Universidade do Vale do Paraíba – UNIVAP
Instituto de Pesquisa e Desenvolvimento - IP&D
Programa de Pós-Graduação em Física e Astronomia

DANIELA OLIVEIRA SILVA MURAJA

IDENTIFICATION OF OCEAN-ATMOSPHERE AND SOLAR PARAMETERS IN ARAUCARIA ANGUSTIFOLIA GROWTH RING CHRONOLOGIES - A COMPARISON BETWEEN CITIES IN SOUTHERN BRAZIL

São José dos Campos - SP

2023

DANIELA OLIVEIRA SILVA MURAJA

IDENTIFICATION OF OCEAN-ATMOSPHERE AND SOLAR PARAMETERS IN ARAUCARIA ANGUSTIFOLIA GROWTH RING CHRONOLOGIES - A COMPARISON BETWEEN CITIES IN SOUTHERN BRAZIL

Doctoral thesis presented to the Graduate Program in Physics and Astronomy at the University of Vale do Paraíba, as a complement to the credits required to obtain the title of Doctor in Physics and Astronomy.

Supervisor: Dr. Virginia Klausner
Co-supervisor: Dr. Alan Prestes and
Dr. Tuomas Aakala

São José dos Campos - SP

2023

Fundação Valeparaibana de Ensino

BIBLIOTECA

TERMO DE AUTORIZAÇÃO DE DIVULGAÇÃO DA OBRA

Ficha catalográfica

Muraja, Daniela Oliveira Silva

Identification of ocean-atmosphere and solar parameters in araucaria angustifolia growth ring chronologies : a comparison between cities in southern Brazil / Daniela Oliveira Silva Muraja; orientadora, Virginia Klausner; co-orientador Alan Prestes, co-orientador Dr. Tuomas Aakala. - São José dos Campos, SP, 2023.

1 CD-ROM, 228 p.

Tese (Doutorado) - Universidade do Vale do Paraíba, São José dos Campos. Programa de Pós-Graduação em Física e Astronomia.

Inclui referências

1. Física e Astronomia. 2. Dendrocronologia. 3. Araucária angustifolia. 4. Oceano-atmosfera. 5. Clima. I. Klausner, Virginia, orient. II. Prestes, Alan, co-orient. III. Aakala, Tuomas, co-orient. IV. Universidade do Vale do Paraíba. Programa de Pós-Graduação em Física e Astronomia. V. Título.

Eu, Daniela Oliveira Silva Muraja, autor(a) da obra acima referenciada:

Autorizo a divulgação total ou parcial da obra impressa, digital ou fixada em outro tipo de mídia, bem como, a sua reprodução total ou parcial, devendo o usuário da reprodução atribuir os créditos ao autor da obra, citando a fonte.

Declaro, para todos os fins e efeitos de direito, que o Trabalho foi elaborado respeitando os princípios da moral e da ética e não violou qualquer direito de propriedade intelectual sob pena de responder civil, criminal, ética e profissionalmente por meus atos.

São José dos Campos, 14 de novembro de 2023.

Daniela O. Silva

Autor(a) da Obra

Data da defesa: 23 / 08 / 2023

Universidade do Vale do Paraíba

Instituto de Pesquisa e Desenvolvimento

DANIELA OLIVEIRA SILVA MURAJA

"IDENTIFICATION OF OCEAN-ATMOSPHERE AND SOLAR PARAMETERS IN ARAUCARIA ANGUSTIFOLIA GROWTH RING CHRONOLOGIES – A COMPARISON BETWEEN CITIES IN SOUTHERN BRAZIL"

Tese aprovada como requisito parcial à obtenção do grau de Doutor, do Programa de Pós-Graduação em Física e Astronomia, do Instituto de Pesquisa e Desenvolvimento da Universidade do Vale do Paraíba, São José dos Campos, SP, pela seguinte banca examinadora:

Irapuan R. de O. Filho	Irapuan Rodrigues
Virginia K. de Oliveira	Virginia K. de Oliveira
Alan Prestes	Alan Prestes
Arian O.González	Arian Ojeda González
Tuomas Aakala	Tuomas Aakala
Luis E. A. Vieira	Luis E. A. Vieira
Francisco C. R. Fernandes	Francisco C. R. Fernandes
Mariza P.de S. Echer	Mariza P. de S. Echer

Prof.ª Dr.ª Lúcia Vieira
Diretora do IP&D – Univap
São José dos Campos, 23 de agosto de 2023.

This work is dedicated to my family and my dogs, because no matter where I am, they will always be by my side.

ACKNOWLEDGEMENTS

First and foremost, I would like to thank my parents, Soraia and Luiz. Without them, I would not be the person I am today, and completing a doctorate would have been nearly impossible. I also want to express my gratitude to my brothers, Danilo and Diego. Regardless of the situation, we have always stood by each other's side, even if it's in an online game. And, of course, my dogs — Cacau, Bela, Maria, Billy, Biba, Cléu, Suzy, Chanel, Mabel, Babi, Leco, Yoke, Taz, Cristal, and Sofia — they played a crucial role in maintaining my mental health during this period. I extend my thanks to my husband Sami and the family he gave to me: Päivi, Kaj, Marjatta, Simo, and Johanna. You are special people, and I am grateful to share my life with you.

I am thankful for my friends who supported me during this period. Bruna and Carol, for grounding me in reality and being honest with their thoughts. Celso and Wandeclayt, for opening my eyes to the quality and importance of my work. Diego and Stella, who bring calmness and laughter. Lucas Brito and Lucas Manfroi, my friends from afar who have always been there for me. Dear Telmo, thank you for your sensitivity and caring friendship. Marcus and Matheus, your continuous support, despite the distance, means a lot. Dear Gargi, it's amazing how a Brazilian and an Indian can be so similar. Stefany Luz, you truly live up to your name—light. To Cecília Lemes Leite, "my first student" and now a dear friend, thank you.

I express my gratitude to Dr. Mariza Echer, Dr. Luis Vieira, Dr. Francisco Rocha (Guga), Dr. Mario Tommazello, Dr. Irapuan Rodrigues, and Dr. Arian González for their valuable contributions to the development of this work. I also want to thank Dr. Marcelo Scipioni for generously providing some of his samples to enhance my work.

I would like to thank Univap and the professors for their guidance since 2012. Throughout this journey, I've encountered exceptional people. Prof Maria Regina (affectionately my *Tia Regina*), your sweetness and strength mean a lot. Prof Eduardo Jorge de Brito Bastos, thank you for your kind words when I shared my dreams. Prof Oli Dors, thanks for making the search for a cup of coffee in your office so enjoyable. Additionally, all the professors at PPGFA have been very special to me over the years.

A big thank you to the entire Univap Observatory team, led by professors Irapuan and Alexandre Oliveira. The Observatory was my favorite activity throughout my postgraduate studies. I learned, had fun, and had unique opportunities with you.

I express my gratitude for the knowledge and patience of my advisors, Dr. Virginia Klausner, Dr. Alan Prestes, and Dr. Tuomas Aakala. I hope I was a good student and person for you. I wish that you have good memories of me, just as I have of you.

"At other times when I hear the wind blow I feel just hearing the wind blow makes it worth being born."

(Fernando Pessoa)

RESUMO

Compreender o clima regional do sul do Brasil é de grande importância devido à alta variabilidade climática na região, que afeta o crescimento das árvores. A Dendrocronologia, que examina os anéis de crescimento das árvores, é uma ferramenta valiosa para estudar parâmetros climáticos e geofísicos que influenciam uma região. Isso permite o desenvolvimento de modelos matemáticos potenciais para reconstruir climas passados e até mesmo identificar ciclos solares antigos. Para este estudo, a espécie *Araucaria angustifolia* foi utilizada devido às suas características morfológicas e anatômicas, anéis de crescimento visíveis, longevidade e adequação para pesquisas dendrocronológicas e dendroclimáticas (sensibilidade climática). As amostras usadas neste estudo fazem parte de um banco de dados do Laboratório de Registros Naturais, onde algumas das quais foram previamente estudadas por outros pesquisadores. Além disso, uma nova série de amostras para a cidade de Canela (29°19' S lat and 50°48' lon) é introduzida e analisada nesta tese. Todas as séries passaram pelo mesmo método de remoção de tendências e correção da variância da cronologia média, e dados estatísticos expressando a qualidade das séries foram obtidos. A região de interesse para este estudo é o sul do Brasil, caracterizada por estações do ano bem definidas e influenciada pelos Oceanos Atlântico e Pacífico, que impactam o clima e os fenômenos atmosféricos na área. O principal objetivo é identificar a influência de parâmetros oceânicos-atmosféricos no crescimento das árvores, como o Índice de Oscilação Sul (IOS) e o NIÑO 3.4 (temperatura da superfície do mar no Oceano Pacífico), ligados à Oscilação Sul *El Niño* (ENSO). Esses parâmetros têm efeitos diretos nos níveis de precipitação, levando a condições anormalmente úmidas ou secas e impactos consequentes na agricultura, no meio ambiente e na economia. Além disso, outros parâmetros climáticos, como níveis de precipitação e temperaturas máximas, médias e mínimas para cada região, bem como a temperatura da superfície do mar do Oceano Atlântico (ATLSW), são avaliados. Além disso, o número de manchas solares (SUNSPOT) é considerado devido à influência da radiação solar na variação do clima da Terra. A identificação dos parâmetros nas cronologias regionais foi inicialmente realizada usando a correlação de Pearson, mas resultados insuficientes foram obtidos. Para superar essa limitação, utilizou-se a análise de coerência cruzada de ondeletas (WTC), que forneceu periodicidades relacionadas aos parâmetros analisados. Os resultados foram primeiramente descritos por cidade para identificar todos os parâmetros que influenciam o crescimento das árvores em cada localização. Em seguida, utilizando a potência média normalizada das ondeletas, comparou-se as respostas das cidades a cada parâmetro. Os resultados mostraram uma influência significativa de parâmetros relacionados ao ENSO, bem como a influência solar nos sinais das cronologias médias de todas as cidades. Surpreendentemente, a precipitação e a temperatura não foram os principais fatores limitantes para as árvores estudadas, possivelmente devido à existência de outros fatores externos que influenciam o crescimento das árvores, e a atividades humanas (desmatamento, poluição, etc). Considerando o impacto humano no meio ambiente, mudanças nas características florestais e microclima podem ter um efeito profundo na sobrevivência das árvores, inclusive na *Araucaria angustifolia*, que já está em risco de extinção devido à atividades intensivas de exploração madeireira nas últimas décadas. Este estudo aprimora nossa compreensão dos parâmetros climáticos, oceânicos-atmosféricos e solares que influenciam o desenvolvimento dessa espécie na região sul do Brasil. Esta tese foi trabalhada com um intuito de gerar um manual com códigos em linguagem R para facilitar a acessibilidade de pesquisadores na área, em especial alunos iniciantes do Laboratório de Registros Naturais (LRN - UNIVAP).

Palavras-chaves: dendrocronologia; araucária angustifolia; oceano-atmosfera; ENSO; clima.

EXPLORING OCEAN-ATMOSPHERE PHENOMENA IN TREE-RING GROWTH OF *ARAUCARIA ANGUSTIFOLIA* FROM SOUTHERN BRAZIL

ABSTRACT

Understanding the regional climate of southern Brazil is of great importance due to the high climate variability in the region, which affects tree growth. Dendrochronology, which examines tree growth rings, is a valuable tool for studying climatic and geophysical parameters that influence a region. It allows for the development of potential mathematical models to reconstruct past climates and even identify ancient solar cycles. For this study, the species *Araucaria angustifolia* was selected due to its morphological and anatomical characteristics, visible growth rings, longevity, and suitability for dendrochronological and dendroclimatic research (climate sensitivity). The samples used in this study are derived from a database at the Laboratory of Natural Records, where some of them have been previously studied by other researchers. Additionally, a new series of samples for Canela city (29°19' S lat and 50°48' lon) is introduced and analyzed in this thesis. All series underwent the same detrending method and mean chronology variance correction and statistical data expressing the quality of the series were obtained. The region of interest for this study is the south of Brazil, characterized by well-defined seasons and influenced by the Atlantic and Pacific Oceans, which impact the climate and atmospheric phenomena in the area. The primary goal is to identify the influence of ocean-atmospheric parameters on tree growth, such as the Southern Oscillation Index (SOI) and the NIÑO 3.4 (sea surface temperature in the Pacific Ocean), linked to the *El Niño*-Southern Oscillation (ENSO). These parameters have direct effects on precipitation levels, leading to abnormal wet or dry conditions and consequential impacts on agriculture, the environment, and the economy. Additionally, other climate parameters, such as precipitation levels and maximum, average, and minimum temperatures for each region, as well as the sea surface temperature of the Atlantic Ocean (ATLSW), are evaluated. Moreover, the number of sunspots (SUNSPOT) is considered due to the influence of solar radiation on Earth's climate variation. The identification of the parameters in the regional chronologies was initially performed using Pearson's correlation, but insufficient results were obtained. To overcome this limitation, we utilized cross-wavelet coherence (WTC) analysis, which provided periodicities related to the analyzed parameters. The results were first described per city to identify all the parameters influencing tree growth in each location. Then, using the normalized average power of the wavelets, we compared the responses of the cities to each parameter. The results showed a significant influence of parameters related to ENSO, as well as solar influence on the signs of the average chronologies of all cities. Surprisingly, precipitation and temperature were not the main limiting factors for the studied trees, possibly due to other external factors influencing tree growth, such as human activities (deforestation, pollution, etc.). Considering the human impact on the environment, changes in forest characteristics and microclimate can have a profound effect on the survival of trees, including the *Araucaria angustifolia*, which is already at risk of extinction due to intensive logging activities in the last decades. This study enhances our understanding of the climatic, ocean-atmospheric, and solar parameters that influence this species' development in the southern region of Brazil. This thesis was designed with the aim of generating a manual with codes in R language to facilitate the accessibility of researchers in the area, especially beginner students of the Laboratory of Natural Records (LRN - UNIVAP).

Keywords: dendrochronology; araucaria angustifolia; ocean-atmosphere; ENSO; climate.

LIST OF FIGURES

LIST OF TABLES

LIST OF ABBREVIATIONS AND ACRONYMS

AÇU - Açungui

ADI - Tropical Atlantic Dipole Index

ALS - Above Sea Level

APM - Atlantic Polar Mass

ATLSW - Alantic Ocean - Southwest Region

ATM - Atlantic Tropical Mass

BCE - Before Common Era

CAN - Canela

CHA - Chapecó

CME - Coronal Mass Ejection

COX - Coxilha

CUR - Curitibanos

CWT - Continuous Wavelet Transform

ENSO - *El Niño* - Southern Oscillation

ERBS - Earth Radiation Budget Satellite

GCA - General Carneiro

IRA - Irani

IRI - Irineópolis

ITCZ - Intertropical Convergence Zone

LLJ - Low-level Jets

MCC - Mesoscale Convective Complexes

MICE - Multiple Imputation

NCEP - National Weather Service - Climate Prediction Center

NOAA - National Oceanic and Atmospheric Administration

PFU - Passo Fundo

PREC - Precipitation

QBO - Quase-Biennial Oscillation

RWI - Ring Width Index

SAAS - South Atlantic Anticyclone System

SACZ - South Atlantic Convergence Zone

SAM - Southern Annular Mode

SASA - South Atlantic Subtropical Anticyclone

SASH - South Atlantic Subtropical High

SFP - São Francisco de Paula

SMM - Solar Maximum Mission

SOI - Southern Oscillation Index

SST - Sea Surface Temperature

SSTA - Sea Surface Temperature Anomaly

TMAX - Maximum Temperature

TMEAN - Mean Temperature

TMIN - Minimum Temperature

WTC - Cross Wavelet Coherence

SUMMARY

1 INTRODUCTION

The global climate has become one of the most important objects of study today, due to climate change and its effects on nature and human life. Because of varying climatic conditions, atmospheric phenomena, and their complex interactions, it is essential to investigate climate on a regional scale. This regional climate analysis contributes to our understanding of the global climate puzzle. In the last three decades studies about climatic phenomena and climatic variability showed that it is mainly driven by the ocean-atmosphere interaction, especially in tropical oceans (RENÉ; PATRICIO, 2007; WANG, 2019). Nowadays the word "climate" is considered a synonym for this ocean-atmosphere interaction, which means that a combination of factors controls a continent's climate (WANG, 2019).

Recent works have focused on studying the interdecadal variability of the ocean-atmosphere system to explain small and large changes in climate. Yet, data obtained by measuring instruments is generally limited (less than 100 years) and there are a lot of missing data, generally caused by equipment reading errors (RENÉ; PATRICIO, 2007). Also, not all regions of the planet contain climatic stations to measure the climatic parameters. There are still a few existing stations in the Brazilian region and most of them have several problems with missing data (GARREAUD; BATTISTI., 1999; RENÉ; PATRICIO, 2007).

Dendrochronology is a valuable tool that studies tree growth rings and can be used together with measured climatic data, enabling the inference of environmental conditions during the time of a ring's development (SPEER, 1971). By analyzing tree rings, it is possible to identify key climatic factors in a region, such as temperature, precipitation, and climatic events, and use this information to help develop mathematical models for reconstructing past climate parameters. Studying past regional climates helps in understanding the global climate puzzle. The pioneering study in applying dendrochronology to study climate and solar activity (dendroclimatology) was conducted by Douglass (1919), who also developed many of the statistical parameters used to check the quality of tree-ring chronologies and, so, its results.

Obtaining reliable data is one of the primary challenges in dendroclimatology. It is important to ensure that the tree-ring chronology is well-dated and has a significant statistical response. Crossdating is applied to check if the rings between the trees are aligned, which involves matching tree ring patterns among samples from different trees and must be performed with great care to avoid introducing erroneous signals into tree growth-climate analysis and paleo reconstructions, which could lead to inaccurate interpretations (SCHWEINGRUBER, 1983).

Liebig's Law of the Minimum is an important principle in dendrochronology, crucial to understanding the factors influencing tree growth (SPEER, 1971). According to this law, a single factor or a few factors can exert the greatest control over the rate of growth. Temperature and precipitation tend to be the most significant factors that affect tree growth (SCHWEINGRUBER, 1983). However, other external factors, including radiation, nutrient availability, and human impacts on the environment, can also influence growth. As demonstrated by Sato & Hirano (2019), phenomena such as atmospheric and radiative changes, as well as complex interactions within the Earth's stratosphere, can have profound effects on global climate by modifying the tropopause structure. This highlights the importance of considering the existence of external factors when studying and understanding tree-growth processes. Depending on the study objectives, filters can be applied to maximize the signal of interest and minimize factors that are not the study target. This method is called detrending, and several types are used, such as Regional Curve Standardization, Spline smoothing, Negative exponential, and others. For instance, applying a detrend method to remove natural tree growth trends will maximize the climatic signal in the tree ring series. These methodologies are further discussed by Helama et al. (2004), Helama, Melvin & Briffa (2017), Silva et al. (2021a).

The choice of *Araucaria angustifolia* as the tree species for the dendroclimatological analysis is based on several factors. The species exhibits morphological and anatomical characteristics of wood that make it suitable for dendrochronological research (SANTA-ROSA et al., 2007). It is found in subtropical/temperate regions, particularly important for studying climate variability. The species is known for its longevity, which allows the construction of long chronologies spanning over 100 years. The dendrochronological potential of *Araucaria angustifolia* has been well-established in Brazil, where it is one of the most studied species. Several studies have used this species to analyze tree growth-climate responses and to reconstruct past climate variability (CATTANEO et al., 2013; MARTIN-KOSKI et al., 2015; LORENSI; PRESTES, 2018; PRESTES et al., 2018b; SILVA et al., 2021b). The widespread use of *Araucaria angustifolia* in dendrochronological research in Brazil highlights its reliability and suitability for this type of analysis.

Brazil is renowned for its rich biodiversity, including a wide variety of plant and animal life, making it an ecologically significant area. Southern Brazil was chosen for this study due to its well-defined climate seasons (each season has a different pattern from the other), which contribute to the formation of distinct annual growth rings in trees. A strong influence of the Atlantic and Pacific oceans affects the climate and oceanic-atmospheric phenomena in this region, which can be identified in the tree ring data (RENÉ; PATRICIO, 2007). These phenomena can have significant impacts on daily life and economic sectors, such as agriculture.

The *El Niño*-Southern Oscillation (ENSO) is an ocean-atmosphere phenomenon

that impacts the precipitation levels in South America, causing unnatural wet conditions in southern Brazil and dry conditions in northern Brazil (RENÉ; PATRICIO, 2007). Its positive and negative phases may bring several consequences to agriculture, economy, tourism, and daily life. Moreover, studies by Rind (2002), Chen & Zhou (2012), Zhou, Chen & Zhou (2013) have shown an influence of solar cycles on the global climate, also affecting ocean-atmosphere dynamics (MEEHL et al., 2003). Furthermore, the findings of (SHIMIZU; AMBRIZZI, 2015) indicate that precipitation and temperature anomalies during ENSO events can be amplified or weakened when they coincide with Madden-Julian Oscillation (MJO), particularly in the austral summer. The MJO is a significant source of intraseasonal variability in the tropics and influences a variety of climate phenomena, including tropical cyclones, monsoons, and atmospheric wave patterns that affect extratropical climate. Additionally, the MJO is associated with regional weather patterns such as atmospheric blocking and weather regimes (WANG; BOYD; WALSH, 2023).

According to studies performed by Hanslmeier (2007), Siingh et al. (2011), Earth's climate is influenced by solar energy, with 50% of the incoming energy being absorbed by the Earth's surface. The variation of the radiation received has two main factors: the Sun and the Earth's position in relation to the Sun. Changes in the position may affect the level o radiation received (VIEIRA et al., 2012), as an example, the Summer for the Southern Hemisphere occurs during the perihelion (point in the planet's orbit at which it is closest to the Sun). To investigate the relationship between the Sun, Earth, and climate, tree growth rings are utilized as a natural record to study this influence (RIGOZO et al., 2008; PRESTES et al., 2011; RIGOZO et al., 2012; PRESTES et al., 2018b). Using fossil wood, Prestes et al. (2013) detected the presence of the 11-year solar cycle approximately 200 million years ago.

Several studies utilizing trees as a natural record for studying the Sun-Earth-Climate relationship have indicated evidence of ocean-atmosphere and solar parameters signals in tree ring growth (RIGOZO et al., 2008; PRESTES et al., 2011; RIGOZO et al., 2012; PRESTES et al., 2018b). In the study conducted by Lorensi & Prestes (2018), they observed a drop in tree growth during periods of high precipitation but noted that higher precipitation levels combined with elevated temperatures can promote tree growth. (LORENSI; PRESTES, 2016) demonstrated that *Araucaria angustifolia* is sensitive to climate variables, enabling the reconstruction of spring-summer precipitation during 1907-2009. Additionally, *El Niño/La Niña* phenomena signals were identified in the tree ring chronology of Prestes et al. (2018b), also using *Araucaria angustifolia* from the South of Brazil.

1.1 STUDY JUSTIFICATION

The present thesis explore ocean-atmosphere and solar parameters in the tree-ring growth of *Araucaria angustifolia* samples collected in southern Brazil. The results can provide insights into the effects of climate variability and regional environmental factors on tree growth patterns, and identify the most significant environmental factors influencing the growth of *Araucaria angustifolia* in different cities of southern Brazil. By studying the periodicities between the tree-ring chronologies and the climatic factors, a better understanding of the climate during the tree's existence and the present climate in this region is possible. This research is expected to contribute to the development of sustainable forest management practices and aid in the preservation of *Araucaria angustifolia* populations, which are threatened by deforestation and climate change, by giving an understanding of how this species' growth responded to climatic parameters.

1.2 GENERAL OBJECTIVES

The main objective is to identify patterns of periodicity and relate them to solar and ocean-atmosphere parameters, such as solar activity, *El Niño*, *La Niña*, and others. Dendrochronological series from different areas of the South region of Brazil, including the states of Rio Grande do Sul, Santa Catarina, and Paraná are used. The species *Araucaria angustifolia* was chosen for the analysis due to its high potential for dendrochronological studies and prevalence in the study region. Furthermore, a GitHub Project called **"DendrochronologySteps"** is provided, with all the codes used in this thesis, to serve as a manual for researchers and beginner students.

1.3 SPECIFIC OBJECTIVES

1. Analyze existing dendrochronological series from different regions of Santa Catarina, Paraná, and Rio Grande do Sul to identify solar and ocean-atmosphere phenomena periodicities;
2. Process tree ring series for Canela City and obtain a new chronology to complement the analysis with samples of *Araucaria angustifolia*;
3. Identify and describe the ocean-atmosphere and solar parameters that influence the tree growth for each of the analyzed cities;
4. Compare and describe the *Araucaria angustifolia* responses to each ocean-atmosphere and solar parameter across the cities.
5. Develop the codes in R language files to be used as a guide/manual for other researchers.

2 LITERATURE REVIEW

This chapter aims to provide a comprehensive understanding of solar and ocean-atmosphere parameters, including solar activity, and their relationship with the Earth's climate. It also explores the use of tree rings as natural proxy records, with a specific focus on the tree species *Araucaria angustifolia*, chosen for investigation in this study.

2.1 SOLAR ACTIVITY

At the heart of the Solar System lies a yellow dwarf star known as the Sun, which emits the majority of its radiation in the visible region of the spectrum. The Sun generates energy through the nuclear fusion process in its core, where hydrogen atoms combine to produce helium and other elements. This fusion process generates energy that manifests as visible light and radiation across the entire electromagnetic spectrum at the Sun's surface (HOYT; SCHATTEN, 1997; MCFADDEN; WEISSMAN; JOHNSON, 2007). The Sun's structure is composed of different layers, each with a distinct function (Figure 1).

- The Core is the innermost part of the Sun, with a temperature of about 15.7 million Kelvin. It is where nuclear fusion occurs continuously, as four hydrogen nuclei fuse to form a helium nucleus. The mass difference between these elements results in the release of energy, which travels throughout the Sun (LEAN, 1991; LANG, 2001).
- The Radiation Zone is the region where energy is transported by radiation, while the Convection Zone is responsible for energy transport through convection (LEAN, 1991; LANG, 2001).
- Photosphere is the visible surface of the Sun, where energy is finally deposited. It is possible to see sunspots on the photosphere, and it has an average temperature of 6400 Kelvin (LEAN, 1991; LANG, 2001). The granulation effect is a result of the convection process occurring in this region.
- Chromosphere is a less dense layer compared to the photosphere, and it is only visible during solar eclipses or by using special equipment. Solar phenomena such as prominence and solar eruptions occur in the chromosphere (SOBRINHO, 2013).
- Corona is the outermost layer. It can be observed during solar eclipses using specific telescopes called coronagraphs (MCFADDEN; WEISSMAN; JOHNSON, 2007). The corona has gases with high velocities that can escape, driven by solar gravitation, and this process generates and powers the solar wind (SOBRINHO, 2013).

Figure 1: The Sun's structure: core, radiative zone, convection zone, photosphere, chromosphere, and corona. Some of the Sun's phenomena are sunspots (black spots present in the photosphere), solar flares, coronal loops, and prominences which can happen in both the chromosphere and corona.

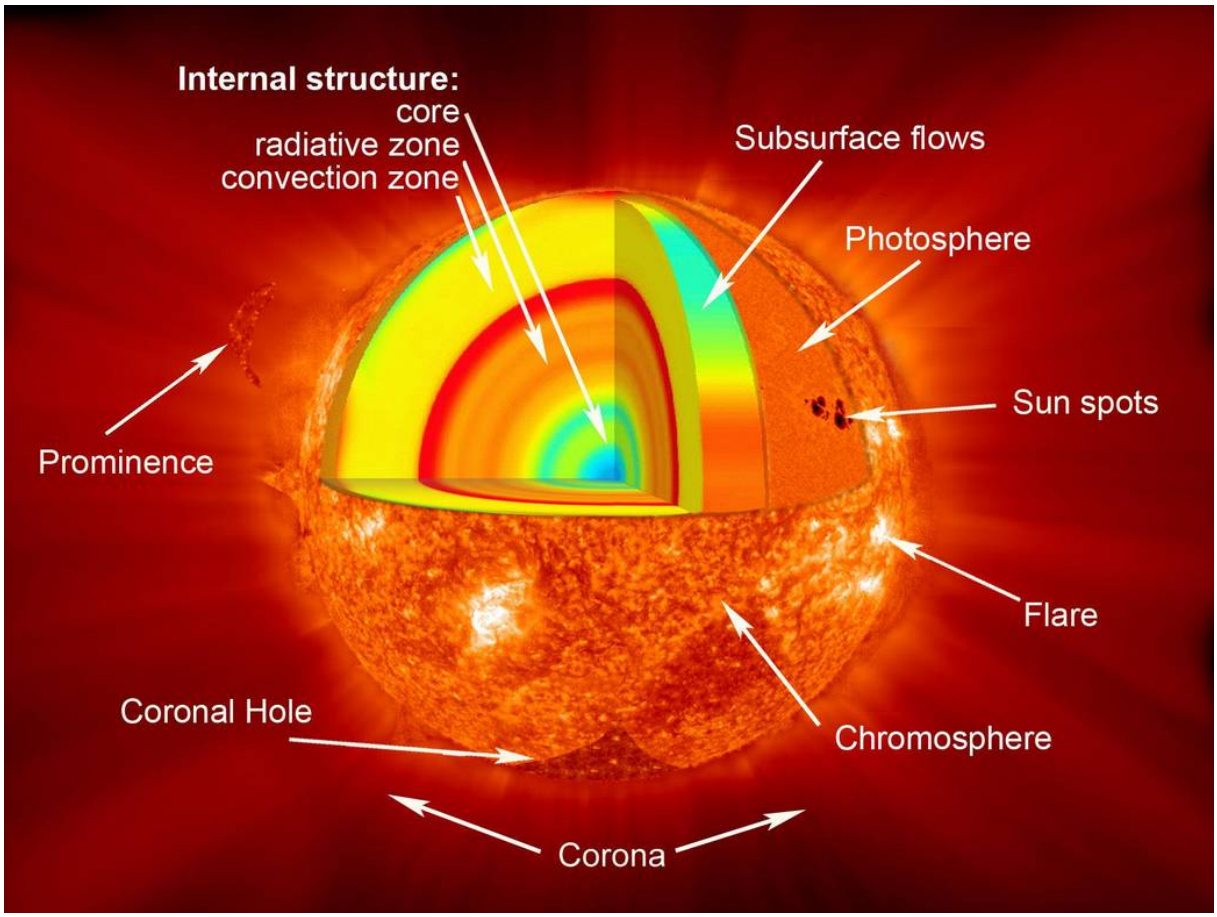

Source: NASA (2017).

According to Gopalswamy, Mewaldt & Torsti (2006), several solar phenomena confirm the true magnetic variability of the Sun. One such phenomenon is the Solar Wind, a supersonic plasma flow responsible for carrying particles, including those reaching the planets, including Earth (AKASOFU, 1998). Additionally, Coronal Mass Ejections (CMEs) and Energetic Solar Particles represent two additional phenomena that mirror solar variability. Another indicator of solar variability is observed through electromagnetic radiation, specifically solar flares (GOPALSWAMY; MEWALDT; TORSTI, 2006). The interaction between the convective layer and its differential rotation creates a magnetic field known as the solar dynamo. This, combined with different rotational speeds at each latitude, leads to distortions in the magnetic field, resulting in various solar phenomena, such as Sunspots, CMEs, and Solar Cycles (HOYT; SCHATTEN, 1997; TSURUTANI; GONZALEZ, 1998; TOBIAS, 2003).

The Solar Cycle exhibits a distinct pattern with a maximum and a minimum of solar activity. During the maximum phase, the number of sunspots increases, while the

minimum phase is characterized by fewer sunspots or none at all (see Figure 2). These sunspots are regions on the Sun with intense magnetic fields that inhibit plasma convection, resulting in darker regions with lower temperatures compared to their surroundings in the solar photosphere. The contrast effect makes them distinguishable, and they can persist for days, while larger sunspots may last for weeks (LEAN, 1991; HOYT; SCHATTEN, 1997; ECHER et al., 2003; HATHAWAY, 2014).

Figure 2: Images captured of the Sun during solar minimum in December 2019 (left) and the solar maximum in April 2014 (right).

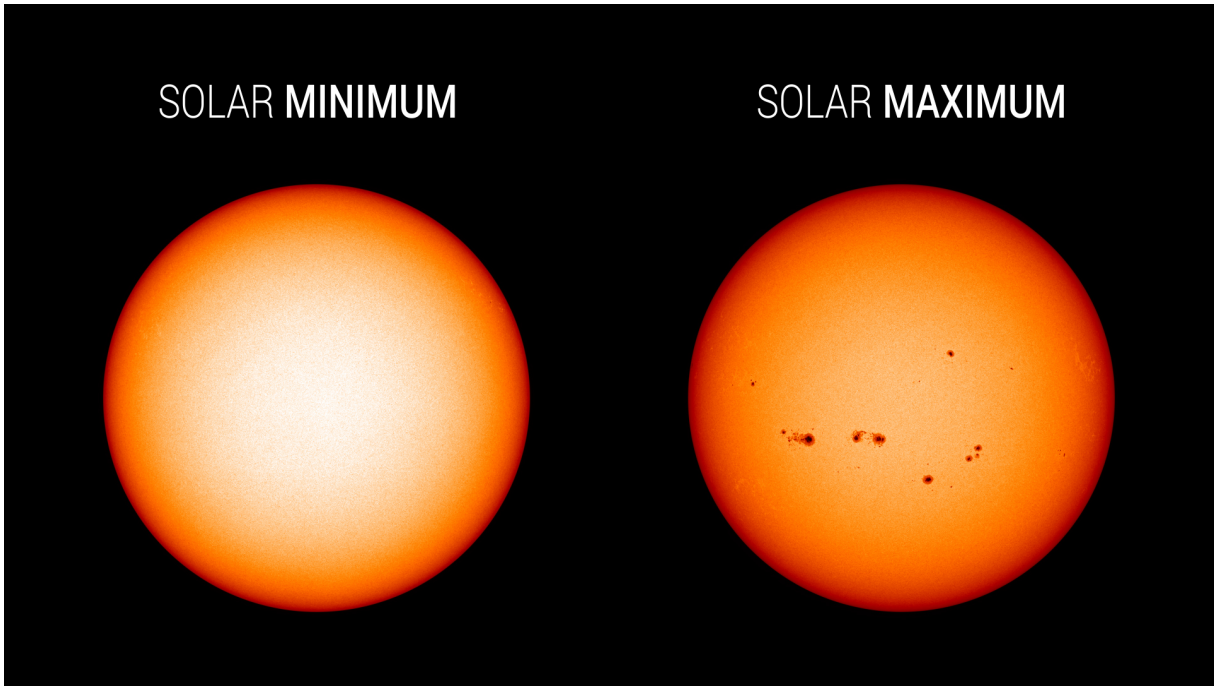

Source: NASA (2020).

Due to the toroidal behavior of the solar magnetic field, plotting the mean daily sunspot area for each latitude as a function of time results in a distinctive pattern known as the "butterfly" diagram (Figure 3). Several solar cycles have been observed through both direct data and proxies. The most common is the 11-year Schwabe Cycle (seen at the bottom of Figure 3), named after Heinrich Schwabe, who first reported groups of sunspots and spotless days, revealing an activity cycle lasting approximately 10 years (SCHWABE, 1844).

The 22-year Hale cycle is essentially two Schwabe cycles, defined by the oscillation of the solar dynamo (SIINGH et al., 2011). On a longer timescale, the 88-year Gleissberg cycle, identified by Gleissberg (1939), encompasses seven or eight cycles, based on data analysis from 1750 to 1928. Additionally, Suess (1980) found evidence of a 200-year cycle using tree-ring radiocarbon records as proxy data.

Historical periods of significantly low solar activity have also been documented. The Maunder Minimum, which occurred from 1570 to 1730 (lasting for approximately 160

Figure 3: Upper: The sunspot area according to its latitude during the time. Bottom: average number of sunspots during a day in which the 11-years cycle is clear.

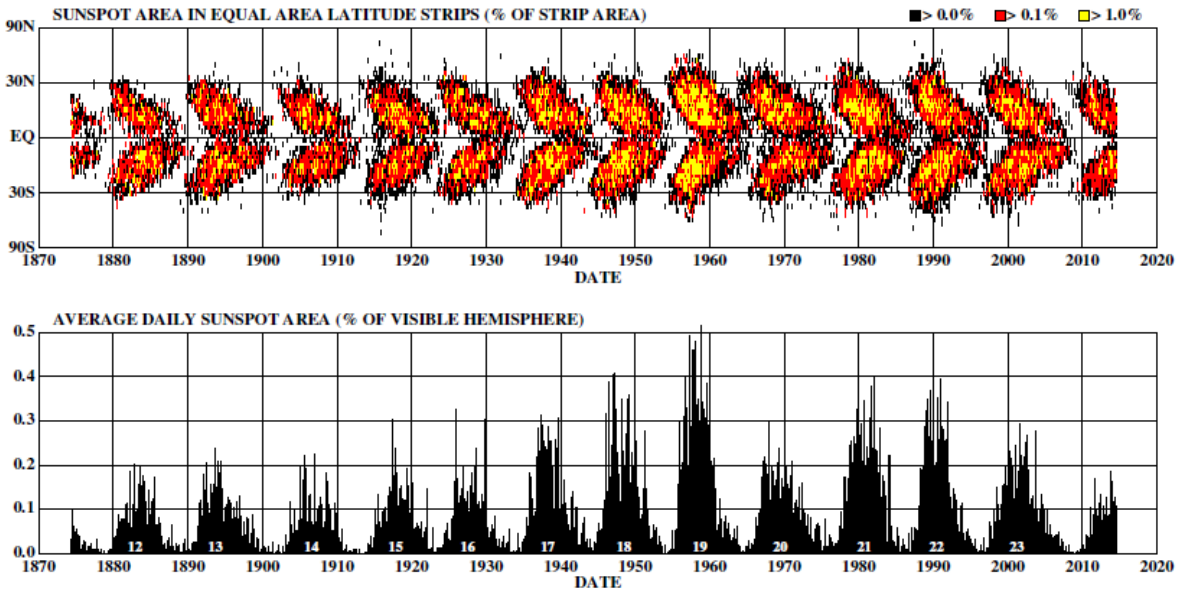

Source: Hathaway (2015)

years), is commonly referred to as a "Little Ice Age", was characterized by significantly reduced solar activity and is believed to have resulted from prolonged atmospheric blocking, possibly exacerbated by elevated levels of greenhouse gases (BRADLEY; JONEST, 1993; LAPOINTE; BRADLEY, 2021). Bradley & Jonest (1993), Usoskin et al. (2015) confirmed this period through the analysis of direct and indirect data (tree-ring and ice cores). Similarly, the Dalton minimum (1797–1827) was observed by John Dalton, who noted a decrease in aurora activity in the early 19th century (SILVERMAN; HAYAKAWA, 2021).

In recent years, tree ring data has gained growing interest as a natural proxy for studying the Sun-Earth-Climate relationship. Several studies have utilized this approach to investigate the relationship between solar activity and tree ring growth, revealing different solar cycles visible in proxy records (RIGOZO et al., 2008; PRESTES et al., 2011; RIGOZO et al., 2012; PRESTES et al., 2018b). For instance, Prestes et al. (2018b) observed a spectral pattern between the sunspot number (SSN) and the dendrochronological series of *Araucaria angustifolia*, finding a consistent Gleissberg cycle. This result aligns with other studies on dendrochronological series from Southern Brazil conducted by Rigozo et al. (2008), Prestes et al. (2011), Rigozo et al. (2012).

The identified solar parameter signals in tree ring growth include the 11-year solar cycle in trees from Southern Italy and Central Europe and Schwabe cycle signals in tree ring carbon isotopes dating back to 969 AD (*Anno Domini* - after Christ) (SIMUNEK et al., 2021; BREHM et al., 2021). These findings imply that trees hold valuable information for understanding the Sun's influence on climate change.

2.2 SUN-EARTH-CLIMATE RELATIONSHIP

The Sun experiences variations in its activity, leading to changes in solar phenomena that can influence space weather and Earth's climate (PARKER, 2001). Throughout history, attempts have been made to relate environmental changes to celestial events, such as sunrise, moonrise, and sunspots levels (HOYT; SCHATTEN, 1997). Nowadays, it is well-known that the Sun plays a crucial role in supporting life on Earth by emitting energy as charged particles through blackbody radiation. The solar activity produces ultraviolet and X-rays that impact the Earth's upper atmosphere, these spectral lines are increased during Solar maximum by a factor of 2 and 100, respectively, resulting in increased temperature and atmospheric density (AKASOFU, 1998; LANG, 2001; LEAN, 1991).

One of the most famous phenomena resulting from particles from the Sun transported through the solar wind that interact with the Earth's atmosphere is the aurora. As described by Akasofu (1998), auroras are luminous ring-shaped belts that appear around the north and south geomagnetic poles of the Earth. They are created by a plasma flux (protons and electrons) from the Sun that reaches the Earth's magnetic field and are carried toward the poles along the magnetic field lines. When these electrons deposit their energy in the upper atmosphere, it excites and/or ionizes the atoms and molecules present in the atmosphere, leading to the release of energy as visible light, resulting in the auroras.

As climate change is finally widely recognized as a serious concern, scientists need to delve deeper and understand every parameter that can influence the climate, including the role of solar variations, the particles in the solar wind that reaches the Earth, and their potential effects on Earth's atmosphere. Data obtained by pyrheliometers flown on the Nimbus-7, Solar Maximum Mission (SMM) satellite, and the Earth Radiation Budget Satellite (ERBS) have allowed for the analysis of long-term trends. It was observed that during its maximum activity, the Sun is brighter and not darker, contrary to initial expectations attributed to the presence of sunspots (FOUKAL, 1998). However, it is now understood that sunspot areas appear darker due to the temperature difference compared to the surrounding areas.

About 400 years BCE (Before Common Era), Meton (Ancient Greek astronomer, engineer and mathematician) began analyzing more than 20 years of solar observations. He found that when the Sun has more black spots, the weather is wetter and rainier (HOYT; SCHATTEN, 1997). Theopharastus (Ancient Greek philosopher) also discovered relations between solar activity and the Earth's climate, but unfortunately, the reports were probably destroyed during the fire at the Alexandria Library, as discussed in Hoyt & Schatten (1997). After that, only a few studies appeared, until a British meteorologist working in India, Meldrum (1872), Meldrum (1885), performed a comparison between sunspot numbers and cyclones in the Indian Ocean, and found a high correlation between them (Figure 4). This work was fundamental in convincing many scientists of the Sun-Earth

relationship.

Figure 4: Comparison of the number of Indian Ocean cyclones and sunspot groups.

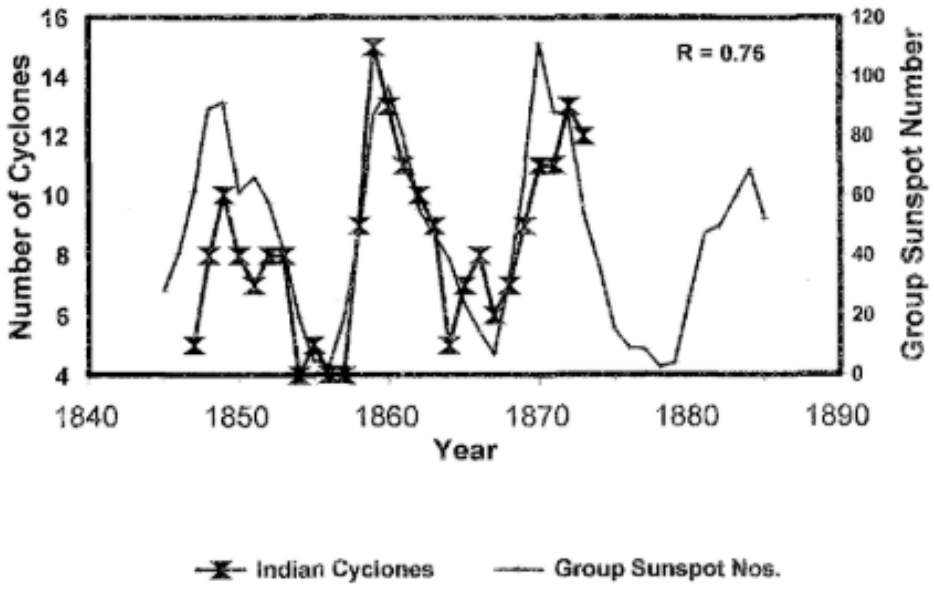

Source: Meldrum (1872).

Hoyt & Schatten (1997) defines that natural variability in climate can originate from solar variations, albedo changes (such as deforestation and ice cover), fluctuations in cloud cover causing variability in the climatic system, volcanic activity, and more. The role of the Sun in climate change is still a subject of debate among scientists. However, researchers studying solar variations through proxies suggest that the increase in solar activity may be linked to global temperature changes. Forest fires in Mexico also seem to be associated with the intensity of the solar cycle variation (VELASCO, 2016). It is important to note that this does not diminish the significance of human impact on climate change.

As a summary of Earth's heat engine, the Earth's surface reflects approximately 30% (albedo = 0.30) of the received solar radiation (short waves) due to clouds (23% of the albedo) and the atmosphere. The remaining 70% of the radiation is absorbed, heating the Earth's surface and causing evaporation or convection. This absorbed radiation is reemitted as infrared radiation (HOYT; SCHATTEN, 1997). According to Seinfeld & Pandis (1998), if the radiation intensity decreases by approximately 5 to 10% without any compensating factors, the planet would be covered in ice within about a century. Throughout history, the Earth has experienced 10 long glacial epochs and 40 smaller ones, all seemingly controlled by the Milankovitch cycles: the Earth's inclination (cycle of 41,000 years), Earth's proximity to the Sun (cycles of 19,000 and 24,000 years), and changes in the Earth's orbit from circular to elliptical (cycle of 100,000 years)

The Maunder Minimum occurred from 1570 to 1730 and it is associated with a

little ice age. During this period, the number of sunspots and auroras was very low. It is now widely accepted in academia that ice ages occur due to changes in the distribution of light received by the Earth. Figure 5 presents another link to the relationship between Earth's climate and solar activity, the sea surface temperature (SST) level data responses to the solar cycles (ZHOU; TUNG, 2010).

Figure 5: (top) The spatial pattern of SST for the period (1854–2007). (bottom) The SST time series (blue) and the total solar irradiance index (red).

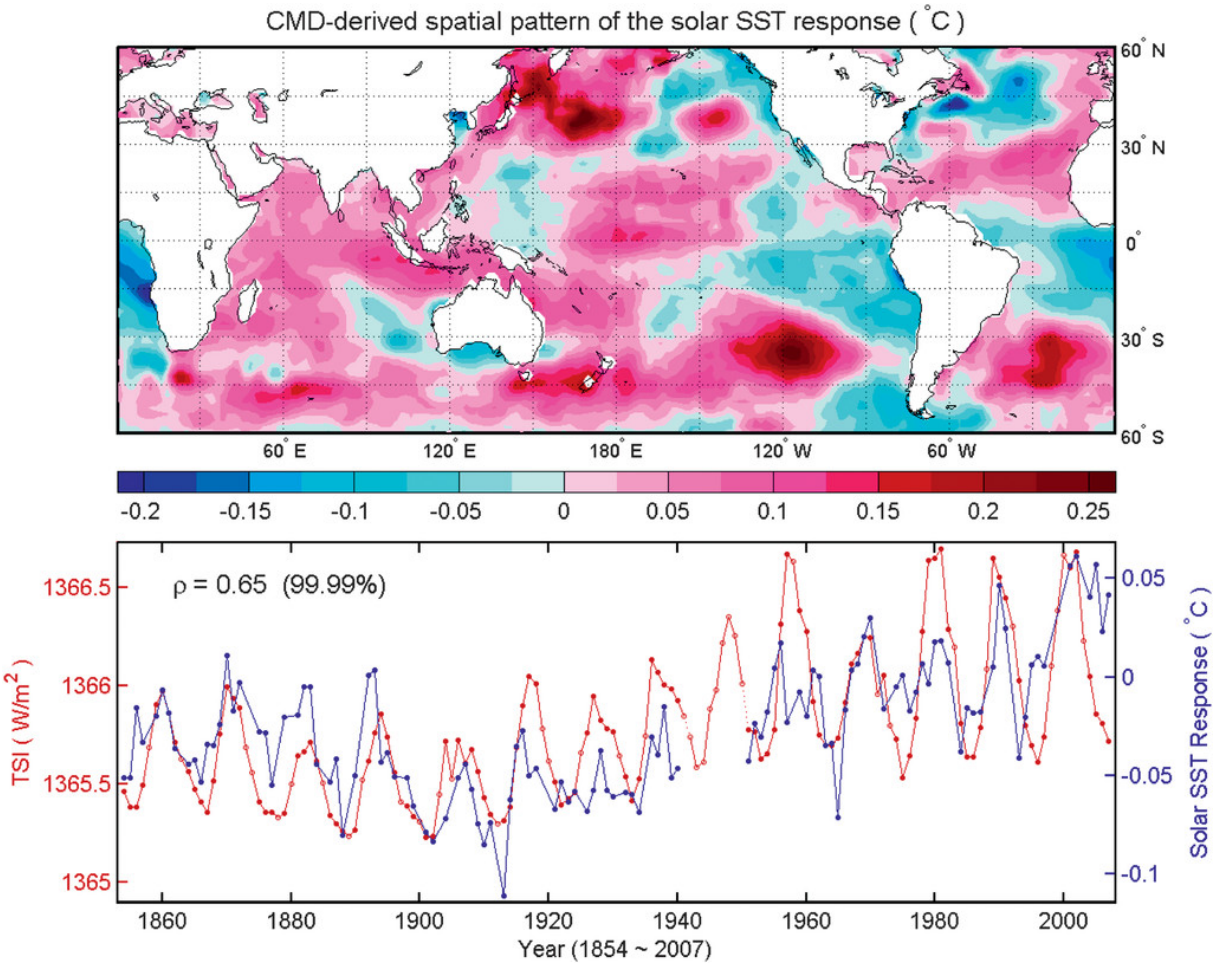

Source: Zhou & Tung (2010).

Earth's temperature has increased by approximately 0.8°C since the 17th century, according to the reconstruction of total solar radiation in the Northern Hemisphere, suggesting a higher solar influence during the pre-industrial period (CROWLEY, 2000). When considering that solar radiation increased by about 0.14% during this time and the temperature rose by 0.28°C, the climate sensitivity is estimated to be 2°C for every 1% change in solar radiation emissions (SEINFELD; PANDIS, 1998). To conduct comprehensive studies of the Sun-Earth-Climate relationship, Hoyt & Schatten (1997) suggests using a large number of spatial and temporal data and applying statistical knowledge, which can lead to successful analysis.

Ongoing research investigates the complex relationship between solar activity and

Earth's climate. Some studies suggest that solar activity can influence climate patterns, particularly on solar cycle timescales (HAIGH, 2011). This influence is observed in non-uniform SST patterns and correlations with climate phenomena like the Pacific Decadal Oscillation (PDO) and North Atlantic Oscillation (NAO). Solar activity also affects climate modes of variability, such as *El Niño*-Southern Oscillation (ENSO) (HAIGH, 2011). Correlations have been found between solar activity and factors like solar wind, radio flux, and cloud cover. However, the precise mechanisms behind these links remain subjects of ongoing research (BOBERG; LUNDSTEDT, 2002; HAIGH, 2007; HAIGH; ROSCOE, 2006).

2.3 SOUTHERN BRAZIL CLIMATE

Regional climate variability is determined by the weather systems that may control the transport of heat and moisture into a region (IPCC, 2014). To begin exploring the climate of Southern Brazil, it is important to highlight that seasons in the Southern Hemisphere occur in different months compared to the Northern Hemisphere. They are commonly divided as follows:

- Spring - Starts around September 23 and ends on December 21. The flowering of flora is a hallmark of spring.
- Summer - Approximately starts on December 21 and ends on March 21. It typically presents higher temperatures and longer days.
- Autumn - Begins on March 21 and ends on June 21. Days are shorter and cooler.
- Winter - Begins on June 21 and ends on September 23. Generally, the temperature drops during this season.

As a country with a large territory, Brazil exhibits a wide range of climate types. An extensive analysis conducted by Dubreuil et al. (2019), using data from 208 meteorological stations for the period of 1990-2015, resulted in Figure 6, which illustrates the diverse climates across the country. This climatic variability is influenced by factors such as latitude, longitude, vegetation, air masses, insolation, atmospheric pressure, humidity, temperature, and interactions with ocean. Even within small regions, the climate can vary significantly, as shown in Figure 6 (b) depicting the vast diversity of climates in Southern Brazil.

Southern Brazil is situated in a transition area between the tropics and mid-latitudes, and it is characterized by a diverse climate due to its topography and altitude. The region has a large part of its territory at 300 m above sea level (ASL), which causes significant contrasts in the rain and temperature levels, even though dry and rainy seasons

Figure 6: (a) Types of climates in Brazil (1990-2015) according to Köppen's classification and a mini-map with the list of Brazilian state abbreviations used in the text. (b) Map of the Southern region of Brazil (scale of 500 km) showing how the climate type can change in a small region.

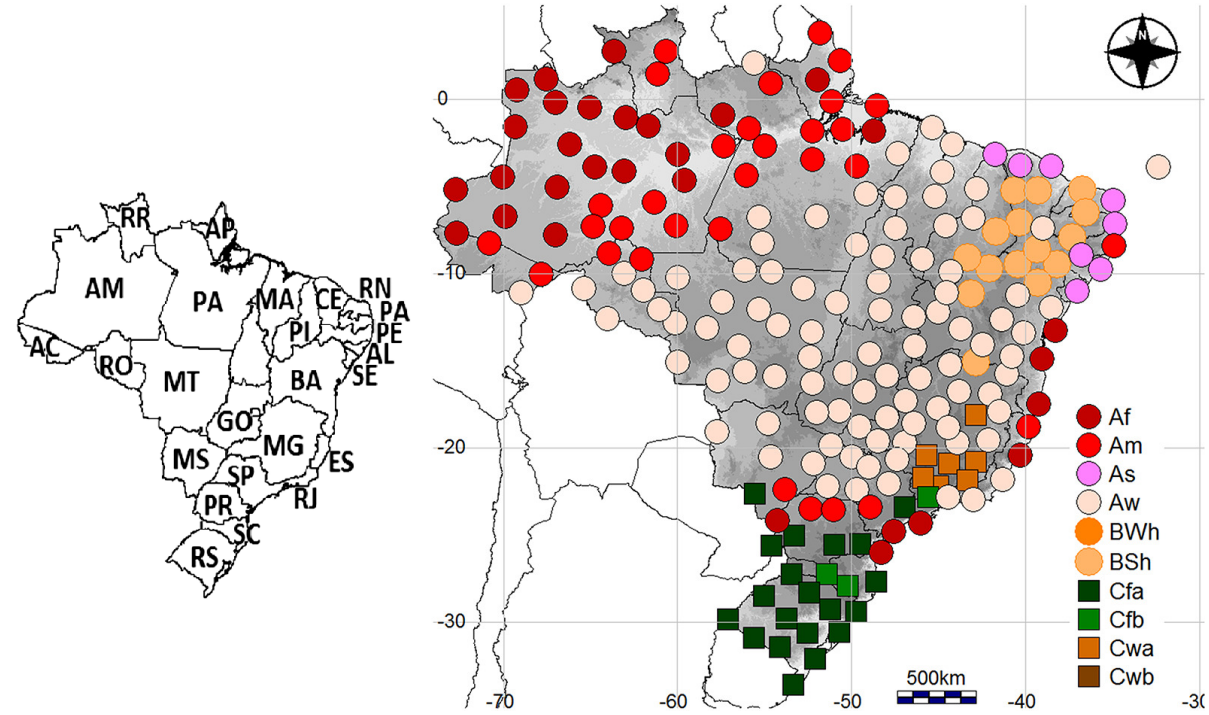

(a)

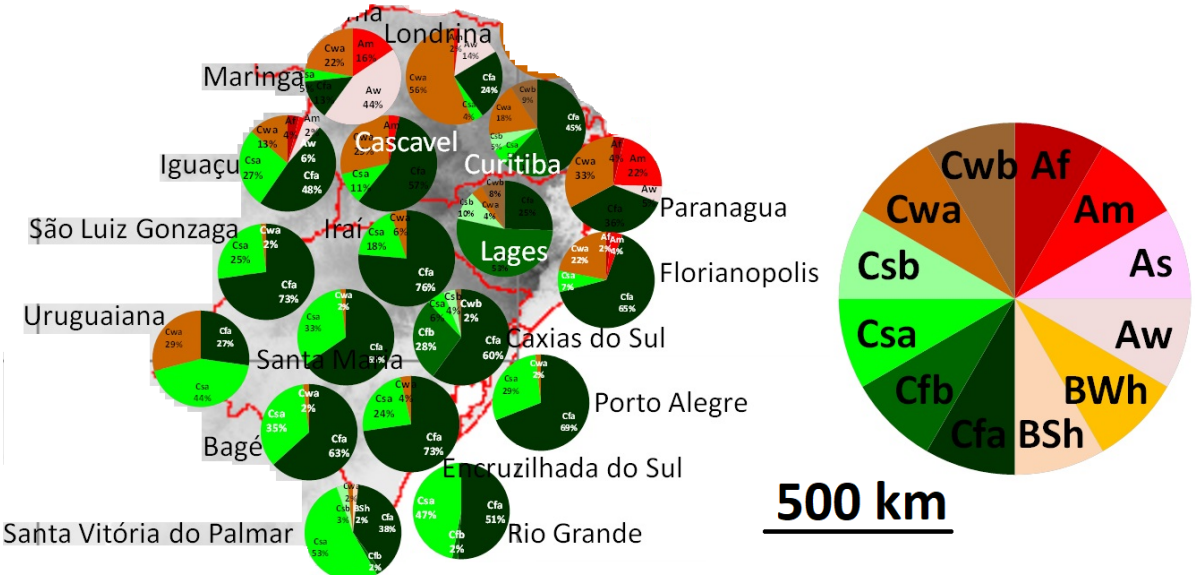

(b)

Source: Modified from Dubreuil et al. (2019).

are not a pattern in the region (GRIMM; BARROS; DOYLE, 2000; HIERA; V., 2014). The precipitation level tends to be similar in all seasons, as illustrated by Figure 7.

Figure 7: Variation in the level of annual precipitation (mm) during the four seasons of the year across Brazil.

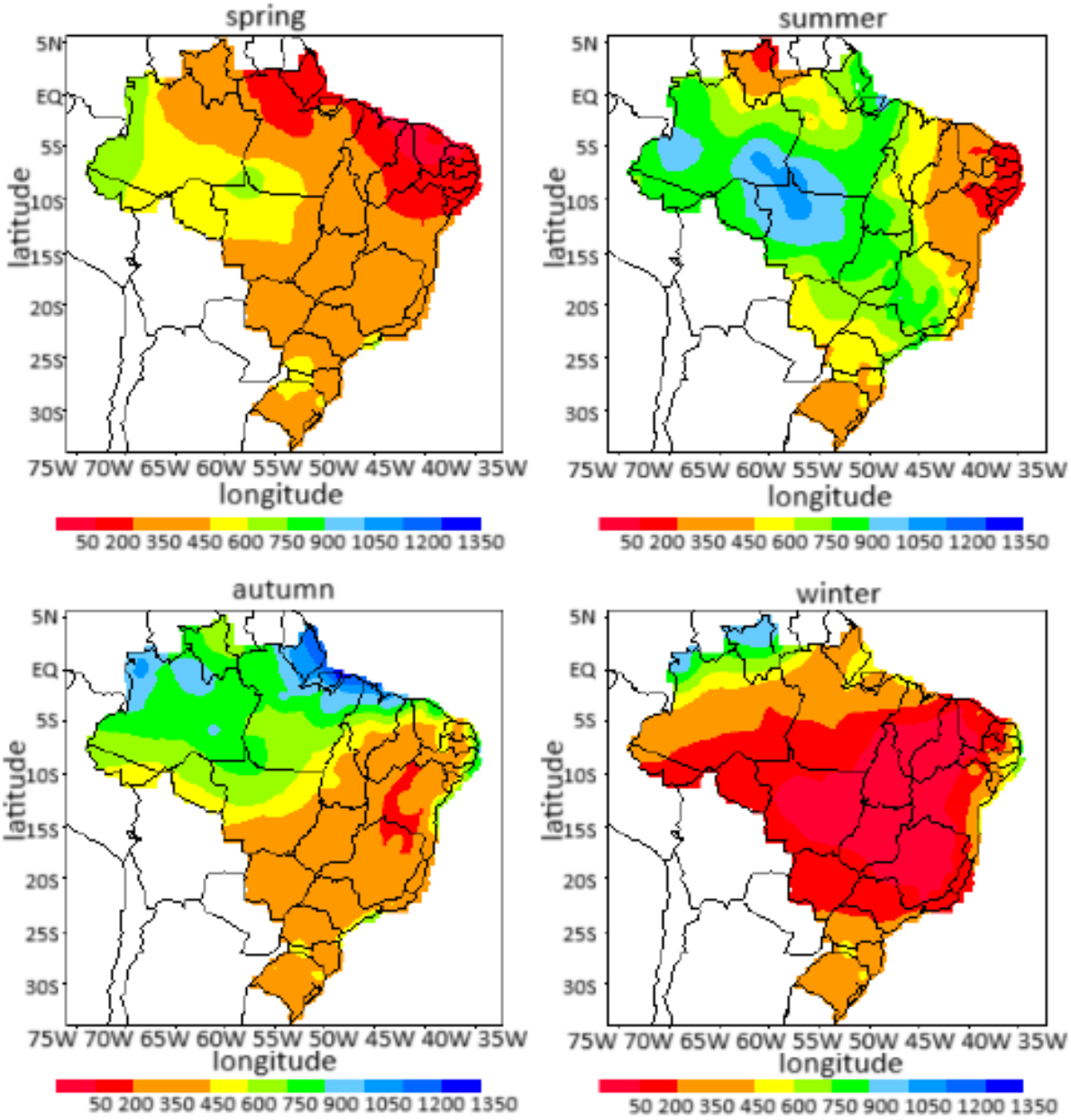

Source: Quadro et al. (1996)

Additionally, Brazil's vast expanse covers a range of latitudes, resulting in variations in the amount of solar energy received. Figure 8 illustrates these differences in incoming sunlight, with regions at lower latitudes receiving more solar energy compared to those at higher latitudes. During summer, almost all areas of Paraná and parts of Santa Catarina experience a decrease in rainfall levels, while in winter, the coastal regions of Paraná and Santa Catarina experience higher rainfall levels (CARVALHO; STIPP, 2004). For example, in the Southern Hemisphere, the summer season coincides with the perihelion, which is

the point in Earth's orbit when it is closest to the Sun. This positioning results in varying levels of solar radiation received at different latitudes, contributing to the region's climate diversity (VIEIRA et al., 2012; WANG; BOYD; WALSH, 2023).

Figure 8: Sunlight energy distribution across Earth is unequal. As depicted in the graph, the angle of incoming sunlight (and hence its intensity) changes with latitude and time of day during the equinoxes.

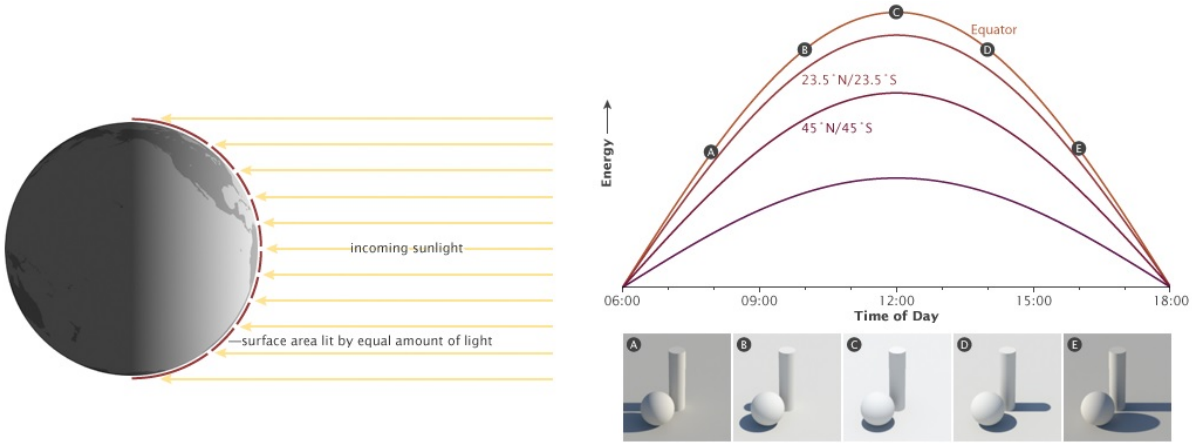

Source: NASA illustration by Robert Simmon.

The climate variability in Southern Brazil is mainly determined by weather systems that control the transport of heat and moisture into the region, which is influenced by factors such as *El Niño* and *La Niña* events and Atlantic Multidecadal Oscillation (AMO) plays a significant role in this climate equation. The AMO, characterized by long-term fluctuations in North Atlantic SSTs, has the potential to further modulate regional climate dynamics, affecting factors such as droughts, heavy rainfall events, and temperature variations in Southern Brazil (IPCC, 2014; SHIMIZU; AMBRIZZI, 2015; TRENBERTH; ZHANG, 2023).

The South of Brazil presents three climate types within the Köppen's classification: Cfb (cold winter with mild summer, wet winter, and summer), Cfa (cold winter with hot summer, wet winter, and summer) and Cwa (moderate temperatures with hot and rainy summer). According to Dubreuil et al. (2019), the uppercase letter "C" is the thermal regimes, the lowercase letters "a" and "b" are subtypes, and the lowercase letters "f" and "w" are subtypes of rainfall. The Table 1 shows the meaning of each Köppen classification from southern Brazil.

The climate in the Southern region of Brazil exhibits a remarkable variation in temperature between the winter and summer seasons. This temperature contrast results in freezing conditions and even snowfall in mountainous areas, which is a rare phenomenon in other regions of Brazil (GRIMM, 2009; HIERA; V., 2014). The annual temperature variation is a crucial characteristic of mid-latitudes, as cold air masses from high latitudes enter the mid-latitude system during winter, leading to lower temperatures (QUADRO,

Table 1: Köppen classification of the climate types from southern Brazil.

Zone - Climate	Type	Acronym	Description
A - Tropical Humid	Tropical wet	Af	No dry season
	Tropical monsoon	Am	Monsoonal, short dry season
	Tropical savanna	As	Dry summer
	Tropical wet and dry	Aw	Winter dry season
B - Dry Climate	Subtropical steppe	BSh	Low-latitude semi arid or dry
	Subtropical desert	BWh	Low-latitude arid or dry
C - Warm temperate (Mid-latitudes) Climates	Humid subtropical	Cfa	No dry season, warm summer
	Marine west coast	Cfb	No dry season, warm and cool summer
	Humid subtropical with dry winter	Cwa	Hot and humid summer, dry winter
	Temperate highland subtropical	Cwb	Warm summer, dry winter

Source: Modified from Drishtiias (2022) according to Arnfield (2023).

1999). In this region, the maximum temperature varies from 10°C in winter to 30°C in summer, as demonstrated in Figure 9 (GRIMM, 2009; HIERA; V., 2014). Moreover, Figure 10 depicts the variation in minimum temperature, ranging from 5 to 20°C (GRIMM, 2009).

The Southern region of Brazil has a climate that combines the features of both Temperate and Tropical climates. In Temperate climates, rainfall is moderate throughout the year, with occasional droughts, mild and/or warm summers, and cool and/or cold winters (SIMMONS, 2015). In contrast, Tropical climates have predictable temperature patterns but unpredictable precipitation patterns (KELLMAN; TACKABERRY, 1997).

The Southern region of Brazil experiences unique weather patterns due to its location outside of the tropics. In the summer, the region receives less light than tropical regions, while in the winter, the Earth's position causes more insolation, leading to higher evaporation rates. The region's proximity to the Atlantic Ocean also contributes to increased cloudiness and higher levels of rainfall (DITTBERNER, 2001). Additionally, the region serves as a passage for polar fronts, resulting in sudden changes in weather throughout the year (LEAL, 1999).

During the period between June and August, southern Brazil encounters an average of 22 frontal system penetrations within the latitudinal range of 25° to 35° S (OLIVEIRA, 1986). These systems accompanied by cold fronts, can induce the formation of squall lines (weather systems characterized by a narrow, elongated line of thunderstorms, often associated with weather fronts) and other phenomena, leading to increased convective precipitation and exerting effects over large areas with tropical climates. The combination of interannual and interdecadal variabilities results in low-frequency climate variations

Figure 9: Variation in the maximum temperature (°C) during the four seasons of the year across Brazil.

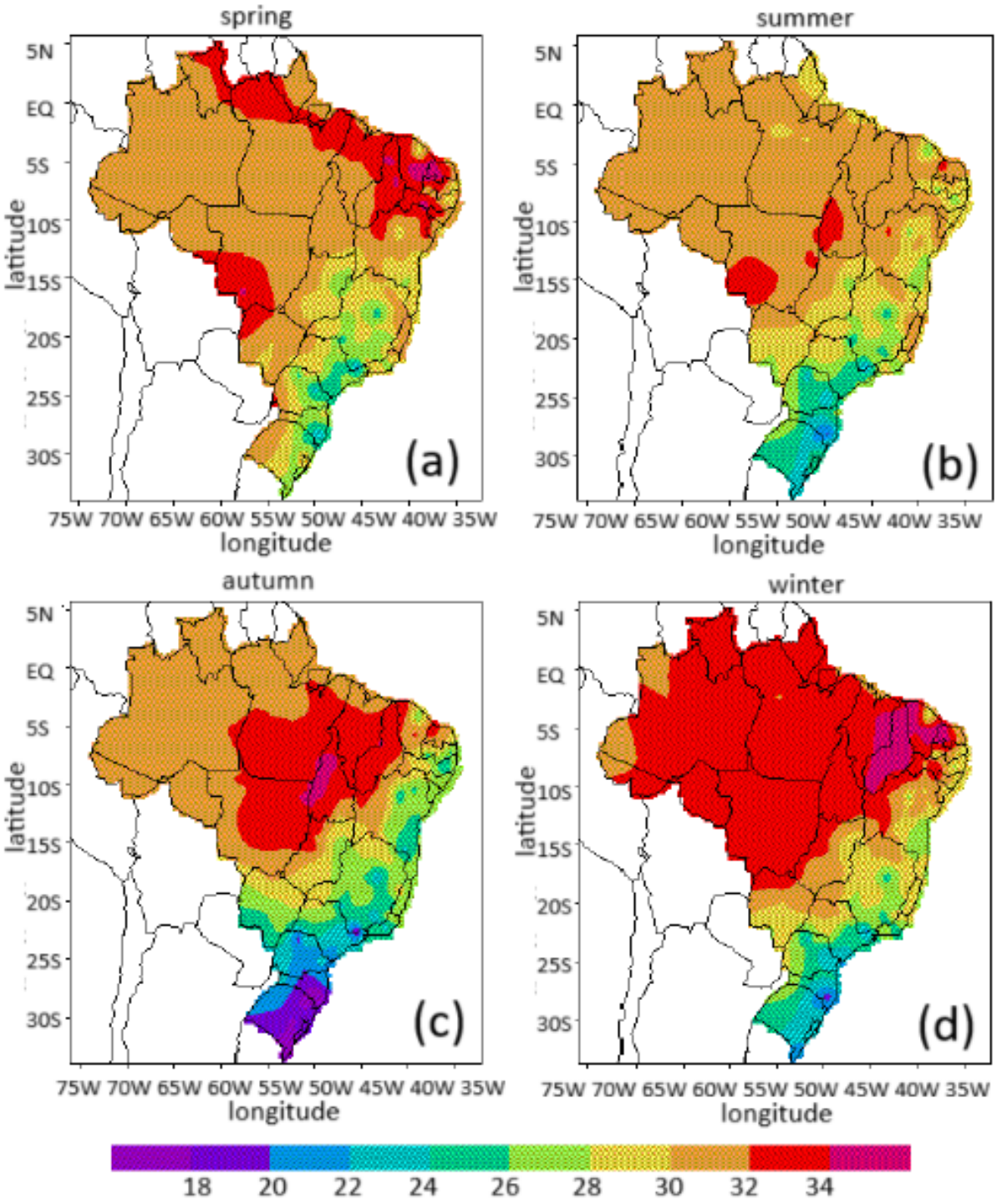

Source: Quadro et al. (1996).

Figure 10: Variation in the minimum temperature (°C) during the four seasons of the year across Brazil.

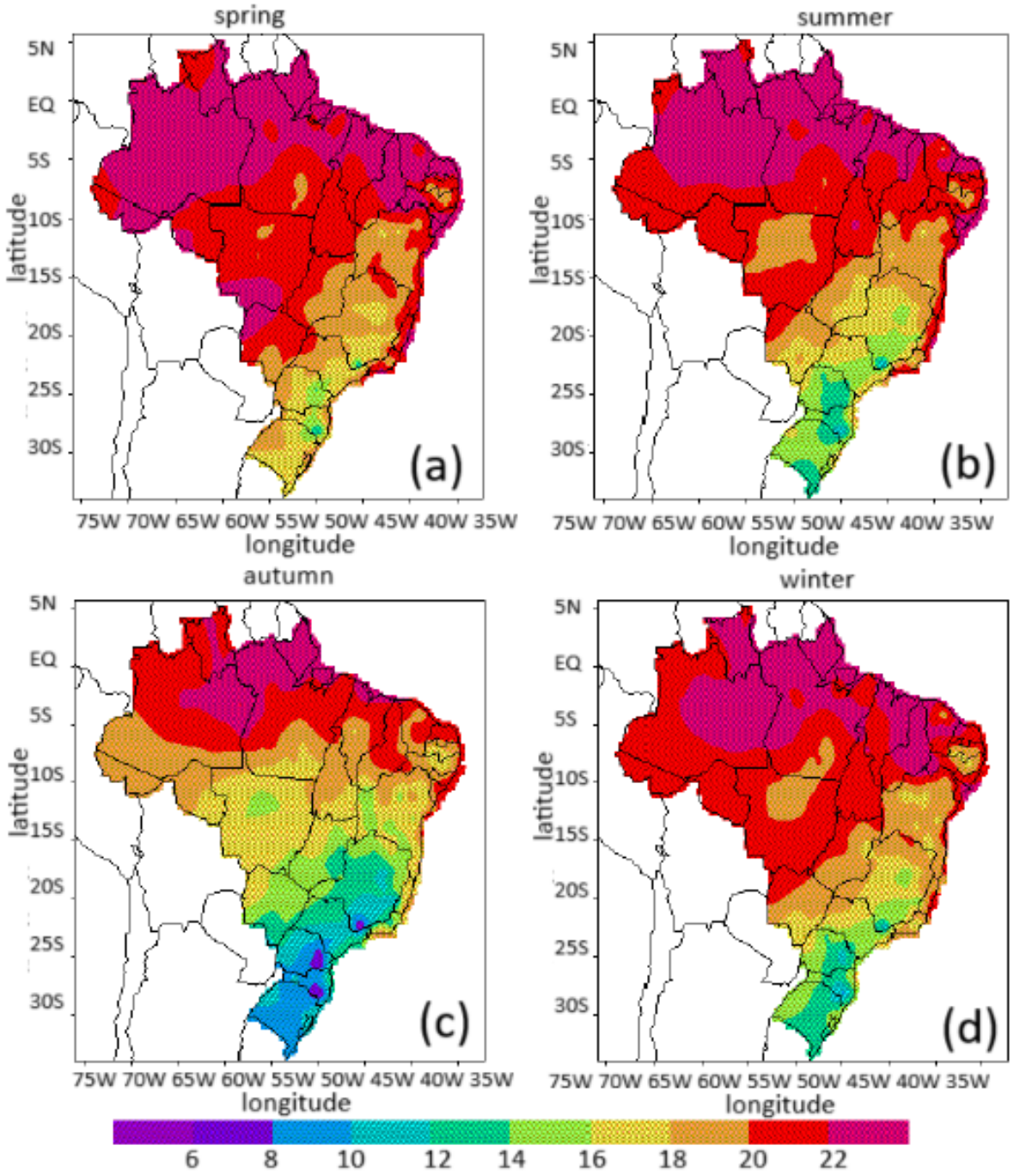

Source: Modified from Quadro et al. (1996)

(RENÉ; PATRICIO, 2007). Although rain variability is a natural random process, it can be influenced by both natural and anthropogenic forcings (SOUZA-ECHER et al., 2008). With the ongoing global warming, there has been a noticeable rise in the frequency of these phenomena, underscoring the significance of comprehending their impacts on different regions (HOYT; SCHATTEN, 1997). Furthermore, studies indicate that ENSO events can be amplified or diminished when they coincide with the MJO, particularly during the southern hemisphere summer (SHIMIZU; AMBRIZZI, 2015).

Mid-latitude systems can also cause an increase in precipitation levels in Southern Brazil (OLIVEIRA, 1986). The trajectory of these systems is linked to the positioning and intensity of the subtropical jet from South America and has a strong influence on precipitation (KOUSKY; CAVALCANTI, 1984; BROWNING, 1986). Climatological studies show that, on average, 5 to 7 cold fronts pass through the region each month (OLIVEIRA, 1986). Among the most important, we can mention the passage of frontal systems over the region, which, together with the interaction with the orographic configurations of the region, are responsible for a large part of the total rainfall recorded (OLIVEIRA, 1986).

Other systems that can contribute to the changes in precipitation levels are the cyclonic vortices that originated from the Pacific and intensify over the South and Southeast of Brazil (CAVALCANTI, 1985). Mesoscale convection is also responsible for intense precipitation in Southern Brazil (GUEDES, 1985). According to Reboita et al. (2012), systems that act directly in the Southern region provide an increase in precipitation level over the years, especially frontal systems, cyclones, Mesoscale Convective Complexes (MCC), instability lines, persistent elongated convective systems, breeze systems, and the low-level jets (LLJ) that are wind systems with speeds higher than 10 m/s with an altitude between one and two kilometers with a horizontal extension of approximately 500 km. Figure 11 shows some of these systems acting in Brazil (REBOITA et al., 2012).

There are synoptic systems acting over South America, one of the most important is the frontal system, which is active throughout the year, as mentioned by Andrade (2005). In Southern Brazil, the South Atlantic ocean indirectly influences the climate through the South Atlantic Anticyclone System (SAAS), which originates a maritime tropical mass. Additionally, the polar anticyclone is the source of the polar mass that displaces and interacts with the heat of the Atlantic, leading to increased precipitation during spring and summer (NIMER, 1989).

2.3.1 OCEAN-ATMOSPHERE PHENOMENA

The oceans play an important role in Earth's climate system since they receive most of the solar energy and are highly effective at absorbing it due to their low albedo. The oceans and continents combined absorb 51% of the total solar radiation that reaches Earth. The first 100 meters of the oceans absorb the majority of this energy, which drives

Figure 11: Atmospheric systems, directly and indirectly, acting in Southern Brazil. SAAS is the South Atlantic Anticyclone System, SACZ South Atlantic Convergence Zone, LLJ is the low-level jets and the MCC are the Mesoscale Convective Complex. Inside the red circle is the Southern region of Brazil.

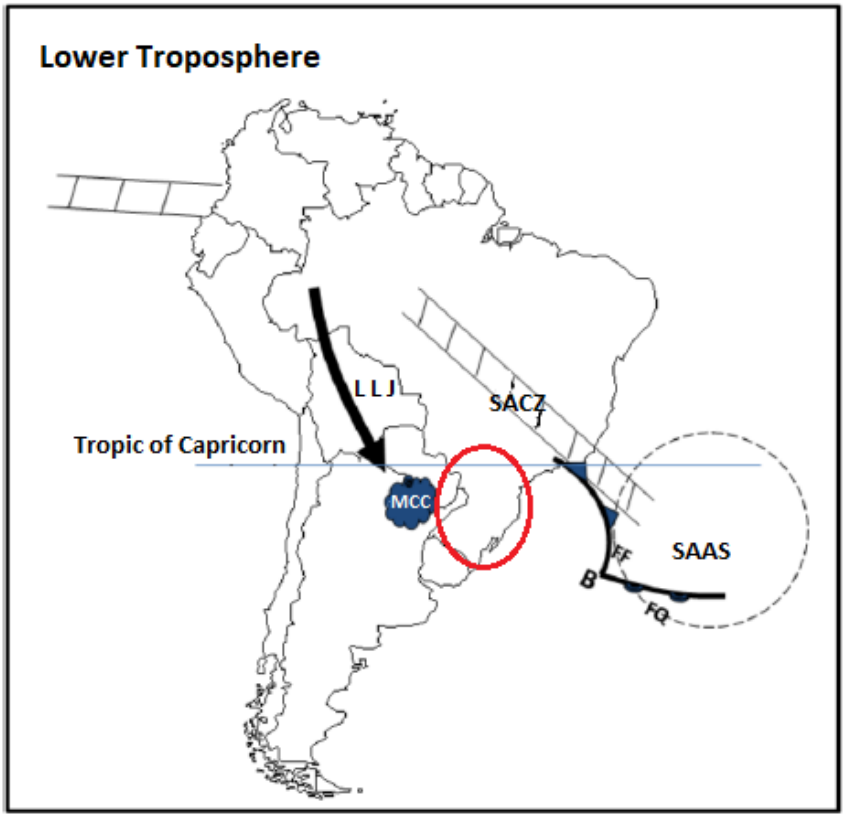

Source: Modified from Reboita et al. (2012).

the process of evaporation. This makes the oceans a primary source of water vapor and heat for the atmosphere, and an essential component of the global hydrological cycle (PHILANDER, 1989).

Because of the high thermal inertia of seawater, the ocean responds relatively slowly to changes in thermal forcing. The annual air-sea heat flux varies greatly from one place to another due to the convergence or divergence of heat transport by ocean currents. In contrast, the atmosphere responds much more quickly to changes in temperature, typically on timescales of weeks and months. Changes in climate over timescales of years to centuries are largely driven by ocean currents, and their interactions with the atmosphere (KAROLY; VINCENT, 1998). These complex interactions define the climate system, as illustrated in Figure 12, and any changes in their intensity can have significant effects on the Earth's climate.

The Southern region of Brazil experiences various meteorological phenomena, with droughts and floods being the most significant (ÁVILA et al., 2016; GRIMM et al., 2020). One of the crucial global climatic events impacting the region is the *El Niño* Southern Oscillation (ENSO), which caused severe flooding in Paraná, Santa Catarina, and Rio

Figure 12: Components, processes and interactions of the climate system. The bold arrows show the direction of the influence, black arrows are natural interactions, the red arrow are antrophogenic interactions and the orange arrow is solar irradiation.

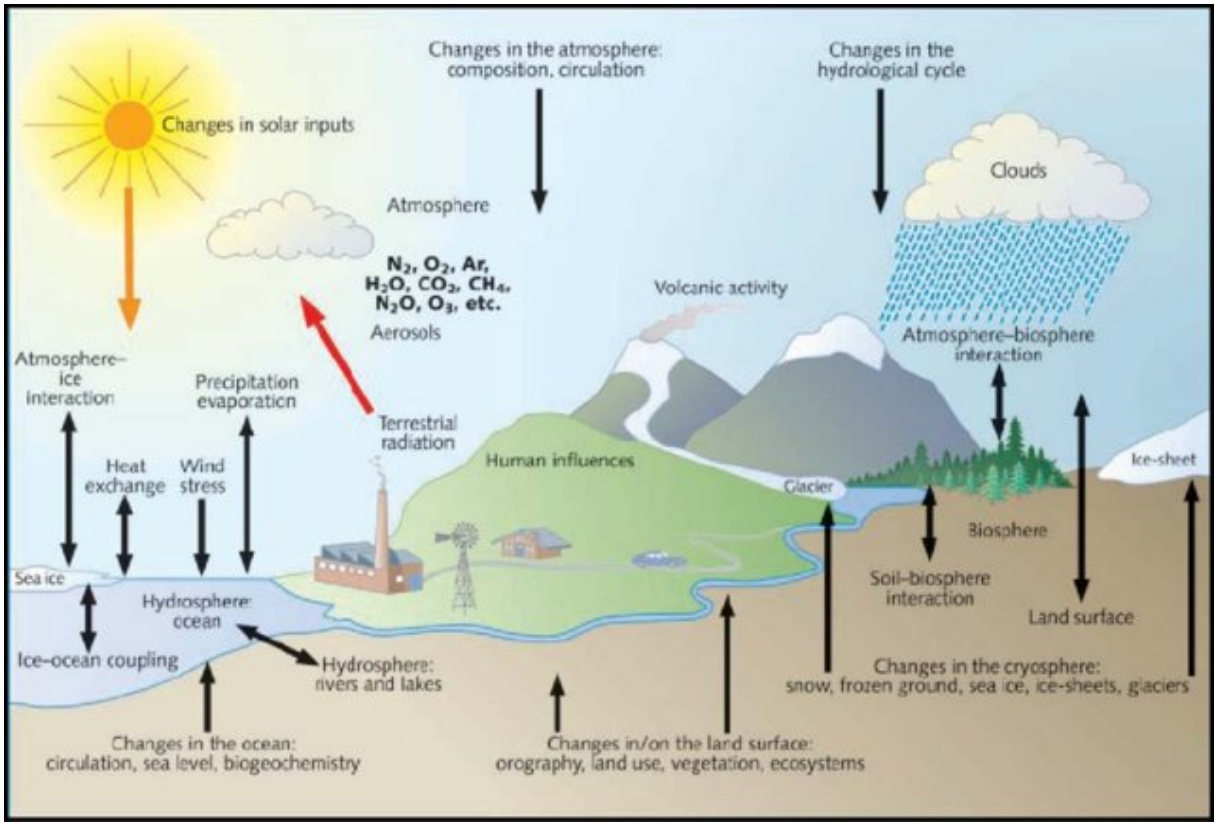

Source: El-Ramady et al. (2012)

Grande do Sul during the 1982-1983 period (ISLA; JUNIOR, 2013). Additionally, the Quasi-Biennial Oscillation (QBO) and the Southern Annular Mode (SAM) influence cyclonic activity in the mid-latitudes (MA; LEMBO; FRANZKE, 2021).

While ENSO significantly affects precipitation in the Southern region, other factors, such as SST boundary conditions across oceans, ice, snow cover, and humidity, are also acting in this area. According to Studzinski (1995), both the Pacific and Atlantic Oceans impact precipitation variability in Southern Brazil. Moreover, the atmospheric circulation system in the region is influenced by various centers of action, including the South Atlantic Subtropical High (SASH), small tropical highs, the polar anticyclone, and the Chaco Low, as described by Nimer (1989).

The influence of the Atlantic Ocean on the precipitation regime of the Southern region has been discussed in several studies, including Studzinski (1995), Grimm, Ferraz & Gomes (1998), GRIMM & FEUSER (1998), SILVA (2001), Kayano & Capistrano (2014). All of these studies have reported similar results, indicating that an increase in precipitation occurs during heating periods of the Pacific SST, along with the warming of the South-Southwest Atlantic SST.

In addition to the Pacific SST, there are also indications that the South Atlantic Ocean Dipole Index (SAODI) influences the precipitation level in the Southern region. According to Prado & Wainer (2013), this is due to the transport of moisture from the ocean to the continent, which can be carried to the south through the Low-Level Jet. The ITCZ also plays a role in the Southern region's precipitation regime, as it is a low-pressure region associated with convection that has an annual cycle in equatorial latitudes, resulting in high cloudiness, convection, and precipitation (WALISER; GAUTIER, 1993; PRADO; WAINER, 2013).

2.3.1.1 SOUTH ATLANTIC OCEAN

The proximity of the Atlantic Ocean to the Southern region of Brazil has a significant influence on the climate due to the ocean's moisture emission through the action of the breeze, which results in rainfall over the continent (REBOITA et al., 2012). Additionally, the South Atlantic Ocean has a semi-stationary high-pressure system, which is known as the South Atlantic Subtropical Anticyclone (SASA), located at 32.5° S and 28.7° S. The SASA is located in the South Atlantic and has a significant impact on the region's climate. The SASA generates the Atlantic Tropical Mass (ATM), which is similar to how the polar anticyclone generates the Atlantic Polar Mass (APM). The displacement of these masses is primarily responsible for the extensive precipitation in the spring and summer seasons in Southern Brazil (NIMER, 1989).

The influence of the South Atlantic Ocean on the climate of Southern Brazil is also related to the South Atlantic Convergence Zone (SACZ), which is a low-level convergence zone that forms over southeastern South America and the adjacent South Atlantic Ocean. The SACZ is an important mechanism for the transport of moisture from the Atlantic Ocean to the continent, leading to intense rainfall in the Southern region (CARVALHO; STIPP, 2004).

In addition to the oceanic influences, atmospheric circulation also plays a critical role in determining the climate of Southern Brazil. The prevailing atmospheric circulation over the region is controlled by several systems, including the SASH, the Chaco Low, and the ITCZ (NIMER, 1989; PRADO; WAINER, 2013).

The SASH is a semi-permanent high-pressure system that forms over the South Atlantic Ocean and extends towards the continent. It is responsible for the control of the South Atlantic Ocean's trade winds, which carry moisture from the ocean towards the continent, leading to precipitation in Southern Brazil (NIMER, 1989). On the other hand, the Chaco Low is a semi-permanent low-pressure system located over the Gran Chaco region, which influences the atmospheric circulation over Southern Brazil and adjacent regions (CARVALHO; STIPP, 2004). The ITCZ, on the other hand, is a low-pressure region that forms over the equatorial Atlantic Ocean, extending towards the continent,

and plays a crucial role in the formation of the SACZ (CARVALHO; STIPP, 2004).

2.3.1.2 EQUATORIAL PACIFIC OCEAN

The Pacific Ocean plays an important role in global climate patterns, with a differential heating process that generates precipitation and air temperature anomalies in various parts of the world, particularly in regions closer to the ascending and descending areas of the Walker cell (located at the equatorial Pacific ocean). In contrast to the South Atlantic's SST Anomalies (SSTA), the Equatorial Pacific's SSTA did not exhibit a cooling trend during the first half of the 20th century or a warming trend in the second half of the 20th century, as shown in studies such as Silva (2018).

The Equatorial Pacific's SSTA is regulated by the *El Niño*-Southern Oscillation (ENSO), which is responsible for most of the global climate variability (TRENBERTH, 1997). During *El Niño* events, the warming of the tropical Pacific Ocean generates anomalous atmospheric convection that alters the atmospheric circulation, including the Walker Circulation, and produces changes in the global climate (TRENBERTH, 1997).

These changes are not limited to the Pacific Ocean region and can affect various regions of the world, including the Southern region of Brazil. During *El Niño* events, the Southern region experiences more rainfall than usual, which can cause floods and landslides (REBOITA et al., 2012). On the other hand, during *La Niña* events, the opposite occurs, the frequency and intensity of precipitation in the Southern region decrease, while the temperature increases, causing droughts and heat waves (REBOITA et al., 2012). The Southern Oscillation Index (SOI) is a metric used to measure the strength of ENSO, and it is calculated from the atmospheric pressure differences between Tahiti and Darwin (TRENBERTH, 1997).

In summary, the Equatorial Pacific's SSTA is influenced by ENSO, and the MJO influences the ENSO, which affects atmospheric circulation and the global climate. *El Niño* and *La Niña* events can cause droughts, floods, and other extreme weather events in various regions of the world, including the Southern region of Brazil.

2.3.1.3 SOUTHERN OSCILLATION INDEX (SOI)

The Southern Oscillation Index (SOI) is a key component of *El Niño* events, which are characterized by a barometric seesaw between Tahiti and Darwin (SILVA, 2018). The SOI has two opposite phases - *El Niño* (positive phase) and *La Niña* (negative phase) - which have a significant impact on the monthly and seasonal precipitation levels in Southern Brazil (GRIMM; FERRAZ; GOMES, 1998; GRIMM; BARROS; DOYLE, 2000). The effects of these phases can be remarkable, causing significant changes in the region's precipitation patterns.

During an *El Niño* phase, the SSTs in the Eastern and Central Pacific oceans become warmer than average, leading to changes in the atmospheric circulation and rainfall patterns around the globe. In Southern Brazil, *El Niño* is typically associated with increased rainfall and flooding, which can also have significant impacts on the region's agriculture and infrastructure (GRIMM; FERRAZ; GOMES, 1998).

In contrast, during a *La Niña* phase, the SSTs in the Eastern and central Pacific Ocean become cooler than average, leading to different atmospheric circulation patterns and precipitation levels. In Southern Brazil, *La Niña* is typically associated with a decrease in precipitation, leading to drought conditions and affecting agriculture and water resources (CAVALCANTI et al., 2011).

Understanding the SOI and its impact on regional weather patterns is essential for predicting and preparing for the potential impacts of *El Niño* and *La Niña* events in Southern Brazil and in other regions of the planet.

2.3.1.4 *EL NINO*-SOUTHERN OSCILLATION (ENSO)

The *El Niño*-Southern Oscillation (ENSO) is the principal interannual climate variability in Brazil (GRIMM, 2003). It involves variations in SST in the equatorial Pacific, along with changes in sea level pressure between Tahiti and Darwin, Australia (BJERKNES, 1966; TRENBERTH, 1976). The ENSO phenomenon is an association of *El Niño* events and the Southern Oscillation, and it affects the climate globally, with a periodicity of 4 to 7 years, and in some cases, between 2 and 7 years (OLIVEIRA, 2001).

The term "*El Niño*" was first used to describe the warm and weak ocean current along the coast of Peru and Ecuador that usually appears around Christmas time (*Niño* means "the child Christ" in Spanish). Later, it became associated with the great warming that occurs every few years, leading to changes in local climate (TRENBERTH, 1997).

The ENSO phenomenon is associated with changes in SST patterns and trade winds in the Equatorial Pacific region, located between the coast of Peru and the western Pacific, where Australia is located. Its measurement is based on indices such as the SST and the Southern Oscillation Index (SOI) (OLIVEIRA, 2001). Figure 13 illustrates the mechanism of *El Niño* and compares it with a year without *El Niño* events. *El Niño* results from hotter temperatures in the west and center of Canada and in the west and north of the United States (SPUDMAN, 2018).

In the study conducted by Ropelewski & Halpert (1987), the relationship between ENSO and precipitation was analyzed for different regions of the world, including Southern Brazil. The results suggested a significant increase in precipitation levels during *El Niño* events from November (beginning of *El Niño*) to February (ending of *El Niño*). Similarly, in a study by Ropelewski & Halpert (1989), the impacts of ENSO's cold phases (*La*

Figure 13: On the top a normal year ocean-atmosphere circulation in the Pacific Ocean. On the bottom, the *El Niño* mechanism, clearly causes the inversion of hot temperature between the Australian coast and the South and North America coast.

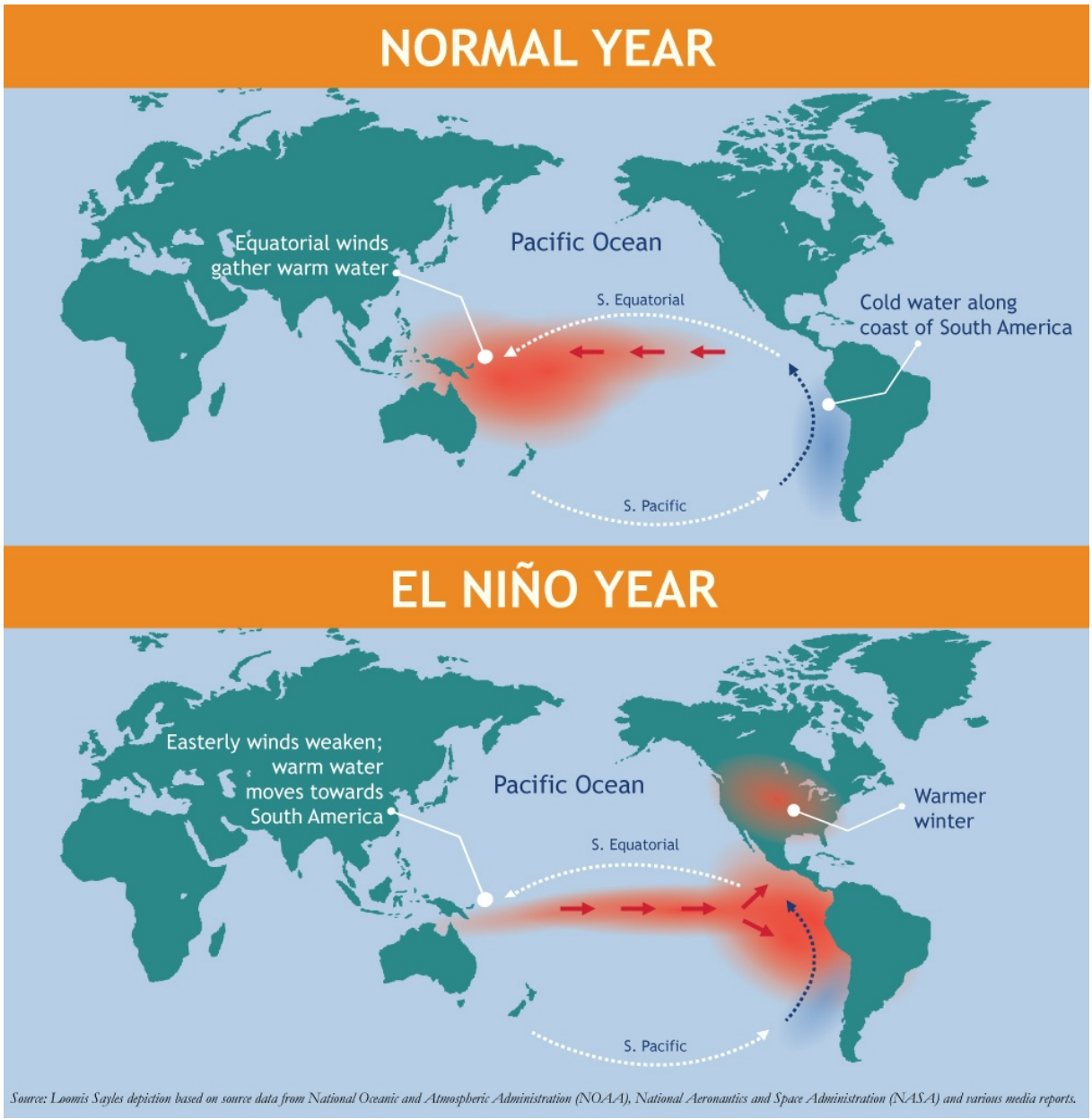

Source: Spudman (2018)

Niña) on global precipitation were investigated, revealing a decrease in precipitation levels from June to December when the *La Niña* year starts and ends. Subsequent studies by Aceituno (1988), Rao & Hada (1990), Studzinski (1995), Diaz, Studzinski & Mechoso (1998) corroborated these findings, suggesting that warm phase years of ENSO generally exhibit excess precipitation in Southern Brazil, Northern Argentina, and Uruguay, while its cold phase years are associated with precipitation deficits.

In South America, ENSO plays a crucial role in inducing dry seasons in the Northeast of Brazil and high precipitation levels in Southern Brazil, primarily during the spring of the event year, as explained by circulation anomalies (GRIMM; BARROS; DOYLE, 2000; NORDEMANN et al., 2002). The relationship between ENSO and precipitation is an indication of how ocean circulation significantly impacts the climate system, leading to atmospheric anomalies (RASMUSSON; WALLACE, 1983).

2.3.2 DENDROCHRONOLOGY

Proxy data like tree stomata, ice cores, isotopic stratigraphy, coral, and tree rings provide valuable insights into Earth's past (NORDEMANN et al., 2002; RIGOZO et al., 2008; GREIN et al., 2010; PRESTES et al., 2011; RIGOZO et al., 2012; DELONG et al., 2013; STEIGER et al., 2017; PRESTES et al., 2018b; RAMSTEIN et al., 2021a; RAMSTEIN et al., 2021b; RAMSTEIN et al., 2021c; RAMSTEIN et al., 2021d).

Dendroclimatology, the study of tree growth rings play a significant role in Dendroclimatology, unraveling climate-tree ring connections for paleoclimatic reconstructions, offering a unique opportunity to analyze patterns of climatic parameters, ocean-atmosphere events, and solar cycles, date events, and assess human impacts on the environment (SPEER, 1971; RAMSTEIN et al., 2021e). Understanding tree growth rings is fundamental to mastering this methodology (RATHGEBER; CUNY; FONTI, 2016).

Trees undergo primary and secondary growth, with primary growth responsible for the lengthening of branches, and secondary growth responsible for the formation of rings. The cambium layer, located below the bark, gives rise to the trunk, branches, and roots. It generates wood, which is responsible for upward sap flow, and phloem, which brings elaborated sap downward. Each year, the previous tissue is pushed inside (to the wood) and outside (to the phloem) (RAMSTEIN et al., 2021e).

When new xylem is generated, it goes through several phases. First, the cambial initial cell forms a new cell, which then begins to grow. The secondary wall of the cell is deposited and lignified simultaneously, and finally, programmed cell death occurs (RATHGEBER; CUNY; FONTI, 2016). A schematic cross-section of an example tree is shown in Figure 14, which illustrates the dormancy period during winter, the active vascular cambium, and the phases of secondary xylem growth.

Figure 14: Schematic cross-section of an example tree. (A) shows the dormancy cambium between the previous xylem and phloem. (B) The active cambium between the new xylem and phloem. The new xylem is in expansion and thickening creating a mature zone. (C) follow all the 5 phases describe in the text, I, II, III, and IV is phase (1); V is phase (2); VI is phase (3); VII is phase (4); and finally VIII and IX is the phase (5).

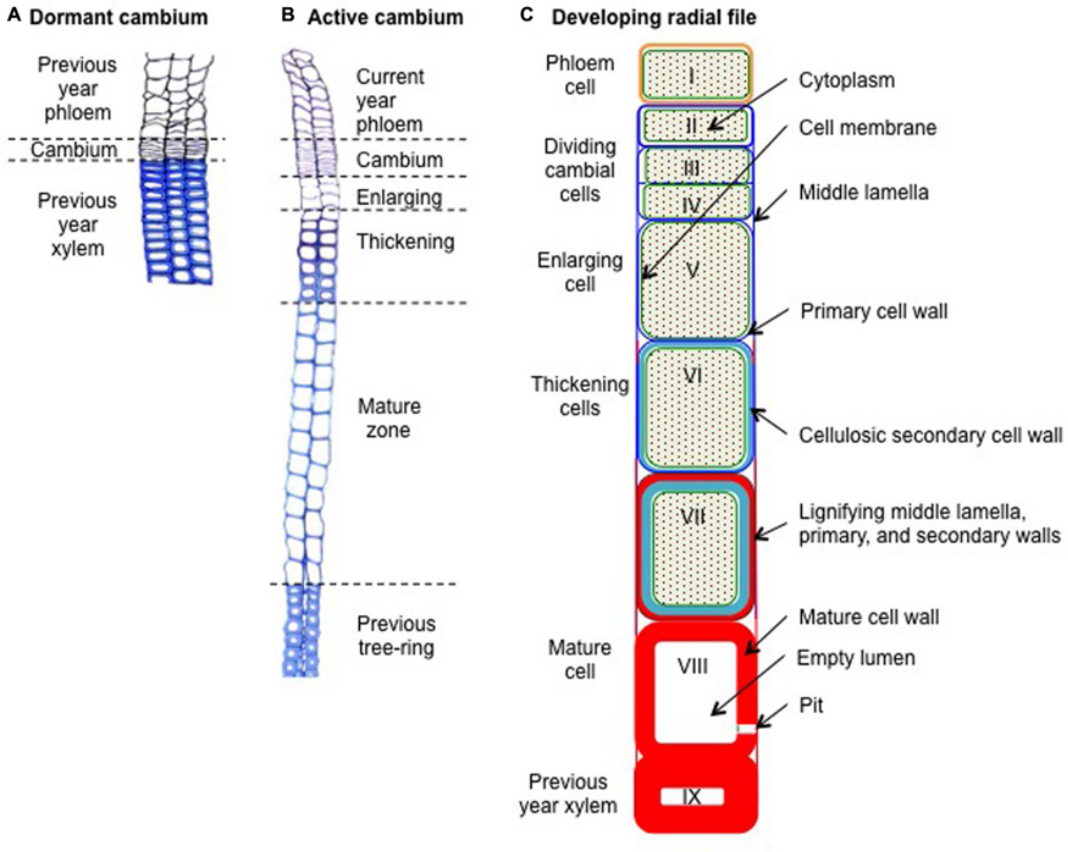

Source: Rathgeber, Cuny & Fonti (2016)

Tree growth ring structure may present significant variations among different species, the differences can be influenced by intrinsic factors of each species, such as its growth rate and physiology, as well as the environmental conditions in which the trees develop. Tree rings are commonly divided into earlywood and latewood (Figure 15). Specifically in conifers, the earlywood forms at the start of the ring with thin cellulosic walls and large cellular diameters, usually lighter wood. Meanwhile the latewood develops at the end of the growing season with thicker cellulosic walls and smaller cellular diameters, resulting in darker wood. Ring thickness variations impact wood density, influenced by intra- and inter-annual variabilities, with a leading limiting factor (RAMSTEIN et al., 2021e).

Tree growth rate depends on various factors, with some species-specific influences, known as Liebig's Law of the Minimum (COOK et al., 1990). Growth cannot exceed the limiting factor's capacity, which can vary annually. Figure 16 illustrates this concept, where a low factor prevents the barrel from being filled despite water input.

In regions with strong climatic variability, trees cannot precisely determine cambial

Figure 15: A tree cross-section with visible rings after the sanding and polishing. The pith is the middle of the tree, where it started developing. The tree starts to create wood radially, increasing the number of rings. The lighter part of the ring is the Earlywood and the dark part is the Latewood.

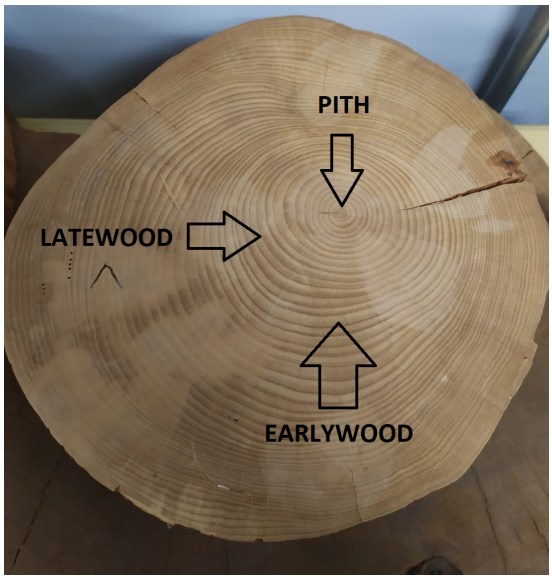

Source: The author.

Figure 16: Liebig's Law of the Minimum example uses a barrel created by diverse factors that would influence the development of a tree and can not fill this barrel with water until the top because one of the factors limit is lower than the others. This will be the limiting factor of the barrel, not allowing it to be filled.

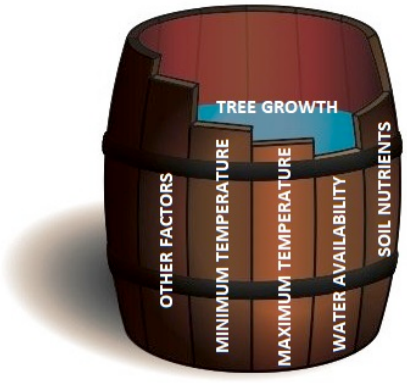

Source: Modified from Longnecker (2016).

activity and dormancy. They respond by following long-term weather changes, leading to the absence of rings or the creation of false rings when signals are misleading (RAMSTEIN et al., 2021e). Despite requiring more time for dating due to these variabilities, species from subtropical/tropical climates are interesting for study due to greater biodiversity and limited research (LISI, 2000).

3 MATERIALS AND METHODS

In Figure 17, the flowchart visually illustrates the main steps and schedule proposed by this thesis. This figure offers an overview of the milestones and activities carried out for the research, helping to understand the organization and planning of subsequent stages. The following sections will detail each of these steps, the materials used, and provide insights into the methodologies and analyzes employed throughout the study.

Figure 17: Methodology proposed and carried out for the development of this study.

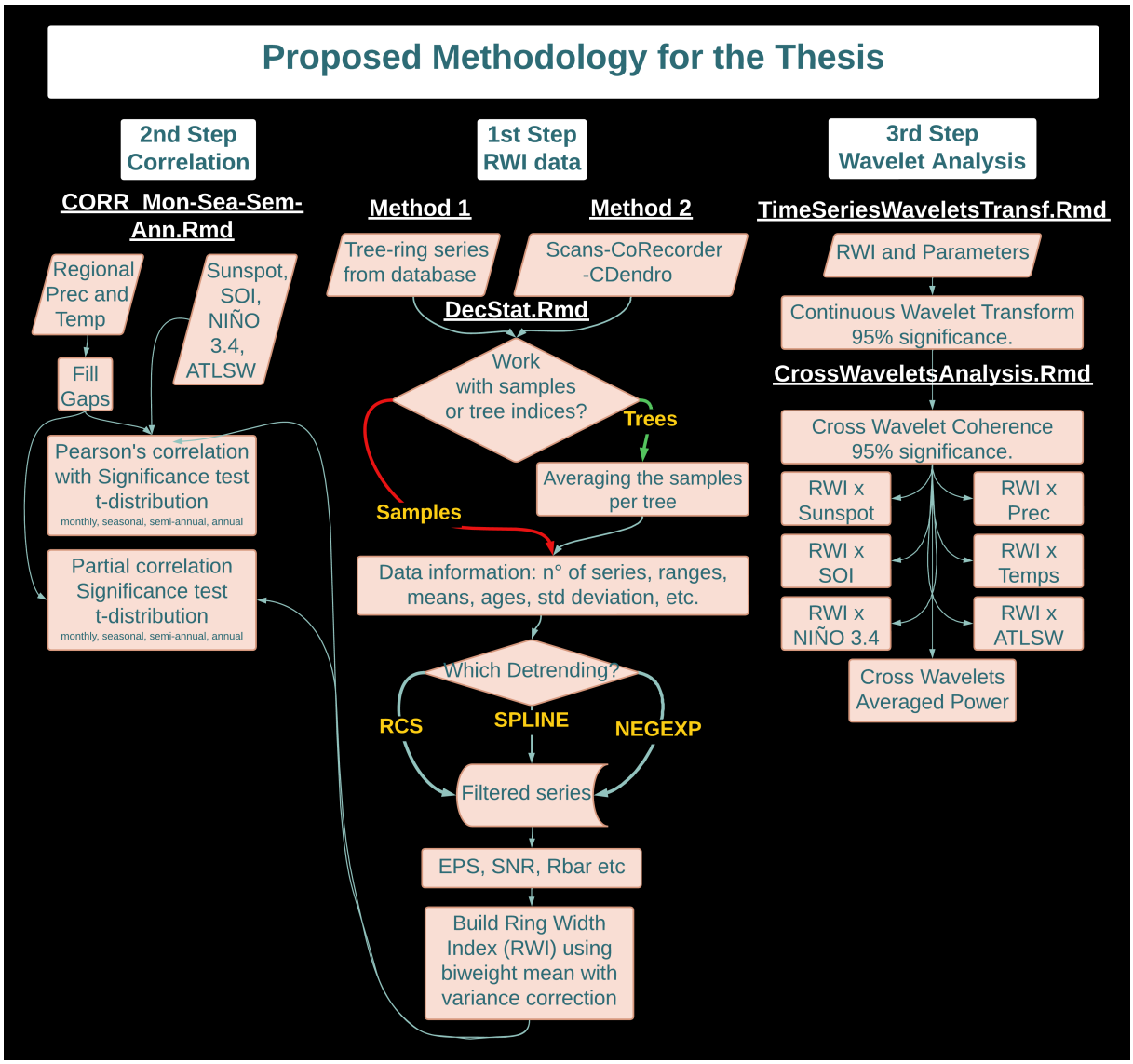

Source: The author.

3.1 TREE-RING SPECIES - *ARAUCARIA ANGUSTIFOLIA*

Native to Brazil and with a widespread distribution, *Araucaria angustifolia* (Figure 18) is a long-lived tree species (between 200 and 300 years) that can also be found in small areas in the extreme northeast of Argentina's province of Misiones (GURGEL; FILHO, 1965; COZZO, 1980). It has a straight and cylindrical trunk, with branches arranged in 8 to 15 whorls, with 6 to 10 branches per whorl. As they get older, they take on a chandelier shape due to the loss of basal whorls (ZANETTE et al., 2017). The tree species exhibit demarcated annual growth rings visible to the naked eye, allowing for easy age estimation. *Araucaria angustifolia* is characterized as an evergreen tree (long life cycle) that can reach heights of approximately 50 m and 250 cm or more in diameter at breast height (DBH) when fully mature, according to Lisi, Pessenda & Filho (1998).

Figure 18: Individual of the *Araucaria angustifolia* species.

Source: Natural Records Laboratory (LRN)

However, the colonization of the country brought about significant changes. From the 19th century onwards, logging activities targeting *Araucaria angustifolia* began, continuing for more than a century. The tree's resistance and malleability made it a valuable resource for constructing houses, furniture, and railways, leading to the species occupying 92% of the country's timber exports. Unfortunately, due to the intense exploitation such as logging activities (which ceased in the 1970s), and lack of replanting, only 2% of the original forest remains. As a result, *Araucaria angustifolia* is now on the brink of extinction (BRASIL, 2008).

After ceasing the logging activities of *Araucaria angustifolia*, other forest species with genetic improvements were introduced in Brazil (e.g. pine and eucalyptus). These trees became more profitable than the araucaria since the araucaria demands a high cost of investment and grows slowly. Moreover, exotic species need much less bureaucracy for cutting and replanting than native species, according to Brazilian law (ZANETTE et al., 2017).

Araucaria angustifolia belongs to the family *Araucariaceae*, which is the most ancestral group of conifers still alive. It appeared around 308 ± 53 million years ago during the Paleozoic Era (ZANETTE et al., 2017). Currently, the family is found exclusively in the Southern Hemisphere (South America and Oceania) as illustrated in Figure 19, and consists of three genera, according to Zanette et al. (2017): Araucaria (divided into 19 species); Agathis (*Agathis dammara*); and Wollemia (*Wollemia nobilis*). Of these, only two are found in South America: *Araucaria angustifolia* in Brazil, Argentina, and Paraguay, and *Araucaria araucana* in Chile and Argentina; the rest of the species are found in Oceania (ZANETTE et al., 2017).

Figure 19: Geographic distribution of the Araycaruaceae family.

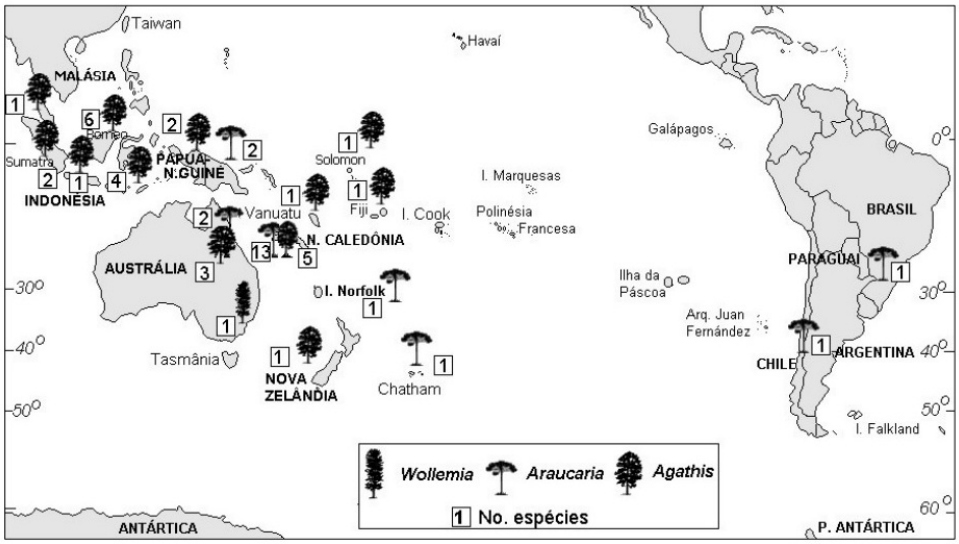

Source: Dutra & Stranz (2003).

Araucaria angustifolia underwent major climatic changes, which modified its dissemination in Brazil. The Pleistocene period (11,500 years ago) marked the end of the last ice age, and the Southern and southeastern regions of Brazil had a cold and dry climate, being an inhospitable environment for the *araucaria*. It developed only in small areas close to rivers. Fossil analysis shows that this region was covered by grass pastures, with no forests. However, during the Holocene (6,000 to 4,000 years ago), the temperature and humidity in the region increased, facilitating the establishment and expansion of areas with araucaria. Around 1,500 years ago, araucarias occupied large areas, forming araucaria forests in the Brazilian South, while the Southeast maintained small communities of the

species (ZANETTE et al., 2017).

3.2 DATA LOCATIONS

The tree ring data used in this thesis were obtained from **10 different cities** in the South of Brazil (Figure 20). The samples from **Canela** were used for the first time in the development of this thesis. The samples from **Curitibanos** belong to Dr. Marcelo Scipionni from the Federal University of Santa Catarina (SCIPIONI et al., 2021), and the time series were provided for this study. The other dendrochronological series were used in previous studies by other LRN researchers and their research partners and published as scientific articles or congress articles, except **Irineópolis** and **Coxilha**. The works generated by the previous studies are listed as follows: Açungui (SOUZA, 2010; SILVA; PRESTES; SOUZA, 2011; SOUZA; PRESTES; SILVA, 2011; SOUZA; SILVA; PRESTES, 2012); General Carneiro (LORENSI; PRESTES, 2013; LORENSI; PRESTES, 2014; LORENSI, 2016); Chapecó (GOERGEN et al., 2014); Irani (LORENSI, 2016); Passo Fundo (PRESTES et al., 2018b; PRESTES et al., 2018a); São Francisco de Paula (SILVA; PRESTES, 2010; SILVA; PRESTES; SOUZA, 2011; SILVA; SOUZA; PRESTES, 2012).

Figure 20: Map of Brazil and a zoom in the Southern region with the location of the sampling places.

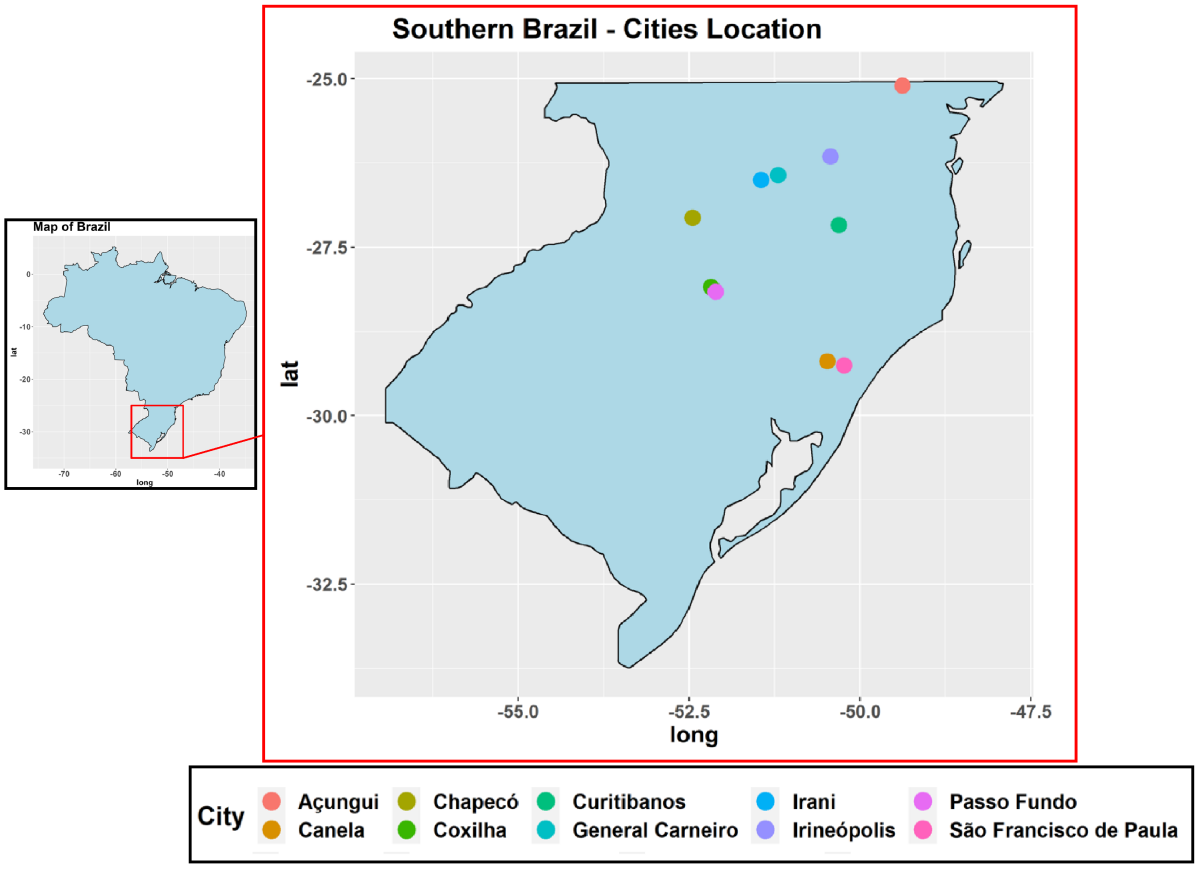

Source: The author.

3.3 TREE-RING DATA

The following tables present important information about the tree ring data; Table 2 for Paraná, Table 3 for Santa Catarina, and Table 4 for Rio Grande do Sul.

Table 2: Fieldwork informations performed by the Laboratory of Natural Records (*Laboratório de Registros Naturais* - LRN) in Paraná state.

Dendrochronology Fieldwork Performed in Paraná State						
City (Acronym)	**Collect Place**	**Altitude ~(m)**	**~Lat ~Lon**	**Year**	**N° Trees**	**N° Samples**
Açungui (AÇU)	National Forest of Açungui	784	-25°10' -49°38'	2005	18	36
General Carneiro (GCA)	Fazenda Pizzatto	1067	-26°43' -51°20'	2013	21	67

Source: The author.

Table 3: Fieldwork informations performed by the Laboratory of Natural Records (*Laboratório de Registros Naturais* - LRN) in Santa Catarina state. The Data from Curitibanos was obtained from Dr. Marcelo Scipionni, from the Federal University of Santa Catarina.

Dendrochronology Fieldwork Performed in Santa Catarina State						
City (Acronym)	**Collect Place**	**Altitude ~(m)**	**~Lat ~Lon**	**Year**	**Nº Trees**	**Nº Samples**
Chapecó (CHA)	National Forest of Chapecó	557	-27°06' -52°45'	2005	15	30
Irani (IRA)	Irani Celulose Factory	1040	-26°50' -51°45'	2011	14	30
Irineópolis (IRI)	In the municipality	767	-26°15' -50°43'	2011	11	35
Curitibanos (CUR)	Campus of the Federal University of Santa Catarina (UFSC)	1100	-27°17' -50°31'	2018	13	16

Source: The author.

Table 4: Fieldwork information performed by the Laboratory of Natural Records (*Laboratório de Registros Naturais* - LRN) in Rio Grande do Sul state.

Dendrochronology Fieldwork Performed in Rio Grande do Sul State						
City (Acronym)	**Collect Place**	**Altitude ~(m)**	**~Lat ~Lon**	**Year**	**Nº Trees**	**Nº Samples**
Passo Fundo (PFU)	National Forest of Passo Fundo and Private properties	740	-28°16' -52°11'	2005	12	32
Canela (CAN)	National Forest of Canela	760	-29°19' -50°48'	2005	6	18
São Francisco de Paula (SFP)	National Forest of São Francisco de Paula	913	-29°25' -50°23'	2005	11	32
Coxilha (COX)	Private properties	702	-28°09' -52°18'	2011	11	43

Source: The author.

The cities where the trees' samples were collected can be classified into two groups that were created following Köppen's classification and using the website Climate Data guidance, these groups are:

1. Group Cfa - This group is composed of the cities Açungui, Chapecó, Passo Fundo, and Coxilha. It has equal distribution of precipitation during the year but with hot summers (the hottest month's mean temperature is higher than 22°C) (DUBREUIL et al., 2019).

2. Group Cfb - The cities that constitute this group are Irati, General Carneiro, Irani, Irineópolis, Curitibanos, Canela, São Francisco de Paula. Similarly to Cfa, it has equal distribution of precipitation over the year, but the difference is the cool summers (the hottest month has a mean temperature lower than 22°C) (DUBREUIL et al., 2019).

3.4 DENDROCHRONOLOGY STEPS

Here the steps of Dendrochronological studies will be explained, from the sampling of the tree samples to the measuring and dating processes, to avoid errors as many as possible in obtaining our tree-ring series. The functions to perform the analysis here are from the dplR package in R.

3.4.1 FIELDWORKS AND TREATMENTS

The samples of *Araucaria angustifolia* were collected during four different fieldwork campaigns in 2005, 2011, 2013, and 2018, using the non-destructive method with a Pressler

Probe (Figure 21). The selected trees were first inspected to ensure they were free of signs of pests, such as ant attacks, both on the tree and its surroundings, to avoid any additional influence on the tree's growth rings.

Figure 21: Sample extraction using a Pressler Probe.

Source: Natural Records Laboratory (LRN).

An average of 4 (four) samples were collected from each tree, although some trees had slightly fewer samples due to collection difficulties or hollowness. To make the growth rings visible, the samples underwent a transverse surface sanding and polishing procedure using sandpaper with different grits, starting from the smallest (300) and progressing to the largest (50) (Figure 22). Each ring was then marked with a pencil using a microscope to facilitate ring measurement.

3.4.2 METHODOLOGIES FOR MEASURING AND CROSSDATING

Andrew E. Douglass, an American astronomer, introduced crossdating in 1904 (SPEER, 1971). This method compares the width of tree rings among different dated samples to reveal environmental conditions. As an example, narrow rings may indicate drought or stress, while wider rings suggest optimal growing conditions. These "marker rings" are compared between trees, but samples must be collected from similar areas with comparable limiting factors (e.g., topography, water, and light availability). False rings can also serve as marker rings but require careful analysis. Crossdating synchronizes samples with unknown dates using dated samples from the same region and species (RAMSTEIN et al., 2021e). Various crossdating techniques exist, all aiming to avoid dating errors or adding/removing rings. The main techniques are illustrated in Figure 23.

Figure 22: (**A**) Samples before being polished and (**B**) sanded, polished and marked samples.

Source: Natural Records Laboratory (LRN).

The correlation coefficient is a measure of the strength of the linear relationship between two variables. In crossdating, it is used to determine correlations between samples. In Figure 23A, correlations are calculated between sample 1 (red) and samples 2 (yellow), 3 (blue), and 4 (green). Then, sample 2 is correlated with samples 3 and 4, sample 3 is only correlated with sample 4, and sample 4 is already correlated with all other samples. The samples with the highest correlations are selected to build the chronology (SILVA et al., 2021b; SPEER, 1971).

The Skeleton Plot (Figure 23 B) involves marking narrow rings with a long mark (blue), leaving normal rings unmarked, and marking wide rings with half the length of the narrow rings' mark (green). Additionally, normal-sized rings that appear narrow compared to the previous and next rings are marked (red). These markings are then correlated between samples to verify if they are dated in the same years (SPEER, 1971).

The List Method (Figure 23C) also focuses on identifying marker rings, which are then compiled in a list and compared between samples. In the example shown in Figure 23C, sample 1A is well-dated, sample 1B is accurately dated until 1915 (although it lacks a marker ring for 1905), followed by an extra ring before 1927 and a missing ring after 1927, and sample 1C appears to be missing one ring, in the beginning, (SPEER, 1971).

Two different methodologies were employed to measure and crossdate the samples. Method 1 was used for samples referenced in previous works, while Method 2 was applied

Figure 23: The Figure shows the Crossdating methods. (A) The correlation coefficients method: In this approach, correlation is performed between all the samples. For example, sample 1 (red) correlates with samples 2, 3, and 4. Sample 2 (yellow) correlates with samples 3 and 4. Sample 3 (blue) correlates with sample 4. Sample 4 (green) already has correlations with all samples. (B) Skeleton Plot: This method uses different marks to represent ring widths. Narrow rings (blue) receive a long mark, wide rings (green) receive a half-size mark, and normal rings that are narrow compared to the previous and following rings receive a small mark in red. (C) Method List: Similar to the Skeleton Plot, but presented in a list shape. This method allows us to observe similarities between the samples, while small differences (one more or one less year) may indicate the presence of an extra or missing ring. (D) CDendro Software combined with CooRecorder Software: CDendro Software creates a reference (mean value) using all the samples, performs the correlation between the reference and all samples, and generates a new reference based on high correlations. The sample time series (red line) with low correlation can be opened and compared to the reference time series (black line) to identify and fix low correlation periods by checking the measurements in CooRecorder.

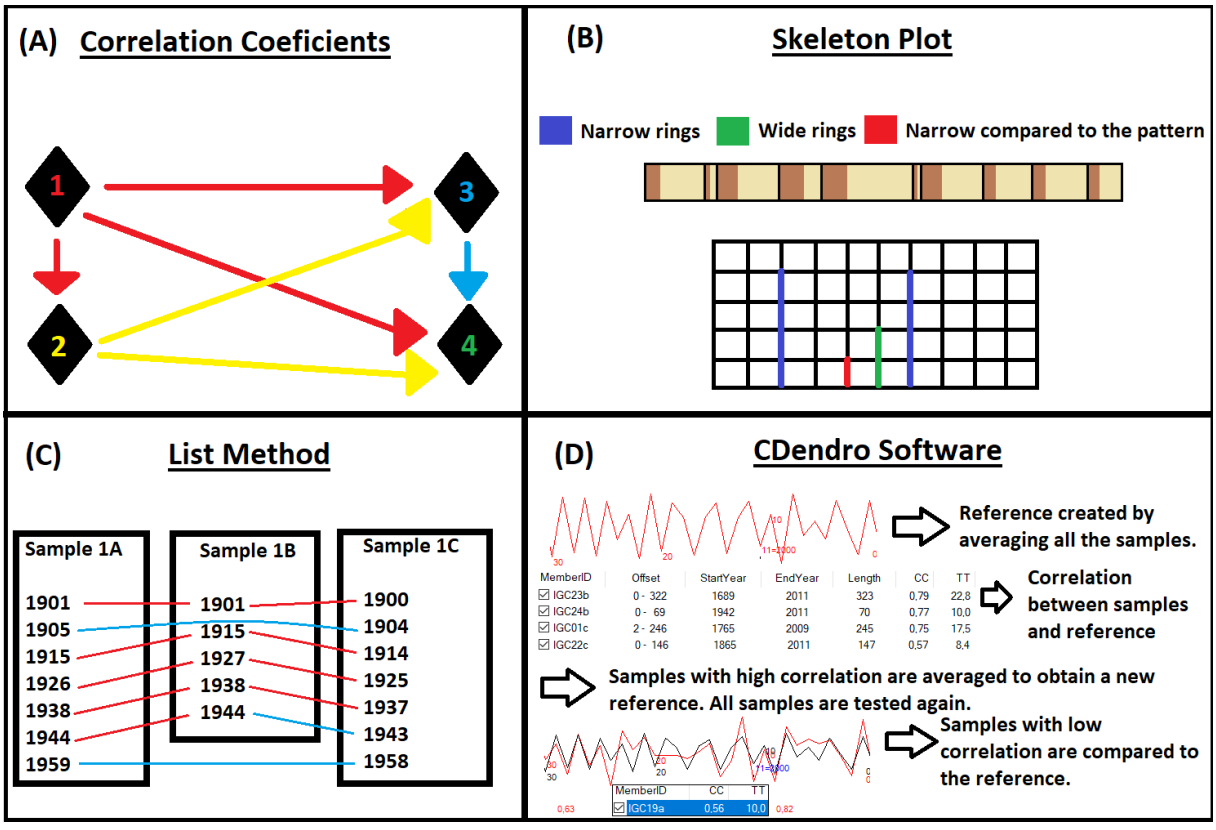

Source: The author.

to the Canela and Curitibanos tree-ring data. For the tree rings from Canela city, Daniela Muraja marked and scanned them. The measurements and crossdating were carried out by the scientific initiation student Cecília Lemes Leite, and Daniela Muraja was responsible for minor adjustments to Canela tree-ring series crossdating. The tree-ring series from Curitibanos had the measuring and crossdating made by Dr. Marcelo Scipioni. Data obtained through Method 1 were provided by Dr. Alan Prestes and by Daniela Muraja performed minor adjustments, by checking the correlation between all the tree-ring series per city and removing those with low correlation values, under Dr. Tuomas Aakala guidance. Daniela Muraja oversaw all subsequent steps in the analysis of tree-ring series, including detrending, calculating series statistics, scripts development, and dendroclimatology analysis.

3.4.2.1 METHOD 1

Method 1 served as the primary approach to measure and crossdate the samples collected in previous fieldwork studies. Measurements were taken using a VELMEX measuring table connected to a stereoscopic microscope with a micrometric reticle, located in the Laboratory of Natural Records at the University of Vale do Paraíba - UNIVAP, with a precision of 0.001 mm. Dating was conducted from the bark to the pith, starting from the known last formed ring, taking into account the collection date, and considering that *Araucaria angustifolia* growth rings begin to form in Spring/Summer (SANTAROSA et al., 2007). Measurement values were recorded in spreadsheets.

Crossdating was performed by calculating correlation coefficients between the dated measurement rings among samples from the same tree. The samples with higher correlations were kept in the analysis. The quality of crossdating was assessed using COFECHA software, and only samples with the best correlations were retained (LORENSI, 2016).

COFECHA is a widely used software to check the crossdating quality, which evaluates the precision of ring measurements. Created by Richard L. Holmes in 1982, Cofecha is an important tool for dendrochronologists, but it is not a crossdating tool itself (GRISSINO-MAYER, 2000).

3.4.2.2 METHOD 2

Method 2 was introduced to measure and crossdate the samples collected in the current thesis. The samples were scanned using an EPSON Scanner with a resolution of 1200 dpi, generating .jpg format files. CooRecorder software was used to measure the rings from the .jpg files. CooRecorder is common software used in dendrochronology studies, specifically for measuring tree rings from digital images of tree core samples (check CYBIS website).

The software offers a zoom function and a support line to ensure measurements were exactly perpendicular to the rings. To determine the beginning and end of each ring, a support line (black line) and marked points were used, as shown in Figure 24. The software was also helpful in identifying possible false rings that could be confused with wood scars. The final file was saved in .pos format and used for CDendro software to perform crossdating.

Figure 24: An example of measurements using CooRecorder. The black line is the support line, the points correspond to the beginning/ending of each ring, and the small window shows the type of data loaded.

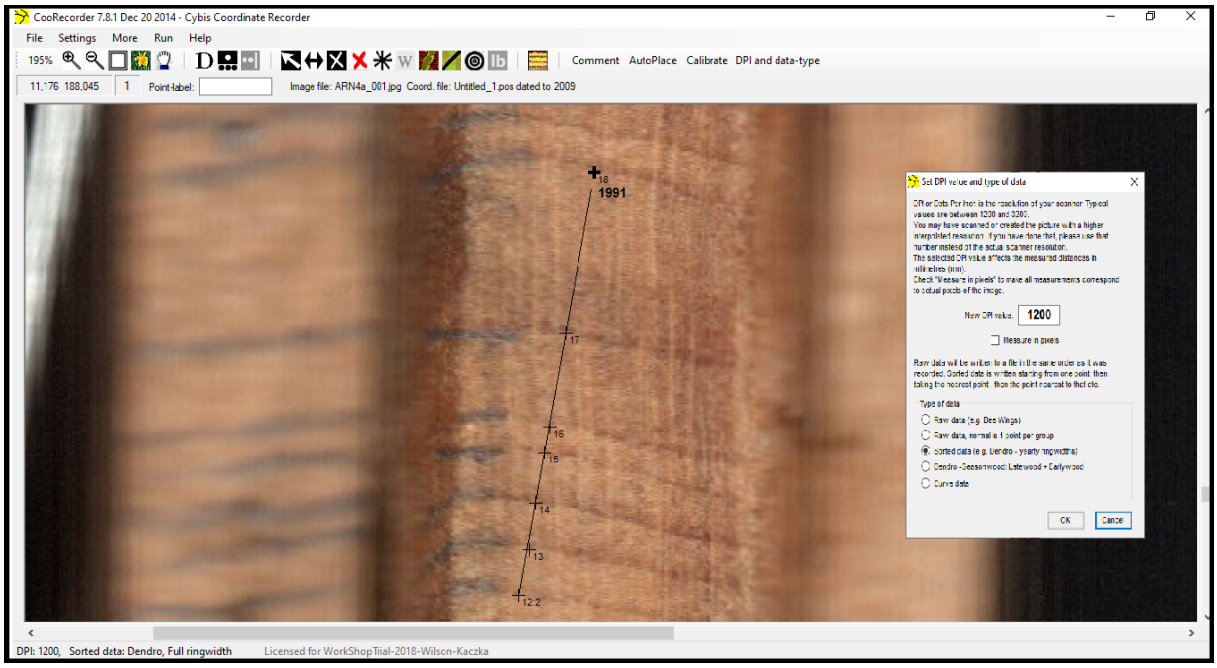

Source: Natural Records Laboratory (LRN).

CDendro is a software widely used in dendrochronology, it helps in crossdating, and quality control, ensuring accurate measurement of tree rings, and identifying missing or false rings (check CYBIS website). In CDendro, all the .pos files were opened and added to a "Collection". A mean series was created from these files, and individual series were compared to this mean series. Series that showed a good correlation with the "first mean" were moved to another collection, where a new mean series was generated. The remaining series from the first collection were compared to the new mean value to obtain new correlations. Each series was then carefully reviewed in both CDendro and CooRecorder to check for possible incorrectly marked or missing rings.

Crossdating was performed by comparing the years from the mean series to each individual series, allowing us to identify false or missing rings, which are common in tropical trees. Once a sample was accurately dated and showed a good correlation with the mean value, it was added to the second collection, and a new mean value was created. This step-by-step process is illustrated in Figure 25.

Figure 25: CDendro software example. Step 1 - load all the samples. Step 2 - create a mean series named reference and test all the samples with it. Step 3 - select the best member (high correlation). Step 4 - create a new reference with the best members and calculate the correlation again. Step 5 - Identify the low correlation members. Step 6 - compare each time series with the reference time series, identify low correlation periods, go back in CooRecorder, and adjust the measurements for that period.

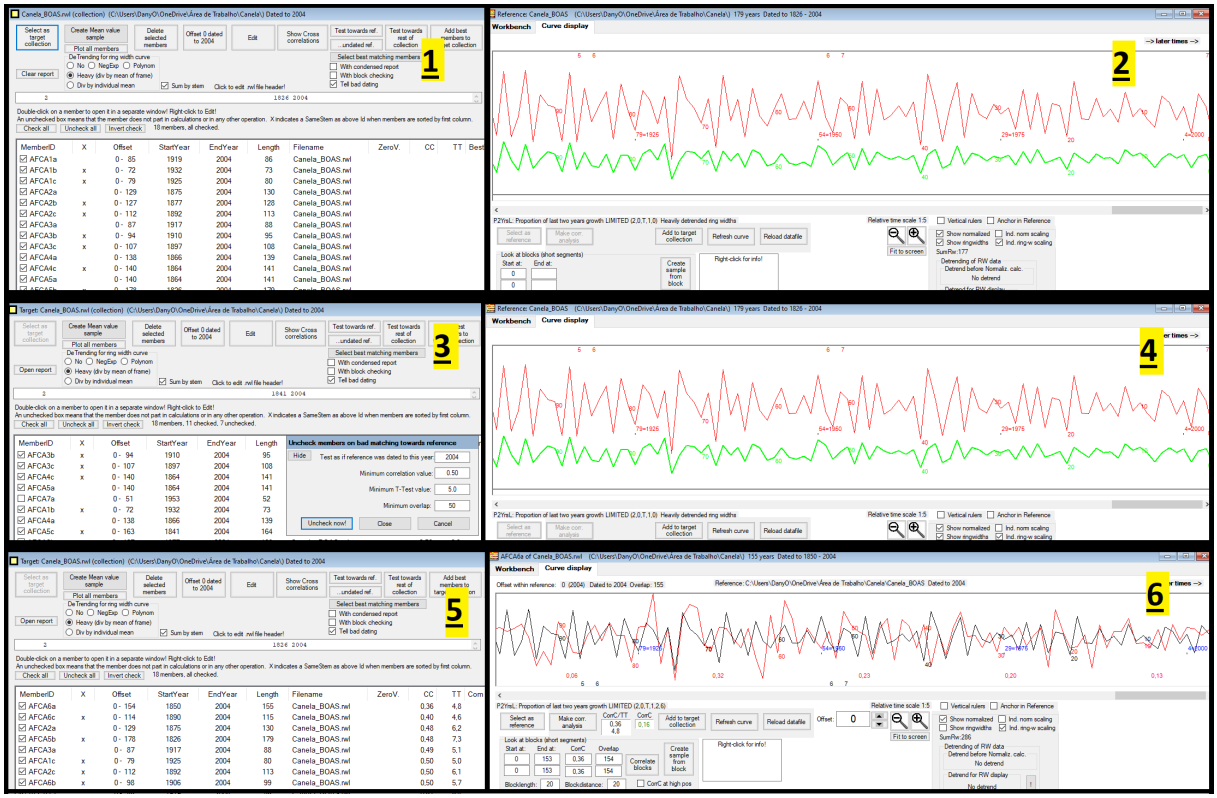

Source: The author.

CDendro software, in conjunction with CooRecorder software, offers multiple crossdating options depending on the samples. For well-behaved trees, a single ideal sample can be used as a reference, and all other samples can be compared to it. For less-behaved trees, an average time series can be created from all or some of the samples, and each sample can be compared to it (RAMSTEIN et al., 2021e).

3.4.3 DETRENDING METHODS

Considering the influence of various factors on tree development, statistical approaches are applied to remove non-intersting signals. It depends on what is the objective of the study, so in this case, climate signals are the focus (what it is wanted to maintain), so other signals, such as the natural growth trend of the species will be removed by the detrending (filtering). The most common methods are the Regional Curve Standardization, the Cubic Spline, and the Negative Exponential or Linear Regression Curve.

Regional Curve Standardization (RCS) uses a 67% spline to create a smooth RCS curve, and each tree-ring series is divided or subtracted by this curve according to its

biological age, resulting in an index (Figure 26A). After filtering, all the time series are realigned to their original dated years (HELAMA et al., 2004; BUNN, 2008; HELAMA; MELVIN; BRIFFA, 2017; SILVA et al., 2021a).

Cubic Spline (SPL) is a stochastic method that uses a low-pass filter (Figure 26B) (SPEER, 1971; COOK, 1985). Different frequencies of splines can be applied, such as a 32-year spline that preserves no more than half the range of variations at wavelengths higher than 32 years, retaining some of the shorter-term fluctuations. On the other hand, the 67-year is more restrictive than the 32-year spline, by emphasizing longer-term trends with a wavelength of two-thirds of the series length (BRIFFA et al., 1990; LINDHOLM et al., 1999; HELAMA et al., 2004; BRIENEN; ZUIDEMA, 2005; BUNN, 2008; SILVA et al., 2021a).

A **Negative Exponential or Linear Regression Curve (NEGEXP)** is calculated for each time series (Figure 26C). In other words, the curve that best fits each tree-ring series is determined, and this curve is then divided or subtracted from the original time series (COOK et al., 1990; BUNN, 2008; PRESTES, 2009; LORENSI; PRESTES, 2016; SILVA et al., 2021a).

All detrending methods can be applied either by taking the difference or by performing the division with the tree-ring series. In this thesis, the division method was chosen, and all three methods were applied to the data, as suggested by Helama, Melvin & Briffa (2017), Silva et al. (2021a), and it was found that all of them maintain climatic signals. After comparing the statistics, the Regional Curve Standardization was selected for the analysis.

3.4.4 SERIES STATISTICS

To guarantee a final chronology with high quality it is necessary to check a few statistics parameters, the Mean Series Intercorrelation ($\overline{r}_{bt}$), Expressed Population Signal (EPS), and Signal to Noise Ratio (SNR) (COOK et al., 1990).

Mean Series Intercorrelation ($\overline{r}_{bt}$) is the mean of all the correlations between different pairs of samples, given by the Equation 3.1:

$$\overline{r}_{bt} = \frac{1}{N_{bt}}(\overline{r}_{tot}N_{tot} - \overline{r}_{wt}N_{wt}) \tag{3.1}$$

considering $\overline{r}_{tot}$ as the mean of all correlations among different samples (within and between different trees), N_{tot} is the total number of samples, N_{wt} is the number of trees (COOK et al., 1990), and $\overline{r}_{wt}$ is the within-tree signal obtained by averaging the coefficients between

Figure 26: Example of three different detrending methods. (A) Original tree-ring series (blue line) and the Cubic Spline with 67% frequency (orange line). (B) The residual tree-ring series by both division (blue line) and subtraction (orange line). (C) Original tree-ring series (blue line) and the Regional Curve Standardization (orange line). (D) The residual tree-ring series by both division (blue line) and subtraction (orange line). (E) Original tree-ring series (blue line) and the Negative Exponential Curve (orange line). (F) The residual tree-ring series by both division (blue line) and subtraction (orange line).

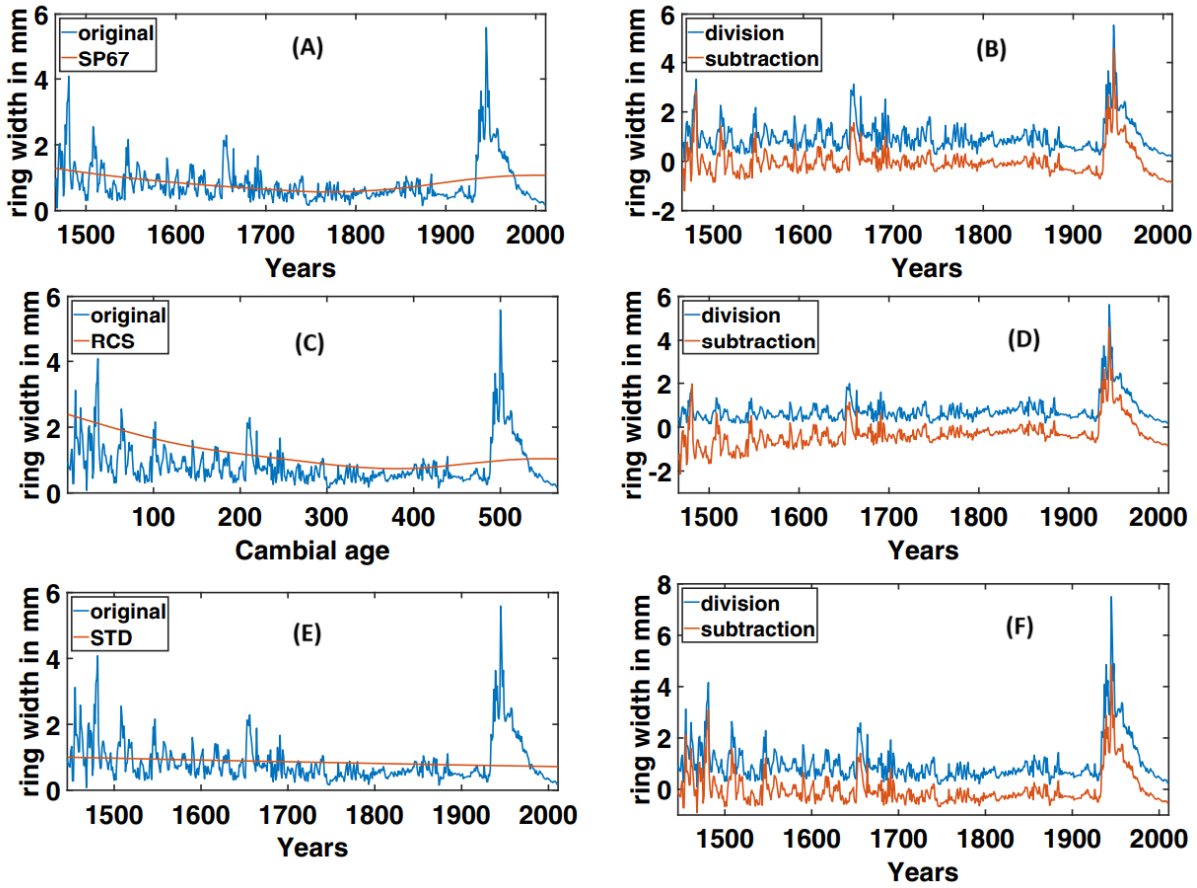

Source: Silva et al. (2021a)

samples from the same tree. And N_{bt} is calculated by Equation 3.2.

$$N_{bt} = N_{tot} - N_{wt} \tag{3.2}$$

Although, $\overline{r}_{bt}$ is not the best parameter to estimate the chronology signal when using a different number of samples per tree. The **Effective Chronology Signal** ($\overline{r}_{eff}$) is an estimation of the chronology-signal using within and between tree signals, used when there is a dissimilarity of the number of samples per tree. It is defined by

$$\overline{r}_{eff} = \frac{\overline{r}_{bt}}{\overline{r}_{wt} + \frac{1-\overline{r}_{wt}}{c_{eff}}} \tag{3.3}$$

where c_{eff} is the effective number of samples (if there is a different number of samples per tree).

Expressed Population Signal (EPS) is the proportion of variance of a population in a chronology that can be described by a subsample, it tells how good the chronology is representing an infinite population (WIGLEY; BRIFFA; JONES, 1984; COOK et al., 1990; BRIFFA et al., 1990), in other words, guarantees that the mean chronology will be created using all tree-ring series in a homogenous way (SILVA et al., 2021b). EPS can be calculated by

$$EPS(t) = \frac{t^* \overline{r}_{bt}}{t^* \overline{r}_{bt} + (1 - \overline{r}_{bt})}, \tag{3.4}$$

where $\overline{r}_{bt}$ can be replaced by $\overline{r}_{eff}$. Moreover, t is the number of tree series (one sample per tree or tree indices made by averaging all the samples per tree).

Figure 27 illustrates the dependency of EPS and $\overline{r}_{eff}$. Statistically significant values are considered above 0.85, this value indicates the number of trees necessary to obtain a good EPS value. If the point is to work with the samples without doing an average per tree, it is possible to just replace $\overline{r}_{bt}$ per $\overline{r}_{eff}$ (COOK et al., 1990).

Figure 27: The plot of mean series intercorrelation effective signal ($\overline{r}_{eff}$ -exponential curves), as y-axis the EPS values and as x-axis the number of trees (t). An EPS with a minimum of 0.85 is considered a chronology with a significance level. With the increase of $\overline{r}_{eff}$ the number of trees needed to reach an EPS > 0.85 is lower.

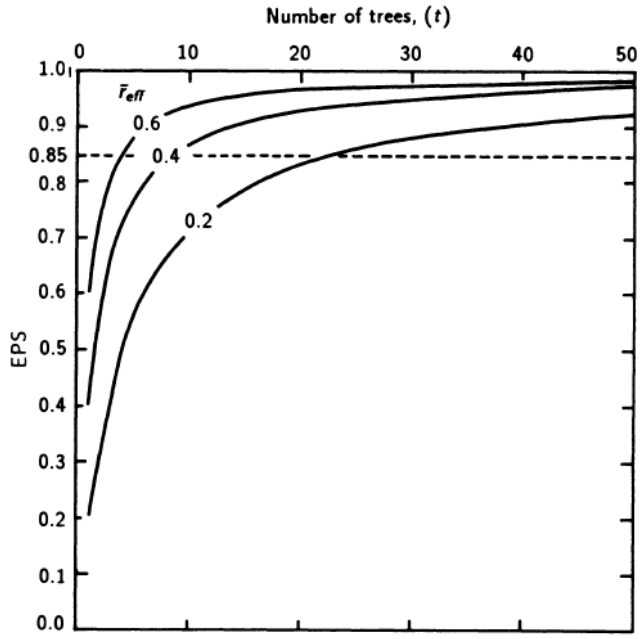

Source: Cook et al. (1990)

Signal to Noise Ratio (SNR) gives the strength of the common signal in the trees and can be used instead of the EPS value (COOK et al., 1990). According to Wigley,

Briffa & Jones (1984), it is defined by

$$SNR = N\overline{r}/(1-\overline{r}), \tag{3.5}$$

considering N as the number of trees and $\overline{r}$ is the average correlation between the trees. The SNR value gives how many times stronger the signals of the series are compared to the noise signals.

3.4.5 OBTAINING THE CHRONOLOGY

To obtain a master chronology (Ring Width Index - RWI) to perform dendroclimatic and paleo reconstructions studies it is necessary to make sure the chronology is well constructed. If the number of samples per tree is different, it is important to create a mean value per tree, to avoid tendency problems.

To estimate the chronology, the averaging of the samples is generally used according to Cook et al. (1990), using the Equation 3.6

$$\overline{I}_t = \sum_{j=1}^{m} I_t/m. \tag{3.6}$$

where I_t is each of the indices, and m is the number of indices.

Therefore, a master chronology can also be made by using the biweight robust mean. This is one way to help with noise reduction outliers or extreme values, since it automatically discounts the influence of noise values, reducing the variance caused by it (MOSTELLER; TUKEY, 1977; COOK et al., 1990). The Equation 3.7 is used to obtain the chronology using biweight robust mean.

$$\overline{I}_t = \sum_{j=1}^{m} w_t I_t, \tag{3.7}$$

considering w_t is calculated by

$$w_t = \left[1 - \left[\frac{I_t - \overline{I}_t^*}{cS_t^*}\right]^2\right]^2, \tag{3.8}$$

for $\left[\frac{I_t-\overline{I}_t^*}{cS_t^*}\right]^2 < 1$ (COOK et al., 1990). Considering c as a constant defined by Mosteller & Tukey (1977) as 6 or 9. Therefore, the choice between const = 6 and const = 9 determines

how smoothing handles extreme values and how sensitive it is to detecting outliers. The constant 6 is more sensitive to outlier detection than 9, as it requires values to be closer to the mean to be considered outliers. Here, the constant 9 is used. And finally, the S_t^* is the standard deviation of the frequency distribution (COOK et al., 1990) obtained by the Equation 3.9:

$$cS_t^* = median\{I_t - \overline{I}_t^*\} \tag{3.9}$$

After estimating the master chronology it is important to correct the variation created if the samples have different sizes, in other words, if the trees do not have the same age . The variance correction is applied for each time period based on the change in the number of trees, as shown in Equation 3.10.

$$I_{cor}^t = (I_{act}^t - I) * k + I, \tag{3.10}$$

where I_{cor}^t is the new chronology (after the variance correction), I_{act}^t is the old chronology (before the variance correction), I is the mean of the chronology, and k is the coefficient of contraction, defined by the division of the coefficient of variation of the maximum time period for the sample size. Cook et al. (1990) and Shiyatov & Mazepa (1987) studies suggest that less than 10 samples is more likely to occur variance effects when creating a chronology.

3.5 OCEAN-ATMOSPHERE AND SOLAR DATA

To analyze the ocean-atmosphere and solar signals in tree growth, specific ocean-atmosphere, and solar parameters were defined for this analysis. The data selected for this thesis are listed as subsections, and the main databases used are the National Oceanic and Atmospheric Administration (NOAA) and the National Weather Service - Climate Prediction Center (NCEP).

3.5.1 SUNSPOT

The solar parameter “Sunspot” is used as a representative of solar activity. The data represents the monthly sunspot numbers, which are the main characteristic defining the 11-year solar cycles. The Sunspot data is accessible at SIDC, RWC Belgium, World Data Center for the Sunspot Index, Royal Observatory of Belgium, covering the time span from 1749 to 2022. The data was transformed into an annual scale to facilitate the analysis (Figure 28).

Figure 28: Annual time series of SUNSPOT numbers. The dashed line marks every 11 years (approximately one solar cycle).

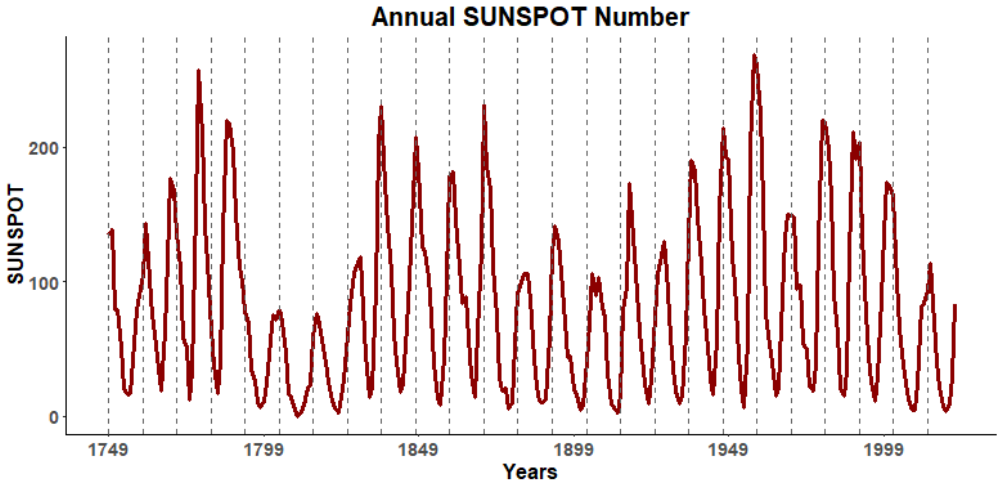

Source: The author.

3.5.2 SOUTHERN OSCILLATION INDEX (SOI)

The Southern Oscillation Index (SOI) used in this thesis is the pressure difference between Tahiti (in the French Polynesia region of the central Pacific) and Darwin (in Northern Australia). It was calculated using the method provided in Ropelewski & Jones (1987) and is accessible on the Climatic Research Unit. The data time span is from 1866 to 2022, and it was calculated into an annual scale for the analysis (Figure 29). As mentioned in the literature review, the SOI is one of the parameters used to study ENSO events, where pressure values above 0 (zero) correspond to *La Niña* events, and values below 0 (zero) indicate *El Niño* events (INPE; CPTEC, 2023).

Figure 29: Annual time series of Southern Oscillation Index (SOI) numbers. The negative values are related to *El Niño* events and positive values indicate *La Niña* events.

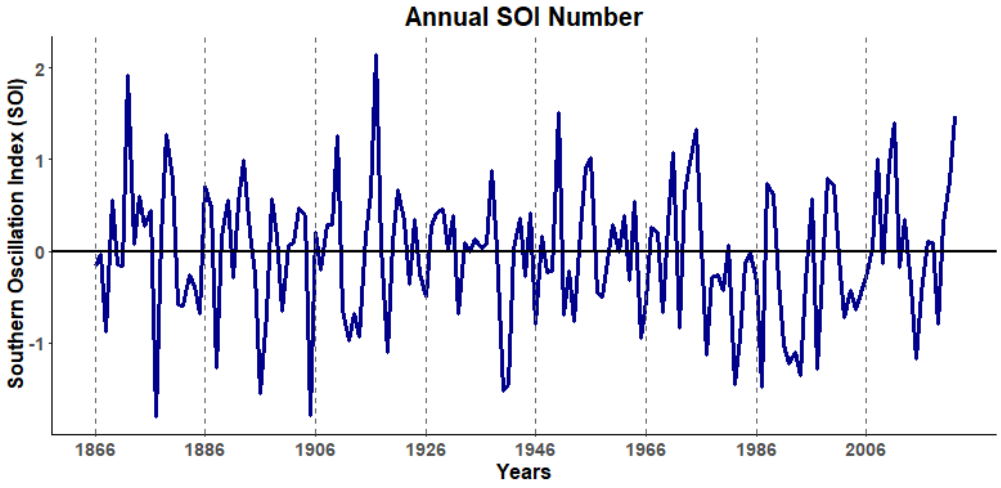

Source: The author.

3.5.3 NIÑO 3.4

To analyze the Equatorial Pacific Ocean's influence on precipitation and the RWI, the NIÑO 3.4 region (5°N - 5°S; 120°W - 170°W) was selected due to its large variability during *El Niño* events, compared to the other NIÑO regions (EDU, 2023). The time series is composed of area-averaged SST measured in this region . In Figure 30a, all the NIÑO regions are illustrated, with "NIÑO 3.4" located between the NIÑO 4 and NIÑO 3 regions. The monthly data was downloaded from the NCEP Database and calculated as annual data (Figure 30b) from 1950 to 2023.

Figure 30: NIÑO 3.4 region location and time series used in this thesis.

(a) The NIÑO regions and the location of NIÑO 3.4 region in the map.

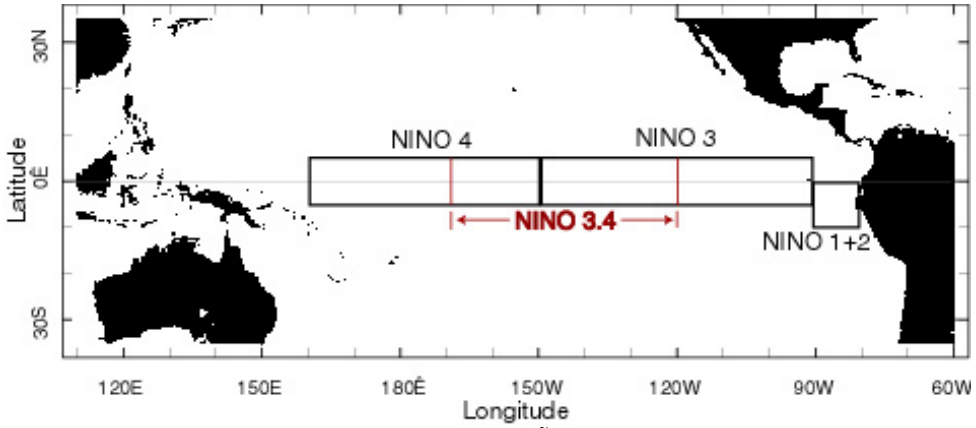

(b) Annual time series of NIÑO 3.4 region in °C.

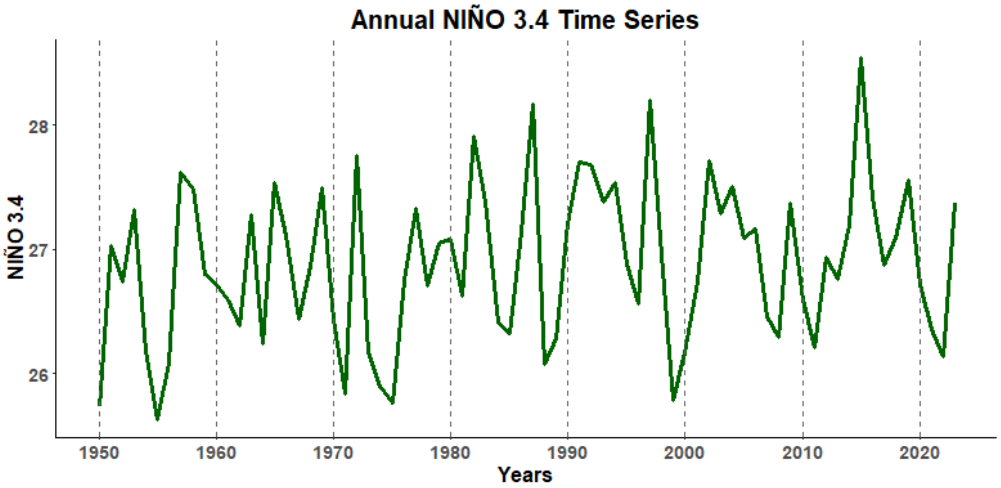

Source: (a) Edu (2023). (b) The author.

3.5.4 ATLANTIC OCEAN - SOUTHWEST REGION (ATLSW)

To analyze the influence of the Atlantic Ocean on precipitation and the RWI, the SST data from the Atlantic Ocean - Southwest region (ATLSW) was used. This region is defined by geographical coordinates ranging from 10°S to 40°S latitude and 60°W to 10°W longitude (see Figure 31). The data covers the period from 1854 to 2015. Monthly

SST data was obtained from the National Weather Service - Climate Prediction Center (NCEP), and the annual mean was computed and used in this thesis (Figure 31).

Figure 31: Atlantic Ocean - Southwest region (ATLSW) Location and Time series

(a) The South Atlantic regions and the location of Atlantic Ocean SST - Southwest region (ATLSW) in the map.

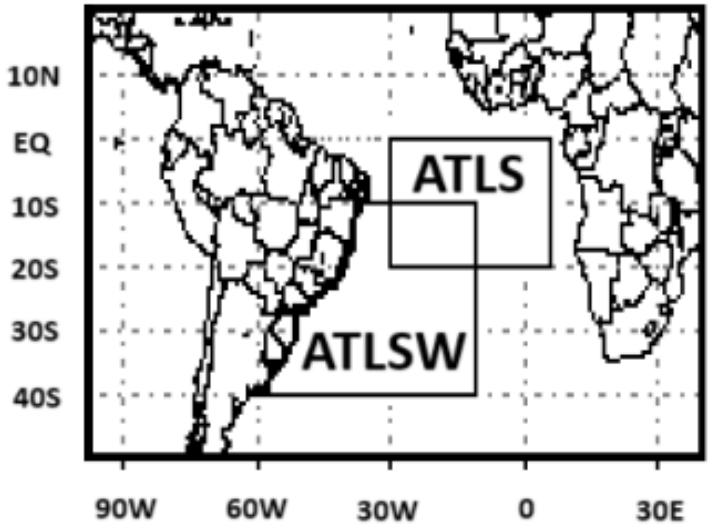

(b) Annual time series of Atlantic Ocean SST - Southwest region (ATLSW) in °C.

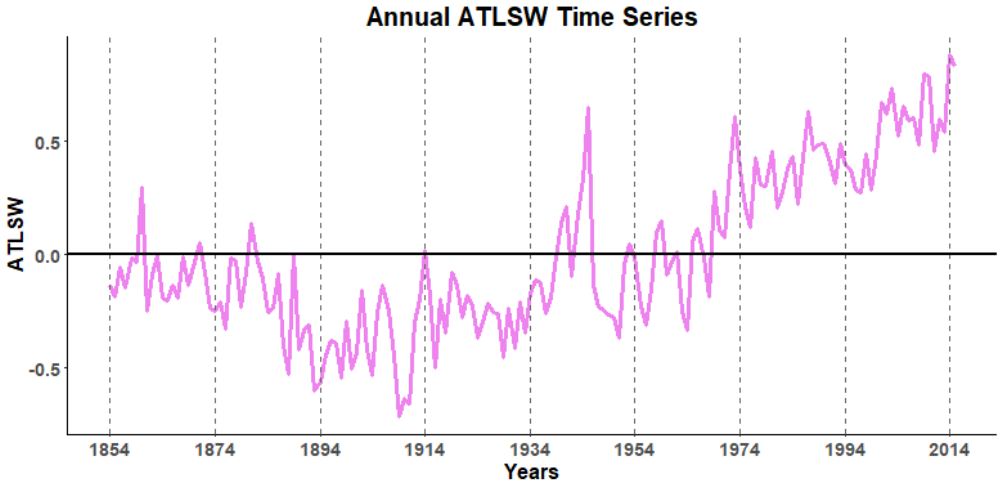

Source: (a) Silva (2004). (b) The author.

3.5.5 REGIONAL PRECIPITATION AND TEMPERATURE

Regional precipitation and temperature monthly data were obtained in the Meteorological Database (BDMEP) of the National Meteorological Institute (INMET). For each city, data from the closest stations (with the same Köppen classification) was collected and a correlation analysis between the parameters and the RWI was performed. The stations chosen are the best correlated to its corresponding RWI. Table 5 presents which precipitation, maximum temperature, mean temperature, and minimum temperature were

used for the cities analyzed in this thesis. The location of the stations in relation to the chronologies can be seem in Figure 32.

Table 5: Precipitation and temperature (maximum, mean, and minimum) information. The station column shows the name of each meteorological station used, and in the City column the corresponding cities that used the same station data. The cities' acronyms can be found in the subsection "Data Locations".

Station	Cities	Precipitation	TMAX	TMEAN	TMIN
Irati	AÇU.	1966-2004	1966-2004	1966-2004	1966-2004
Caxias do Sul	CAN. SFP.	1961-2004	1961-2004	1961-2004	1961-2004
Chapecó	CHA.	1973-2004	1973-2004	1973-2004	1973-2004
Passo Fundo	COX. PAF.	1961-2010	1961-2022	1961-2022	1961-2022
Curitibanos	CUR.	2008-2022	2008-2022	2008-2022	2008-2022
Porto União	GCA IRI.	1961-1991	1961-1991	1961-1991	1961-1991
Joaçaba	IRA.	1986-2007	1986-2007	1986-2007	1986-2007

Source: The author.

Figure 32: Map of southern Brazil with the location of the cities and the climatic stations (**X**).

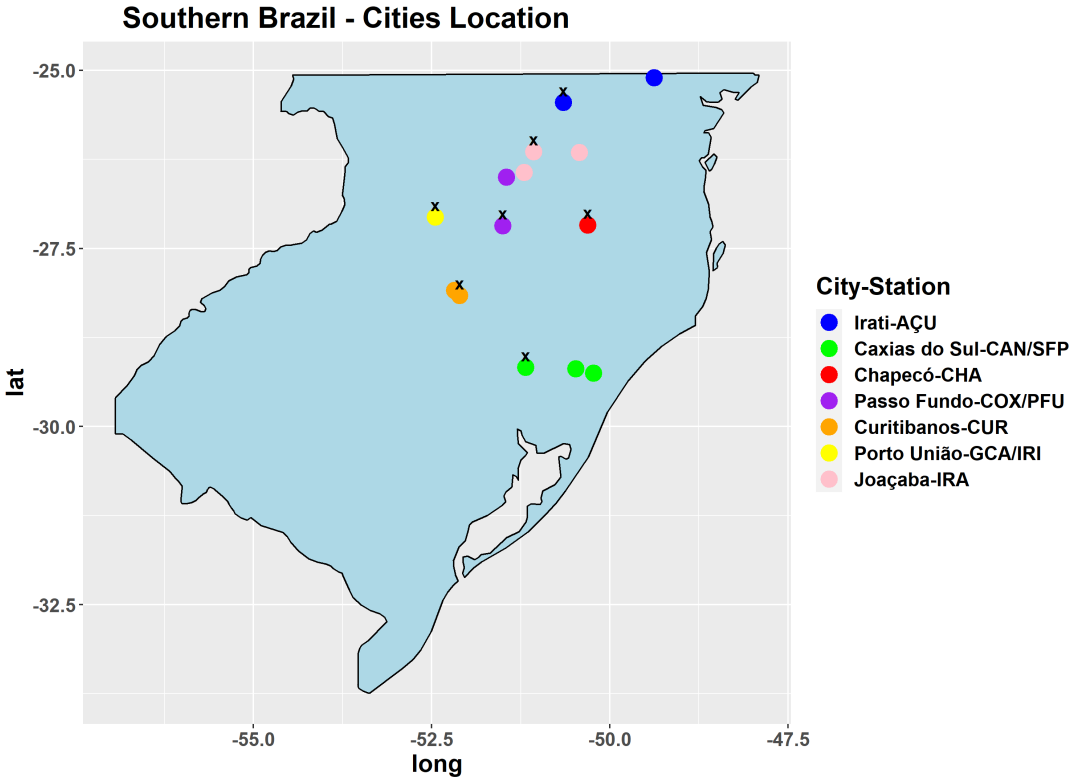

Source: The author.

The provided data by INMET unfortunately has a lot of missing data (gaps). Some approaches widely used in research were applied in order to overcome this problem, these

methods were Multiple Imputation (MICE), MissForest, Principal Component Regression with MICE, and Mean Imputation. The choice of the methodology to deal with missing data is crucial to maintaining important information from the original and inputting fewer errors as possible, as discussed in Patrician (2002), the best approach can vary with each data type (SHRIVE et al., 2006). Here, all the aforementioned methodologies were tried, but the mean imputation approach was the only one that worked for the data used here, considering the large gaps found in the data. This approach can also be found in the literature as "individual mean", and it consists in filling the gaps with the mean of the variable, so in this case, the monthly mean was used to fill gaps in the corresponding month column.

3.6 DENDROCLIMATOLOGY

To analyze the relationship between RWI and ocean-atmosphere and solar parameters, Pearson's correlation and Partial correlation were used as a pre-analysis to identify strong linear responses. The t-distribution was employed as the significance test for correlation. For identifying non-linear responses in this relationship, the cross wavelet coherence methodology was chosen, as it is commonly used in geophysical series (GRINSTED; MOORE; JEVREJEVA, 2004; RIGOZO et al., 2012; SILVA et al., 2021b; MURAJA et al., 2023). The Continuous Wavelet Transform and the Cross Wavelet Coherence are further described in the following subsections.

3.6.1 CORRELATION AND PARTIAL CORRELATION

Pearson correlation is commonly used to measure the linear relationship between two variables, especially in Dendrochronology studies (CORREA-DíAZ et al., 2019; CORREA-DíAZ et al., 2020; RUBIO-CUADRADO; CAMARERO; BOSELA, 2022) It is defined by the Equation 3.11:

$$r_{X,Y} = \frac{\sum_{i=1}^{n}(X_i - \bar{X})(Y_i - \bar{Y})}{\sqrt{\sum_{i=1}^{n}(X_i - \bar{X})^2 \sum_{i=1}^{n}(Y_i - \bar{Y})^2}} \tag{3.11}$$

where $r_{X,Y}$ represents the Pearson correlation coefficient between variables X and Y. n is the number of data points in the sample. X_i and Y_i are the individual data points of variables X and Y, respectively. $\bar{X}$ and $\bar{Y}$ are the sample means of variables X and Y , respectively (MARTINS, 2014).

However, climatic parameters can be influenced by other variables; for instance, the precipitation level may be affected to some extent by the temperature of the region. The correlation between two variables can thus be influenced by a third variable (ZUO

et al., 2014). The Equation 3.12 shows the partial correlation between X and Y while excluding the influence of the variable Z.

$$r_{XY \cdot Z} = \frac{r_{XY} - r_{XZ} r_{ZY}}{\sqrt{(1 - r_{XZ}^2)(1 - r_{ZY}^2)}} \tag{3.12}$$

where $r_{XY \cdot Z}$ represents the partial correlation between variables X and Y, controlling for Z. r_{XY} is the correlation between variables X and Y. r_{XZ} is the correlation between variables X and Z. r_{YZ} is the correlation between variables Y and Z.

The denominator $\sqrt{(1 - r_{XZ}^2)(1 - r_{ZY}^2)}$ adjusts the partial correlation, taking into account the variability of Z in relation to X and Y, avoiding it from being excessively influenced by strong correlations between X and Z or between Y and Z (EPSKAMP; FRIED, 2018).

3.6.2 CONTINUOUS WAVELET TRANSFORM (CWT)

The wavelet transform of a time series involves decomposing it into time-frequency space, allowing the identification of periodicities in the frequency domain and their occurrence in time. This provides a significant advantage over other frequency analyses, such as Fourier analysis, because it not only identifies frequency patterns but also reveals when these patterns occur in time (GRINSTED; MOORE; JEVREJEVA, 2004; HADDAD; SERDIJN, 2009). In this thesis, the CWT is utilized on the RWI, ocean-atmosphere, and solar time series to extract patterns or cycles of behavior (periodicities), these could be short-term fluctuations or longer-term trends. The wavelet transform has been extensively used in dendrochronology, particularly in studying the *El Niño*-Southern Oscillation (GRINSTED; MOORE; JEVREJEVA, 2004; RIGOZO et al., 2012; PRESTES et al., 2018b; SILVA et al., 2021b; MURAJA et al., 2023).

According to Torrence & Compo (1998), for a function to be considered a "wavelet", it must be localized in both time and frequency space with a mean value of zero. Thus, the time series x_n CWT can be represented as the convolution of x_n with a scaled version of the "mother wavelet" function ψ:

$$W_n(s) = \sum_{n'=0}^{N-1} x_{n'} \psi^* \left[\frac{(n' - n)\, \delta t}{s} \right] \tag{3.13}$$

where (*) indicates the complex conjugate. The scale (s) can be adjusted to fit the characteristics of each signal, depending on the time series being analyzed. However, it is essential to be cautious with scale adjustments, as significant increments can lead to the loss of time information, and vice versa (TORRENCE; COMPO, 1998). This is analogous

to the Heisenberg Uncertainty principle, which sets limitations on operational possibilities in quantum physics (BUSCH; HEINONEN; LAHTI, 2007).

Since this work deals with finite-length time series, edge effects may occur at the beginning and end of the wavelet power spectrum, as mentioned by Torrence & Compo (1998). To determine the region where there are no edge effects, a Cone of Influence (COI) is defined for each "mother wavelet". In this work, the Morlet wavelet was employed as the "mother wavelet" with central frequency of 6 and the standard deviation is implicit in the formula used to calculate the Morlet wavelet (using the scale, wavenumber vector, and central frequency), and its COI is defined as half of the time-series length. The period scale was chosen accordingly for each time series' COI or, more specifically, in the period where the COI ends.

Here, the R package "dplR" was employed to obtain the CWT for each time series, the default parameters can be found in the Torrence Wavelet program (wavelet.pro), used to build the function. The wavelet spectrums were visualized using "wavelet.plot" (BUNN, 2020).

3.6.3 CROSS WAVELET COHERENCE (WTC)

To evaluate the non-linear relationship between the RWI and each ocean-atmosphere and solar parameter, the cross-wavelet coherence (WTC) was applied. The WTC is a measure used to investigate the coherent phase relationship between two non-stationary time series in the time-frequency domain. It is an extension of classical coherence analysis for the analysis of non-stationary signals, such as climatic or geophysical time series.

As described in Torrence & Compo (1998), the wavelet coherence of two time series is defined as:

$$R_{xy} = \frac{\sum_{i=0}^{N-1} W_x^*(a,b,i) \cdot W_y(a,b,i)}{\left[\sum_{i=0}^{N-1} |W_x(a,b,i)|^2 \cdot \sum_{i=0}^{N-1} |W_y(a,b,i)|^2\right]^{\frac{1}{2}}} \tag{3.14}$$

where R_{xy} represents the wavelet cross coherence between two time series $x(t)$ and $y(t)$. $W_x(a,b,i)$ and $W_y(a,b,i)$ are the wavelet coefficients of $x(t)$ and $y(t)$ in the scale a, time displacement b, and N is the total number of points in the time series. This definition closely resembles that of a traditional correlation coefficient, making it useful to consider wavelet coherence as a localized correlation coefficient in time-frequency space.

In the context of wavelet analysis, the phase represents the local relative phase between two-time series in the time-frequency domain. It indicates the synchronization or lag between two signals at different time points and frequencies. The phase can be

visualized using arrows in the time-frequency plane. In Figure 33, the arrows illustrate the direction of cross-wavelet coherence. Arrows pointing to the right indicate in-phase synchronization, while arrows pointing to the left represent anti-phase (lag). The angle of the arrows reflects the degree of this synchrony or lag (VACHAA; BARUNIK, 2012).

Figure 33: This diagram illustrates the phase representation of the coherence wavelet based on the arrow's direction. In the upper left box, the arrow points 90° to the left in the 2nd quadrant, indicating that series x lags behind series y. In the upper right frame, the arrow is in the 1st quadrant, pointing 90° to the right, signifying that y lags behind x. In the lower left box, the arrow is in the 3rd quadrant, suggesting that y lags behind x. Lastly, in the lower right frame, the arrow points 90° to the right in the 4th quadrant, indicating that x lags behind y.

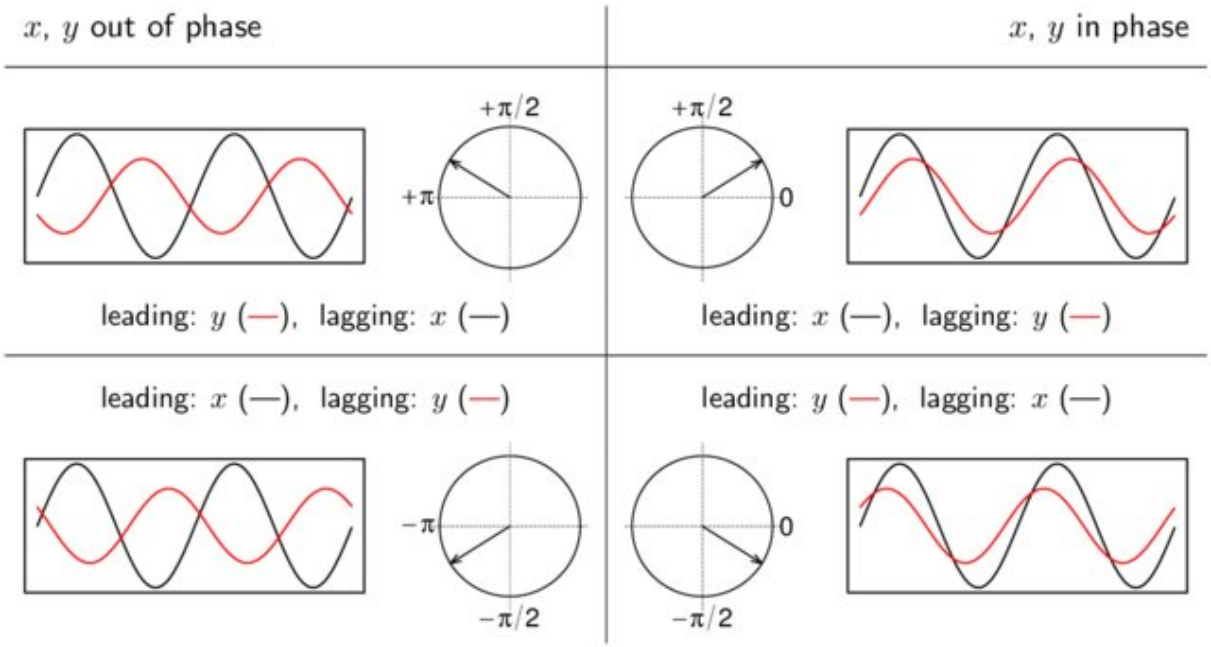

Source: Schmidbauer & Roesch (2018).

According to the Nyquist criterion, finding periodicities between a RWI and ocean-atmosphere-solar time series is possible. In Sidhu, Bhajla & Das (2023), the maximum order of frequency (N_F) is defined as:

$$N_F = \frac{\frac{f_s}{2}}{f} \tag{3.15}$$

where f_s is the sampling frequency and f is the fundamental frequency. The energy of high order harmonics will reflect into the low order harmonics if the original signal contains harmonics greater than N_F (aliasing effect). To avoid this it is crucial to ensure that the sampling rate is adequate, otherwise, high-frequency components may be wrongly represented as low-frequency components, introducing errors into signal analysis.

The R package biwavelet was implemented with the function "wtc" to compute the cross wavelet coherence between the time-series. To plot the results, the function "plot.biwavelet" using the normalized power by variance (type = power.norm) was applied.

4 RESULTS AND DISCUSSION

In this chapter, the main findings regarding the identified patterns in the time series, as well as their implications for understanding the interactions between climatic factors and the RWI are presented. The results obtained from the analysis of data in the stages of Regional Chronologies Processing; Ocean-Atmosphere, and Solar Data Processing; Pearson's correlation; Continuous Wavelet Transform; and the Cross Wavelet Coherence are discussed. The scripts developed for the analysis are available at **GitHub**.

4.1 REGIONAL CHRONOLOGIES PROCESSING

The tree-ring time series per city were averaged so it would become a tree-ring index per city, here called RWI. Each city tree-ring time series and respective chronology (RWI) are shown in Appendix A (Figures 41, 42, 43, 44, 45, 46, 47, 48, 49, 50).

Three detrending methods were applied to the RWIs, and based on the EPS values obtained, the Regional Curve Standardization (RCS) method was selected for this thesis. RCS consistently yielded superior EPS values across most of the chronologies, and its widespread utilization in dendroclimatic studies made it the preferred choice. Table 6 contains the EPS, Rbt, and SNR values for each RWI. The AÇU, CHA, COX, GCA, IRA, PFU, and SFP RWIs had EPS values between 0.5 and 0.6. For CAN, CUR, and IRI RWIs, the EPS values were greater than 0.6.

Table 6: The statistics per chronology (city). Expressed Population Signal (EPS) values greater than 0.6 are colored in blue. The only EPS value that almost reached the 0.85 criteria is in bold.

RWI	Rbt	EPS	SNR
Açungui (AÇU)	0.073	0.572	1.338
Canela (CAN)	0.474	**0.844**	5.399
Chapecó (CHA)	0.089	0.595	1.468
Coxilha (COX)	0.111	0.578	1.367
Curitibanos (CUR)	0.145	0.670	2.03
General Carneiro (GCA)	0.052	0.545	1.199
Irani (IRA)	0.088	0.575	1.355
Irineópolis (IRI)	0.205	0.740	2.844
Passo Fundo (PFU)	0.093	0.551	1.226
São Francisco de Paula (SFP)	0.088	0.516	1.065

Source: The author.

The RWIs are not reaching the required EPS value (> 0.85), Canela RWI is the only one that was close enough (EPS = 0.84) to be considered statistically significant. This suggests that all the trees collected in Canela are responding to the same limiting factor, and consequently, are well-dated. For the other cities, there are two possibilities for

the lower values: some trees were affected by a very specific regional external factor or there is an issue with the cross-dating. Since these trees' time series were worked on by other researchers, there is no easy way to find the original problem, besides re-doing the measurements and cross-dating. However, doing this is very time-demanding and not the scope of this thesis, so the RWIs will be used for the analysis anyway. It is important to highlight that the climate affects these trees, the only thing the statistics are showing is that there are other limiting factors between the trees.

Furthermore, the choice of the detrending method may influence these statistics. For example: using SPL detrending, the EPS value for Curitibanos RWI is 0.821; for Irineópolis RWI using NegExp, the EPS value is 0.855. Moreover, adding more trees to the study can help in identifying errors in cross-dating, such as the existence of missing and false rings. It's crucial to emphasize that working with trees in tropical regions presents significant challenges due to the influence of climate variability and other ecological processes, which can lead to the formation of false or missing rings.

4.2 OCEAN-ATMOSPHERE AND SOLAR DATA PROCESSING

In this section, the ocean-atmosphere and solar time series are displayed in Figures 34, 35, 36, 37, 38, 39, 40. The regional precipitations and temperatures with missing values were filled with the mean imputation methodology.

The climate in the Irati station (Figure 34), located in the state of Paraná, Brazil, is primarily influenced by two climatic systems. During the spring and summer months (October to March), the area experiences a warm and humid tropical continental climate, characterized by higher temperatures and more frequent rainfall, with January being the rainiest month. In contrast, during autumn and winter (April to September), Irati is affected by the polar Atlantic system, resulting in lower temperatures and drier conditions, with August being notably dry. This seasonal variation leads to a distinct pattern of rainy and hot seasons in spring and summer, followed by dry and cold conditions in autumn and winter.

For Chapecó station (Figure 35), the high precipitation level, averaging around 250 mm, is primarily influenced by two distinct climatic systems. The rainiest months, February (summer) and October (spring), can be attributed to the influence of the tropical continental climate, which brings warm, moist air. In contrast, the remaining months maintain an average of approximately 150 mm of rainfall per month, reflecting the impact of the polar Atlantic system, which contributes to drier and cooler conditions. As a result, Chapecó maintains a consistent rainy characteristic throughout the year, with no dry months or seasons. While temperatures vary by only about 5°C, there is a noticeable pattern between the hotter months of spring and summer, driven by the tropical influence, and the colder months of autumn and winter, influenced by the polar Atlantic system,

Figure 34: (a) Precipitation,(b) mean temperature, (c) maximum temperature, and (d) minimum temperature bar series for Irati station (used with Açungui RWI). It was calculated as the mean per month through the time period.

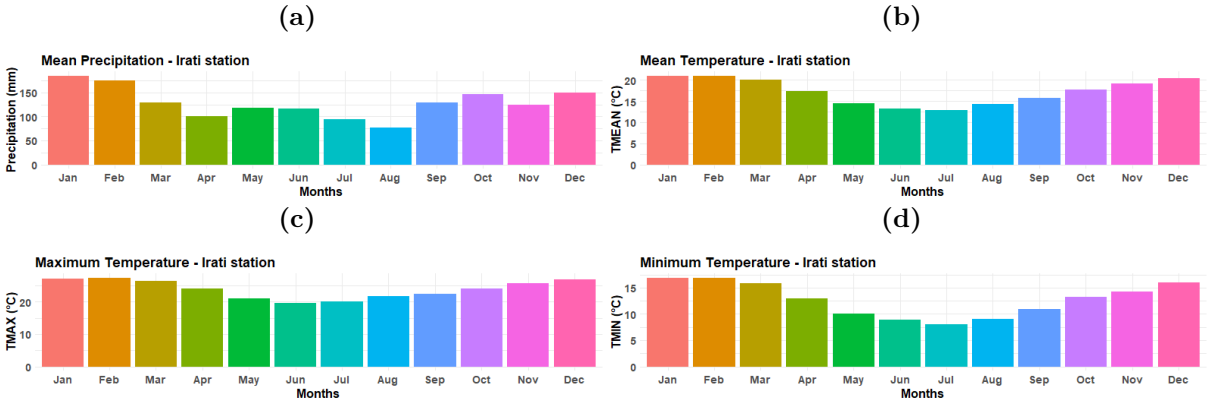

Source: The author.

making Chapecó distinct in its climatic patterns compared to the other cities analyzed.

Figure 35: (a) Precipitation,(b) mean temperature, (c) maximum temperature, and (d) minimum temperature bar series for Chapecó station (used with Chapecó RWI). It was calculated as the mean per month through the time period.

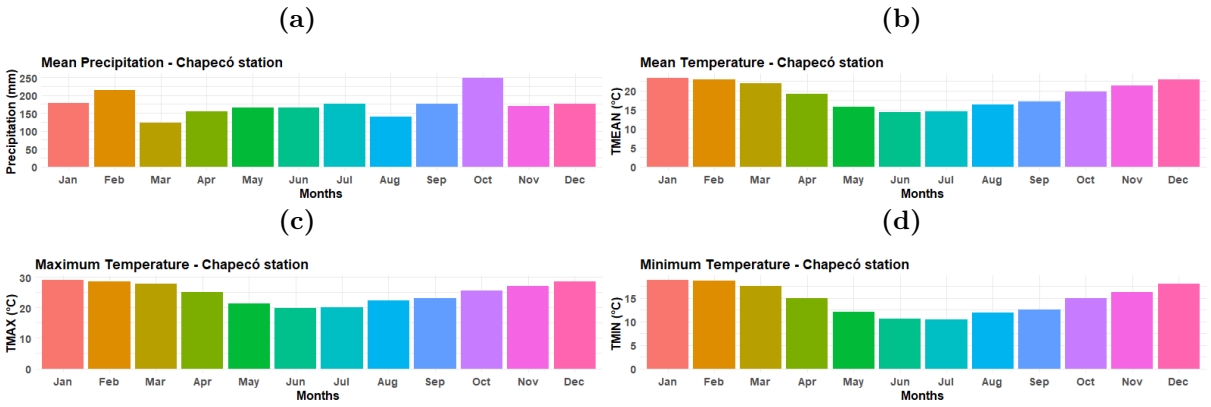

Source: The author.

The Passo Fundo station (Figure 36) exhibits a higher level of precipitation, averaging around 200 mm, particularly during September and October, which corresponds to the spring season. Similar to Chapecó station, the remaining months maintain an average precipitation level of approximately 150 mm. Additionally, temperatures in Passo Fundo show significant variations of more than 5°C, with distinct patterns evident between the hotter seasons of spring and summer. The tropical continental climate and the polar Atlantic systems plays a similar role in this region as described for Irati and Chapecó.

In Caxias station (Figure 37), the precipitation levels are lower (< 175 mm) and they vary from 100 mm in May (end of autumn) to 175 mm in September, October, and December (spring and beginning of summer). Interesting to notice that June and July are the coldest months but also one of the rainiest. Two key factors may be contributing to it. Firstly, the influence of polar air masses from the south leads to lower temperatures,

Figure 36: (a) Precipitation,(b) mean temperature, (c) maximum temperature, and (d) minimum temperature bar series for Passo Fundo station (used with Coxilha and Passo Fundo RWIs). It was calculated as the mean per month through the time period.

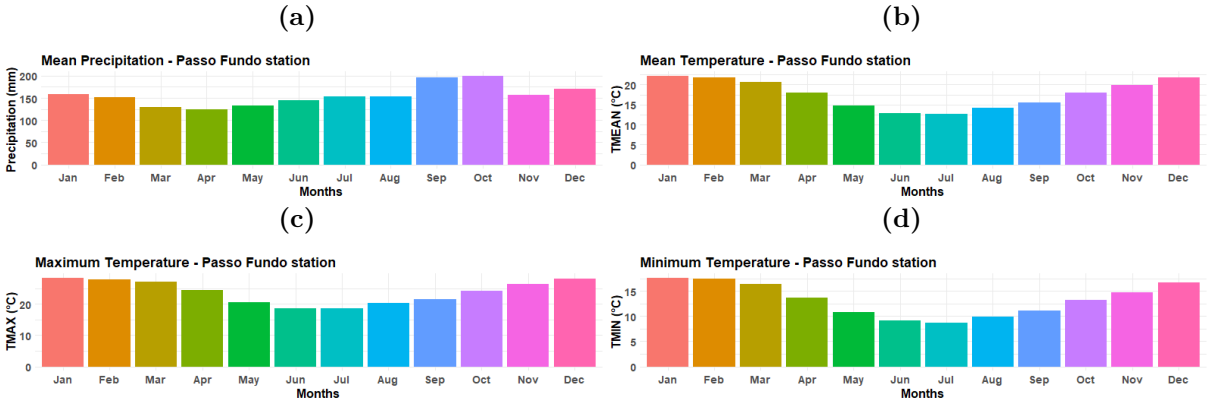

Source: The author.

making these months the coldest of the year. Secondly, the proximity to the Atlantic Ocean plays a crucial role, as ocean moisture can be transported inland, resulting in substantial winter precipitation. Temperature patterns can vary until 10°C in mean temperature. Winter contains the coldest months, but the difference for this station is that spring is colder than autumn. Summer months are very hot here, compared to the other stations' patterns.

Figure 37: (a) Precipitation,(b) mean temperature, (c) maximum temperature, and (d) minimum temperature bar series for Caxias do Sul station (used with Canela RWI, and São Francisco de Paula RWI). It was calculated as the mean per month through the time period.

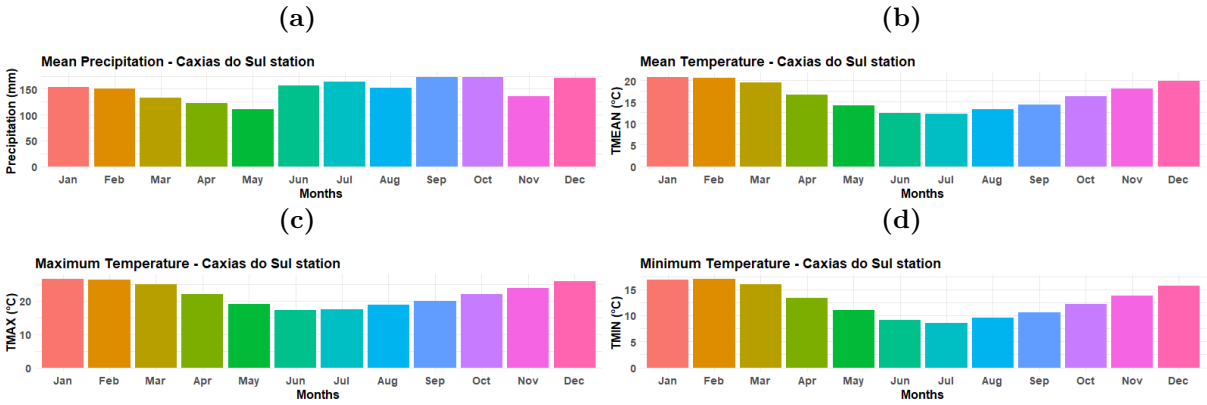

Source: The author.

Upon analyzing the data from Porto União station (Figure 38), it becomes apparent that the patterns of precipitation and temperatures closely resemble those of Caxias station. However, there is a noteworthy distinction in the minimum temperature pattern, with June and July experiencing colder temperatures. This divergence in minimum temperatures can be attributed to localized factors such as geographical variations, elevation differences, and microclimatic influences that may exist in the Porto União area. These factors can intensify the cooling effect during winter months, leading to the observed colder nights in Porto União as compared to Caxias

Figure 38: (a) Precipitation,(b) mean temperature, (c) maximum temperature, and (d) minimum temperature bar series for Porto União station (used with General Carneiro RWI, and Irineópolis RWI). It was calculated as the mean per month through the time period.

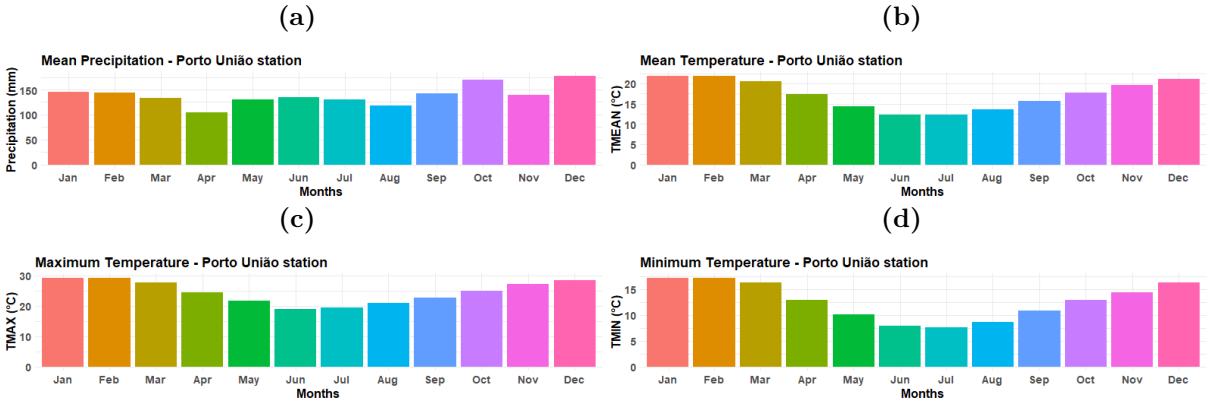

Source: The author.

In Joaçaba station (Figure 39), high levels of precipitation (> 175mm) were identified for January, February, and October. These increased precipitation levels during the warmer months can be attributed to the influence of the regional tropical continental climate system, which brings warm and humid air masses, leading to more intense rainfall. Conversely, very low precipitation values occur in March and August. Regarding temperature, the values are consistently high, particularly for maximum temperatures. Spring, summer, and autumn are considered hot seasons, characterized by warm temperatures. This temperature pattern aligns with the influence of the tropical continental climate. However, there is a notable shift to colder temperatures only at the beginning of winter, specifically in June and July. This cooling trend during early winter can be attributed to the influence of the polar Atlantic system, which brings cooler air masses to the region. These climatic factors contribute to the unique precipitation and temperature patterns observed in Joaçaba throughout the year. Additionally, local topography and geography may play a role in climate variability in Joaçaba

Figure 39: (a) Precipitation,(b) mean temperature, (c) maximum temperature, and (d) minimum temperature bar series for Joaçaba station (used with Irani RWI). It was calculated as the mean per month through the time period.

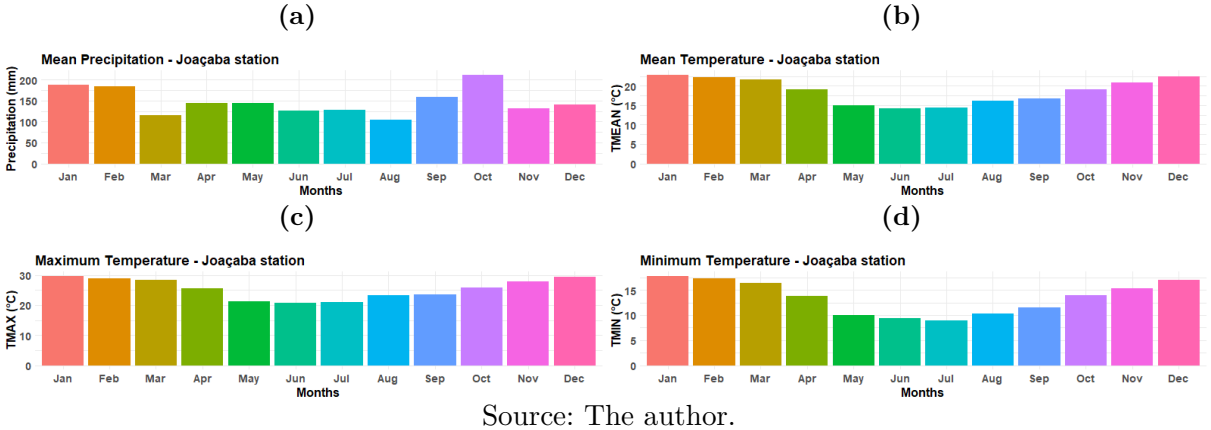

Source: The author.

On the INMET website, only the mean temperature for Curitibanos (Figure 40) was provided. However, this data allows us to identify the presence of distinct hot and cold seasons, even though the temperature variation doesn't exceed 10°C. This pattern can be attributed to the influence of regional climatic systems. Conversely, a distinct pattern is observed for precipitation. Curitibanos experiences rainy months during the summer and at the beginning of spring, particularly in September and October. This seasonal rainfall pattern aligns with the influence of the tropical continental climate system, characterized by warm and humid air masses, leading to more intense rainfall during these periods. Surprisingly, the lowest precipitation levels occur in April, which is typically considered mid-autumn. This deviation from the expected pattern suggests that, unlike the other stations, winter is not the driest season in Curitibanos. These unique climate characteristics reflect a combination of regional climatic influences, geographical factors, and local topography, which collectively shape the temperature and precipitation patterns in Curitibanos.

Figure 40: (a) Precipitation and (b) mean temperature bar series for Curitibanos station (used with Curitibanos RWI). It was calculated as the mean per month through the time period.

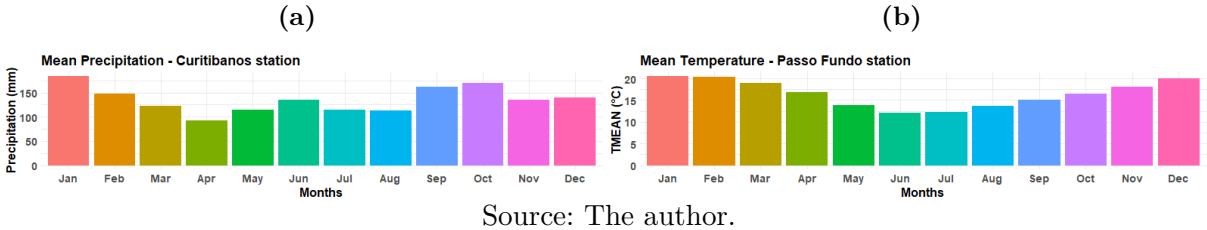

Source: The author.

4.3 DENDROCLIMATOLOGY ANALYSIS

In this Chapter, the results obtained from the analysis of the RWIs are presented as stages: Regional Chronologies Processing; Ocean-Atmosphere, and Solar Data Processing; Pearson's correlation; Continuous Wavelet Transform; and Cross Wavelet Coherence. The relationship between RWI and climatic or solar parameters was investigated using Pearson's correlation to identify linear connections and the Cross Wavelet Coherence to uncover non-linear relationships between the analyzed series.

4.3.1 PRE-ANALYSIS

Pearson's correlation is the most common and easy tool to apply. Here it was applied as a pre-analysis to identify how the trees are responding to the selected parameters for this thesis. The RWI was correlated to the parameters using monthly, seasonal, semester, and annual data. The t-test was applied to obtain a **significance level of 95%**. The significance t-test is a statistical method used to determine whether the difference between the means of two groups is statistically significant or due to random chance. Next, a brief description of the correlations obtained by parameter, as in general the values were

not significant. The correlation was also calculated with precipitation and temperature (TMAX, TMEAN, TMIN) using partial correlation, for example, the correlation between RWI and precipitation excluding the variance of temperature (TMAX, TMEAN, TMIN) in the precipitation time series.

1. **Precipitation (PREC):** Monthly correlations were greater than 20% and greater than -20% (indicating that, as one variable increases, the other tends to decrease), but most of them were not significant (p-value < 0.05), except by SFP RWI. Similarly, for Seasonal and Semester, SFP RWI responded with positive correlations for spring-summer. And Annual only SFP RWI and GCA RWI obtained high correlations with significance levels.

2. **Temperature (TMAX, TMEAN, TMIN):** Similarly to precipitation, the monthly correlations of each temperature were not significant for most of the RWI, except for IRI and IRA for TMIN. For Seasonal correlation, most of them responded to summer with negative correlations (anticorrelations). In Seasonal evaluation, the spring-summer had a greater response, especially for TMEAN, also all correlations were negative. And finally, for Annual correlations, 5 cities had significant correlation values, especially in TMEAN, and again, only negative values.

3. **Southern Oscillation Index (SOI):** Mainly correlation values were low and not significant, with a better response only in Seasonal correlations during autumn for 3 RWI, where 2 of them were negative correlations (anticorrelations).

4. **Sunspot:** Here good correlation (significant) values were found. In the Monthly, Seasonal, and Semester correlation, 6 RWI (CAN, CHA, COX, IRI, PFU, SFP) presented high correlation values. And in Annual correlation, CHA and SFP RWIs presented highly significant correlations.

5. **NIÑO 3.4:** Two RWIs (COX, GCA) presented positive high correlations during April. For Annual analysis, SFP RWI presented high correlation values, -20% and 18%, respectively.

6. **Atlantic Ocean - Southwest Region (ATLSW):** All the cities responded with high significant correlation values for Monthly, Seasonal, and Semester analyses. For Annual analysis, CAN RWI, and COX RWI had high positive correlations, and IRA, IRI, and PFU RWIs obtained high negative correlations (anticorrelations).

7. **Precipitation excluding Temperature (TMAX, TMEAN, TMIN) variance:** The results of the partial correlation here were better than the common correlation. SFP RWI is still the city with better correlation values. What changes is that correlation values are greater in autumn-winter now. An important observation

worth noting is that the correlation results improved notably when the variance in maximum temperature (TMAX) was excluded. This observation suggests a strong influence of higher temperatures on the availability of water.

8. **Temperature (TMAX, TMEAN, TMIN) excluding Precipitation:** In this partial correlation analysis, IRI RWI has much less significant values compared to the temperature correlation analysis. The RWIs IRA and GCA have greater correlation values, positive for IRA and negative for GCA. Better responses were obtained for Semester and Annual analyses, with 6 RWIs, for TMAX, TMED, and TMIN.

Evaluating the results obtained in this pre-analysis, it would be expected more significant responses to the parameters that are known to influence the region, such as precipitation, as obtained in Lorensi & Prestes (2018). Negative values of correlation were expected for precipitation when followed by low temperatures, since the *Araucaria angustifolia* tree species has a tendency to suffer with the increase of water it receives (ZANON, 2007). The absence of more significant correlation values can be attributed to several factors. Firstly, there may be potential cross-dating issues in some of the RWIs, as detailed in section 4.1.1 on Regional Chronologies Processing. Secondly, the relatively short duration of the precipitation and temperature (TMAX, TMEAN, TMIN) time series could also contribute to this outcome. Finally, the presence of gaps within the aforementioned time series may further impact the ability to establish stronger correlations.

4.3.2 CONTINUOUS WAVELET TRANSFORM (CWT)

The CWTs were computed to identify non-linear responses between the RWIs and the climatic and solar parameters, benefiting from wavelet analysis's ability to handle outliers in time series. CWTs serve as the initial step for the Cross Wavelet Coherence analysis, offering an exploration of the RWI signal's time-frequency characteristics and enabling further investigation of climate-environment interactions and their impact on tree growth dynamics in the region. Significant areas are represented by black color contours inside the cone of influence (COI), all the Figures are located in Appendix B, for better visualization.

For the Açungui RWI (Figure 51a), a significant region within the cone of influence is revealed, spanning approximately from 1930 to 1965. This region displays pronounced wavelet power concentration in the 16 to 32-year period band, potentially indicating the Hale Solar Cycle, and can be associated with relevant climate phenomena or environmental influences on tree growth during the mid-20th century.

Canela RWI (Figure 51b) exhibits two small yet significant regions within the period range of approximately 2 to 4 years. The first significant region is around 1950,

while the second region is centered around 1920, indicating short-term cyclic variations in the RWI data during those periods.

The CWT analysis of Chapecó RWI (Figure 51c) reveals a significant cyclic pattern between 1930 and 1945, with a periodicity of 16 to 32 years. This may be associated with Hale Solar Cycle and/or other climatic factors impacting tree growth during this period.

For Coxilha RWI (Figure 51d), a significant and prominent region emerges within the period range from 1925 to 1965. This region is characterized by a robust concentration of wavelet power within the 32-64 year period band. This indicates the presence of a distinct and prolonged cyclic variation in the RWI signal during this time frame, which may be associated with longer-term solar cycles, such as the 60-year cycle known as the Solar Gleissberg Cycle. Additionally, these long-term cyclic patterns could be influenced by other climatic factors and oceanic oscillations that might have impacted tree growth over several decades.

For Curitibanos RWI (Figure 51e), the CWT analysis reveals two significant regions at different period ranges. The first one, with a periodicity of 2 to 4 years, centered around the year 1970, suggests short-term cyclic variations in the RWI signal. These short-term fluctuations may be associated with climate patterns influenced by phenomena such as the *El Niño*-Southern Oscillation (ENSO) or other regional atmospheric systems. The second region, spanning 8 to 16 years and covering the period from 1960 to 1990, indicates longer-term cyclic variations in the RWI data. These longer-term patterns may potentially be associated with solar cycles, including the 11-year Schwabe solar cycle or the 22-year Hale solar cycle. Additionally, regional climatic factors, such as variations in temperature and precipitation, could contribute to these longer-term cyclic variations, impacting tree growth over extended periods.

The CWT analysis of General Carneiro RWI (Figure 51g) reveals significant short-term cyclic variations within the 4 to 8-year period range, particularly around 1650 to 1670. These variations may be associated with a combination of climatic influences, including regional climatic systems like the South American Monsoon, as well as shorter solar cycles such as segments of the 11-year Schwabe solar cycle. These factors could have collectively influenced tree growth during this specific period, leading to the observed cyclic pattern in the RWI data.

The CWT analysis for Irani RWI (Figure 51h) uncovers several significant regions, primarily outside the Cone of Influence (COI), with some extending into the COI. These regions correspond to different time periods, indicating the presence of cyclic variations and oscillations in the RWI signal. While the specific climatic systems and solar cycles aren't explicitly identified in this analysis, the observed cyclic variations could potentially be associated with a combination of factors, including regional climatic systems such as the South American Monsoon and shorter solar cycles like segments of the 22-year Hale

solar cycle. Further detailed analysis and research may be necessary to pinpoint the exact climatic and solar influences on the tree growth patterns observed in Irani RWI.

For Irineópolis RWI (Figure 51i), a continuous significant region spanning approximately 32 to 128 years, from 1825 to 1970, suggests the presence of longer-term periodicities. While specific climatic systems and solar cycles aren't explicitly identified, these longer-term patterns may be associated with segments of the 87 to 96-year Gleissberg solar cycle, as well as regional climatic systems like the South American Monsoon and the Pacific Decadal Oscillation, which could collectively influence tree growth over extended periods.

The CWT analysis of the Passo Fundo RWI (Figure 51j) reveals various significant regions at different time periods. Short-term patterns emerge within the 8-year period around 1920, potentially associated with regional climatic systems such as the South American Monsoon. Additionally, longer-term cyclic variations spanning from 1902 to 1945 within the 16 to 32-year period range suggest the influence of solar cycles, such as segments of the 22-year Hale solar cycle. These findings indicate a combination of climatic and solar influences shaping tree growth patterns during the early to mid-20th century in Passo Fundo.

No significant regions are detected within the COI for the São Francisco de Paula RWI (Figure 51k). This might indicate the possibility of other factors influencing the RWI signal.

The CWTs were also calculated for the climatic and solar parameters (Figure 52) following the same setting as for the RWIs. Figure 52a displays the CWT plot for SUNSPOT, revealing a significant area covering the period range of approximately 8 to 16 years, spanning the entire analyzed time period. This suggests pronounced cyclic variations in sunspot activity at these time scales. Another significant region is observed in the period range of approximately 32 to 128 years, both inside and outside the COI, with the inside part extending from 1815 to 1915. These findings indicate cyclic patterns in sunspot activity at both shorter (8-16 years) and longer (32-128 years) time scales.

The CWT analysis for the SOI data (Figure 52b) shows multiple significant areas within the period range of approximately 2 to 8 years, from 1885 to 1975. These regions suggest short-term cyclic variations in the SOI data during this time frame, reflecting potential variations in the *El Niño*-Southern Oscillation (ENSO) phenomenon at interannual time scales. Another significant area is observed in the period range of approximately 8 to 16 years, from 1975 to 2010, indicating longer-term cyclic variations in the SOI signal at decadal time scales, reflecting potential variations in ENSO. Furthermore, these variations can interact with other long-term climate phenomena, such as the Pacific Decadal Oscillation (PDO), further influencing global climate patterns.

The CWT analysis of the NIÑO 3.4 data (Figure 52c) also reveals multiple significant areas at different period ranges, similar to the SOI analysis. Additionally, a significant area is observed within the period range of approximately 16 to 32 years, from 1875 to 1900. These results are expected as both the SOI and NIÑO 3.4 are essential components of the *El Niño*-Southern Oscillation (ENSO) phenomenon, which exhibits variability at various time scales, ranging from interannual (2-8 years) to decadal (8-16 years) and longer.

However, the ATLSW CWT Figure 52d) did not show significant regions inside the COI, indicating that cyclic variations present in the data may not well-resolved by the wavelet analysis. However, the wavelet power is stronger from periods 8 to around 32, around 1940. Caution should be exercised when interpreting results at certain time scales.

Figures 53, 54, 55, 56, 57, and 58 present the CWTs for precipitation, maximum temperature, minimum temperature, and mean temperature per station. It is important to note that the short length of some time series can pose challenges for wavelet analysis, impacting the reliability and interpretability of the results.

For the Irati station, the precipitation CWT plot (Figure 53a) shows significant regions within the period range of approximately 2 to 4 years, spanning from 1978 to 1990, and within the period range of approximately 4 to 8 years, from 1967 to 1974 and from 1993 to 2002. The maximum temperature CWT (Figure 53b) reveals a significant region within the period range of approximately 8 to 16 years, from 1995 to 2007. The CWT analysis of minimum temperature data (Figure 53c) does not show any significant cyclic patterns within the COI. The CWT for mean temperature (Figure 53d) identifies a significant region around the period of approximately 4 years, specifically from 2000 to 2005. While both precipitation and mean temperature data display repetitive fluctuations over certain years, no significant cyclic patterns are observed for maximum and minimum temperatures during the examined time scales.

At the Caxias do Sul station, the CWT analysis (Figures 54a) for precipitation did not reveal any significant cyclic patterns or variations within the analyzed time scales. The CWT plot for maximum temperature (Figure 54b) shows a significant region within the period range of approximately 8 to 16 years, spanning from 1973 to 1987. For minimum temperature (Figure 54c) and mean temperature (Figure 54d), a significant point around a period of approximately 2 years is observed, specifically around 1965.

At Chapecó station, the CWT analysis reveals short-term cyclic variation in precipitation (Figure 55a), while the temperature parameters (maximum, minimum, and mean temperature) do not show clear cyclic patterns during the examined period. This highlights the importance of considering different climate variables separately, as they may exhibit distinct temporal behaviors and responses to climatic and environmental influences.

For Passo Fundo station, the CWT analysis shows short-term cyclic variations in precipitation (Figure 56a) over different periods, ranging from 1967 to 2005. The CWT plot for maximum temperature (Figure 56b) indicates cyclic variations within the period range of approximately 2 to 4 years, spanning from 1974 to 1982. Significant areas are also observed for minimum temperature (Figure 56c) and mean temperature (Figure 56d) around the period of approximately 2 years, specifically around 1965, with another significant region around the year 2000.

At Porto União Station, the CWT analysis indicates significant cyclic patterns in precipitation (Figure 57a) at short to medium-term time scales around 1977 and from 1977-1985. A significant cyclic pattern is observed at a short-term time scale for mean temperature around the year 1965 (Figure 57b). Similar cyclic patterns are observed in maximum temperature (Figure 57c) from 1975 to 1980. However, no significant cyclic patterns are identified in the minimum temperature data (Figure 57d) during the analyzed time scales.

Regarding Curitibanos stations, due to the short length of the time series for precipitation and temperature, the CWT analysis did not yield meaningful results. Therefore, they were not evaluated by cross-wavelet coherence.

Finally, for Joaçaba station, precipitation, maximum and minimum temperature (Figure 58a, b, and c) did not show any significant periodicities in their CWT. However, a significant cyclic pattern is observed at short to medium-term time scales (periods 2-4) for mean temperature (Figure 58d).

The significant areas in the CWTs between periods 2-8 are expected to be related to the ENSO influence on tree-ring development and will be further analyzed using SOI and NIÑO 3.4 time series in the next section using cross-wavelet coherence. The periods between 8-14 years may likely be related to the Schwabe Solar Cycle, while periods from 20 to 28 years are expected to indicate the influence of the Hale Solar Cycle. These aspects will be detailed in the following section.

4.3.3 CROSS WAVELET COHERENCE (WTC)

For the graphical representations of the Cross Wavelet Coherence analysis, please refer to Appendix C (Figures 59, 60, 61, 62, 63, 64, 65, 66, 67, 68. The white arrows on the coherence plots indicate the phase angle and direction of the relationships between the RWI and the ocean-atmosphere and solar parameters within the significant regions.

Açungui City:

Analyzing the WTC between Sunspot and Açungui RWI, in the time-frequency domain of Figure 59a, there are significant short-term periodicities between periods 2 and 8. The most prominent feature in the WTC analysis appears between periods 8

and 16. This significant coherence region spans a substantial time period (1940 to 1980). The extended duration of coherence suggests a more prolonged and potentially impactful interaction between the Açungui RWI and the Schwabe solar cycle (~ 11 years). The right-pointing arrows suggest an "in-phase" relationship, where RWI is in lag related to sunspot, indicating that both the Açungui RWI and Sunspot Activity share similar variations at specific time-frequency intervals.

Figure 59b shows two distinct time intervals for the WCT between Açungui RWI and SOI, from 1910 to 1925 and 1935 to 1965, with small regions of statistical significance in periods 4 to 8. The appearance of arrows pointing left within these coherence regions indicates an "anti-phase" (negative) relationship (correlation), where SOI is lagging relating to RWI. Between 1910 and 1930, a more prolonged coherence region is observed in periods 8 to 16, characterized by similar arrows pointing left.

The WTC analysis between Açungui RWI and the NIÑO 3.4 (Figure 59c) shows a strong in-phase influence between the periods 4 to 16, starting in 1910 and ending in 1965, with NIÑO 3.4 lagging related to the RWI. Periods 2-4 also present only one anti-phase periodicity around 1925. Similar years were obtained in the SOI responses described before.

The ATLSW periodicities in the Açungui RWI (Figure 59d) were found between periods 2 and 4 around 1965 and around 1980. Between the periods 4 to 8, a unique significant region was obtained from the WTC analysis from 1910 to 1920.

Figure 59e shows the precipitation periodicities in the Açungui RWI, around the periods 2-4 from 1972-1979 (in phase), and another between the periods 4-8 from 1987-1995. These periods of years indicate that precipitation has an intense influence on tree growth. Precipitation in Açungui, is influenced by several climate systems, including the SACZ, the ITCZ, ENSO (*El Niño-La Niña*), and the SAM, which can influence precipitation patterns in the region. These weather systems can interact in complex ways, resulting in variations in precipitation conditions over time.

The temperature periodicities in the Açungui RWI are presented between 2 to 6 periods, around 1980 (anti-phase), for maximum (Figure 59f), minimum (Figure 59g), and mean temperature with a lag of TMEAN related to the RWI ((Figure 59h). The latitude of the region plays a fundamental role in determining seasonal variations in temperature. In addition, the local topography, proximity to the ocean and the air masses that predominate in the area play an important role. The influence of tropical, polar and Atlantic air masses, as well as global climate systems such as *El Niño* and *La Niña*, can also affect temperature conditions in the region, leading to interannual variations in temperature averages.

Canela City:

For the WTC between Canela RWI and Sunspot (Figure 60a) one small region of statistical significance is observed in periods 2 to 4 around 1975 and again in periods 4

to 8 around 1890. Two significant coherence regions are observed for the period 8 to 16 (Schwabe Cycle), spanning from 1850 to 1875 in phase (Sunspot lagged in relation to the RWI), and from 1960 to 1985 also in-phase, with the RWI lagging behind the Sunspot series (during the same time period of Açungui city responses). A response to the Hale Cycle was also identified (periods 16 to 32) during the years 1875-1925 and 1940-1975, both in anti-phase, probably indicating a lagged response from the tree's growth to the solar effect.

The analysis of the WTC between Canela RWI and SOI (Figure 60b) provided small significant regions approximately in the period of 4, around the years 1900, 1915, 1940, and 1965. These last 3 years were also found in the WTC for SOI and Açungui RWI.

The results for NIÑO 3.4 WTC and Canela RWI (Figure 60c) show almost the same years as the WTC for the SOI. The differences are that the periods extend from 2 to 8 periods, and were obtained periodicities around 1890, 1910 (anti-phase where the RWI is lagging behind NIÑO 3.4), and 1920 (in-phase, RWI is algo lagged behing NINÑO 3.4), which may indicate just a lagged response of the tree's growth to the ENSO events.

The WTC between Canela RWI and ATLSW (Figure 60d) showed periodicities from 2-4 periods in 1865 (in-phase, ATLSW lagging behind the RWI), from 4-8 periods in 1880 (anti-phase, ATLSW lagging behind the RWI) and in 1965, and from 8-16 periods in 1870 (in-phase) and in 1960. No similarities were found between Canela and Açungui ATLSW periodicities.

Figure 60e present periodicities between the periods 2-4 around 1962, 1965-1975 (similarly, Açungui responded in 1965), and 1990-1993; periods from 4-8 around 1962-1967; and a strong anti-phase (with the RWI lagging behind the precipitation series) periodicity between the periods 4-16 from 1952-1985, showing a strong influence of precipitation on tree growth. The region is significantly influenced by larger climate systems, such as the SACZ, the MJO and the *El Niño-La Niña* phenomena, which influence rainfall conditions in the southern region of the Atlantic Ocean. Brazil.

Mean and minimum temperature (Figure 60g and Figure 60h, respectively) do not show any temperature influence, probably because there is a strong influence of precipitation in the RWI. However, mean temperature (Figure 60f) presented one periodicity between 2-4 periods around 1980, similar to Açungui RWI. The temperature in Canela can be influenced by several climatic factors, including atmospheric circulation, which involves changes in the position of high and low pressure systems, such as the South Atlantic subtropical high pressure system (SASH), which affect regional temperatures. In addition, movements of cold fronts, polar or tropical air masses, and variations in SST and ocean patterns, also play crucial roles in determining local thermal conditions.

Chapecó City:

The Sunspot relationship with the Chapecó RWI analyzed by the WTC (Figure 61a), similar to the previous cities identified small significant regions between 2 and 4 (around 1915 and 1955) and a small significant region around 1990 between the periods 8 and 16 (in phase). Differently from other cities, Chapecó didn't show much response to solar activity influence. This can maybe be caused by stronger signals from other influences in the RWI, such as, local climatic factors, extreme weather events and non-climatic nature factors, such as disturbances in the environment, changes in the surrounding vegetation, among others.

The WTC between SOI and Chapecó RWI (61b) provided significant areas in phases between 2 and 4 periods, from 1910 to 1925 (same period as Açungui but anti-phase) with SOI series lagging behind RWI, and around 1965 (also obtained for Açungui as anti-phase and in-phase for Canela) with RWI lagging behing SOI, 1985, and 1995. There is also a long-term response between the periods 8 to 16 from 1970 to 1990 in anti-phase (also obtained for Canela in 1975) with SOI series lagging behind RWI.

Figure 61c provides the WTC between the NIÑO 3.4 and the Chapecó RWI. Most of the areas are similar to what was obtained for the SOI WTC, besides that the periodicities 1965 and 1970-1990 present opposite phases compared to the SOI. The periodicity in 1985 was found between periods 2-8, differently from the SOI analysis. Another significant area was observed from 4 to 8 around 1945 and 1950.

In-phases (ASTLSW lagging behind RWI) periodicities were found in the ATLSW and Chapecó RWI WTC in (Figure 61d) the 2-4 period (1915-1920 and 1985-1990) and in the 16-32 (1910-1960). Again, no similar periodicities were found with the previously analyzed RWIs (Açungui and Canela).

Figure 61e shows a very strong anti-phase influence of precipitation in the Chapecó RWI from 2-8 periods between 1980 and 1990. This is expected since the analyzed species (*Araucaria angustifolia*) tends to suffer with the increase in precipitation, affecting its growth. The 1980 periodicity is also found in the Açungui WTC response to precipitation. The result suggests a possible interaction of local and regional climate systems, such as the SACZ and atmospheric circulation patterns.

Chapecó RWI has a strong influence by the maximum temperature (Figure 61f) in the periods 2-4 around 1977 and from 1987 to 199 (in-phase with RWI lagging behind TMAX); two small influences in the period 2-4 for mean temperature (Figure 61h) located between 1987 to 1997 (in-phase with TMEAN lagging behind RWI), and nothing was obtained for minimum temperature (Figure 61g). Due to the strong anti-phase influence of precipitation, it is expected that the increase in temperature can keep a balance in the quantity of water acquired by the trees.

Coxilha City:

In Figure 62a, the WTC between Coxilha RWI and Sunspot is displayed. As in the previous sunspot analysis, small significant regions between 2-4 (1890, 1950 in-phase with Sunspot lagging behind RWI, and 1975 anti-phase with Sunspot also lagging) were obtained. Around 1950 there is also a significant region between the periods 4 and 8. And the Schwabe Cycle (8-16 period) appears here again between 1900-1925, with a positive correlation, close to the time period where Açungui RWI also responds to the Sunspot number. Furthermore, there is a full-time period significant answer between periods 32 and 64, where both time series are in-phase. The study of (PRESTES et al., 2018b) provides the possibility of a combination between the Hale and the Gleissberg cycle exactly in this time period.

For Coxilha RWI and SOI WTC (Figure 62b), there are several significant regions between the periods 2 to 8, around 1900, 1910, 1920, 1940, 1970, and 1980, and a longer period from 1945 to 1965 (in-phase with RWI lagging behind the NIÑO 3.4). The periods between 8 and 16 present a small region around 1955 and an in-phase region from 1980 to 1995 (in-phase similarly with RWI lagging behind the NIÑO 3.4).

The NIÑO 3.4 periodicities in the Coxilha RWI (Figure 62c) are very similar to the periodicities found in the SOI analysis but with opposite phases to the areas where was obtained the phase arrows. The differences are that some areas extend to the 8-16 periods and 3 areas presented in period 2 around 1910, 1915, and 1925.

Periodicities related to ATLSW were found in the Coxilha RWI (Figure 62d). Between the periods 2-4, the significant areas correspond to the years 1815 (in phase), 1825 (anti-phase), and, similarly to Chapecó, there are periodicities in 1915 and 1985-1995 (anti-phase). Between periods 2 to 8, there is one significant region around 1935. And between periods 4 to 16, there is a strong in-phase (RWI lagging behind ATLSW) periodicity from 1875 to 1935.

Figure 62e shows a small periodicity with precipitation around the period 2 in 1970, and a strong intensity between 2-8 periods from 1987-2002 in phase. Açungui, Canela, and Chapecó RWI also showed some of the periodicities found here. Systems such as the SACZ, the MJO, the ITCZ and the Chaco Low play a role in varying precipitation conditions in the region , which in turn can affect tree growth.

The temperature, time series (Figures 62f, g, and h) obtained similar periodicities between the periods 2-4 from 1975-1980 and between 4-8 from 1995-2000. The maximum temperature still has a strong influence in the Coxilha RWI between periods 4-8 from 1970 to 1983. Some regional climate systems and climate phenomena, such as the SACZ and variations in atmospheric circulation, may be related to these temperature variations.

Curitibanos City:

The WTC analysis between Sunspot and Curitibanos RWI (Figure 63a) shows

the same pattern of significant regions between periods 2 and 8, that it was found in the previous sunspot analysis. Here, the in-phase regions occur around 1970 and around 2005, an anti-phase region between 1980-1990 (RWI lagging behind Sunspot), and there is a significant region around 1990. The Schwabe Cycle also appears in this analysis between the years 1960 and 2005 in anti-phase, where Agunçui, Canela, and Chapecó also presented significant regions.

The relationship between Curitibanos RWI and the Southern Oscillation Index (SOI) was examined in Figure 63b. Noteworthy regions of significance were identified within the 2 to 8-year period range, spanning approximately 1955, 1970-1975 (in anti-phase, RWI lagging behind SOI), 1970-1985, 1985 (in-phase, SOI lagging behind RWI), and 1990-2000. Some of these influences align with findings from previous cross-wavelet coherence analyses of RWI and SOI. Additionally, an anti-phase relationship (RWI lagging behind SOI) was observed around the year 2000 within the 8 to 16-year period range.

Figure 63c presents the analysis for the NIÑO 3.4, showing exactly the same periodicities found in the SOI analysis, but similarly to other cities, they are in opposite phases.

Curitibanos RWI has periodicities of ATLSW (Figure 63d) between the periods 2-4, from 1980 to 1990 and from 2000 to 2005. Some of the same years were obtained in Açungui (~ 1980) and in Coxilha and Chapecó (~ 1985-1990).

As discussed previously, it wasn't possible to analyze Curitibanos RWI with precipitation and temperature due to the short length of the climatic time series.

General Carneiro City:

The WTC between SUNSPOT and General Carneiro RWI (Figure 64a) shows small regions between periods 2 and 4 (the same as the other cities). Two regions between 8 and 16 periods, one around 1800 and another from 1925 to 1960 (anti-phase, RWI lagging behind Sunspot) correspond to the Schwabe Cycle, also found in the WTC in Açungui, and Coxilha RWIs. A longer significant region was found between the periods 16 and 32, from 1840 to 1900, probably related to the Halee Cycle, in a similar time period as in the analysis for Canela RWI.

SOI periodicities were found in the WTC analysis (Figure 64b), especially between periods 2 and 8, around the years 1965, 1970, 1975, and 1980 (in-phase, SOI lagging behind RWI). Again, similar to the previous SOI analysis for other cities. Between periods 8-16, the periodicities are located from 1925-1945 and around 1975. The years 1925-1930 were also part of the Açungui periodicities of SOI.

General Carneiro RWI responded to NIÑO 3.4 (Figure 64c) similarly to the SOI, with opposite phases. A few more significant regions can be found in the periods from 2 to 8. There is also a strong periodicity from 16-32 periods between 1875 to 1900 and

another periodicity in period 32 from 1945-1975. An interesting aspect of this graphic is that all graphics that present arrows are in anti-phase. All phases indicates NIÑO 3.4 lagging behind RWI.

General Carneiro RWI presents several periodicities related to the ATLSW in Figure 64d. They are presented in periods from 2 to 4 (1945, 1955, and 2000), from 4 to 8 (1880-1890, 1905, and 1955-1975), in-phase from 4-16 (around 2000), between 8 and 16 (around 1950), anti-phase between the periods 16-32 (1875-1910, with ATLSW lagging behind RWI) and an in-phase around the period 32 (from 1915 to 1970, with RWI lagging behind ATLSW). Some of these periods were also present in Açungui, Canela, Chapecó, and Curitibanos WTC.

No influences of precipitation were found in the General Carneiro RWI (Figure 64e), this may be caused by the lack of climatic series close to the analyzed region, and/or to the several GAPS in the time series, or to the other climatic parameters having a stronger influence in the tree growth.

The maximum temperature (Figure 64f) shows a strong anti-phase influence during the years in the period band from 4 to 8, and a strong in-phase periodicity from periods 2-4 between 1973 to 1982 years, with RWI lagging behind TMAX in all periodicities. The minimum temperature (Figure 64g) seems to have a small effect around 1975 in the 4-8 period band,and similarly to TMAX, RWI is lagging. And the mean temperature (Figure 64h) presented the same periodicity from 1973 to 1982. Again, here it is possible to notice that while the temperatures seem to be very strongly influencing the RWI of General Carneiro, the precipitation presented zero influence, probably indicating that temperature is one of the main limiting factors in the regions where these trees were collected.

Irani City:

Similar to the WTC analysis between Açungui RWI and Sunspot (Figure 65a), small regions of statistical significance are observed in the WTC analysis between the Irani RWI and Sunspot Activity at periods 2 to 8. Two significant coherence regions are identified for the period 8 to 16. The first region, centered around 1840, does not exhibit any arrows, implying that during this time, the relationship between the Irani RWI and Sunspot is not characterized by a specific phase direction. The second coherence region, centered around 1975, shows arrows pointing to the left, in other words, a negative correlation (anticorrelation). And differently from Açungui city, here there is a single coherence region around 1850 observed in periods 16 to 32 (left-pointing arrow meaning that RWI is lagging behind Sunspot).

Irani (Figure 65b) showed periodicities in the period of 2 around 1945 and 1990 anti-phase. Between the periods 4 to 8, periodicities were found around 1880, 1895-1905, 1900-1910. And more periodicities from 8 to 16 periods, around the years 1885-1910

(anti-phase, SOI lagging behind RWI) and again in 1995. The significant responses found for periods between 2 to 8 were mostly similar in years compared to the other cities' analysis. For the period 8-16, Açungui, Canela, and Coxilha also obtained some similar years.

Irani RWI obtained periodicities (Figure 65c) in some similar years as the SOI, but much more was found here. Between 2 and 8 periods, the significant areas were found around 1875, 1900, 1915, 1945 (anti-phase), and 1985. Between the 4 and 16 periods there is a strong periodicity from 1900 to 1925. A similar anti-phase region that appeared in period 16 of the SOI is also found here but from 1900 to 1930.

Figure 65d presents the ATLSW periodicities in the Irani RWI from periods 2 to 4, from 1965-1980 and 1985 (in-phase); and from 4-16 a strong periodicity from 1920-1960 in anti-phase; a small significant area was found around the period 4 in 1910. Similar periodicities were found among the ATLSW responses to the previous cities analyzed until here.

Similarly to General Carneiro WTC with precipitation (Figure 65e), Irani RWI does not present significant areas.

The maximum temperature (Figure 65f) seems to be lagging in relation to the RWI of Irani. since it has the same time period as the mean temperature (Figure 65h) in the 4-8 period band. The minimum temperature (Figure 65g) presented influence during the same period, but it is in phase (RWO lagging behind TMIN) and in a shorter time, indicating that the trees might have positive growth responses to cold temperatures.

Irineópolis City:

Several significant regions were found in the WTC analysis between Sunspot and Irineópolis RWI (Figure 66a). Similarly to the other WTC RWIs with Sunspot, small regions were found between periods 2 to 4. A bigger in-phase (RWI lagging behind Sunspot) region can be seen in between periods 2 to 8 around 1775. Schwabe Cycle influence the RWI around 1825 and from 1900 to 1950, similar time periods were obtained for Açungui, Coxilha, and General Carneiro RWIs. The Halee Cycle is influencing the RWI from 1950 to 1975, like the Canela RWI response.

Irineópolis presented periodicities with SOI (Figure 66b) between the periods 2-4 around 1870, 1915 (anti-phase), 1930 (anti-phase, SOI lagging behind RWI), 1945 (in-phase, RWI lagging behind SOI), and 1980, similar to the other cities responses. The periods from 4 to 8 also presented periodicities around 1880, 1940, 1990 and from 1975-1990. Another periodicity can be seen between 16-32 from 1955-1960. Canela, Chapecó, and Coxilha RWIs also presented periodicities in similar years for the period 4-16, and in Canela for the period 16-32.

For the NIÑO 3.4 periodicities in Irineópolis RWI, Figure 66c shows just a few

regions were found, and all of them are also present in the SOI analysis for Irineópolis.

Figure 66d presents the ATLSW periodicities found in the Irineópolis RWI, mainly anti-phase between the periods 2 to 4 (1905 and 1975-1985), and in the periods 16-32 (from 1905 to 1930). The short periods were also found in the other ATLSW WTC analysis for other RWIs. On the other hand, periodicities from 16-32 in similar years were only found in the Chapecó and the General Carneiro RWI.

There is a strong anti-phase influence of the precipitation (leading) in the Irineópolis RWI (Figure 66e) between 1974 to 1986 around the periods 2-4. A few of these periodicities were found in Canela and Chapecó RWIs' responses to precipitation. The influence of precipitation may be related to several listed weather systems, such as the SACZ or the MJO, which may affect rainfall patterns in the region.

For Irineópolis RWI, the maximum temperature (Figure 66f) presented a periodicity around the period of 4 from 1977 to 1985. minimum temperature (Figure 66g) also presented an anti-phase leading influence in RWI but in the 2-4 period, from 1972 to 1977. And mean temperature (Figure 66h) did not show any influence on the RWI, indicating that the precipitation level with cold temperatures leads the trees to not have optimal growth.

Passo Fundo City:

The Sunspot and Passo Fundo RWI WTC analysis is displayed in Figure 67a. Small significant regions exist between 2 and 8 periods. Schwabe Cycle influenced the RWI around 1780, 1950 (also found in Açungui, Canela, General Carneiro, and Irineópolis RWIs), and around 1980 (similarly found in Açungui and Curitibanos RWIs). And the Halee Cycle was identified around the year 1800.

In Passo Fundo WTC (Figure 67b) analysis with SOI, periodicities between 2-8 periods were found in 1875-1900 (the first half period is anti-phase with RWI lagging and the second half is in-phase with SOI lagging), 1920 (anti-phase with RWI lagging), and around 1945. Between 8-16 periods periodicities were found around 1905-1925, 1930, and 1975-1985 (anti-phase and SOI lagging in relation to RWI). The periodicities of the 8-16 periods presented similar years as in Açungui, Canela, Chapecó, Coxilha, General Carneiro, Irani, and Irineópolis analysis. It is likely that other long-term phenomena are acting in conjunction with the SOI, such as the influence of solar cycles, oceanic patterns such as the Pacific Decadal Oscillation (PDO) that influence precipitation in these regions.

The NIÑO 3.4 periodicities (Figure 67c) in Passo Fundo RWI show a slight similarity to the SOI WTC analysis. From 2 to 8 periods, there are periodicities during 1860, 1865, 1880 (anti-phase), 1890-1900 (anti-phase), and 1910-1920 (anti-phase). The periods from 8 to 16 also present a periodicity from 1890-1925 (similarly to Chapecó, Irineópolis, and General Carneiro RWIs).

Figure 67d presents ATLSW periodicities in Passo Fundo RWI between 2-4 periods

around 1875 (in-phase) and in 1980; between the periods 8-16 from 1880 to 1895, around 1945 and 1970; and in the 16-32 periods from 1920 to 1955.

Precipitation periodicities in the Passo Fundo RWI (Figure 67e) were obtained between periods 2 to 4, around 1970-1972 and 1982, and between periods 4 to 8 around 1970. Similar periodicities were obtained for most of the other RWIs analyzed (Açungui, Canela, Chapecó, Coxilha, and Irineópolis). The analyzes show that several of these cities presented similar periodicities in both SOI/NIÑO 3.4 and precipitation, in terms of specific years in which the variations occurred. This suggests that fluctuations in *El Niño/La Niña* conditions, represented by SOI/NIÑO 3.4, may be related to precipitation patterns in the analyzed regions.

The mean temperature periodicities (Figure 67h) found in the WTC for Passo Fundo RWI are located between the periods 2-6 , around the years 1977 (in-phase), 1982, 1986-1992 (in-phase, RWI lagging behind TMEAN), and 1995 (anti-phase, where RWI is lagging). maximum temperature (Figure 67f) presented the same periodicity in the year 1982 where RWI is lagging behind TMAX, and the minimum temperature (Figure 67g) presented the same periodicity around the year 1995 (anti-phase).

São Franciso de Paula City:

The WTC between Sunspot and São Francisco de Paula RWI (Figure 68a) presents the same small regions as for the other cities' responses, between the periods 2 and 4, during 1890-1900 (with an anti-phase lag of Sunspot), and around 1945. Two more periodicities where found between 4 and 8 bands, in 1950-1960, and a in-phase periodicitie during 1970-1980.

São Francisco de Paula WTC analysis with SOI (Figure 68b) presents similar periodicities between 2 and 8 periods as the other cities, mostly every 5-10 years, around 1900, 1910, 1915, 1930 (in-phase), 1935, 1950-1960 (anti-phase, where the SOI is lagging in relation to the RWI), 1985, and 1995 (in-phase).

The WTC analysis of NIÑO 3.4 and São Francisco de Paula RWI (Figure 68c) showed similar regions found in the SOI analysis (1930, 1950-1960, 1985, and 1995). Moreover, the period of 16 shows a strong in-phase periodicity from 1930 to 1985 where the RWI is lagged in relation to NIÑO 3.4.

Figure 68d presents very few periodicities, from 2-4 periods around 1900 and 1930 (anti-phase, ATLSW lagged in relation to the RWI); in 1920 between 8-16 periods; and around 1945 between 16-32 periods. It does not show much influence of the ATLSW in the tree ring development of the trees in the São Francisco de Paula RWI analysis, or maybe other parameters are influencing more the RWI signals. For periodicities of 2-8 periods, the SOI, NIÑO 3.4 and ATLSW analyzes present some common dates, such as 1930, 1950-1960 and 1985, where significant oscillations occur. Furthermore, some oscillations

are in-phase, while others are anti-phase, indicating coordinated or opposite variations in the time series.

São Francisco de Paula RWI presented only two periodicities related to precipitation (Figure 68e). One in anti-phase around 1962 in the period of 2, where RWI is leading in relation to precipitation. And a small periodicity around 1965, between the periods 8 to 16.

The maximum temperature (Figure 68f) presented stronger periodicities compared to the mean and minimum. The periodicities were found in the periods from 2 to 4 around 1985 (anti-phase, TMAX lagging in relation to the RWI), from 2 to 6 around 1990-1997, and from 6 to 8 around 1968-1977. minimum temperature WTC (Figure 68g) captured a periodicity from 2-4 periods around 1990. The mean temperature (Figure 68g) basically responded in the same periods as maximum temperature but in the years 1975-1980 (2-4 periods), anti-phase during 1987-1997 (2-6 periods), and around 1970 (6-8 periods).

Overview:

The solar activity effects in tree-ring growth were also studied in Southern Brazil (Passo Fundo city) by Rigozo et al. (2012), where they obtained similar short-term periodicities between the period 2-8 similar to what was obtained in all Sunspot CWTs. When long-term responses were found in the analysis, they were generally between the period 16-32, indicating a Halee Cycle influence, and again similarly to what Rigozo et al. (2012) found in their study. In the study of Lorensi (2016), most of the periodicities found in the RWI from Southern Brazil of *Araucaria angustifolia* correspond to the Schwabe Cycle. Moreover, the Schwabe Cycle was also found in other dendrochronological series from Southern Brazil, indicating that this region is affected by the short-term solar cycles (RIGOZO et al., 2004; MURAJA et al., 2023).

The normal periods of frequency where the SOI responds during a time-frequency analysis are between 2 and 8, mostly between 4 to 8. In the study of Lorensi (2016) the second most common periodicity found in the *Araucaria angustifolia* RWI was the SOI. The years with periodicities obtained here agree with the findings in Muraja et al. (2023), where they used a different species (*Ocotea Porosa Barroso*) to analyze the city of General Carneiro, Southern Brazil. Similar periodicities were also found in the study of Rigozo et al. (2012), where they also analyzed other regions of Brazil besides the South. Similar SOI periodicities were also found when analyzing the Amazon region and a different species, but it is important to highlight that the ENSO events have opposite effects in Southern and Northern Brazil (SCHÖNGART et al., 2004).

There are still few studies using the NIÑO 3.4 index with dendrochronological series, which is one of the reasons this study presents this analysis. Recently, a significant negative relationship between NIÑO 3.4 region and tree-ring chronology was found by

Granato-Souza et al. (2018), mostly after 1970, but they analyzed a different species (*Alchornea triplinervia*) in Southern Brazil. In the study of Schöngart et al. (2004), Muraja et al. (2023) they also obtained similar frequency bands for the SOI when performing a cross-wavelet coherence analysis.

Both SOI and NIÑO 3.4 are indexes used to refer to the ENSO events. *El Niño* events of Canonical type can be also named the "Eastern Pacific type", the mature phase of ENSO has observations during 1905-06; 1911-12; 1918-19; 1930-31; 1939-40; 1972-73; 1976-77; 1982-83; 1986-87; and 1997-98 according to the study of Viegas et al. (2019). All the ENSO events are observed in the results of this thesis analyzing the periods from 2 to 8, where it is expected to have the ENSO frequency.

As reported by Viegas et al. (2019), between the years 1905 and 1998, there were 10 observed *El Niño* events of the Eastern Pacific-type (or Canonical-type), 5 of which correspond to the years of periodicities found in the chronology (1911–1912, 1918–1919, 1976–1977, 1982–1983, and 1986–1987). Additionally, 14 Central Pacific-type (or Modoki-type) *El Niño* events were observed between 1902 and 2005, but only one event (1914–1915) occurred within the periodicities found in this study. This may indicate a positive response in tree growth to Eastern Pacific-type *El Niño* events, as they cause higher precipitation levels in Southern Brazil due to their propagation further westward to the Eastern Equatorial Pacific from the coast of South America, as explained in Rasmusson & Carpenter (1982).

Most of the RWIs presented periodicities related to the ATLSW, especially in the 2-4 and 4-8 period bands. The studies of Silva (2018), Muraja et al. (2023) analyzed the relationship between the ATLS and tree-ring chronologies for General Carneiro using the *Ocotea Porosoa Barroso* species, they also found most of its periodicities between the band 2-4. A reason for the existence of the 4-8 periods in the present thesis may be related to the different locations between the ATLSW and ATLS, here the ATLSW is being used.

The periodicities related to precipitation were obtained mostly from periods 2 to 4 and 4 to 8, in sporadic years and two cities (General Carneiro and Irani) did not show the influence of the precipitation. This goes accordingly to the results obtained by Rigozo et al. (2012), Silva (2018). The climate in the southern region of Brazil is affected by several factors. The MJO, a tropical oscillation pattern, can bring intense rains or droughts, depending on the phase it is in. High and low atmospheric pressure systems also play an important role, bringing climate stability or instability. Additionally, ocean currents, such as the Brazil Current, impact SSTs and influence coastal weather patterns. The region's topography, including mountains and mountain ranges, plays a role in air circulation and local climate variations. These factors, together with other climate systems, interact in complex ways to shape the varied and dynamic climate of the southern region of Brazil, and can influence the non-linear signals that Cross Wavelet Coherence seeks to identify.

An interesting finding here is that temperature influences in the RWIs started after the year 1960, maybe as a response to the intensive logging activity in the area and cities development (industry, land use, etc), which changed the characteristics of the forests and the environment around the location of these trees (CABRAL; CESCO, 2008; MATOS et al., 2016; NODARI, 2016). Most negative and strong periodicities are related to the maximum temperature, for example in Curitibanos RWI where there is a 45 years of anti-phase periodicity. It is important to note that only analyzing the mean temperature of a region can mask the real influence of the temperatures. In this study, the minimum temperature did not show much influence on the RWI, which can also reflect in the lower responses to mean temperatures. Moreover, the RWIs which presented strong periodicities with the temperature presented a low relationship with the precipitation. This anti-phase relation between temperature and tree growth can be related to temperature-induced stress since it causes high levels of evapotranspiration, decreasing the air-water potential, which is common in tropical regions, and can decrease the tree-ring development rate, as discussed by Rolland (1993), Locosselli, Schöngart & Ceccantini (2016).

The book of Gadow, Pukkala & Tomé (2000) discusses the important information to develop forest management practices, as a collection of papers. The ecological considerations in forestry have an important role, especially on a planet going through climate change and loss of biodiversity. For this thesis, the trees' responses to the solar and ocean-atmosphere parameters can be valuable when developing this sustainable forest management practice, since it gives information on how trees responded during the years to specific patterns.

Several climate systems operate in the South region, including the MJO, SACZ, and ITCZ, among others. These systems can indeed impact tree growth in the region, as they directly affect climate variability, specifically precipitation levels and temperature regulation—two essential factors for the development of trees.

Analyzing the relationship between tree growth and climate in the region poses challenges due to the limited number of climate stations available. As a result, researchers often use the nearest stations that fall within the same Köppen climate classification as the study location. However, it's crucial to acknowledge that regional characteristics, such as variations in topography, can introduce complexities into the analyses, as these factors may differ even within the same climate classification.

4.4 HIGHLIGHTS

The main results (highlights) of this thesis are:

1. The research addresses how solar activity, ENSO events and climate variables influence the growth of tree rings in southern Brazil, with implications for studies on climate change and tree growth dynamics in the region.

2. Canela was identified as having a consistent tree response to one limiting factor, while other sites may have additional factors or small dating errors.

3. Short- and long-term periodicities have been observed in tree ring time series, possibly representing the Schwabe Cycle and the Hale Cycle, respectively.

4. ENSO events, such as *El Niño*, can influence tree growth in the region, affecting precipitation levels.

5. After 1960, temperature began to have a more significant impact on tree growth, possibly related to changes in forest and land use.

6. The quality of climate data is an important consideration for future studies.

5 CONCLUSIONS

Overall, this thesis contributes to the understanding of how solar activity, ENSO events, and climate variables influence tree-ring growth in southern Brazil. The findings underscore the importance of considering these factors in dendrochronological research and provide valuable information for future studies on climate change and tree growth dynamics in the region.

In the analysis of the EPS values for each RWI, only CAN RWI presented an EPS value (0.84) close to 0.85. This suggests that the trees collected in Canela are responding to a consistent limiting factor, leading to well-dated chronologies. Despite the lower EPS values for the other RWIs, it is crucial to emphasize that climate does indeed influence the trees in this region, and the statistics presented here only suggest the presence of additional limiting factors among the trees studied or small dating errors. The periodicities in time series are not as sensitive to dating errors as the linear correlations, so when applying the WTC, the cycles can still be visible in the time series even if the rings are a few years off.

The WTC findings revealed probable significant short-term periodicities in tree-ring growth between the periods of 2-8, and ~ 11 periods consistent with the Schwabe Cycle observed in other dendrochronological studies. Long-term responses were also detected, particularly in the period 16-32, indicating a Hale Cycle influence, which aligns with other research in the area.

The SOI and the NIÑO 3.4 index, both associated with ENSO events, were also analyzed, and their periodicities (2-8 years) corresponded to those found in the tree-ring chronology. This suggests that ENSO events play a role in influencing tree growth in the region, with El Niño (negative phase) events of the Eastern Pacific type potentially leading to higher precipitation levels in southern Brazil.

The study provided valuable insights into the relationship between the ATLSW and tree-ring growth, with most periodicities observed in the 2-4 and 4-8 periods. This information adds to the limited existing research on the interaction between ATLSW and tree-ring chronologies.

Regarding climate variables, temperature showed a more pronounced impact on tree-ring growth after the year 1960, possibly due to changes in forest characteristics and land use in the region during that period. The study highlighted that higher temperatures led to strong negative responses in tree growth, particularly evident in Curitibanos RWI with a 45-year anti-phase periodicity. Additionally, an opposite-phase relationship between temperature and precipitation responses was observed, indicating potential temperature-induced stress on tree growth in tropical regions, after the water availability by evapotranspiration.

Furthermore, the analysis of temperature and precipitation data demonstrated varying responses in different RWIs for different time scales. The mean temperature analysis showed diverse regional responses, indicating that the impact of temperature and precipitation on tree-ring growth varies across different periods and locations. It's worth noting that the climatic data suffer from data gaps, which can introduce complexities in the interpretation of results.

In general, the trees collected in southern Brazil seem to suffer significant influences from solar activity's short-term periodicities (2-8 years) and long-term responses (16-32 years) in tree-ring growth. These long-term periodicities align with the Hale Cycle. ENSO events, particularly El Niño (negative phase) events in the Eastern Pacific, may influence tree growth in the region by potentially leading to higher precipitation levels. Insights into the relationship between the ATLSW and tree-ring growth were obtained with periodicities in the 2-4 and 4-8 year range, which could be further investigated for other tree-ring series in southern Brazil in order to better understand its effects on the region's climate. After the year 1960, temperature appeared to have a more pronounced impact on tree-ring growth, potentially related to changes in forest characteristics and land use in the region. However, the presence of missing data in climatic series highlights the need for further data quality improvement in future studies. The thesis provides valuable insights into the complex interactions between solar activity, ENSO events, climate variables, and tree-ring growth in southern Brazil. These findings have implications for dendrochronological research and contribute to the understanding of climate change impacts on tree growth dynamics in the region.

This thesis offers a substantial contribution to the comprehension of the factors influencing tree-ring growth in southern Brazil. It unveils the roles in tree-growth of solar activity, ENSO events, climate variables, and possible action of climatic systems, including the MJO. Through an analysis of short-term and long-term periodicities, such as the Schwabe Cycle and Hale Cycle, it enriches our understanding of the complex interplay of these factors. The study also highlights the potential impact of El Niño events in the Eastern Pacific on tree growth. The increasing influence of temperature on tree-ring growth after 1960 and the importance of improving data quality in climatic series are noteworthy findings. In conclusion, this research deepens our insights into the multifaceted interactions shaping tree-ring growth dynamics in the region, with broader implications for dendrochronological studies and a better understanding of how climate change affects tree growth patterns.

As future research, the chronologies EPS can be improved by incorporating additional series, particularly in the Canela and São Francisco de Paula regions. These new series can be derived from tree images already captured by Daniela Muraja, Cecília Lemes Leite (scientific initiation student at the Laboratory of Natural Records) and Wandeclayt

Melo (specialist in high-speed video and scientific images at the Image Registration Laboratory of the Brazilian Institute of Aeronautics and Space). Furthermore, develop climatic reconstructions of chronologies that exhibit an EPS (Expressed Population Signal) higher 0.85 after the improvement will allow to deepen the understanding and provide a more comprehensive analysis of the climatic patterns in southern Brazil associated with these tree-ring datasets.

REFERENCES

ACEITUNO, P. On the functioning of the southern oscillation in the south american sector. part i: Surface climate. *Monthly Weather Review*, American Meteorological Society, Boston MA, USA, v. 116, n. 3, p. 505 – 524, 1988.

AKASOFU, S.-I. Aurora. In: *From the sun: Auroras, magnetic storms, solar flares, cosmic rays*. [S.l.]: American Geophysical Union, 1998.

ANDRADE, K. M. *Climatologia e comportamento dos sistemas frontais sobre a América do Sul*. Dissertação (Masters Dissertation) — Instituto Nacional de Pesquisas Espaciais - INPE, São José dos Campos - São Paulo, Brazil, 2005.

ARNFIELD, A. J. *Köppen climate classification. Encyclopedia Britannica.* 2023. Disponível em: <https://www.britannica.com/science/Koppen-climate-classification>.

BJERKNES, J. A possible response of the atmospheric hadley circulation to equatorial anomalies of ocean temperature. *Tellus*, v. 18, n. 4, p. 820–829, 1966.

BOBERG, F.; LUNDSTEDT, H. Solar wind variations related to fluctuations of the north atlantic oscillation. *Geophysical Research Letters*, v. 29, p. 1718, 2002. Related online version (cited on 06 September 2007). Disponível em: <https://ui.adsabs.harvard.edu/abs/2002GeoRL..29.1718B/abstract>.

BRADLEY, R. S.; JONEST, P. D. "little ice age" summer temperature variations: their nature and relevance to recent global warming trends. *The Holocene*, v. 3, n. 4, p. 367–376, 1993.

BRASIL. *Ministério do Meio Ambiente. Instrução normativa nº 6 de 23 de setembro de 2008. Lista as espécies da flora brasileira ameaçadas de extinção e com deficiência de dados*. Brasília, DF, 2008. N. 185, seção 1, p. 75-85.

BREHM, N. et al. Eleven-year solar cycles over the last millennium revealed by radiocarbon in tree rings. *Nature Geoscience*, v. 14, 2021.

BRIENEN, R. J. W.; ZUIDEMA, P. A. Relating tree growth to rainfall in bolivian rain forests: a test for six species using tree ring analysis. *Ecophysiology*, 2005.

BRIFFA, K. et al. A 1,400-year tree-ring record of summer temperatures in fennoscandia. *Nature*, v. 346, p. 434–439, 1990.

BROWNING, K. A. Conceptual models of precipitation systems. *Weather and Forecasting*, American Meteorological Society, Boston MA, USA, v. 1, n. 1, p. 23 – 41, 1986. Disponível em: <https://journals.ametsoc.org/view/journals/wefo/1/1/1520-0434_1986_001_0023_cmops_2_0_co_2.xml>.

BUNN, A. *dplR: Dendrochronology Program Library in R*. [S.l.], 2020. Available at: https://cran.r-project.org/web/packages/dplR/dplR.pdf.

BUNN, A. G. A dendrochronology program library in r (dplr). *Dendrochronologia*, v. 26, n. 2, p. 115–124, 2008. ISSN 1125-7865. Disponível em: <https://www.sciencedirect.com/science/article/pii/S1125786508000350>.

BUSCH, P.; HEINONEN, T.; LAHTI, P. Heisenberg's uncertainty principle. *Physics Reports*, v. 452, n. 6, p. 155–176, 2007. ISSN 0370-1573.

CABRAL, D. d. C.; CESCO, S. Notas para uma história da exploração madeireira na mata atlântica do sul-sudeste. *Ambiente & Sociedade*, ANPPAS - Revista Ambiente e Sociedade, v. 11, n. 1, p. 33–48, Jan 2008. ISSN 1414-753X. Disponível em: <https://doi.org/10.1590/S1414-753X2008000100004>.

CARVALHO, S. M.; STIPP, N. A. F. Contribuição ao estudo do balanço hídrico no estado do paraná: Uma proposta de classificação qualitativa. *Geografia*, v. 13, n. 1, 2004.

CATTANEO, F. et al. Climate signals in tree-ring widths of araucaria angustifolia in an altitudinal gradient in southern brazil. *Trees*, v. 27, n. 5, p. 1329–1338, 2013.

CAVALCANTI, I. F. A. *Casos de intensa precipitação nas Regiões Sul e Sudeste do Brasil no período de inverno de 1979 a 1983*. São José dos Campos - São Paulo, Brazil, 1985.

CAVALCANTI, I. F. A. et al. The south american monsoon system and the 1970s climate transition. *International Journal of Climatology*, Wiley Online Library, v. 31, n. 9, p. 1248–1256, 2011.

CHEN, W.; ZHOU, Q. Modulation of the arctic oscillation and the east asian winter climate relationships by the 11-year solar cycle. *Advances in Atmospheric Sciences*, v. 29, p. 1861–9533, 2012.

COOK, E. et al. Tree-ring standardization and growth-trend estimation. *Methods of Dendrochronology: Applications in the Environmental Sciences*, 01 1990.

COOK, E. R. *A Time Series Analysis Approach to Tree Ring Standardization*. Dissertação (Mestrado) — University of Arizona, 1985.

CORREA-DíAZ, A. et al. Linking remote sensing and dendrochronology to quantify climate-induced shifts in high-elevation forests over space and time. *Journal of Geophysical Research: Biogeosciences*, v. 124, n. 1, p. 166–183, 2019.

CORREA-DíAZ, A. et al. From trees to ecosystems: Spatiotemporal scaling of climatic impacts on montane landscapes using dendrochronological, isotopic, and remotely sensed data. *Global Biogeochemical Cycles*, v. 34, n. 3, p. e2019GB006325, 2020.

COZZO, D. Distribución fitogeográfica en la argentina de araucaria araucana y a. angustifolia. In: FUPEF. *Meeting on Forestry problems of the genus Araucaria*. Curitiba, Brazil, 1980. v. 1, p. 1–3.

CROWLEY, T. J. Causes of climate change over the past 1000 years. *Science*, v. 289, n. 5477, p. 270–277, 2000.

DELONG, K. L. et al. Improving coral-base paleoclimate reconstructions by replicating 350 years of coral sr/ca variations. *Palaeogeography, Palaeoclimatology, Palaeoecology*, v. 373, p. 6–24, 2013. ISSN 0031-0182. Unraveling environmental histories from skeletal diaries - advances in sclerochronology. Disponível em: <https://www.sciencedirect.com/science/article/pii/S0031018212004956>.

DIAZ, A. F.; STUDZINSKI, C. D.; MECHOSO, C. R. Relationships between precipitation anomalies in uruguay and southern brazil and sea surface temperature in the pacific and atlantic oceans. *Journal of Climate*, American Meteorological Society, Boston MA, USA, v. 11, n. 2, p. 251 – 271, 1998.

DITTBERNER, M. R. Causas e efeitos das turbulências nas operações aéreas do aeroporto internacional hercílio luz. Graduation Monograph. Departamento de Geografia - Universidade Federal de São Carlos - UFSC. 2001.

DOUGLASS, A. E. *Climatic Cycles and Tree-Growth. A Study of the Annual Rings of Trees in Relation to Climate and Solar Activity*. Washington: the Carnegie Institution of Washington, 1919.

DRISHTIIAS. *Climatic Regions of World: Part-I*. 2022. Disponível em: <https://www.drishtiias.com/to-the-points/paper1/climatic-regions-of-world-part-i>.

DUBREUIL, V. et al. Climate change evidence in brazil from köppen's climate annual types frequency. *International Journal of Climatology*, v. 39, n. 3, p. 1446–1456, 2019.

DUTRA, T. L.; STRANZ, A. História das araucariaceae: a contribuição dos fósseis para o entendimento das adaptações modernas da família no hemisfério sul, com vistas a seu manejo e conservação. In: _____. [S.l.]: São Leopoldo: UNISINOS, 2003. cap. Tecnologia, diagnóstico e planejamento ambiental.

ECHER, E. et al. O Número de Manchas Solares, Índice da Atividade do Sol. *Revista Brasileira de Ensino de Física*, scielo, v. 25, p. 157 – 163, 06 2003. ISSN 1806-1117. Acesso em 23 de novembro de 2019. Disponível em: <http://www.scielo.br/scielo.php?script=sci_arttext&pid=S1806-11172003000200004&nrm=iso>.

EDU, C. *Monitoring ENSO*. 2023. Accessed on July 5, 2023. Disponível em: <https://iridl.ldeo.columbia.edu/maproom/ENSO/Diagnostics.html>.

EL-RAMADY, H. et al. *Contemporary Environmental Readings Volume 1 Climate Change A Blessing or a Curse for Agriculture*. [S.l.: s.n.], 2012.

EPSKAMP, S.; FRIED, E. I. Psychological methods. *A tutorial on regularized partial correlation networks*, v. 23, n. 4, p. 617–634, 2018.

FOUKAL, P. Solar irradiance variations and climate. In: *From the sun: Auroras, magnetic storms, solar flares, cosmic rays*. [S.l.]: American Geophysical Union, 1998.

GADOW, K. von; PUKKALA, T.; TOMé, M. *Sustainable Forest Management*. [S.l.]: Kluwer Academic Publishers, 2000.

GARREAUD, R. D.; BATTISTI., D. S. Interannual (enso) and interdecadal (enso-like) variability in the southern hemisphere tropospheric circulation. *Journal of Climate*, v. 12, p. 2113–2123, 1999.

GLEISSBERG, W. A long-periodic fluctuation of the sun-spot numbers. *Observatory 62*, v. 62, p. 158–159, jun 1939.

GOERGEN, L. C. B. et al. Análise de registros naturais em anéis de árvores com relação aos parâmetros meteorológicos locais. In: *V Simpósio Brasileiro de Geofísica Espacial e Aeronomia - SBGEA*. [S.l.: s.n.], 2014. ANAIS (ABSTRACTS).

GOPALSWAMY, N.; MEWALDT, R.; TORSTI, J. Solar eruptions and energetic particles: An introduction. In: *: NATCHIMUTHUKONAR GOPALSWAMY, Richard. Solar eruptions and energetic particles.* Washington DC: American Geophysical Union, 2006.

GRANATO-SOUZA, D. et al. Dendrochronological analyses and climatic signals of alchornea triplinervia in subtropical forest of southern brazil. *Austral Ecology*, v. 43, n. 4, p. 385–396, 2018.

GREIN, M. et al. Mechanistic modelling of Middle Eocene atmospheric carbon dioxide using fossil plant material. In: *EGU General Assembly Conference Abstracts*. [S.l.: s.n.], 2010. (EGU General Assembly Conference Abstracts), p. 9798.

GRIMM, A. M. The el niño impact on the summer monsoon in brazil: Regional processes versus remote influences. *Journal of Climate*, American Meteorological Society, Boston MA, USA, v. 16, n. 2, p. 263 – 280, 2003. Disponível em: <https://journals.ametsoc.org/view/journals/clim/16/2/1520-0442_2003_016_0263_teniot_2.0.co_2.xml>.

GRIMM, A. M. Tempo e clima no brasil. In: _____. first. São Paulo, Brazil: Oficina de Textos, 2009. cap. Clima da Região Sul do Brasil.

GRIMM, A. M. et al. The combined effect of climate oscillations in producing extremes: the 2020 drought in southern brazil. *RBRH*, Associação Brasileira de Recursos Hídricos, v. 25, p. e48, 2020. ISSN 2318-0331. Disponível em: <https://doi.org/10.1590/2318-0331.252020200116>.

GRIMM, A. M.; BARROS, V. R.; DOYLE, M. E. Climate variability in southern south america associated with el niño and la niña events. *Journal of Climate*, American Meteorological Society, Boston MA, USA, v. 13, n. 1, p. 35 – 58, 2000.

GRIMM, A. M.; FERRAZ, S. E. T.; GOMES, J. Precipitation anomalies in southern brazil associated with el niño and la niña events. *Journal of Climate*, American Meteorological Society, Boston MA, USA, v. 11, n. 11, p. 2863 – 2880, 1998.

GRIMM, A. M.; FEUSER, V. R. Relações entre temperaturas da superfície do mar sobre o atlântico e precipitação no sul e sudeste do brasil. Congresso Brasileiro de Meteorologia. 1998.

GRINSTED, A.; MOORE, J. C.; JEVREJEVA, S. Application of the cross wavelet transform and wavelet coherence to geophysical time series. *Nonlinear Processes in Geophysics*, v. 11, n. 5/6, p. 561–566, 2004. Disponível em: <https://npg.copernicus.org/articles/11/561/2004/>.

GRISSINO-MAYER, H. Evaluating crossdating accuracy: a manual and tutorial for the computer program cofecha. *Tree-Ring Research*, v. 57, 11 2000.

GURGEL, J.; FILHO, O. G. Evidências de raças geográficas no pinheiro-brasileiro, araucaria angustifolia (bert.) o. ktze. *Ciência e Cultura*, v. 17, n. 1, p. 33–39, 1965.

HADDAD, S. A. P.; SERDIJN, W. A. *Wavelet versus Fourier Analysis*. Dordrecht: Springer Netherlands, 2009. 33–50 p. ISBN 978-1-4020-9073-8.

HAIGH, J. The sun and the earth's climate. *Living Reviews in Solar Physics*, v. 4, 10 2007.

HAIGH, J. Solar influences on climate. *Imperial College London - Grantham Institute for Climate Change*, 2011. Briefing paper No 5. Disponível em: <https://www.imperial.ac.uk/media/imperial-college/grantham-institute/public/publications/briefing-papers/Solar-Influences-on-Climate---Grantham-BP-5.pdf>.

HAIGH, J.; ROSCOE, H. Solar influences on polar modes of variability. *Meteorologische Zeitschrift*, v. 15, p. 371–378, 2006.

HANSLMEIER, A. *The sun and space weather*. second. New York: Springer, 2007.

HATHAWAY, D. H. *Photospheric Features*. 2014. Disponível em: <https://solarscience.msfc.nasa.gov/feature1.shtml>.

HATHAWAY, D. H. The solar cycle. *Living Rev. Solar Phys.*, v. 12, 2015.

HELAMA, S. et al. Detection of climate signal in dendrochronological data analysis: a comparison of tree-ring standardization methods. *Theoretical and Applied Climatology*, v. 79, 2004.

HELAMA, S.; MELVIN, T. M.; BRIFFA, K. R. Regional curve standardization: State of the art. *The Holocene*, v. 27, n. 1, p. 172–177, 2017.

HIERA, M. D. S.; V., E. E. A. As chuvas de junho e a primeira onda de frio intenso de 2013: A atuação dos sistemas atmosféricos e o ritmo climático para a região de maringá. *Geoingá: Revista do Programa de PósGraduação em Geografia*, v. 6, n. 1, p. 78–94, 2014.

HOYT, D. V.; SCHATTEN, K. H. *The Role of the Sun in Climate Change*. [S.l.]: Oxford University Press, 1997.

INPE; CPTEC. *Condições Atuais do ENOS: Caracterização do El Niño*. 2023. Accessed on July 5, 2023. Disponível em: <http://enos.cptec.inpe.br/>.

IPCC, I. P. on C. C. Climate phenomena and their relevance for future regional climate change. In: _____. *Climate Change 2013 – The Physical Science Basis: Working Group I Contribution to the Fifth Assessment Report of the Intergovernmental Panel on Climate Change*. [S.l.]: Cambridge University Press, 2014. p. 1217–1308.

ISLA, F. I.; JUNIOR, E. E. T. Enso impacts on atlantic watersheds of south america. *Quaternary and Environmental Geosciences*, v. 4, n. 1-2, 2013.

KAROLY, D. J.; VINCENT, D. G. *Meteorology of the Southern Hemisphere*. second. [S.l.]: American Meteorological Society Boston, MA, 1998. (Meteorological Monographs, v. 27). ISSN 0065-9401.

KAYANO, M.; CAPISTRANO, V. How the atlantic multidecadal oscillation (amo) modifies the enso influence on the south american rainfall. *International Journal of Climatology*, v. 34, 01 2014.

KELLMAN, M.; TACKABERRY, R. *Tropical Environments: The Functioning and Management of Tropical Ecosystems*. New York: Routledge, 1997.

KOUSKY, V. E.; CAVALCANTI, I. F. A. Eventos oscilação sul - el niño: características, evolução e anomalias de precipitação. *Revista Ciência e Cultura*, p. 1888–1889, 1984.

LANG, K. R. *The Cambridge Encyclopedia of the Sun*. Medford, Massachusetts, USA: Tufs University, 2001.

LAPOINTE, F.; BRADLEY, R. S. Little ice age abruptly triggered by intrusion of atlantic waters into the nordic seas. *Science Advances*, v. 7, n. 51, p. eabi8230, 2021. Disponível em: <https://www.science.org/doi/abs/10.1126/sciadv.abi8230>.

LEAL, P. C. *Sistema Praial Moçambique – Barra da Lagoa – Ilha de Santa Catarina – Brasil: Aspectos Morfológicos, Morfodinâmicos, Sedimentológicos e Ambientais*. Dissertação (Masters Dissertation) — Universidade Federal de Santa Catarina, Santa Catarina, Brazil, 1999.

LEAN, J. Variation in the sun's radiative output. *Reviews of Geophysics*, v. 29, n. 4, p. 505–535, 1991.

LINDHOLM, M. et al. A ring-width chronology of scots pine from northern lapland covering the last two millennia. *Annales Botanici Fennici*, v. 36, p. 119–126, 11 1999.

LISI, C. S. *Atividade de C14 do Fallout e Razão Isotópica C13/12 em Anéis de Crescimento de Clima Tropical e Subtropical do Brasil. 2000*. Tese (Doutorado) — Escola Superior de Agricultura Luiz de Queiroz, Universidade de São Paulo, 2000.

LISI, C. S.; PESSENDA, L. C. R.; FILHO, M. T. Análise da variação da largura dos anéis de crescimento de araucaria angustifolia (b.) o. kuntze – pinheiro-do-paraná para estudos dendrocronológicos. In: BIOLOGIA, U. F. da Bahia: Instituto de (Ed.). *Congresso Nacional de Botânica*. Salvador: [s.n.], 1998. v. 49, p. 44.

LOCOSSELLI, G.; SCHöNGART, J.; CECCANTINI, G. Climate/growth relations and teleconnections for a hymenaea courbaril (leguminosae) population inhabiting the dry forest on karst. *Trees*, v. 30, p. 1127–1136, 2016.

LONGNECKER, N. An integrated model of science communication — more than providing evidence. *Journal of Science Communication*, v. 15, p. Y01, 09 2016.

LORENSI, C. *Resposta dos anéis de crescimento de Araucaria angustifolia (Bertol.) O. Kuntze da região sul do Brasil aos forçantes geofísicos e climáticos*. Tese (Doutorado) — Universidade do Vale do Paraíba – UNIVAP, Instituto de Pesquisa e Desenvolvimento Programa de Pós-Graduação em Física e Astronomia, 2016.

LORENSI, C.; PRESTES, A. Estudo da relação sol-terra em anéis de crescimento de árvores de general carneiro/pr. In: *International Workshop of Tropical Dendrochronology*. [S.l.: s.n.], 2013. ANAIS (ABSTRACT).

LORENSI, C.; PRESTES, A. Study of solar-terrestrial interactions in tree growth rings from general carneiro, pr/ brazil. 2014.

LORENSI, C.; PRESTES, A. Dendroclimatological Reconstruction of Spring-Summer Precipitation for Fazenda Rio Grande, PR, with samples of *Araucaria angustifolia (Bertol.) Kuntze*. *Revista árvore*, scielo, v. 40, p. 347 – 354, 2016.

LORENSI, C.; PRESTES, A. Dendroclimatologia com amostras de araucaria angustifolia coletadas em santa catarina. *Revista Univap*, v. 24, p. 1, 06 2018.

MA, Q.; LEMBO, V.; FRANZKE, C. L. E. The lorenz energy cycle: trends and the impact of modes of climate variability. *Tellus A: Dynamic Meteorology and Oceanography*, Taylor & Francis, v. 73, n. 1, p. 1–15, 2021.

MARTINKOSKI, L. et al. Climatic influences on the radial growth of araucaria angustifolia in the brazilian south atlantic forest. *iForest - Biogeosciences and Forestry*, v. 9, p. 102–108, 2015.

MARTINS, M. E. G. Coeficiente de correlação amostral. *Revista de Ciência Elementar*, 2014.

MATOS, D. U. et al. Habitat dynamics in subtropical south america: Socioeconomic determinants and landscape patterns at a forest-grassland ecotone. *Neotropical Biology and Conservation*, 2016.

MCFADDEN, L. A.; WEISSMAN, P.; JOHNSON, T. *Encyclopedia of the Solar System*. 2nd. ed. [S.l.]: Academic Press, 2007. ISBN 9780120885893,0120885891.

MEEHL, G. A. et al. Solar and greenhouse gas forcing and climate response in the twentieth century. *Journal of Climate*, American Meteorological Society, Boston MA, USA, v. 16, n. 3, p. 426 – 444, 2003.

MELDRUM, C. On a periodicity in the frequency of cyclones in the indian ocean south of the equator. In: *REPORT OF THE BRITISH ASSOCIATION FOR THE ADVANCEMENT OF SCIENCE, 42nd., Brighton, 1872. Proceedings...* ,Brighton: [s.n.], 1872.

MELDRUM, C. On a supposed periodicity of the cyclones of the indian ocean south of the equator. *Nature*, v. 32, p. 613–614, 1885.

MOSTELLER, F.; TUKEY, J. W. *Data Analysis and Regression: A Second Course in Statistics*. [S.l.]: Reading, MA: Addison-Wesley Pub Co., 1977.

MURAJA, D. O. S. et al. Theoretical & applied climatology. *Ocean–atmosphere interaction identified in tree-ring time series from southern Brazil using cross-wavelet analysis*, 2023.

NIMER, E. *Climatologia do Brasil*. Rio de Janeiro: Instituto Brasileiro de Geografia e Estatística - IBGE, 1989.

NODARI, E. S. Historia de la devastación del bosque de araucaria en el sur del brasil. *áreas. Revista Internacional de Ciencias Sociales*, n. 35, p. 75–85, dic. 2016. Disponível em: <https://revistas.um.es/areas/article/view/279171>.

NORDEMANN, D. J. R. et al. Solar activity and el ninõ effects on southern brazil araucaria ring widths (1955-1997). In: *INTERNATIONAL CONFERENCE ON DENDROCHRONOLOGY, 6., 2002. Quebec City. Proceedings...* Quebec: [s.n.], 2002. (Poster).

OLIVEIRA, A. S. *Interações entre sistemas na América do Sul e convecção na Amazônia*. Dissertação (Master Dissertation) — Instituto Nacional de Pesquisas Espaciais, 1986.

OLIVEIRA, S. G. El niño e você – o fenômeno climático. *Transtec Editorial*, 2001.

PARKER, E. N. Space weather and the changing sun. In: *Space Weather*. [S.l.]: American Geophysical Union, 2001.

PATRICIAN, P. A. Multiple imputation for missing data. *Research in Nursing & Health*, v. 25, n. 1, p. 76–84, 2002.

PHILANDER, S. *El Niño, La Niña, and the Southern Oscillation*. New York: Academic Press, 1989. (International Geophisics Series, v. 46).

PRADO, L.; WAINER, I. Planetary-scale climatic indices and relationship between decadal variability of rainfall in northeastern and southern brazil. *Brazilian Journal of Geophysics*, v. 31, n. 1, p. 31–41, 2013. ISSN 2764-8044.

PRESTES, A. *Relação Sol-Terra Estudada Através de Anéis de Crescimento de Coníferas do Holoceno Recente e Triássico. 2009*. Tese (Doutorado) — Instituto Nacional de Pesquisas Espaciais, São José dos Campos, 2009.

PRESTES, A. et al. Resposta do crescimento da araucária à variabilidade solar e climática na região de passo fundo - rs. In: *VII Simpósio Brasileiro de Geofísica Espacial e Aeronomia - SBGEA*. [S.l.: s.n.], 2018. ANAIS (ABSTRACTS).

PRESTES, A. et al. Araucaria growth response to solar and climate variability in south brazil. *Annales Geophysicae*, v. 36, p. 717–729, 05 2018.

PRESTES, A. et al. Sun–earth relationship inferred by tree growth rings in conifers from severiano de almeida, southern brazil. *Journal of Atmospheric and Solar-Terrestrial Physics*, v. 73, 07 2011.

PRESTES, A. et al. Imprint of climate variability on mesozoic fossil tree rings: Evidences of solar activity signals on environmental records around 200 million years ago? *Pure and Applied Geophysics*, v. 171, p. 1983–1991, 08 2013.

QUADRO, M. Estudo de episódios de zonas de convergência do atlântico sul (zcas) sobre a américa do sul. *Revista Brasileira de Geofísica*, v. 17, 1999.

QUADRO, M. F. L. et al. *Boletim da Climanalise - CLIMATOLOGIA DE PRECIPITAÇÃO E TEMPERATURA*. 1996. Centro de Previsão de Tempo e Estudos Climáticos - CPTEC/INPE. Accessed on March 12, 2023. Disponível em: <http://climanalise.cptec.inpe.br/~rclimanl/boletim/cliesp10a/chuesp.html>.

RAMSTEIN, G. et al. Paleoclimatology. In: _____. [S.l.]: Springer, 2021. (Frontiers in Earth Sciences), cap. The Climate System: Its Functioning and History.

RAMSTEIN, G. et al. Paleoclimatology. In: _____. [S.l.]: Springer, 2021. (Frontiers in Earth Sciences), cap. Carbon-14.

RAMSTEIN, G. et al. Paleoclimatology. In: _____. [S.l.]: Springer, 2021. (Frontiers in Earth Sciences), cap. Dating of Corals and Other Geological Samples via the Radioactive Disequilibrium of Uranium and Thorium Isotopes.

RAMSTEIN, G. et al. Paleoclimatology. In: _____. [S.l.]: Springer, 2021. (Frontiers in Earth Sciences), cap. The Dating of Ice-Core Archives.

RAMSTEIN, G. et al. Paleoclimatology. In: _____. [S.l.]: Springer, 2021. (Frontiers in Earth Sciences), cap. Dendrochronology.

RAO, V. B.; HADA, K. Characteristics of rainfall over brazil: Annual variations and connections with the southern oscillation. *Theoretical and Applied Climatology*, v. 42, 1990.

RASMUSSON, E.; CARPENTER, T. Variations in tropical sea surface temperature and wind associated with the southern oscillation/el niño. *Monthly Weather Review*, v. 110, p. 354–384, 1982.

RASMUSSON, E. M.; WALLACE, J. M. Meteorological aspects of the el ninõ/southern oscillation. *Science*, American Association for the Advancement of Science, v. 222, n. 4629, p. 1195–1202, 1983.

RATHGEBER, C. B. K.; CUNY, H. E.; FONTI, P. Biological basis of tree-ring formation: A crash course. *Frontiers in Plant Science*, v. 7, 2016. ISSN 1664-462X. Disponível em: <https://www.frontiersin.org/articles/10.3389/fpls.2016.00734>.

REBOITA, M. S. et al. Entendendo o tempo e o clima na américa do sul. *Terra E Didática*, v. 8, n. 1, p. 34–50, 2012.

RENÉ, D. G.; PATRICIO, A. The physical geography of south america. In: _____. 198 Madison Avenue, New York, New York 10016: OXFORD UNIVERSITY PRESS, 2007. cap. Atmospheric Circulation and Climatic Variability. ISBN 978-0-19-531341-3.

RIGOZO, N. et al. Solar-terrestrial signal record in tree ring width time series from brazil. *Pure and Applied Geophysics*, v. 169, 12 2012.

RIGOZO, N. et al. Solar maximum epoch imprints in tree-ring width from passo fundo, brazil (1741–2004). *Journal of Atmospheric and Solar-Terrestrial Physics*, v. 70, p. 1025–1033, 05 2008.

RIGOZO, N. R. et al. Search for solar periodicities in tree-ring widths from concórdia (s.c., brazil). *Pure and Applied Geophysics*, v. 161, p. 221–233, 2004.

RIND, D. The sun's role in climate variations. *Science*, v. 296, n. 5568, p. 673–677, 2002.

ROLLAND, C. Tree-ring and climate relationships for abies alba in the internal alps. *Tree Ring Bull*, v. 53, p. 1–11, 1993.

ROPELEWSKI, C. F.; HALPERT, M. S. Global and regional scale precipitation patterns associated with the el niño/southern oscillation. *Monthly Weather Review*, American Meteorological Society, Boston MA, USA, v. 115, n. 8, p. 1606 – 1626, 1987.

ROPELEWSKI, C. F.; HALPERT, M. S. Precipitation patterns associated with the high index phase of the southern oscillation. *Journal of Climate*, American Meteorological Society, Boston MA, USA, v. 2, n. 3, p. 268 – 284, 1989.

ROPELEWSKI, C. F.; JONES, P. D. An extension of the tahiti–darwin southern oscillation index. *Monthly Weather Review*, American Meteorological Society, Boston MA, USA, v. 115, n. 9, p. 2161 – 2165, 1987. Disponível em: <https://journals.ametsoc.org/view/journals/mwre/115/9/1520-0493_1987_115_2161_aeotts_2_0_co_2.xml>.

RUBIO-CUADRADO, ; CAMARERO, J. J.; BOSELA, M. Applying climwin to dendrochronology: A breakthrough in the analyses of tree responses to environmental variability. *Dendrochronologia*, v. 71, p. 125916, 2022. ISSN 1125-7865.

SANTAROSA, E. et al. Crescimento sazonal em araucaria angustifolia: Evidências anatômicas. *Revista Brasileira de Biociências*, v. 5, p. 618–620, 2007.

SATO, K.; HIRANO, S. The climatology of the brewer–dobson circulation and the contribution of gravity waves. *Atmospheric Chemistry and Physics*, v. 19, n. 7, p. 4517–4539, 2019. Disponível em: <https://acp.copernicus.org/articles/19/4517/2019/>.

SCHMIDBAUER, H.; ROESCH, A. Waveletcomp 1.1: A guided tour through the r package. 03 2018.

SCHÖNGART, J. et al. Teleconnection between tree growth in the amazonian floodplains and the el niño–southern oscillation effect. *Global Change Biology*, v. 10, n. 5, p. 683–692, 2004.

SCHWABE, H. Sonnen-beobachtungen im jahre 1843. *Astron. Nachr*, v. 21, n. 495, p. 233–236, 1844.

SCHWEINGRUBER, F. H. *Tree Rings Basics and Applications of Dendrochronology*. Dordrecht / Boston / London: Kluwer Academic Publishers, 1983.

SCIPIONI, M. et al. Effects of cold conditions on the growth rates of a subtropical conifer. *Dendrochronologia*, v. 68, p. 125858, 06 2021.

SEINFELD, J. H.; PANDIS, S. N. *Atmospheric chemistry and physics*. New York: John Wiley |& Sons, Inc., 1998.

SHIMIZU, M.; AMBRIZZI, T. Mjo influence on enso effects in precipitation and temperature over south america. *Theoretical and Applied Climatology*, v. 124, 03 2015.

SHIYATOV, S. G.; MAZEPA, V. S. *Some New Approaches in the Consideration of More Reliable Dendroclimatological Series and in the Analysis of Cycle Components*. International Institute for Applied Systems Analysis, Laxenburg, Austria and Polish Academy of Sciences-System Research Institute, Warsaw, Poland: Kairiukstis, L. et al. (eds.), 1987. (Methods of Dendrochronology).

SHRIVE, F. M. et al. Dealing with missing data in a multi-question depression scale: a comparison of imputation methods. *BMC Med Res Methodol*, v. 6, n. 57, 2006.

SIDHU, T.; BHAJLA, B.; DAS, S. Numerical algorithms for protection and metering devices. In: GARCíA, J. (Ed.). *Encyclopedia of Electrical and Electronic Power Engineering*. Oxford: Elsevier, 2023. p. 45–87. ISBN 978-0-12-823211-8.

SIINGH, D. et al. Solar activity, lightning and climate. *Surveys in Geophysics*, v. 32, 2011.

SILVA, A. C. da; PRESTES, A. Estudo dendroclimático da região de São Francisco de Paula - RS. In: *XIV Encontro Latino Americano de Iniciação Científica, X Encontro Latino Americano de Pós Graduação e IV Encontro Latino América de Iniciação Científica Junior*. [S.l.: s.n.], 2010. ANAIS (ABSTRACTS).

SILVA, A. C. da; PRESTES, A.; SOUZA, T. G. G. Estudo comparativo dos fenômenos geofísicos, climáticos e solares, comuns nas florestas nacionais de Açungui - PR e de são francisco de paula - rs. In: *XV Encontro Latino Americano de Iniciação Científica, XI Encontro Latino Americano de Pós Graduação e V Encontro Latino América de Iniciação Científica Junior*. [S.l.: s.n.], 2011. ANAIS (Abstracts).

SILVA, A. C. da; SOUZA, T. G. G.; PRESTES, A. Análise da resposta dos anéis de crescimento de araucárias da região de São Francisco de Paula - RS à eventos El Niño e La Niña e sua influência na preciptiação e temperatura. In: *XVI Encontro Latino Americano de Iniciação Científica, XII Encontro Latino Americano de Pós Graduação e VI Encontro Latino América de Iniciação Científica Junior*. [S.l.: s.n.], 2012. ANAIS (Abstracts).

SILVA, D. et al. Principal components analysis: An alternative way for removing natural growth trends. *Pure and Applied Geophysics*, 2021. Https://doi.org/10.1007/s00024-021-02807-x.

SILVA, D. O. et al. Climate influence in dendrochronological series of araucaria angustifolia from Campos do Jordão, Brazil. *Atmosphere*, v. 12, n. 8, 2021. ISSN 2073-4433. Disponível em: <https://www.mdpi.com/2073-4433/12/8/957>.

SILVA, I. R. *Variabilidade sazonal e interanual das precipitações na região sul do Brasil associadas às temperaturas dos oceanos Atlântico e Pacífico*. Dissertação (Masters Dissertation) — Instituto Nacional de Pesquisas Espaciais - INPE, São José dos Campos - São Paulo, Brazil, 2001.

SILVA, I. R. *Relações Entre o Crescimento da (Ocotea porosa (Nees & Mart) Barroso) e as Forçantes Climatológicas do Sudeste do Paraná. 2018*. Tese (Doutorado) — Universidade do Vale do Paraíba, São José dos Campos, 2018.

SILVA, I. R. da. *Variabilidade Sazonal e Interanual das Precipitações na Região Sul do Brasil Associadas às Temperaturas dos Oceanos Atlântico e Pacífico*. Dissertação (Mestrado) — Instituto Nacional de Pesquisas Espaciais - INPE, 2004.

SILVERMAN, S. M.; HAYAKAWA, H. The dalton minimum and john daltons auroral observations. *J. Space Weather Space Clim.*, v. 11, p. 17, 2021. Disponível em: <https://doi.org/10.1051/swsc/2020082>.

SIMMONS, M. T. Climates and microclimates: Challenges for extensive green roof design in hot climates. In: _____. *Green Roof Ecosystems*. Cham: Springer International Publishing, 2015. p. 63–80. Disponível em: <https://doi.org/10.1007/978-3-319-14983-7_3>.

SIMUNEK, V. et al. Tree rings of european beech (*Fagus sylvatica L.*) indicate the relationship with solar cycles during climate change in central and southern europe. *Forests*, MDPI AG, v. 12, n. 3, p. 259, Feb 2021. ISSN 1999-4907.

SOBRINHO, J. L. G. *O Sol e o seu interior*. Madeira: [s.n.], 2013.

SOUZA-ECHER, M. P. et al. Climatic change. *Wavelet analysis of a centennial (1895–1994) southern Brazil rainfall series (Pelotas, 31°46'19"S 52°20'33"W)*, v. 87, 2008.

SOUZA, T. G. G. Dendrocronologia das araucárias coletadas na Floresta Nacional de Açungui. Completion of course work. (Bachelor of Biological Sciences) - University of Vale do Paraíba. 2010.

SOUZA, T. G. G.; PRESTES, A.; SILVA, A. C. da. Dendroclimatologia da Floresta Nacional de Açungui - PR. In: *XV Encontro Latino Americano de Iniciação Científica, XI Encontro Latino Americano de Pós Graduação e V Encontro Latino América de Iniciação Científica Junior*. [S.l.: s.n.], 2011. ANAIS (ABSTRACTS).

SOUZA, T. G. G.; SILVA, A. C.; PRESTES, A. Estudo da influência da temperatura e precipitação em anéis de crescimento de araucaria angustifolia da Floresta de Açungui - PR. In: *XVI INIC, XII EPG, VI INIC-Júnior*. [S.l.: s.n.], 2012. ANAIS (ABSTRACTS).

SPEER, J. H. *Fundalmentals of Tree-Ring Research*. [S.l.]: Library of Congress Cataloging-in-Publication Data, 1971.

SPUDMAN. *El Niño present in Pacific, could mean drier 2019 for Pacific Northwest*. 2018. Disponível em: <https://spudman.com/news/el-nino-dry-pacific-northwest/>. Acesso em 12 de março de 2023.

STEIGER, N. J. et al. Climate reconstruction using data assimilation of water isotope ratios from ice cores. *Journal of Geophysical Research: Atmospheres*, v. 122, n. 3, p. 1545–1568, 2017. Disponível em: <https://agupubs.onlinelibrary.wiley.com/doi/abs/10.1002/2016JD026011>.

STUDZINSKI, C. D. *Um estudo da precipitação na Região Sul do Brasil e sua Relação com os Oceanos Pacífico e Atlântico Tropical Sul*. Dissertação (Master Dissertation) — Instituto Nacional de Pesquisas Espaciais - INPE, São José dos Campos - São Paulo, Brazil, 1995.

SUESS, H. E. The radiocarbon record in tree rings of the last 8000 years. *Radiocarbon*, Cambridge University Press, v. 22, n. 2, p. 200–209, 1980.

TOBIAS, S. M. The solar dynamo. *Philosophical transactions. Series A, Mathematical, physical, and engineering sciences*, v. 360, 2003.

TORRENCE, C.; COMPO, G. P. A Practical Guide to Wavelet Analysis. *Bulletin of the American Meteorological Society*, v. 79, n. 1, p. 61–78, jan. 1998.

TRENBERTH, K.; ZHANG, R. *The Climate Data Guide: Atlantic Multi-decadal Oscillation (AMO) and Atlantic Multidecadal Variability (AMV)*. 2023. Last modified 2023-09-01, Accessed on 2023-09-19. Made together with the National Center for Atmospheric Research Staffs. Disponível em: <https://climatedataguide.ucar.edu/climate-data/atlantic-multi-decadal-oscillation-amo>.

TRENBERTH, K. E. Spatial and temporal variations of the southern oscillation. *Quarterly Journal of the Royal Meteorological Society*, v. 102, n. 433, p. 639–653, 1976.

TRENBERTH, K. E. The definition of el niño. *Bulletin of the American Meteorological Society*, v. 78, n. 12, 1997.

TSURUTANI, B. T.; GONZALEZ, W. D. Magnetic storms. In: *From the sun: Auroras, magnetic storms, solar flares, cosmic rays*. [S.l.]: American Geophysical Union, 1998.

USOSKIN, I. G. et al. The maunder minimum (1645–1715) was indeed a grand minimum: A reassessment of multiple datasets. *Astronomy & Astrophysics*, 2015.

VACHAA, L.; BARUNIK, J. Co-movement of energy commodities revisited: Evidence from wavelet coherence analysis. *arxiv.org*, 2012. Preprint arXiv:1201.4776v1 [q-fin.ST].

VELASCO, G. Mexican forest fires and their decasal variations. *Adv. Space Res.*, v. 10, 2016.

VIEGAS, J. et al. Caracterização dos diferentes tipos de el niño e seus impactos na américa do sul a partir de dados observados e modelados. *Revista Brasileira de Meteorologia*, Sociedade Brasileira de Meteorologia, v. 34, n. 34, Jan 2019. ISSN 0102-7786. Disponível em: <https://doi.org/10.1590/0102-7786334015>.

VIEIRA, L. E. A. et al. How the inclination of earth's orbit affects incoming solar irradiance. *Geophysical Research Letters*, v. 39, n. 16, 2012. Disponível em: <https://agupubs.onlinelibrary.wiley.com/doi/abs/10.1029/2012GL052950>.

WALISER, D. E.; GAUTIER, C. A satellite-derived climatology of the itcz. *Journal of Climate*, American Meteorological Society, Boston MA, USA, v. 6, n. 11, p. 2162 – 2174, 1993.

WANG, C. Interações de três oceanos e variabilidade climática: uma revisão e perspectiva. *Clim Dyn*, n. 53, p. 5119–5136, 2019.

WANG, Z.; BOYD, K.; WALSH, J. E. Modulation of polar low activity by the madden-julian oscillation. *Geophysical Research Letters*, v. 50, n. 12, p. e2023GL103719, 2023. Disponível em: <https://agupubs.onlinelibrary.wiley.com/doi/abs/10.1029/2023GL103719>.

WIGLEY, T. M. L.; BRIFFA, K. R.; JONES, P. D. On the average value of correlated time series, with applications in dendroclimatology and hydrometeorology. *Journal of Applied Meteorology and Climatology*, American Meteorological Society, Boston MA, USA, v. 23, n. 2, p. 201 – 213, 1984. Disponível em: <https://journals.ametsoc.org/view/journals/apme/23/2/1520-0450_1984_023_0201_otavoc_2_0_co_2.xml>.

ZANETTE, F. et al. Araucária: particularidades, propagação e manejo de plantios. In: _____. Brasília, DF: Embrapa Florestas, 2017. chapter in book Particularidades e biologia reprodutiva de Araucaria angustifolia.

ZANON, M. L. B. *Crescimento da Araucaria angustifolia (Bertol.) Kuntze diferenciado por dioicia*. Tese (Doutorado) — Universidade Federal de Santa Maria (UFSM), 2007.

ZHOU, J.; TUNG, K.-K. Solar cycles in 150 years of global sea surface temperature data. *Journal of Climate*, American Meteorological Society, Boston MA, USA, v. 23, n. 12, p. 3234 – 3248, 2010. Disponível em: <https://journals.ametsoc.org/view/journals/clim/23/12/2010jcli3232.1.xml>.

ZHOU, Q.; CHEN, W.; ZHOU, W. Solar cycle modulation of the enso impact on the winter climate of east asia. *Journal of Geophysical Research: Atmospheres*, v. 118, n. 11, p. 5111–5119, 2013. Disponível em: <https://agupubs.onlinelibrary.wiley.com/doi/abs/10.1002/jgrd.50453>.

ZUO, Y. et al. Biological network inference using low order partial correlation. *Methods*, v. 69, n. 3, p. 266–273, 2014. ISSN 1046-2023. Recent development in bioinformatics for utilizing omics data.

ÁVILA, A. et al. Recent precipitation trends, flash floods and landslides in southern brazil. *Environmental Research Letters*, IOP Publishing, v. 11, n. 11, p. 114029, nov 2016. Disponível em: <https://dx.doi.org/10.1088/1748-9326/11/11/114029>.

Appendix

APPENDIX A – TREE-RING SERIES AND CHRONOLOGIES (RWI) FIGURES

In this appendix, the tree-ring time series and chronologies (RWIs) per city are demonstrated.

Figure 41: (a) Tree-ring time series of the samples collected in Açungui city; (b) Tree-ring time series for the trees (after averaging the samples per tree); (c) Ring Width Index (RWI) as black line and sample depth in red line for Açungui city.

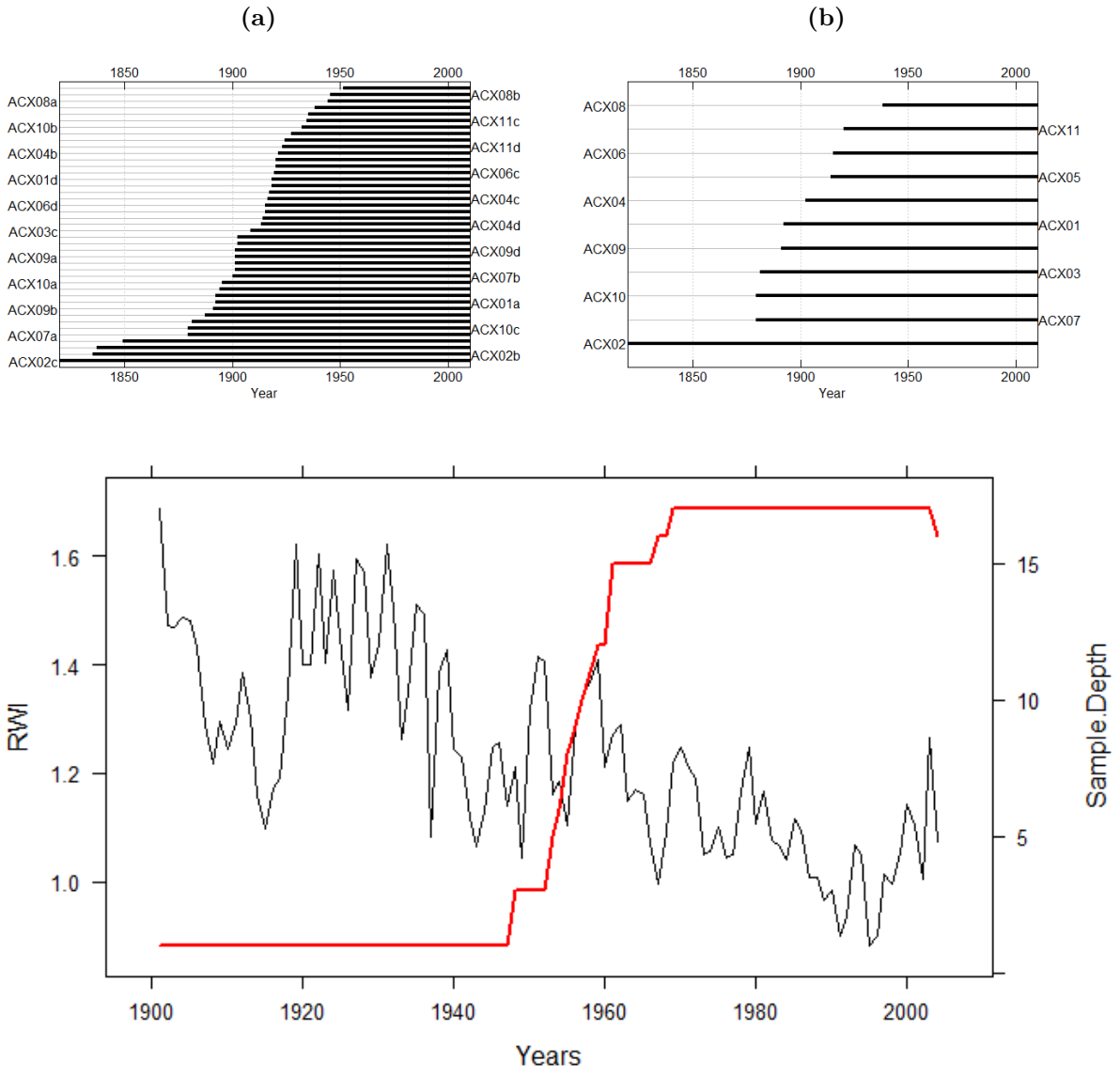

Source: The author.

Figure 42: (a) Tree-ring time series of the samples collected in Canela city; (b) Tree-ring time series for the trees (after averaging the samples per tree); (c) Ring Width Index (RWI) as black line and sample depth in red line for Canela city.

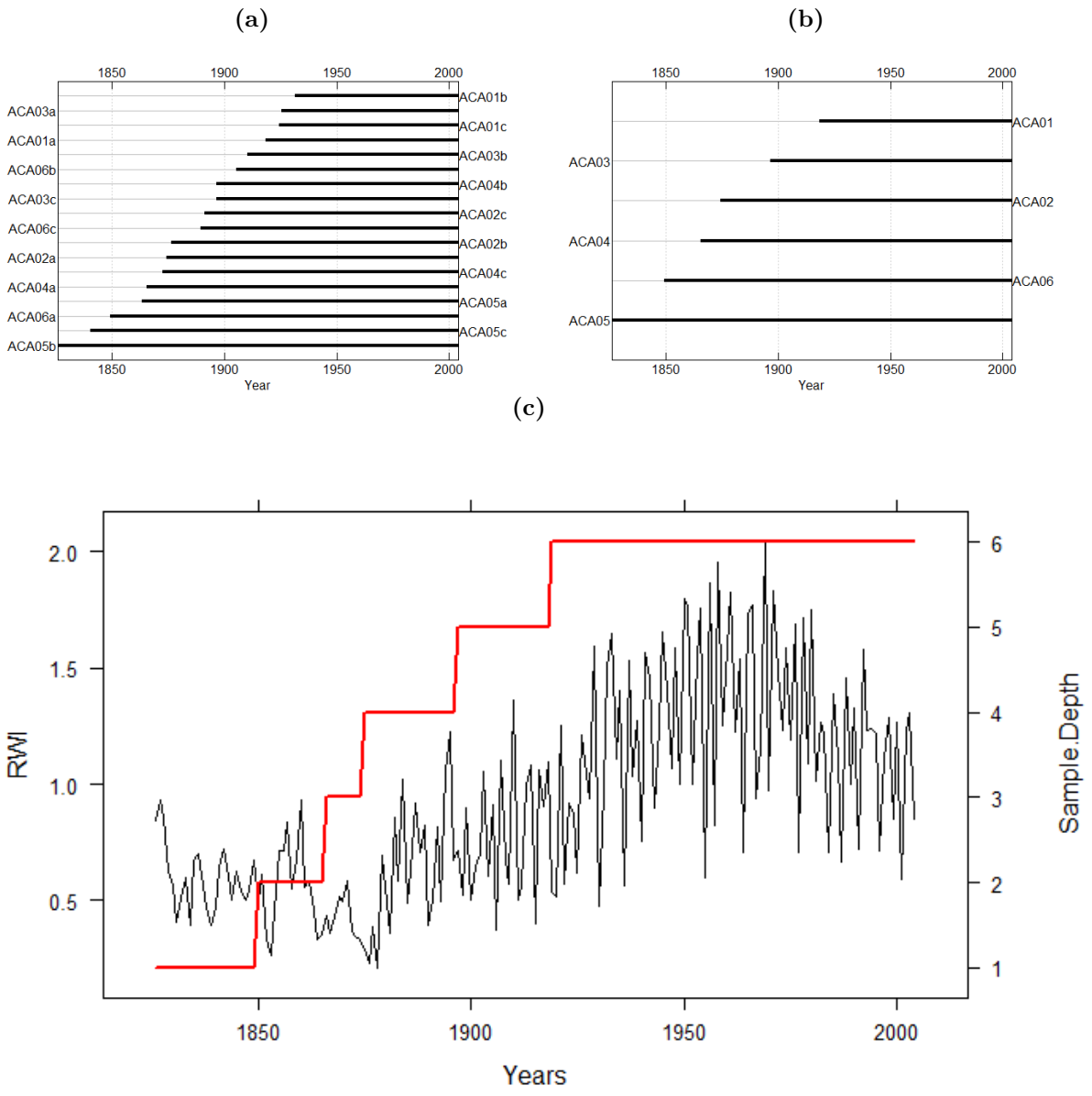

Source: The author.

Figure 43: (a) Tree-ring time series of the samples collected in Chapecó city; (b) Tree-ring time series for the trees (after averaging the samples per tree); (c) Ring Width Index (RWI) as black line and sample depth in red line for Chapecó city.

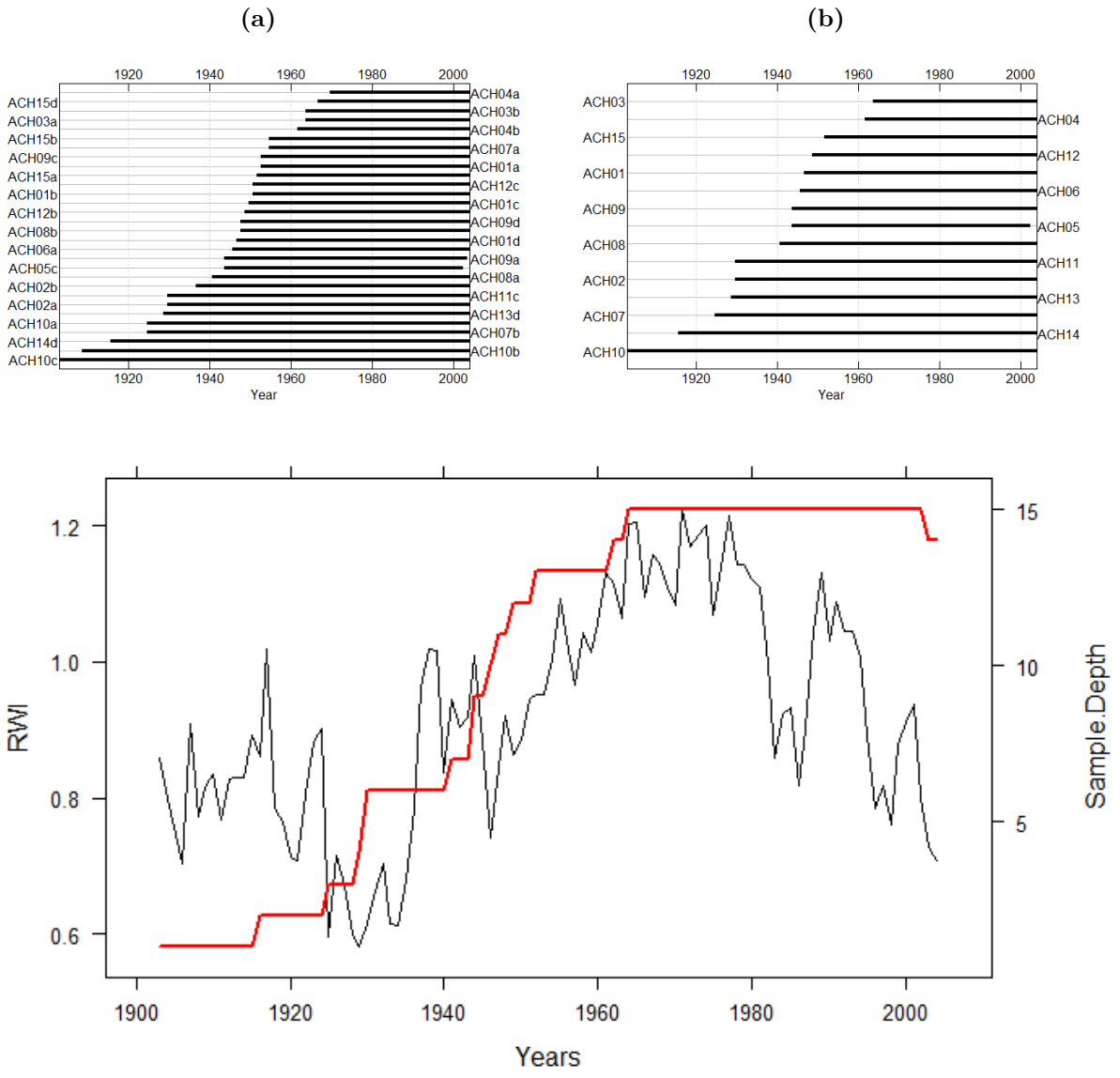

Source: The author.

Figure 44: (a) Tree-ring time series of the samples collected in Coxilha city; (b) Tree-ring time series for the trees (after averaging the samples per tree); (c) Ring Width Index (RWI) as black line and sample depth in red line for Coxilha city.

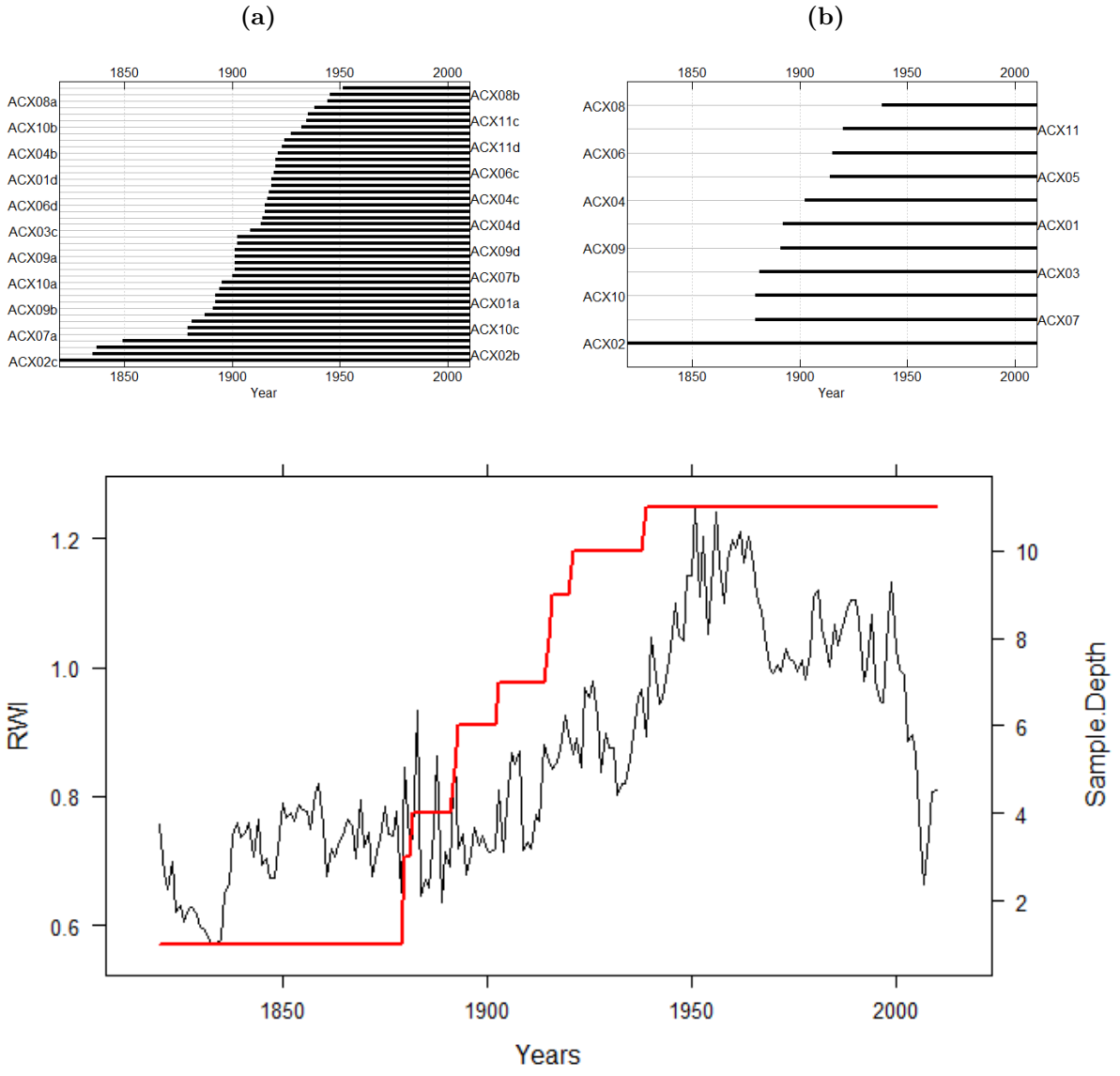

Source: The author.

Figure 45: (a) Tree-ring time series for the trees (after averaging the samples per tree), the samples were collected in Curitibanos City, and only the tree indices were obtained for this thesis; (b) Ring Width Index (RWI) as black line and sample depth in red line for Curitibanos city.

(a)

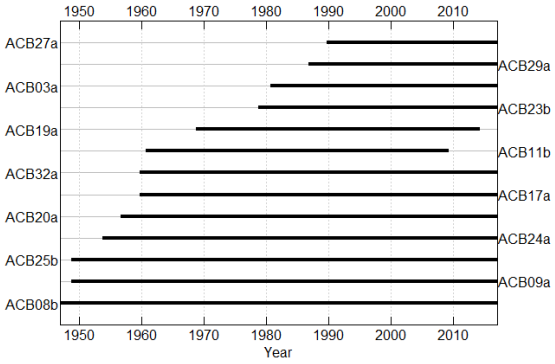

(b)

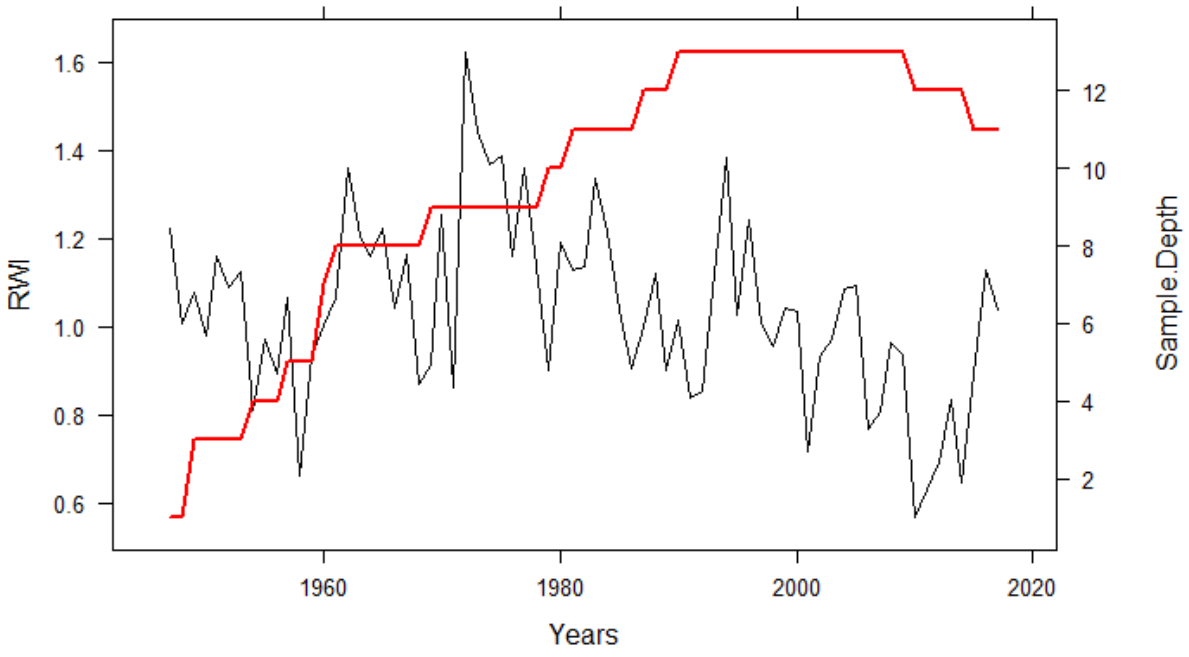

Source: The author.

Figure 46: (a) Tree-ring time series of the samples collected in General Carneiro City; (b) Tree-ring time series for the trees (after averaging the samples per tree); (c) Ring Width Index (RWI) as black line and sample depth in red line for General Carneiro City.

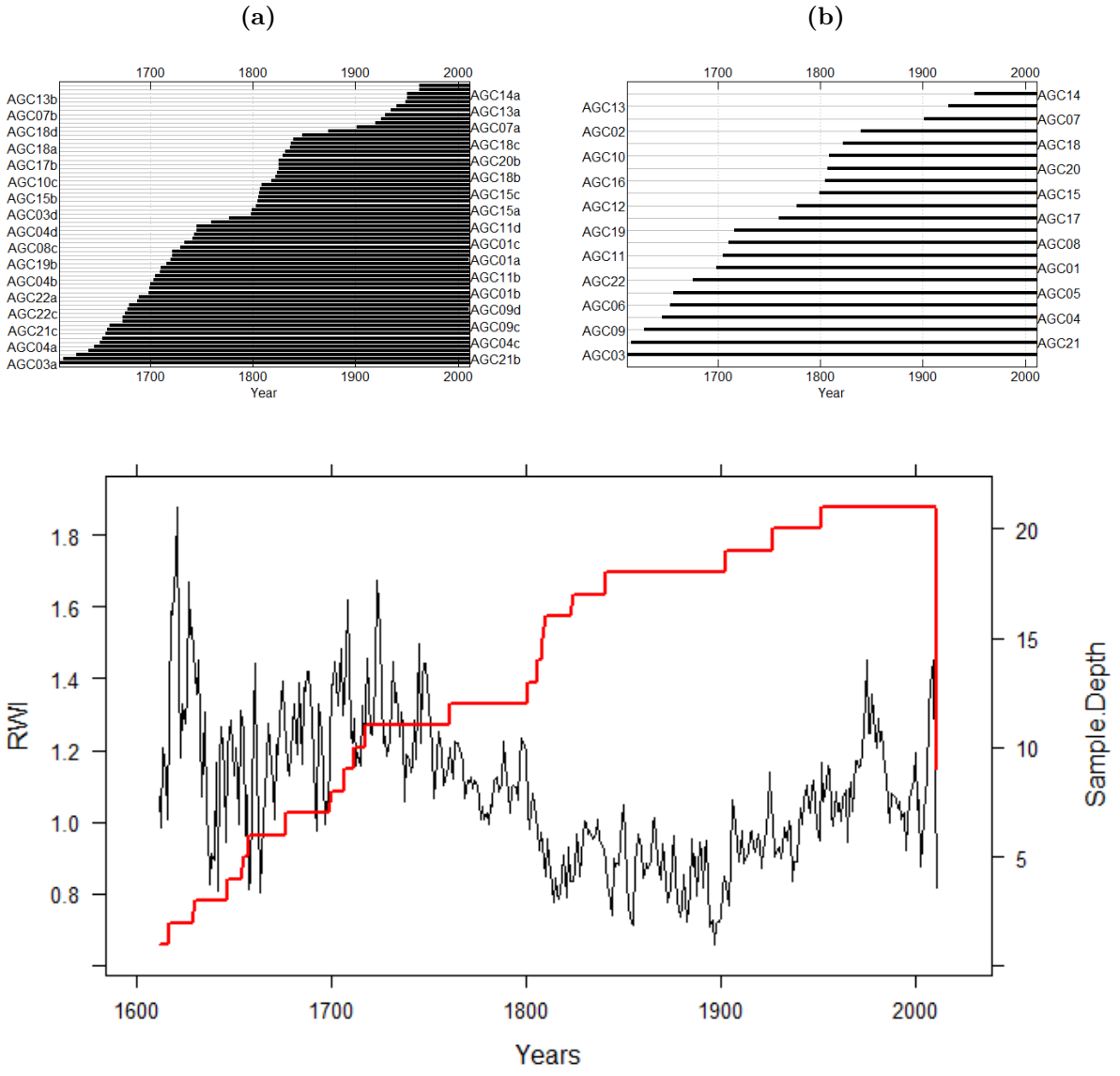

Source: The author.

Figure 47: (a) Tree-ring time series of the samples collected in Irani City; (b) Tree-ring time series for the trees (after averaging the samples per tree); (c) Ring Width Index (RWI) as black line and sample depth in red line for Irani City.

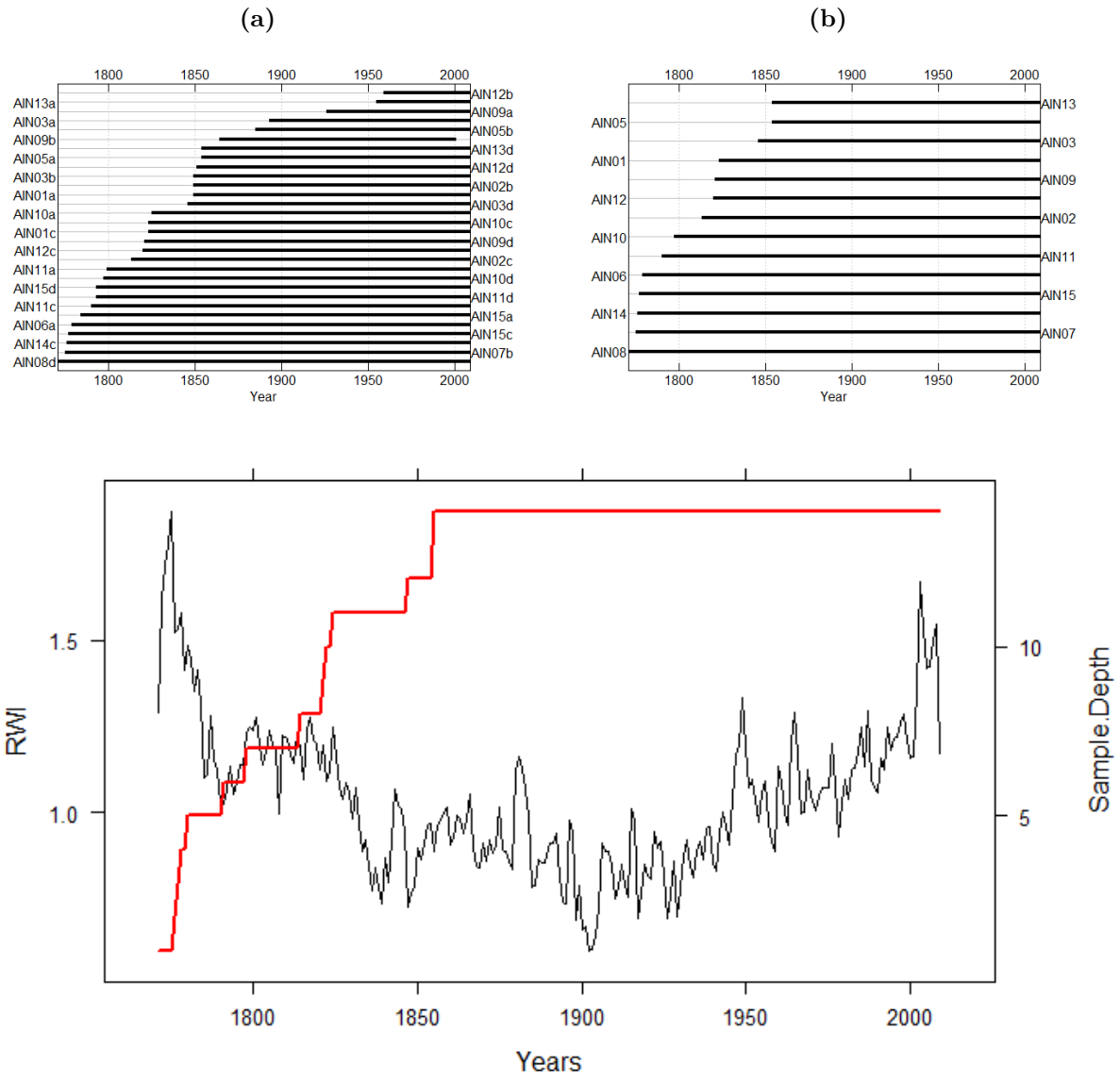

Source: The author.

Figure 48: (a) Tree-ring time series of the samples collected in Irineópolis City; (b) Tree-ring time series for the trees (after averaging the samples per tree); (c) Ring Width Index (RWI) as black line and sample depth in red line for Irineópolis City.

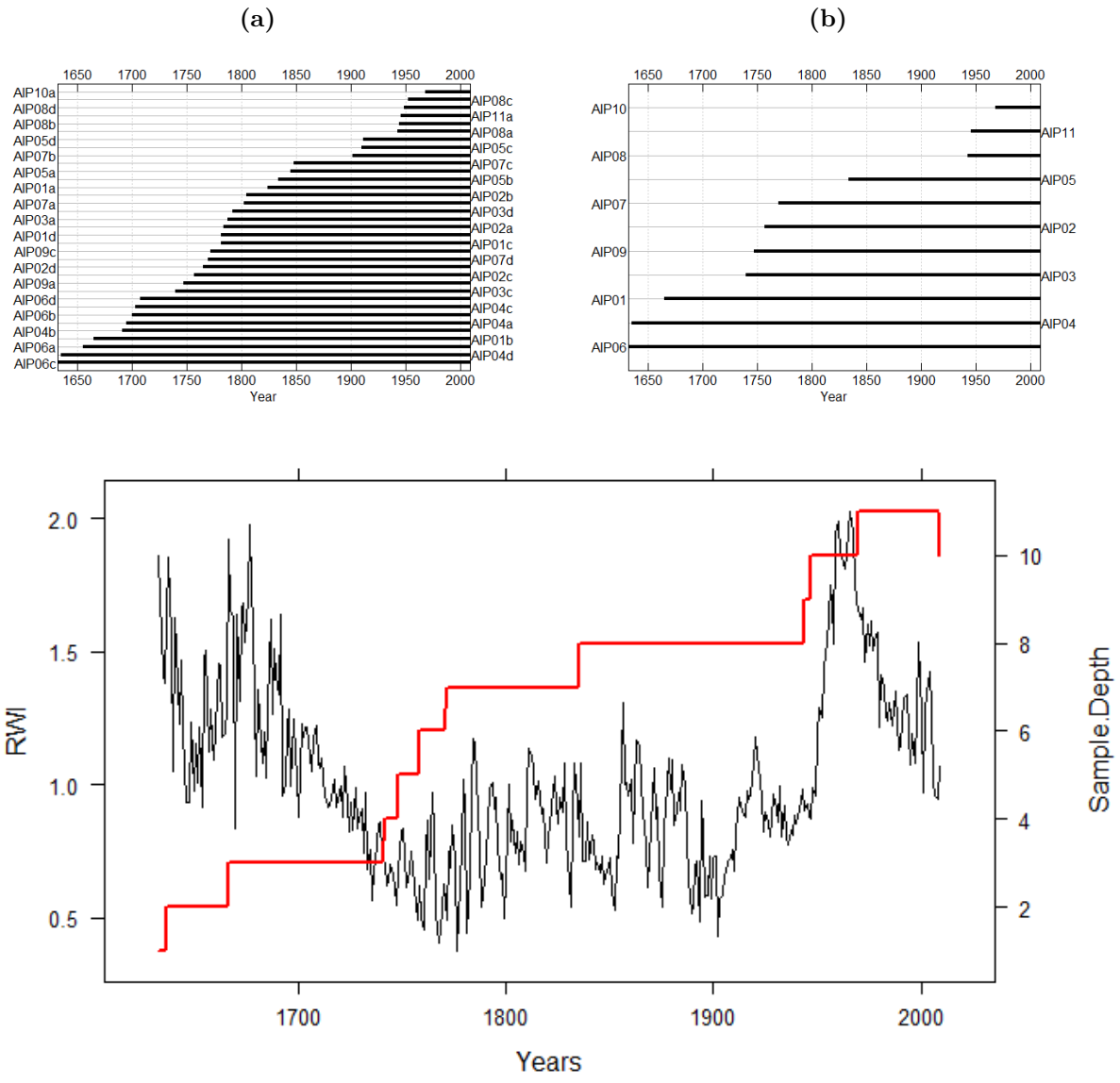

Source: The author.

Figure 49: (a) Tree-ring time series for the trees (after averaging the samples per tree), the samples were collected in Passo Fundo City, and only the tree indices were obtained for this thesis; (b) Ring Width Index (RWI) as black line and sample depth in red line for Passo Fundo City.

(a)

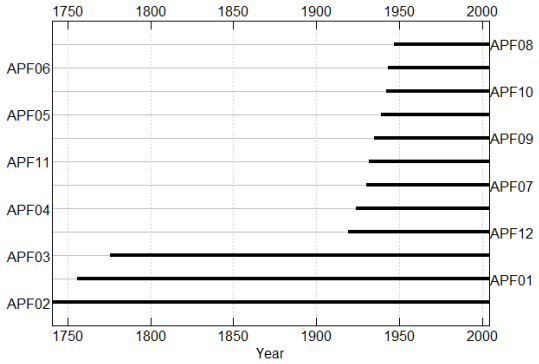

(b)

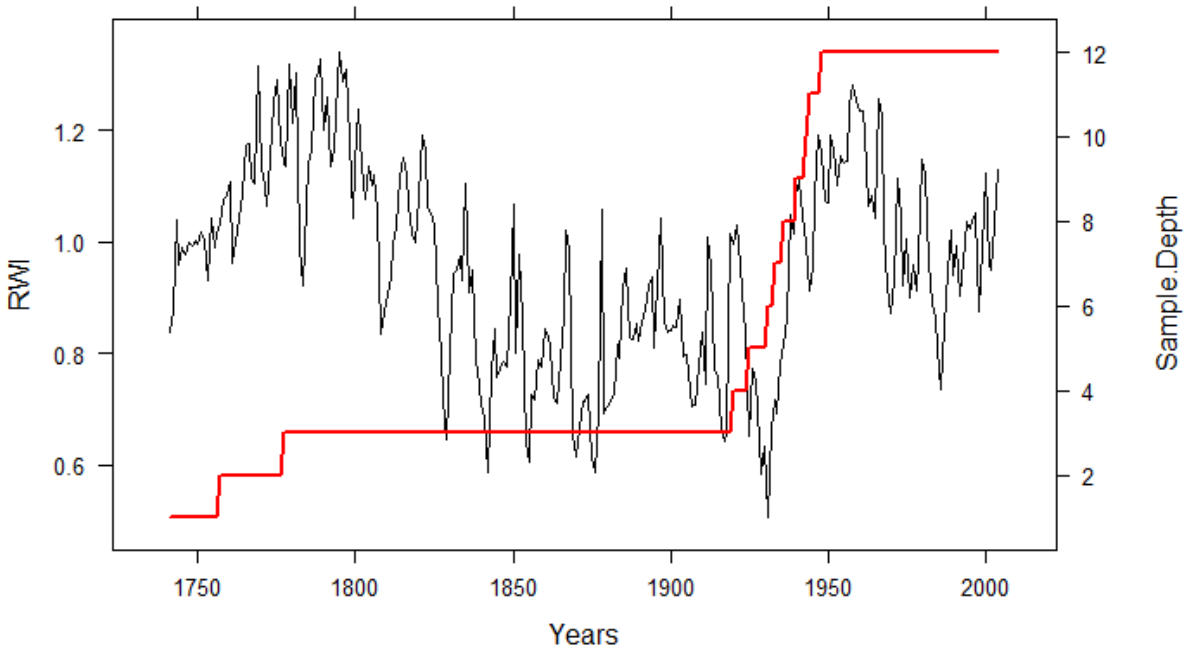

Source: The author.

Figure 50: (a) Tree-ring time series of the samples collected in São Francisco de Paula City; (b) Tree-ring time series for the trees (after averaging the samples per tree); (c) Ring Width Index (RWI) as black line and sample depth in red line for São Francisco de Paula City.

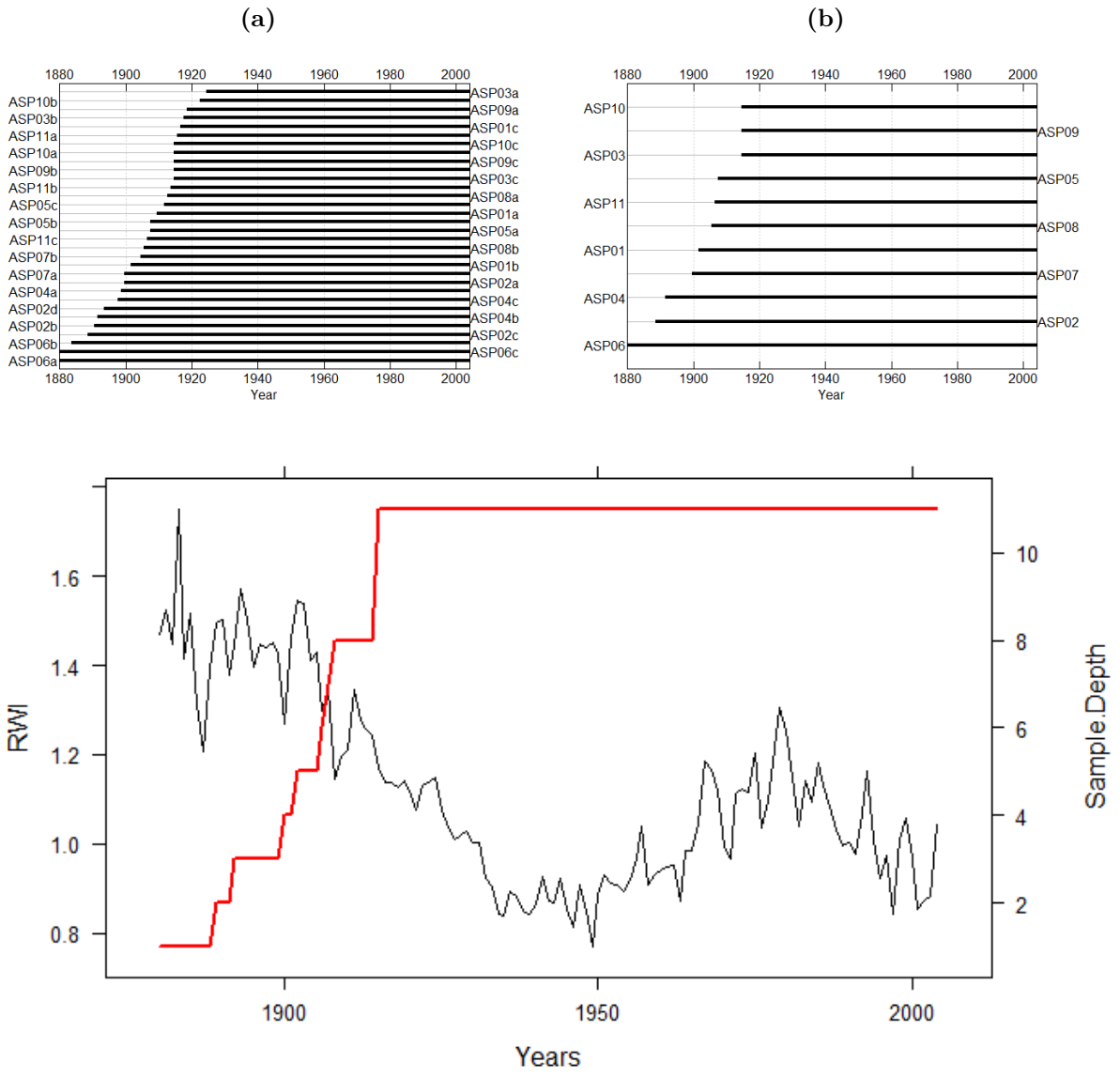

Source: The author.

APPENDIX B – CONTINUOUS WAVELET TRANSFORM (CWT) FIGURES

The figures presented in this appendix display the results of the continuous wavelet transform (CWT) analysis conducted on the time series data for each parameter and RWI for each city in this study. Each CWT figure represents the time-evolving wavelet power spectrum and highlights potential periodicities and their time-localization. The detailed analysis is provided in the **Results - Continuous Wavelet Transform (CWT)** section.

Figure 51: Continuous Wavelet Transforms (CWTs) of the Ring Width Index (RWI) of (a) Açungui, (b) Canela, (c) Chapecó, (d) Coxilha, (e) Curitibanos, (f) General Carneiro, (g) Irani, (h) Irineópolis, (i) Passo Fundo, and (J) São Francisco de Paula. The black contours indicate regions with a significance level > 0.95.

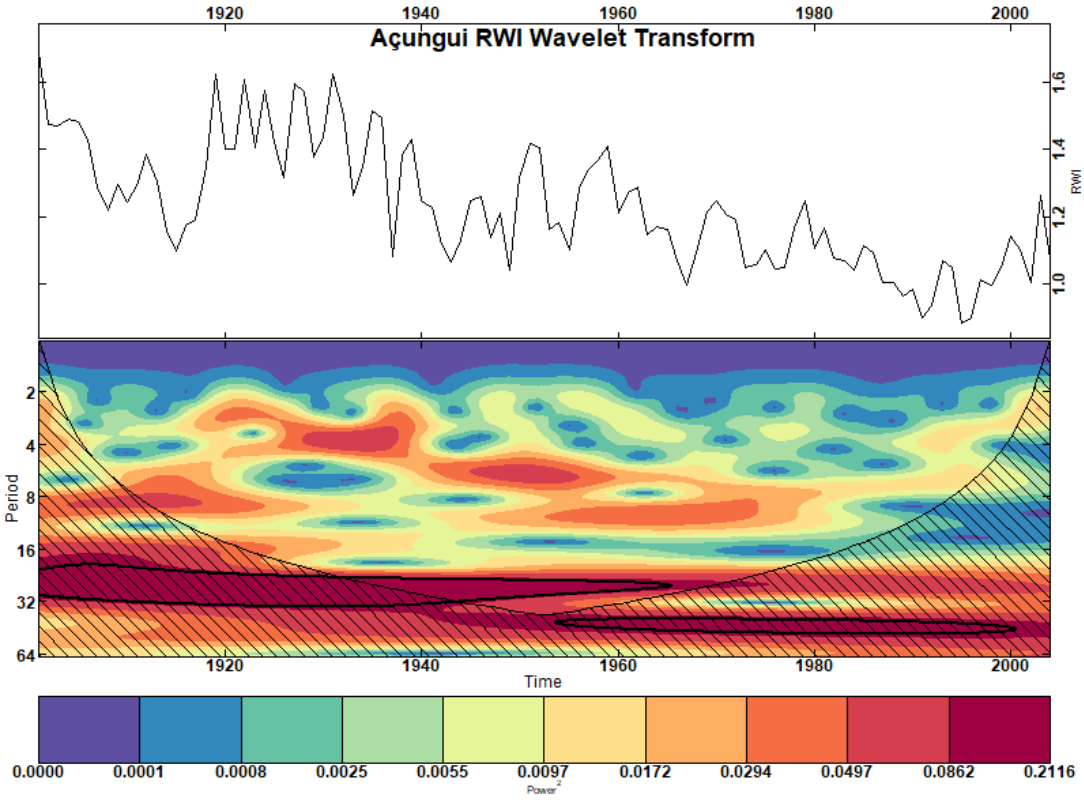

(a)

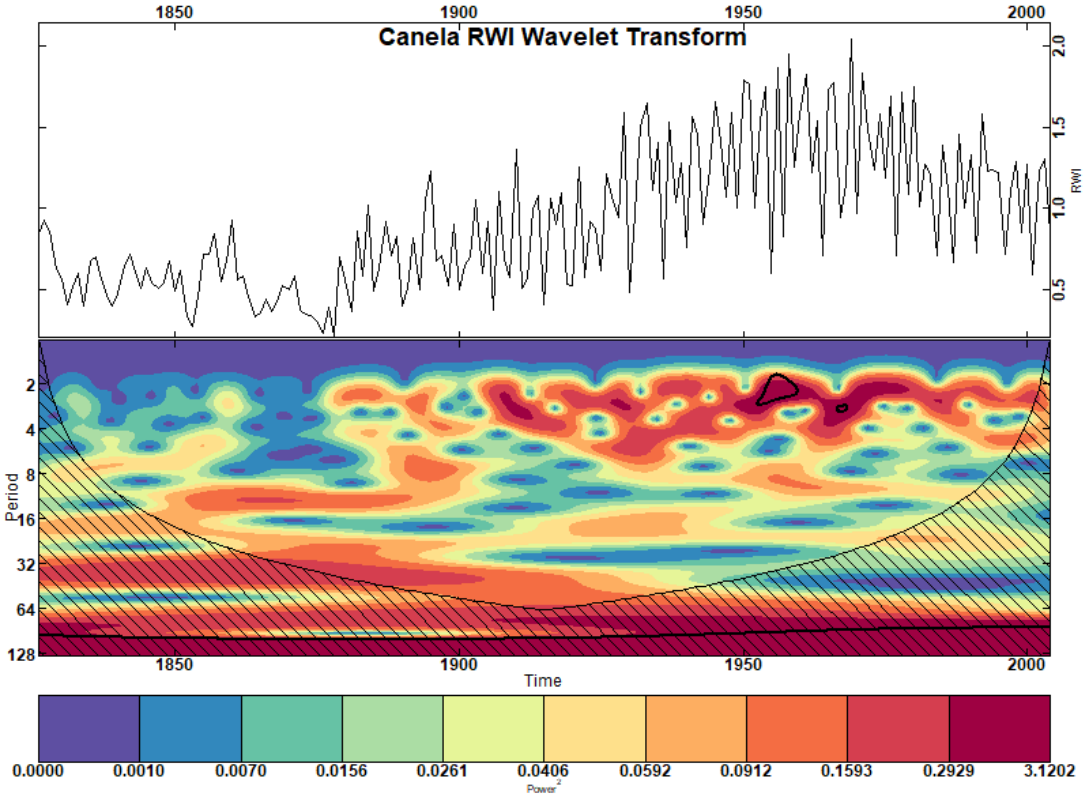
Canela RWI Wavelet Transform
1850
1900
1950
2000
RWI
0.5
1.0
1.5
2.0
Period
2
4
8
16
32
64
128
Time
0.0000
0.0010
0.0070
0.0156
0.0261
0.0406
0.0592
0.0912
0.1593
0.2929
3.1202
Power²

(b)

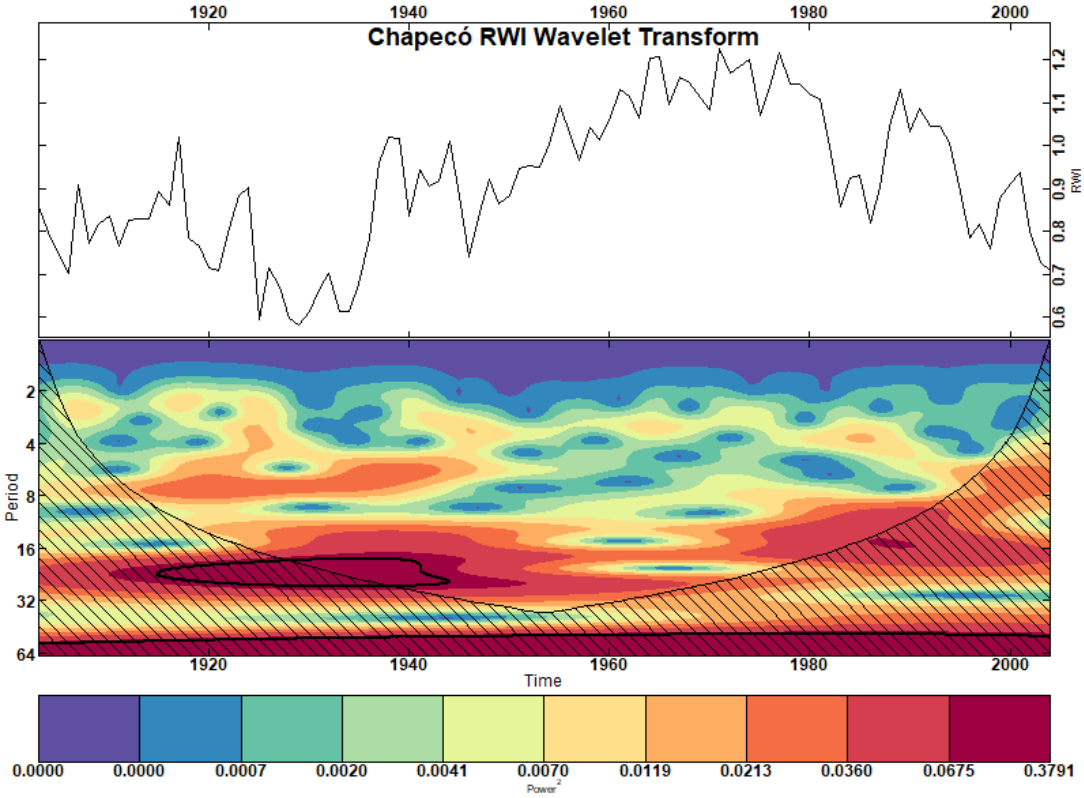
Chapecó RWI Wavelet Transform
1920
1940
1960
1980
2000
RWI
0.6
0.7
0.8
0.9
1.0
1.1
1.2
Period
2
4
8
16
32
64
Time
0.0000
0.0000
0.0007
0.0020
0.0041
0.0070
0.0119
0.0213
0.0360
0.0675
0.3791
Power²

(c)

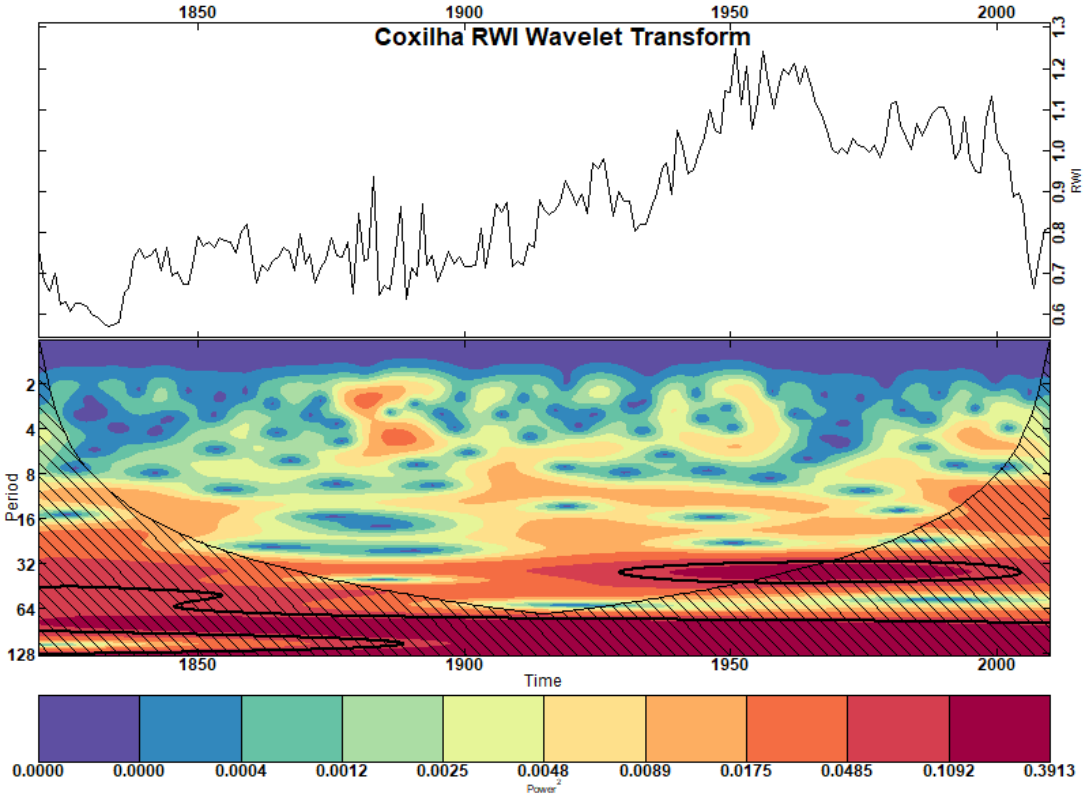
Coxilha RWI Wavelet Transform
1850
1900
1950
2000
RWI
Period
Time
0.0000
0.0000
0.0004
0.0012
0.0025
0.0048
0.0089
0.0175
0.0485
0.1092
0.3913
Power²

(d)

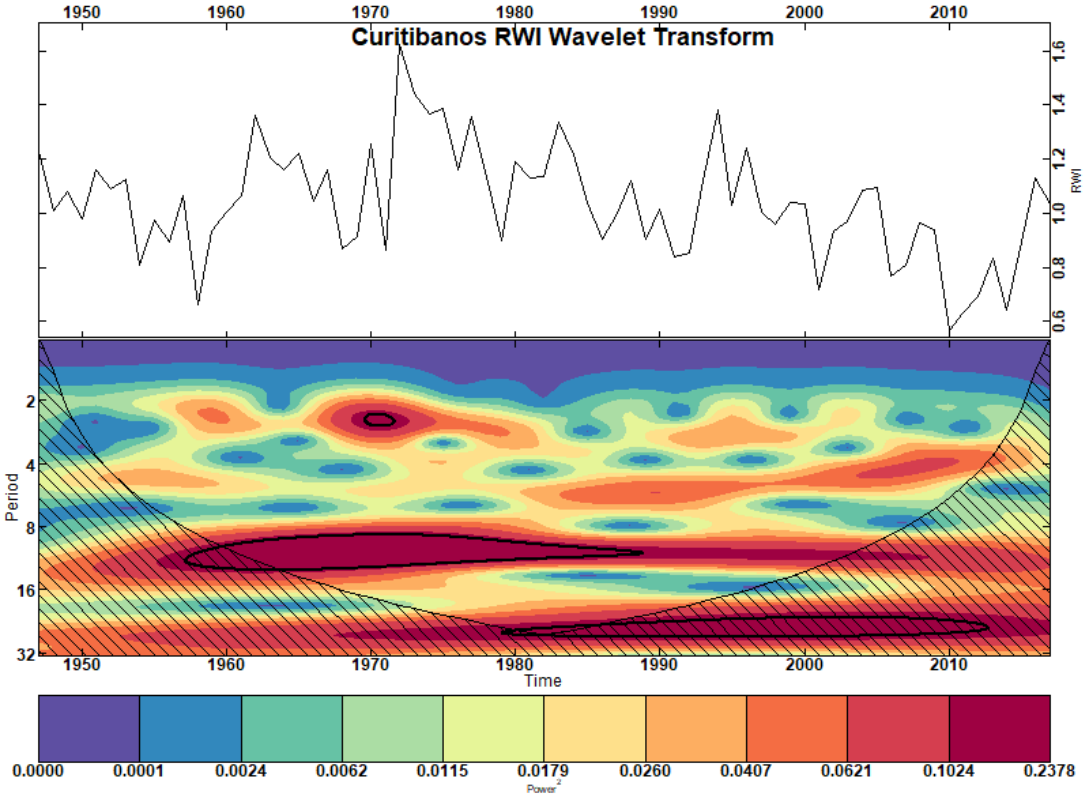
Curitibanos RWI Wavelet Transform
1950
1960
1970
1980
1990
2000
2010
RWI
Period
Time
0.0000
0.0001
0.0024
0.0062
0.0115
0.0179
0.0260
0.0407
0.0621
0.1024
0.2378
Power²

(e)

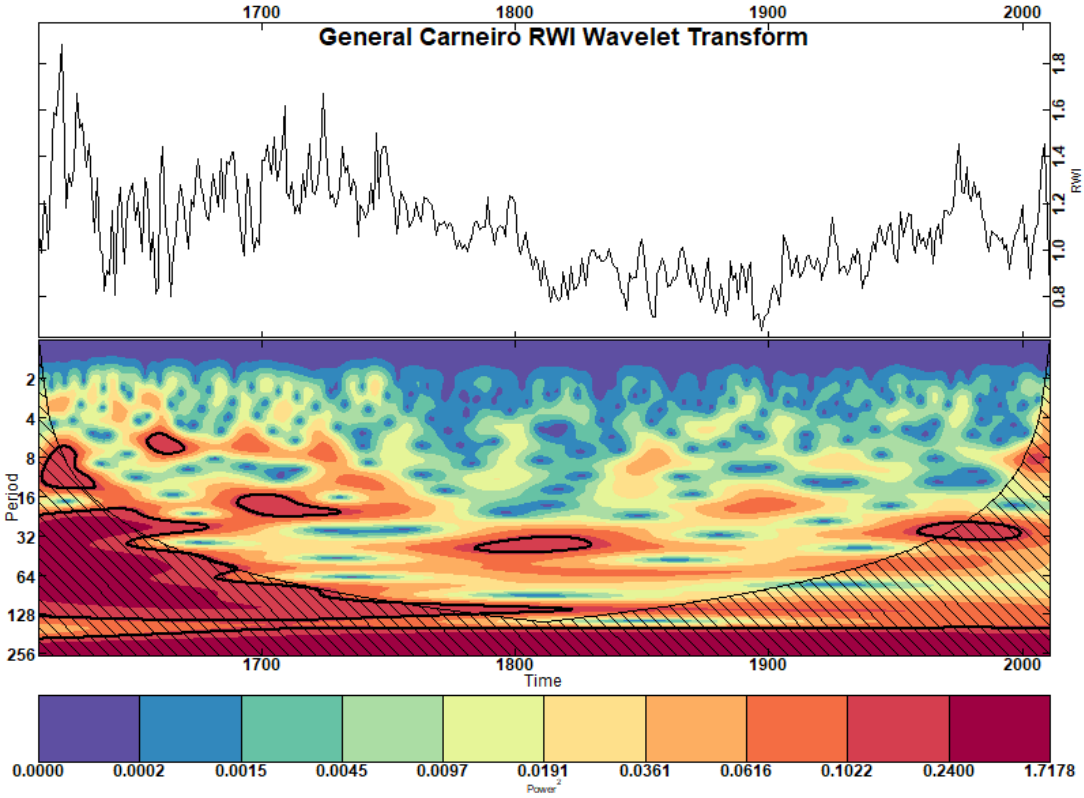
General Carneiro RWI Wavelet Transform
1700
1800
1900
2000
RWI
0.8
1.0
1.2
1.4
1.6
1.8
Period
2
4
8
16
32
64
128
256
Time
0.0000
0.0002
0.0015
0.0045
0.0097
0.0191
0.0361
0.0616
0.1022
0.2400
1.7178
Power²

(f)

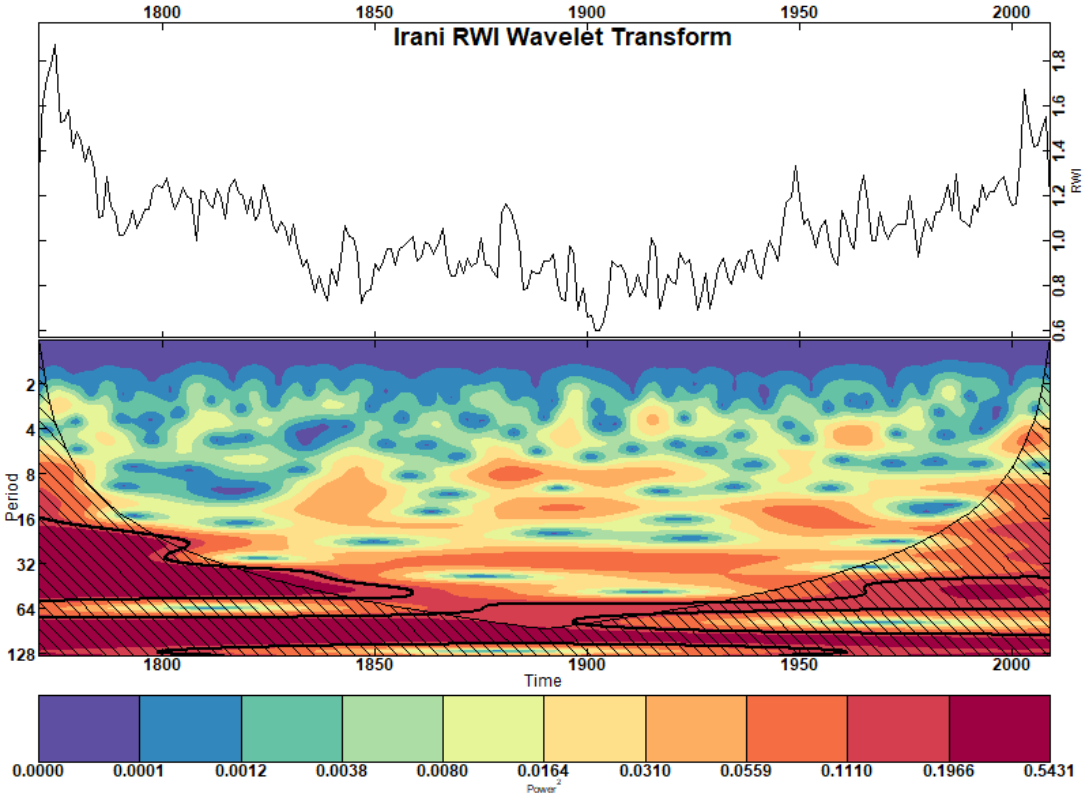
Irani RWI Wavelet Transform
1800
1850
1900
1950
2000
RWI
0.6
0.8
1.0
1.2
1.4
1.6
1.8
Period
2
4
8
16
32
64
128
Time
0.0000
0.0001
0.0012
0.0038
0.0080
0.0164
0.0310
0.0559
0.1110
0.1966
0.5431
Power²

(g)

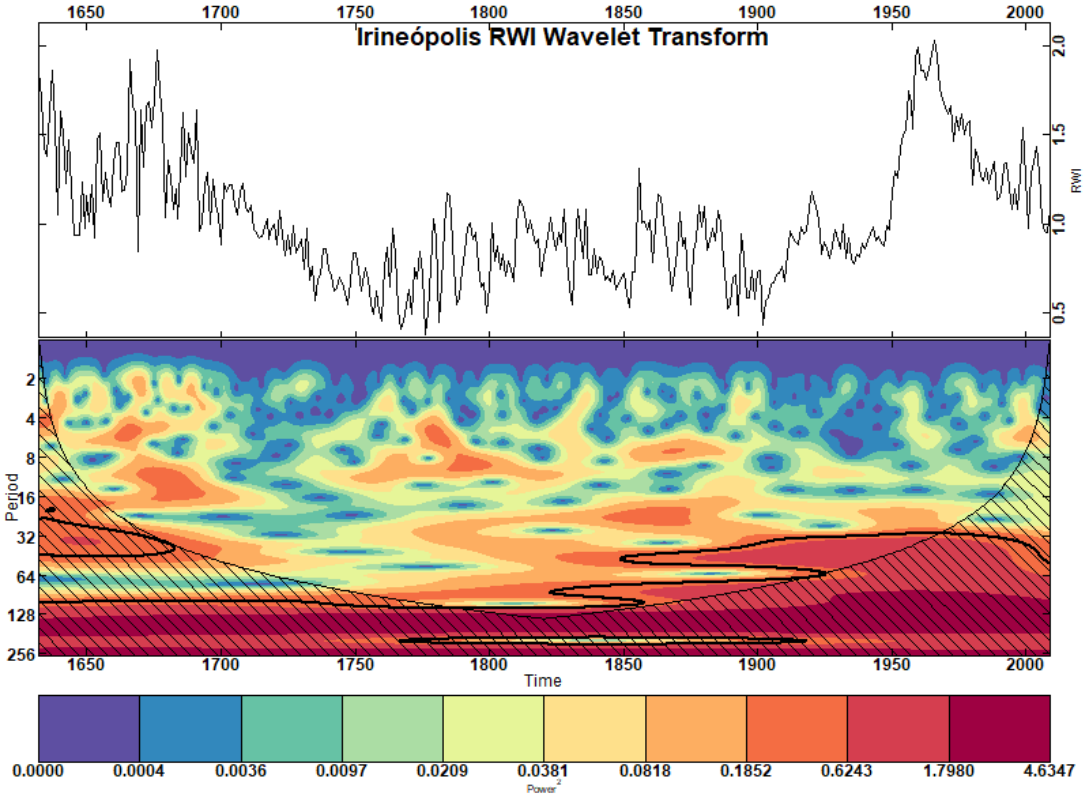
Irineópolis RWI Wavelet Transform
1650
1700
1750
1800
1850
1900
1950
2000
RWI
0.5
1.0
1.5
2.0
Period
2
4
8
16
32
64
128
256
Time
0.0000
0.0004
0.0036
0.0097
0.0209
0.0381
0.0818
0.1852
0.6243
1.7980
4.6347
Power²

(h)

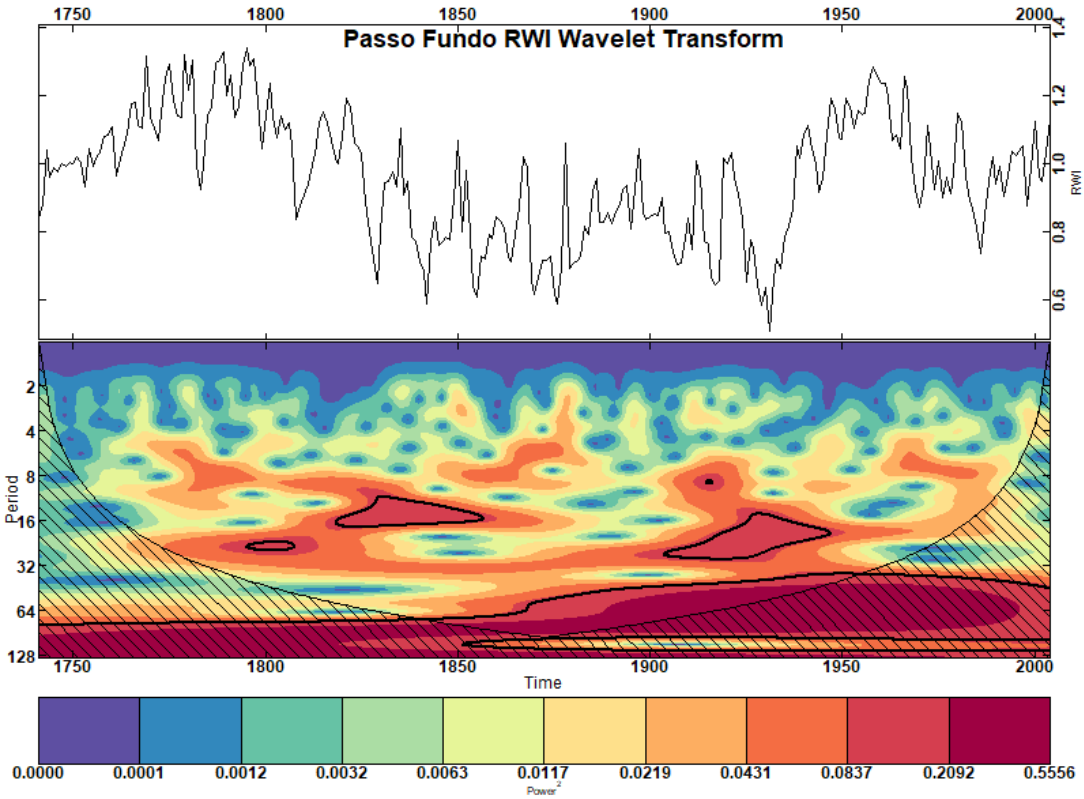
Passo Fundo RWI Wavelet Transform
1750
1800
1850
1900
1950
2000
RWI
0.6
0.8
1.0
1.2
1.4
Period
2
4
8
16
32
64
128
Time
0.0000
0.0001
0.0012
0.0032
0.0063
0.0117
0.0219
0.0431
0.0837
0.2092
0.5556
Power²

(i)

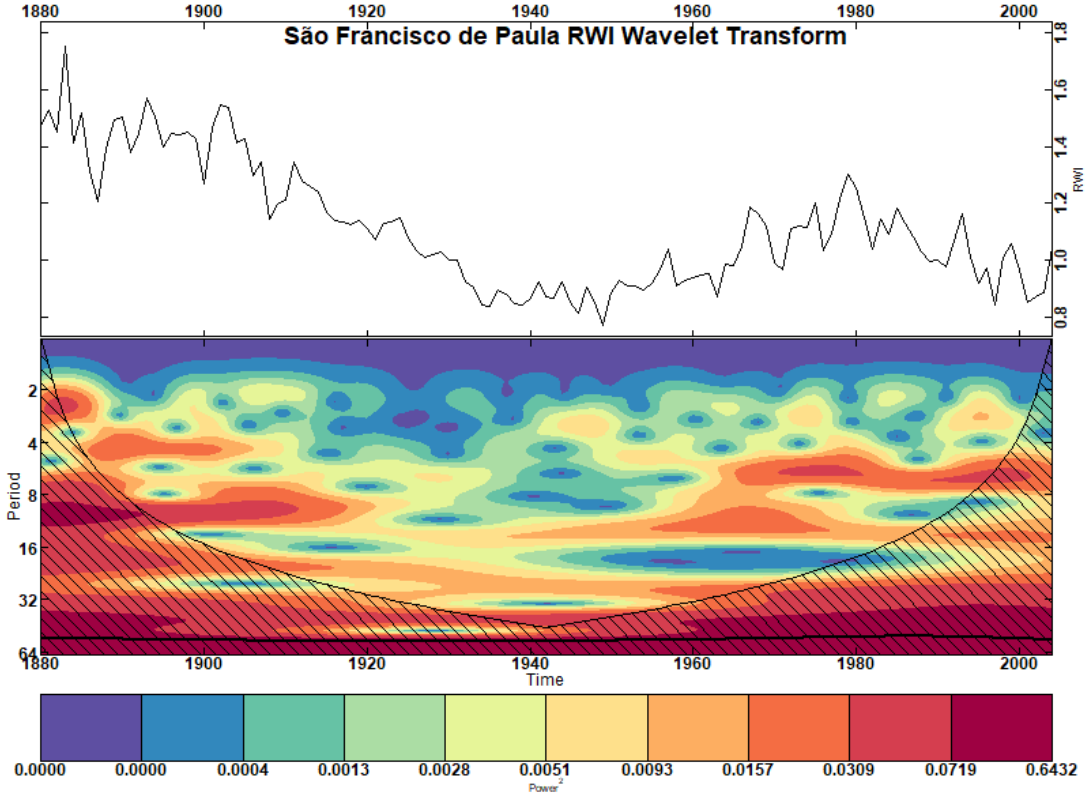

(j)
Source: The author.

Figure 52: Continuous Wavelet Transforms (CWTs) of the time-series: (a) SOI, (b) NIÑO 3.4, (c) SUNSPOT, (d) and ATLSW. The black contours indicate regions with a significance level > 0.95.

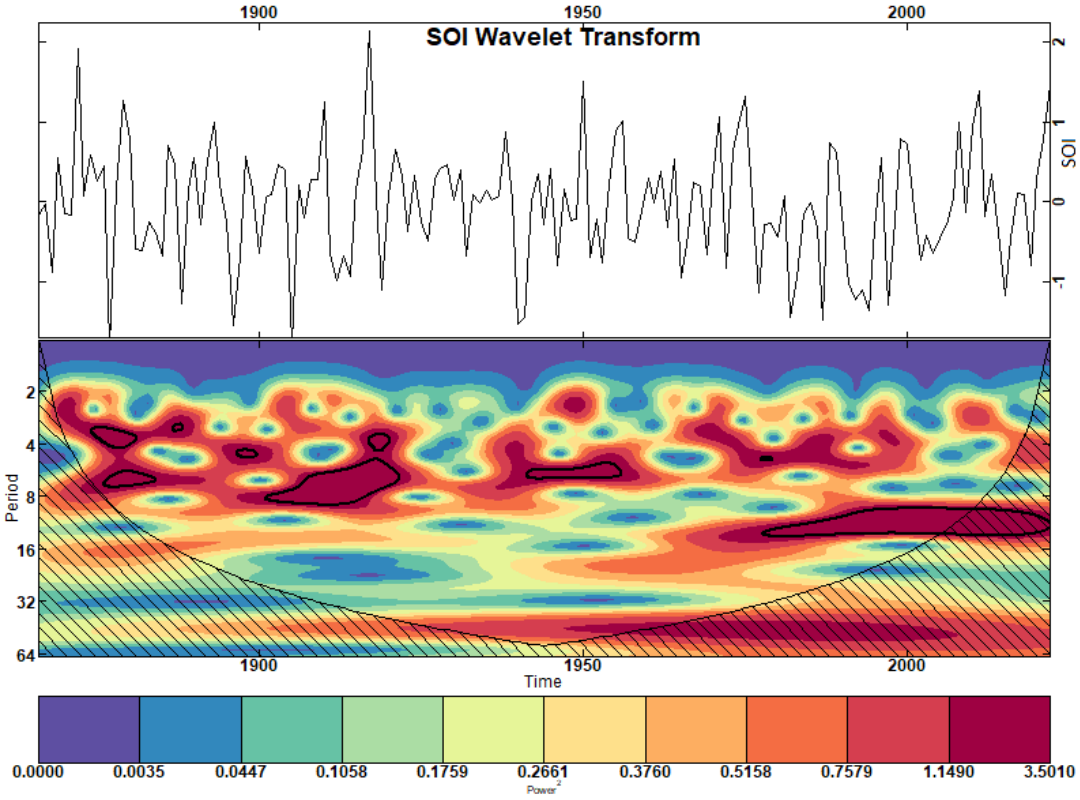

(a)

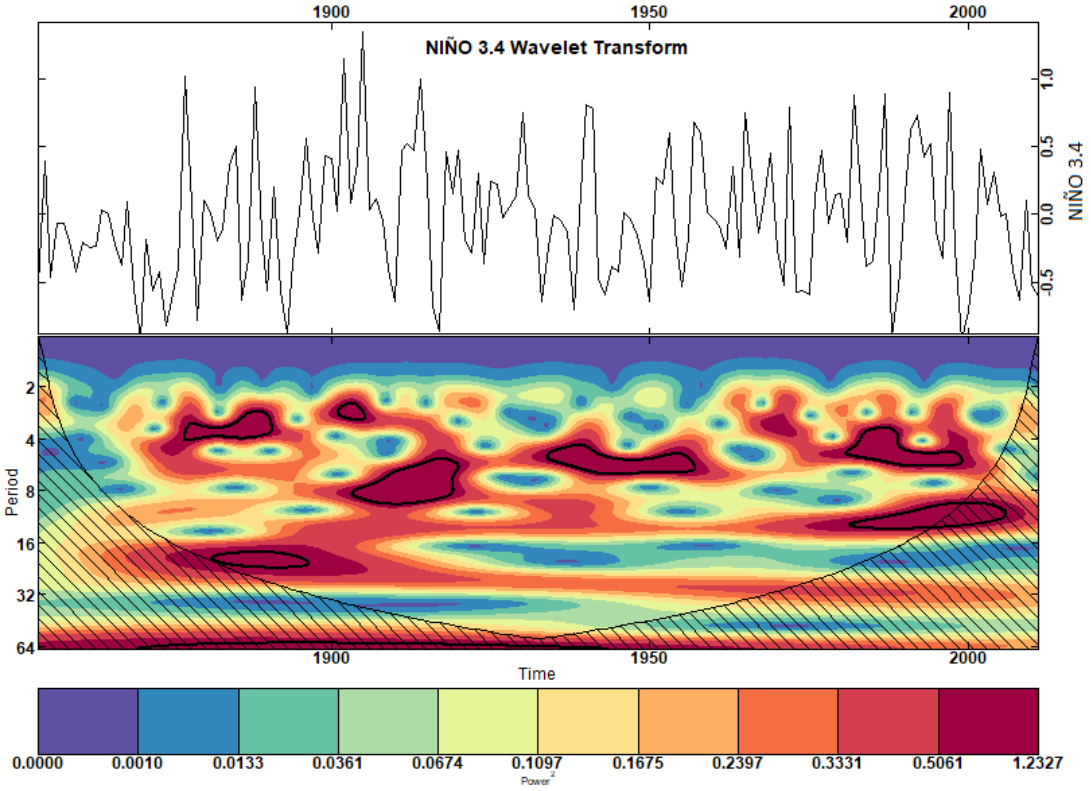

(b)

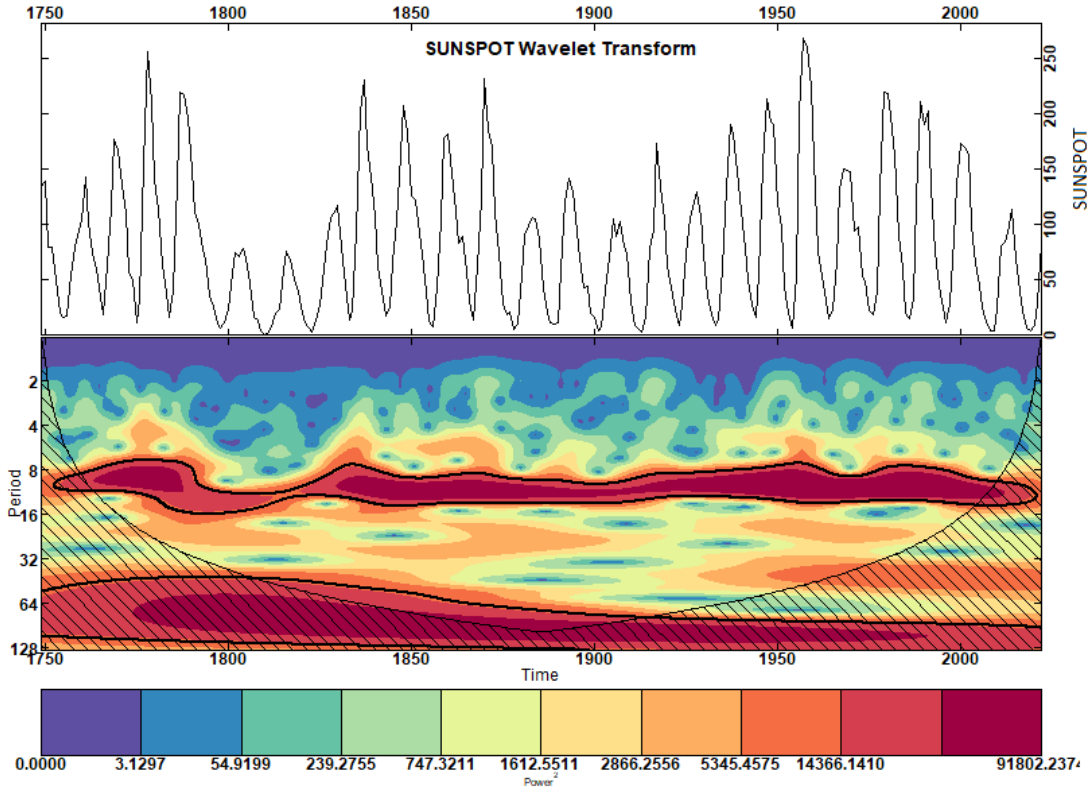

(c)

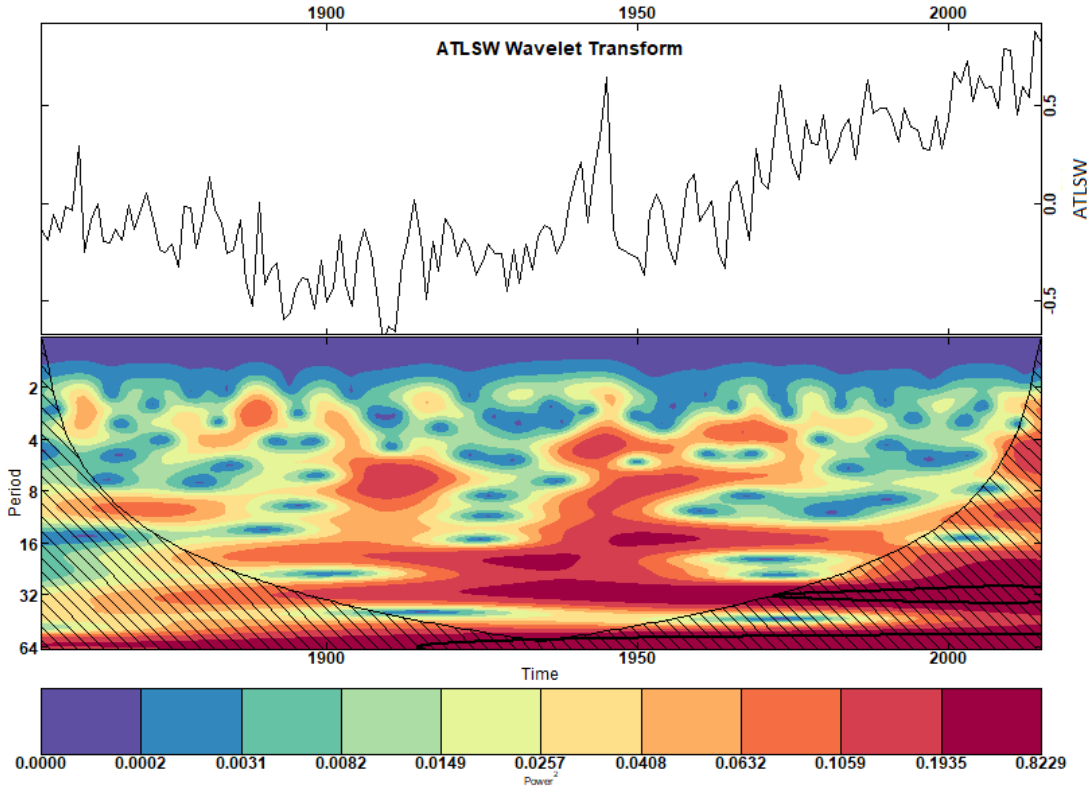

(d)

Source: The author.

Figure 53: Continuous Wavelet Transforms (CWTs) of Climate Variables at Irati Station. (a) Precipitation, (b) Mean Temperature, (c) Minimum Temperature, and (d) Maximum Temperature. The black contours represent regions with a significance level greater than 0.95, indicating statistically significant patterns.

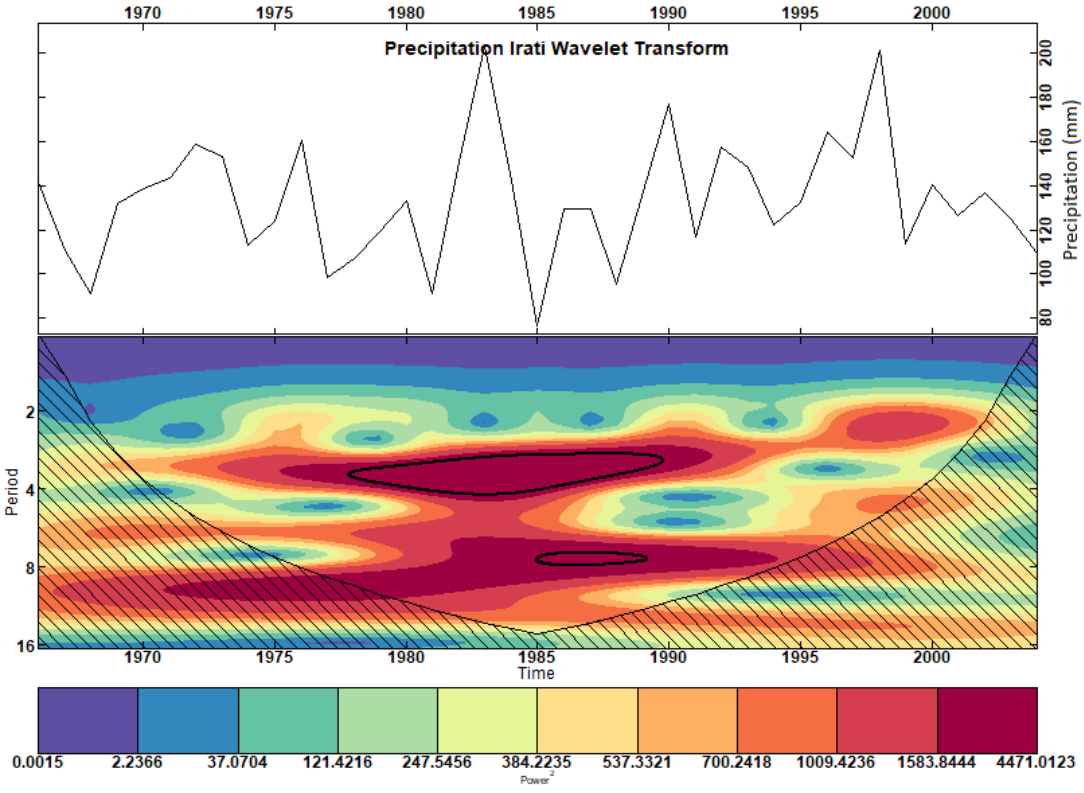

(a)

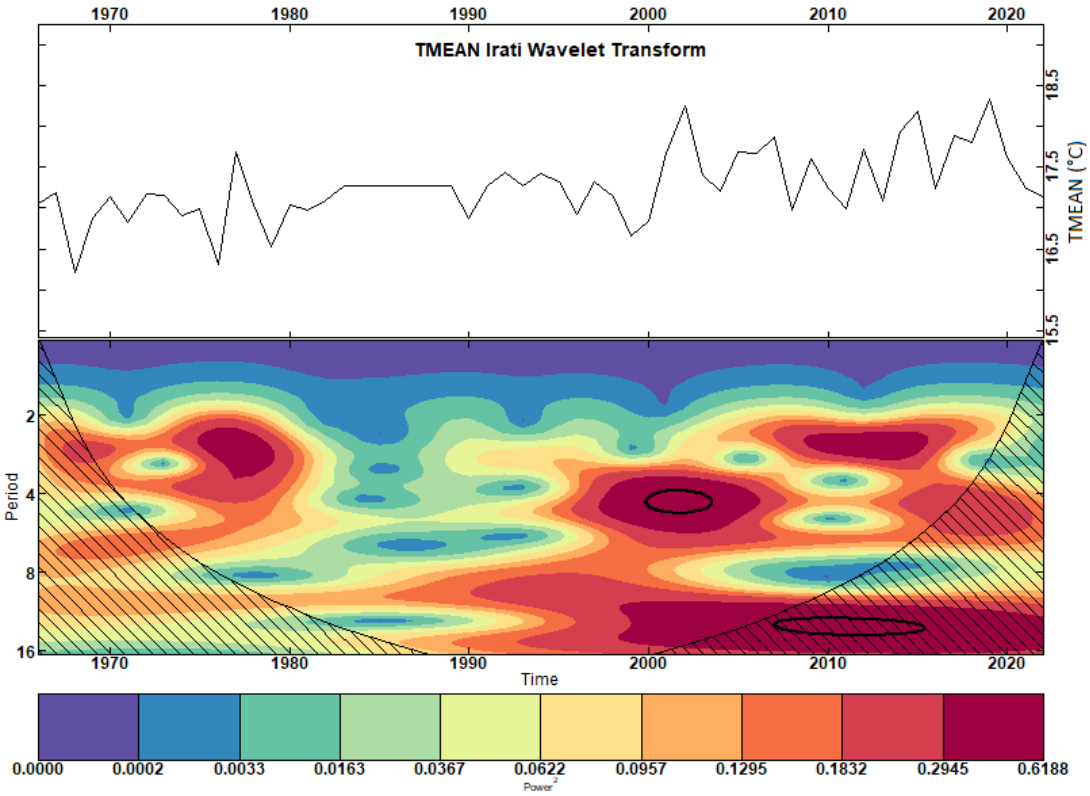

(b)

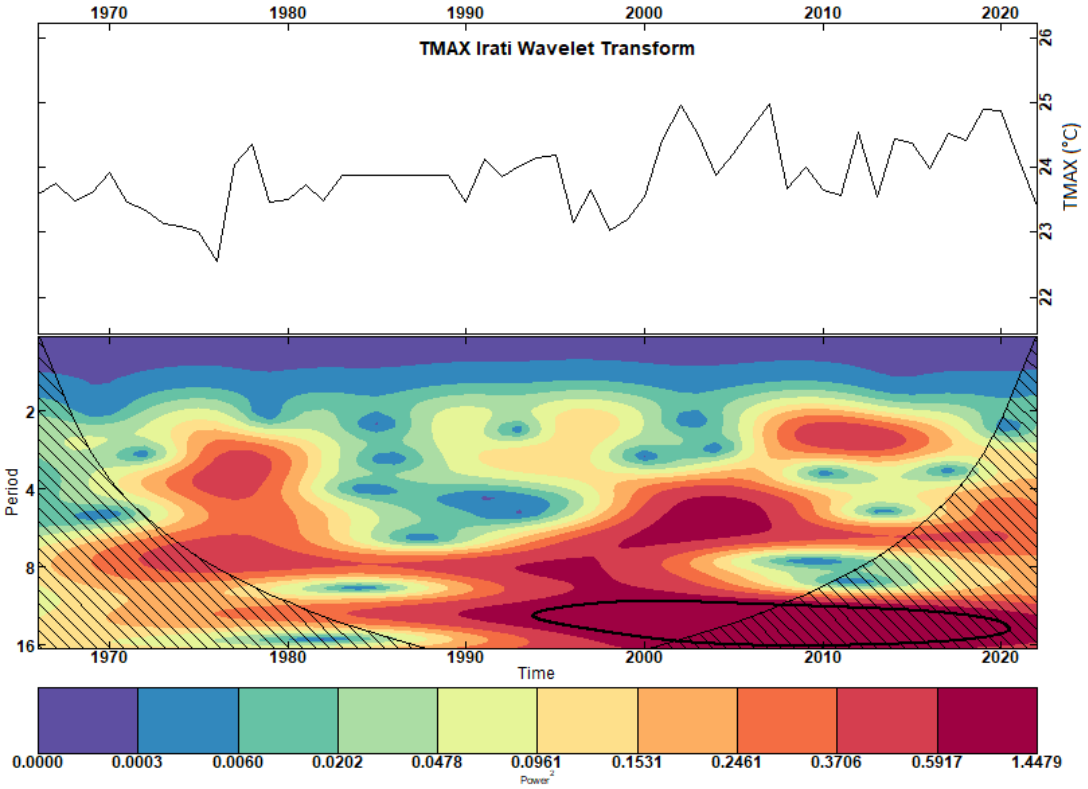

(c)

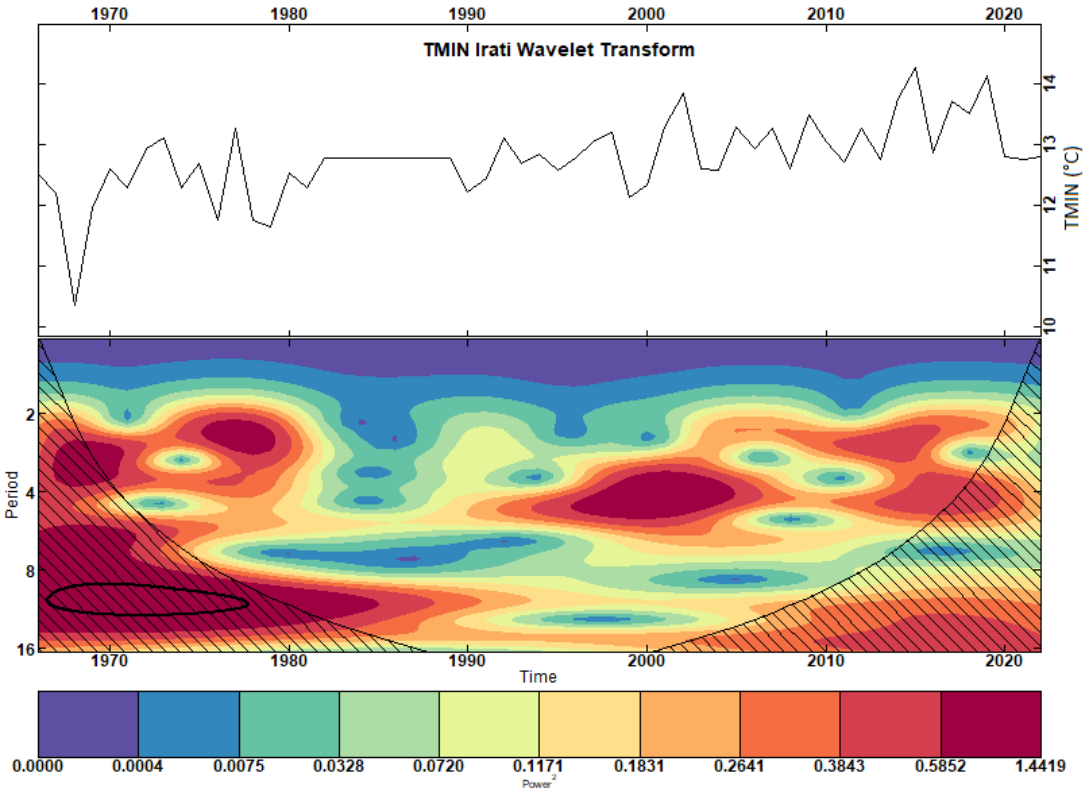

(d)

Source: The author.

Figure 54: Continuous Wavelet Transforms (CWTs) of Climate Variables at Caxias do Sul Station. (a) Precipitation, (b) Mean Temperature, (c) Minimum Temperature, and (d) Maximum Temperature. The black contours represent regions with a significance level greater than 0.95, indicating statistically significant patterns.

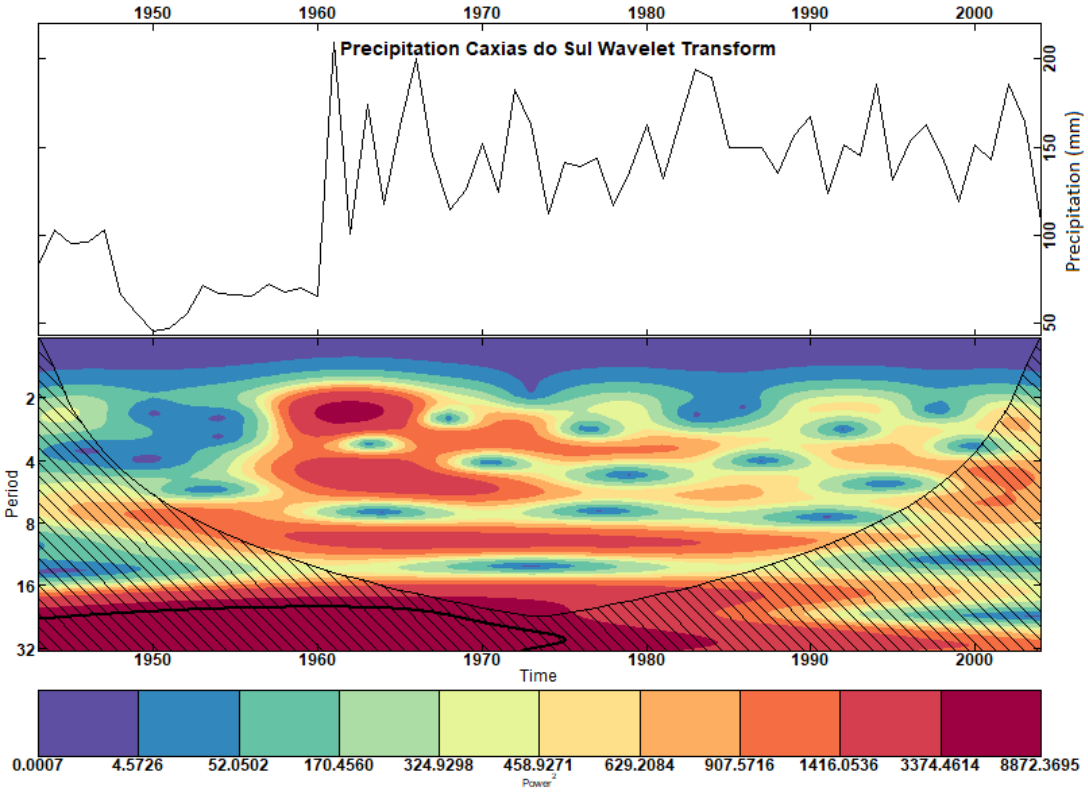

(a)

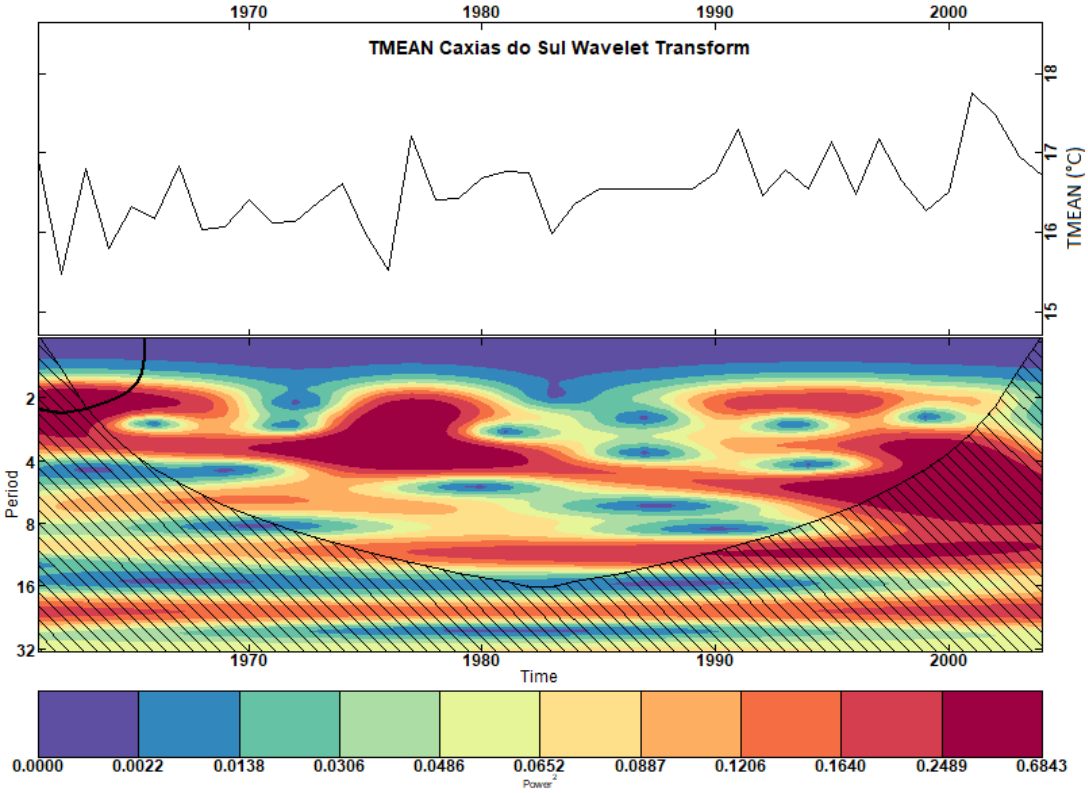

(b)

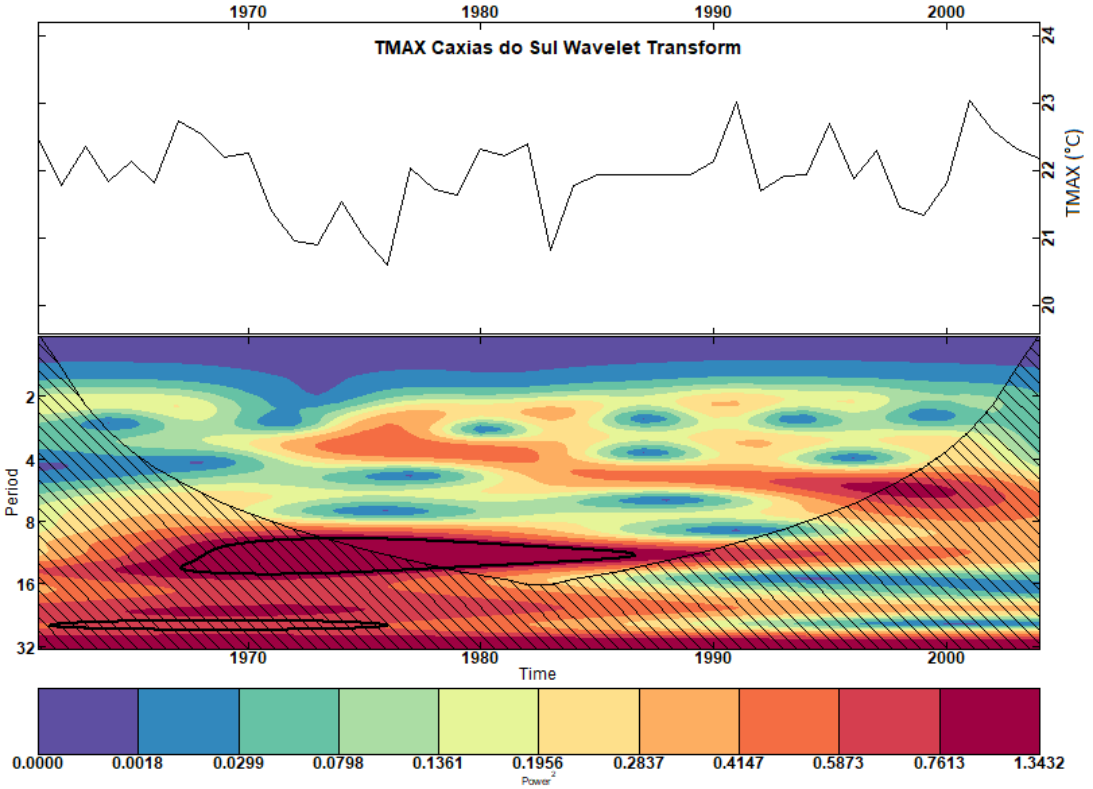

(c)

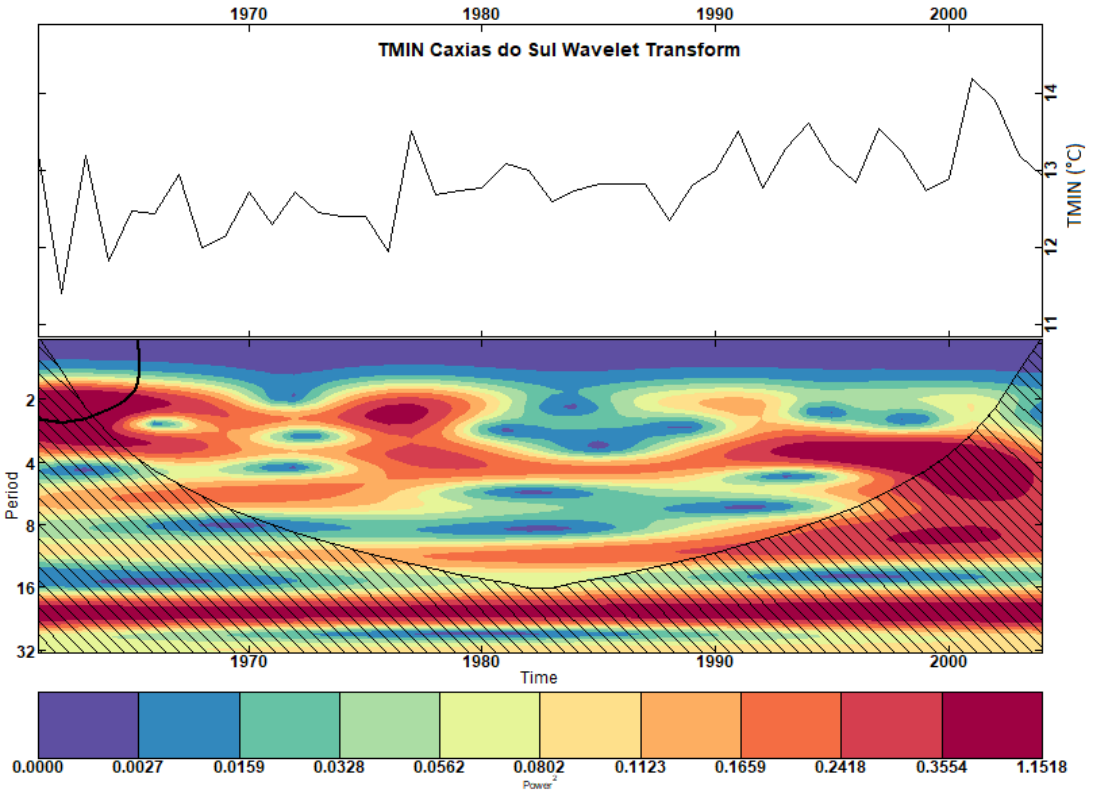

(d)

Source: The author.

Figure 55: Continuous Wavelet Transforms (CWTs) of Climate Variables at Chapecó Station. (a) Precipitation, (b) Mean Temperature, (c) Minimum Temperature, and (d) Maximum Temperature. The black contours represent regions with a significance level greater than 0.95, indicating statistically significant patterns.

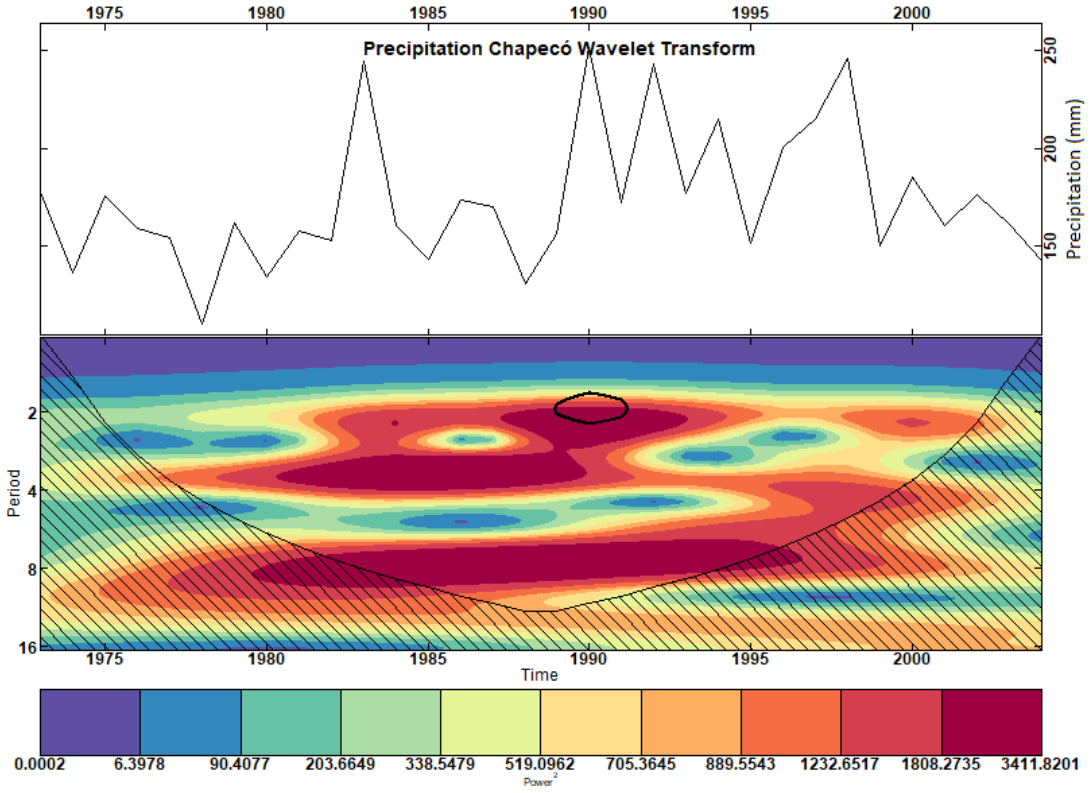

(a)

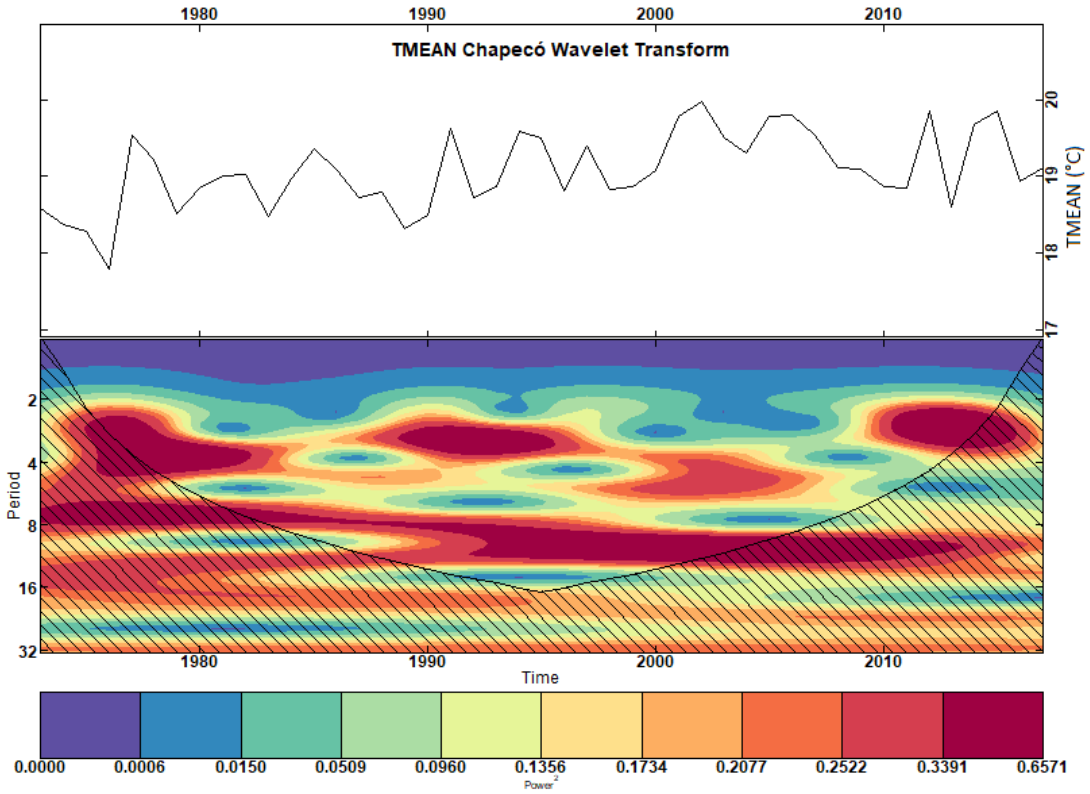

(b)

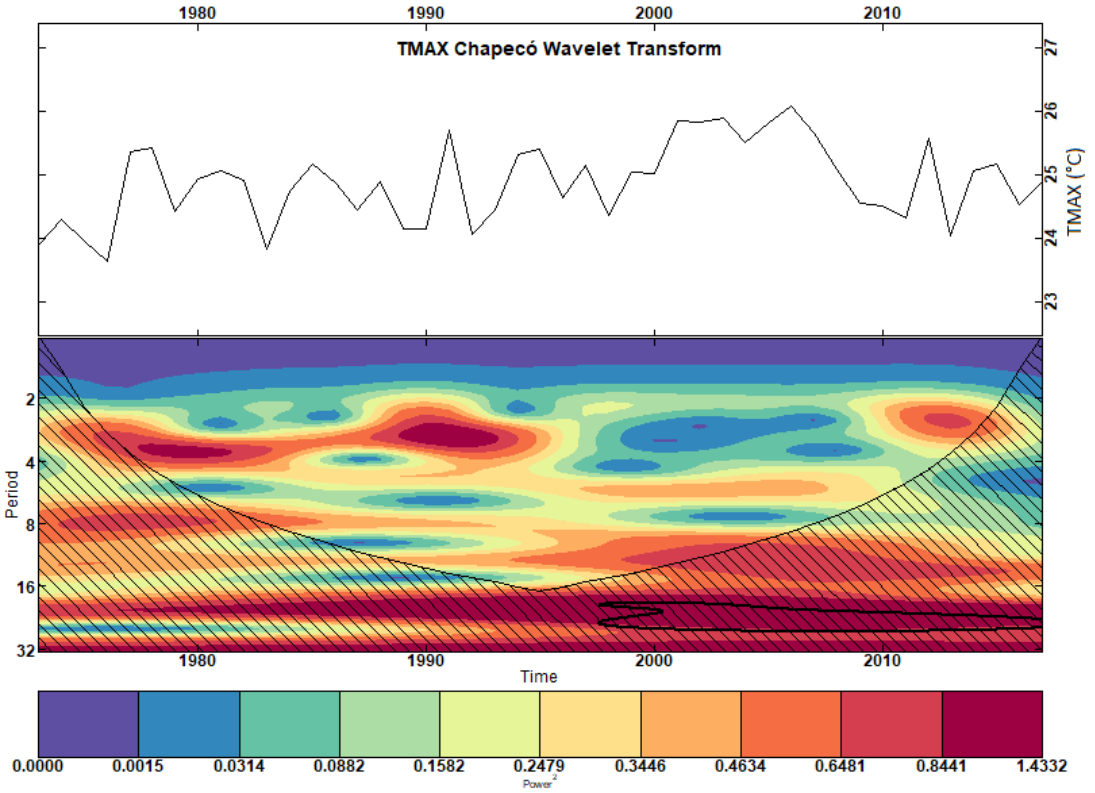

(c)

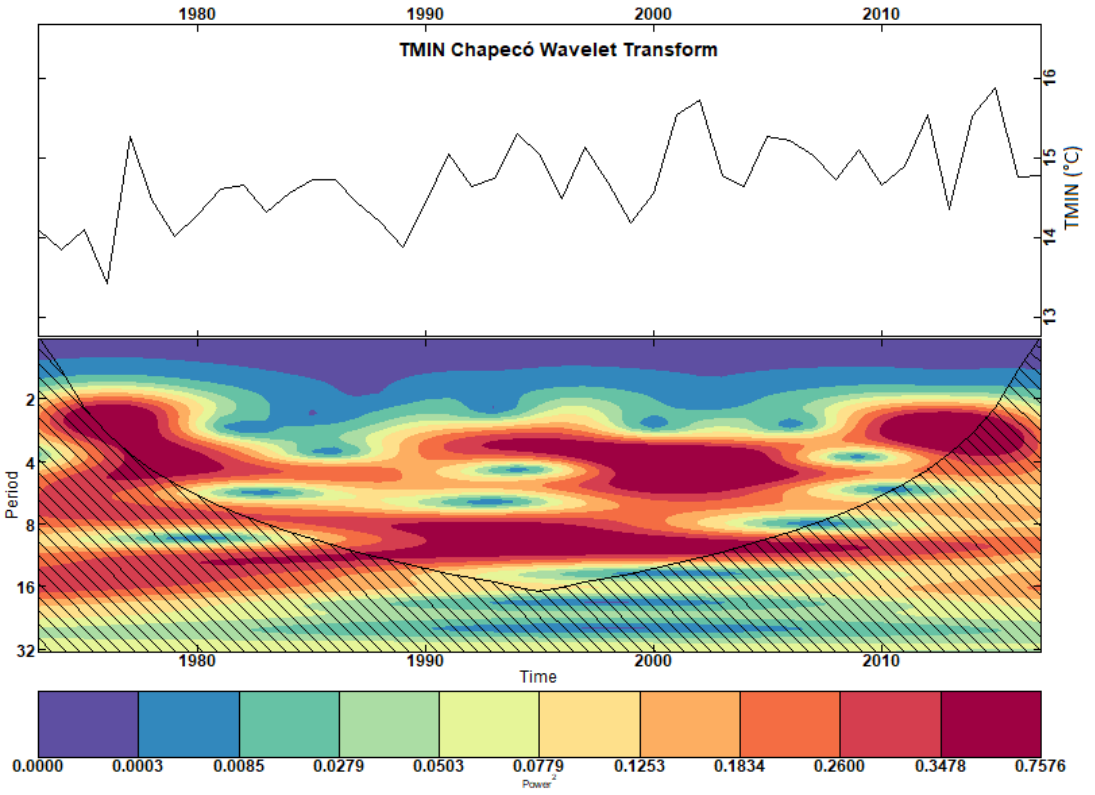

(d)

Source: The author.

Figure 56: Continuous Wavelet Transforms (CWTs) of Climate Variables at Passo Fundo Station. (a) Precipitation, (b) Mean Temperature, (c) Minimum Temperature, and (d) Maximum Temperature. The black contours represent regions with a significance level greater than 0.95, indicating statistically significant patterns.

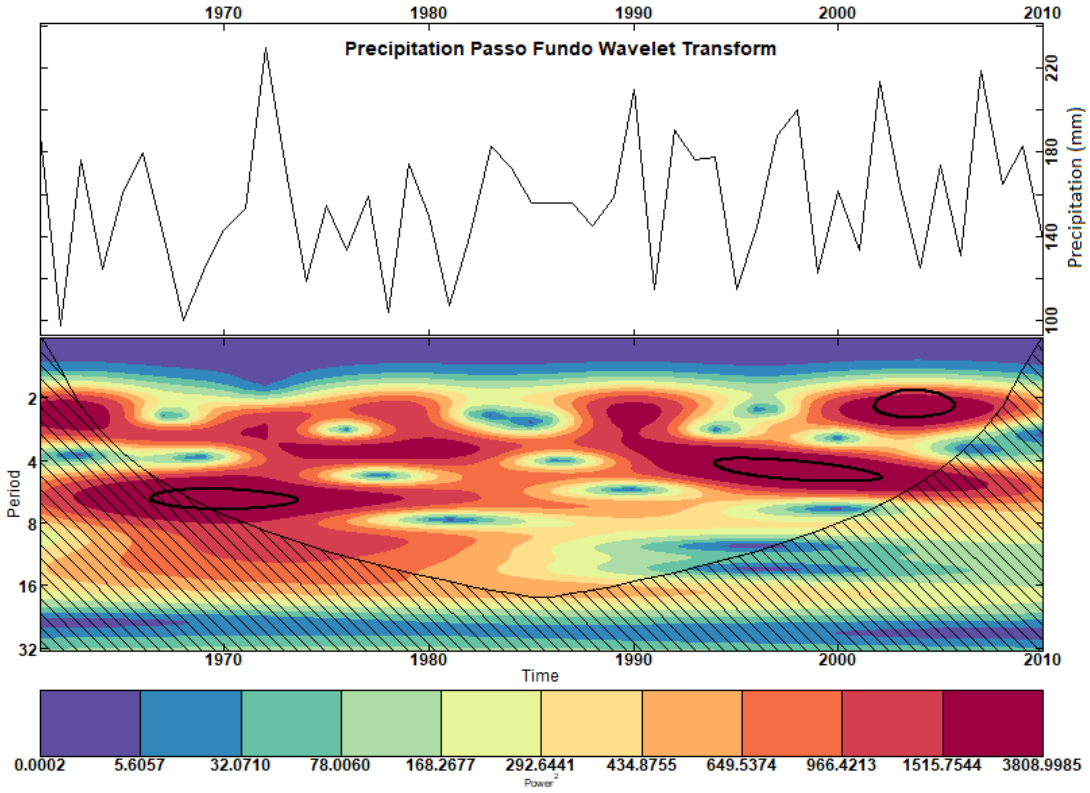

(a)

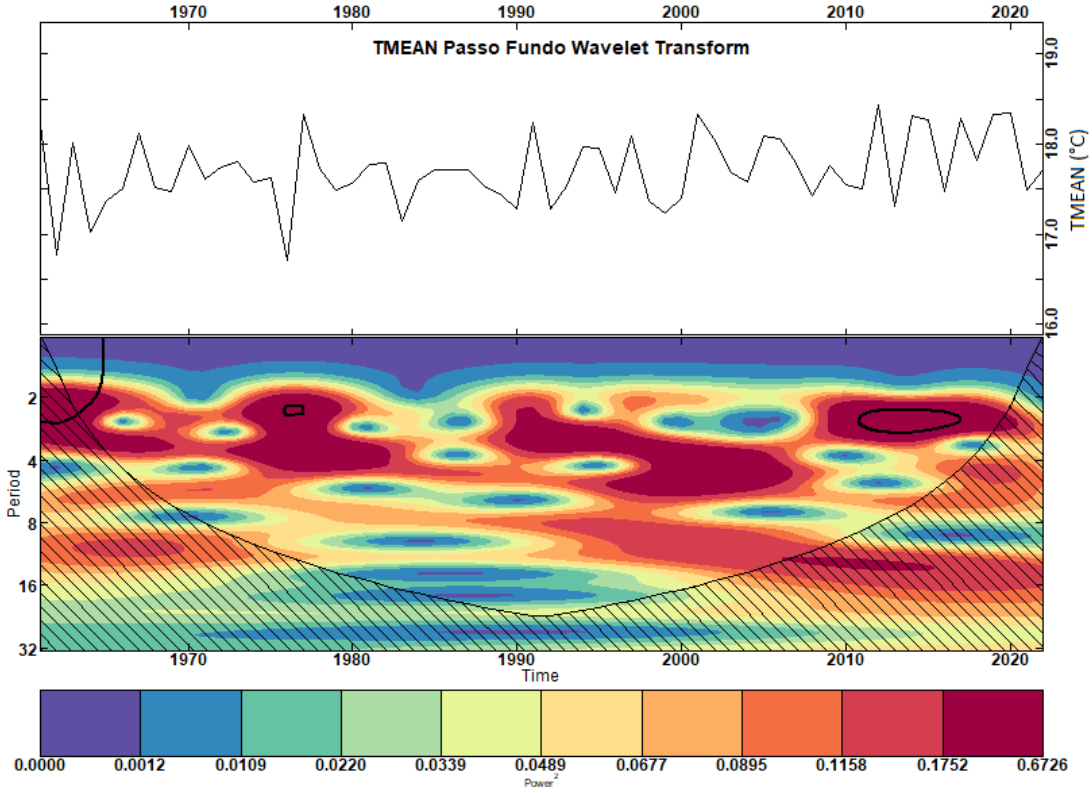

(b)

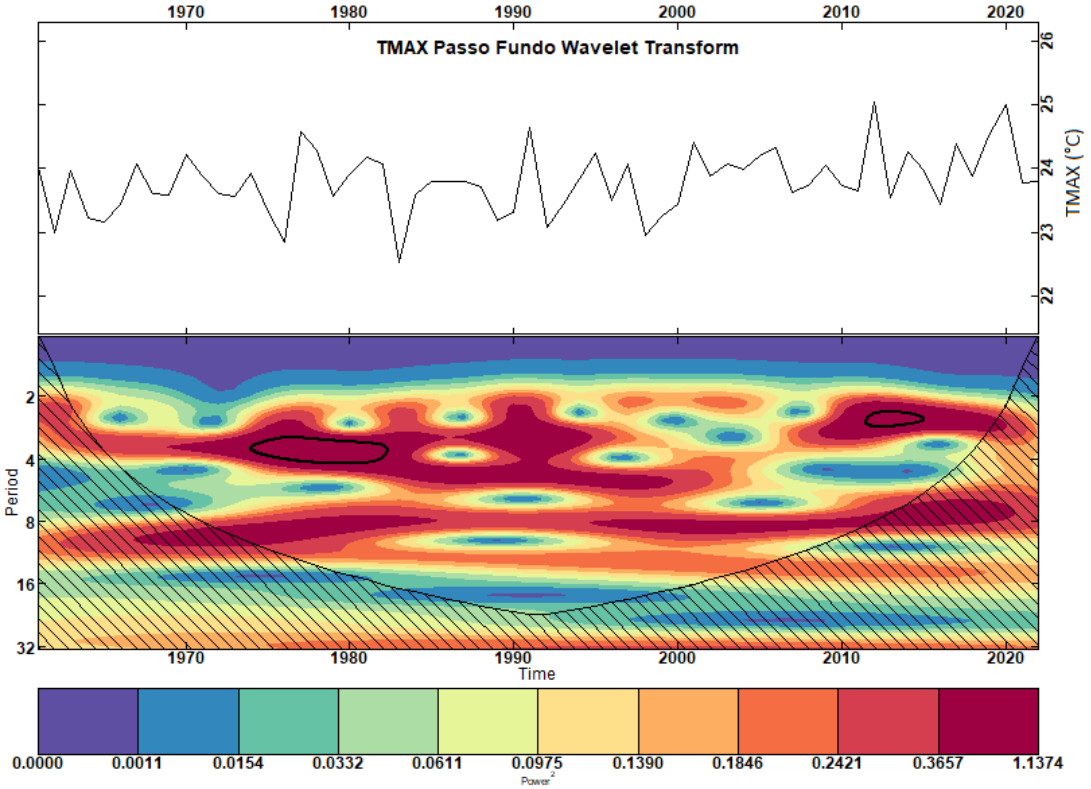

(c)

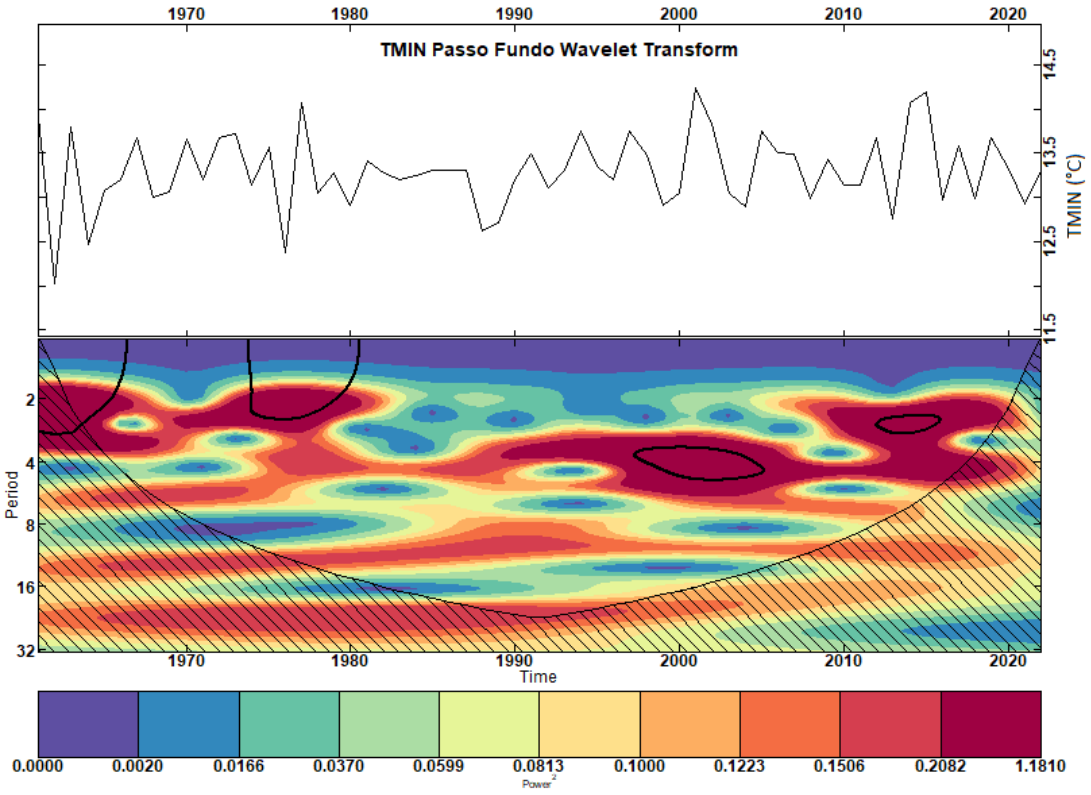

(d)

Source: The author.

Figure 57: Continuous Wavelet Transforms (CWTs) of Climate Variables at Porto União Station. (a) Precipitation, (b) Mean Temperature, (c) Minimum Temperature, and (d) Maximum Temperature. The black contours represent regions with a significance level greater than 0.95, indicating statistically significant patterns.

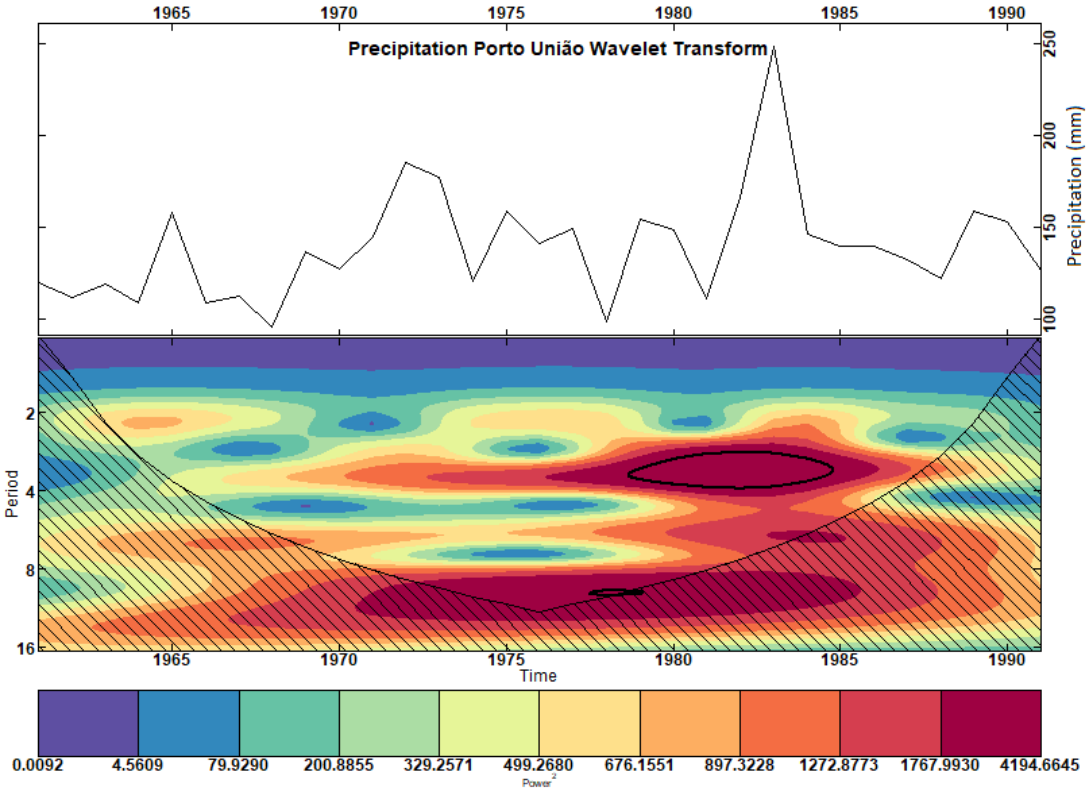

(a)

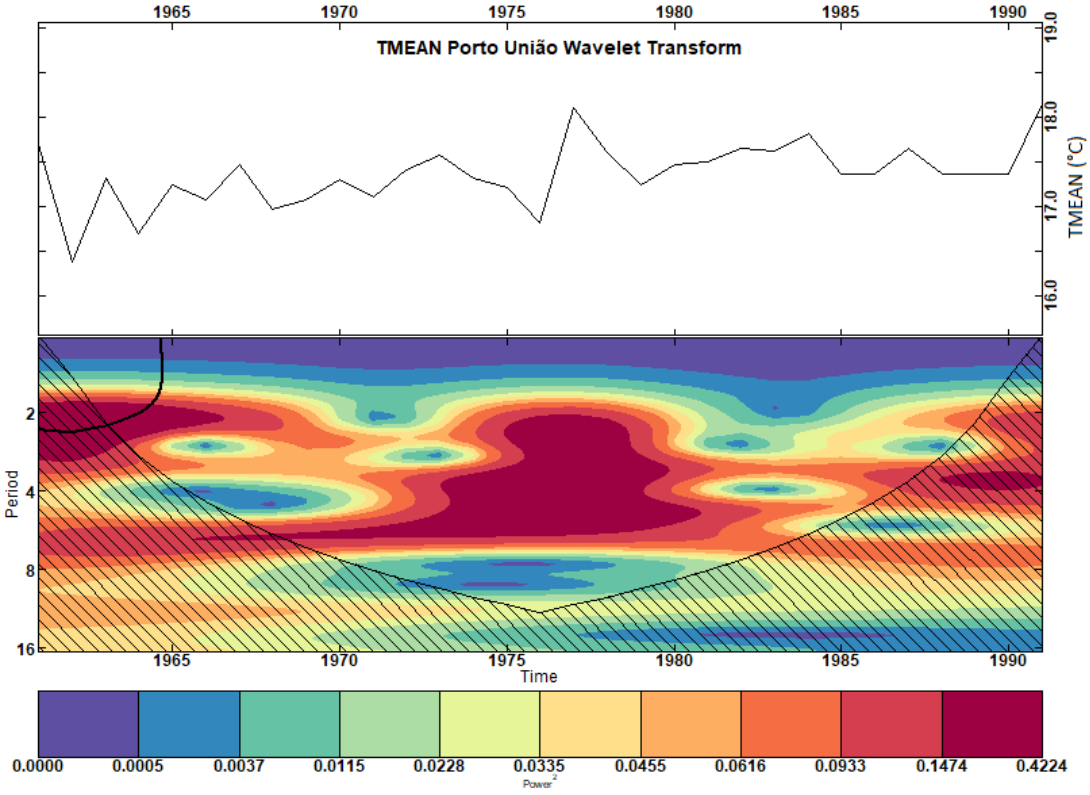

(b)

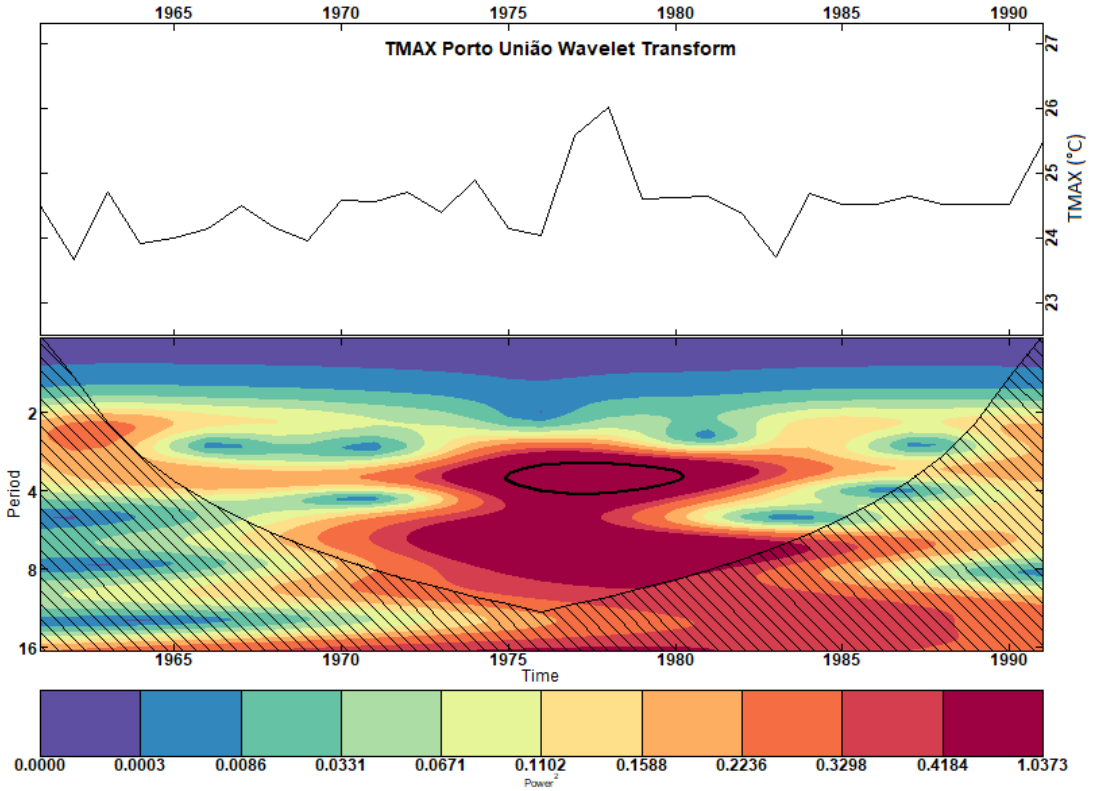

(c)

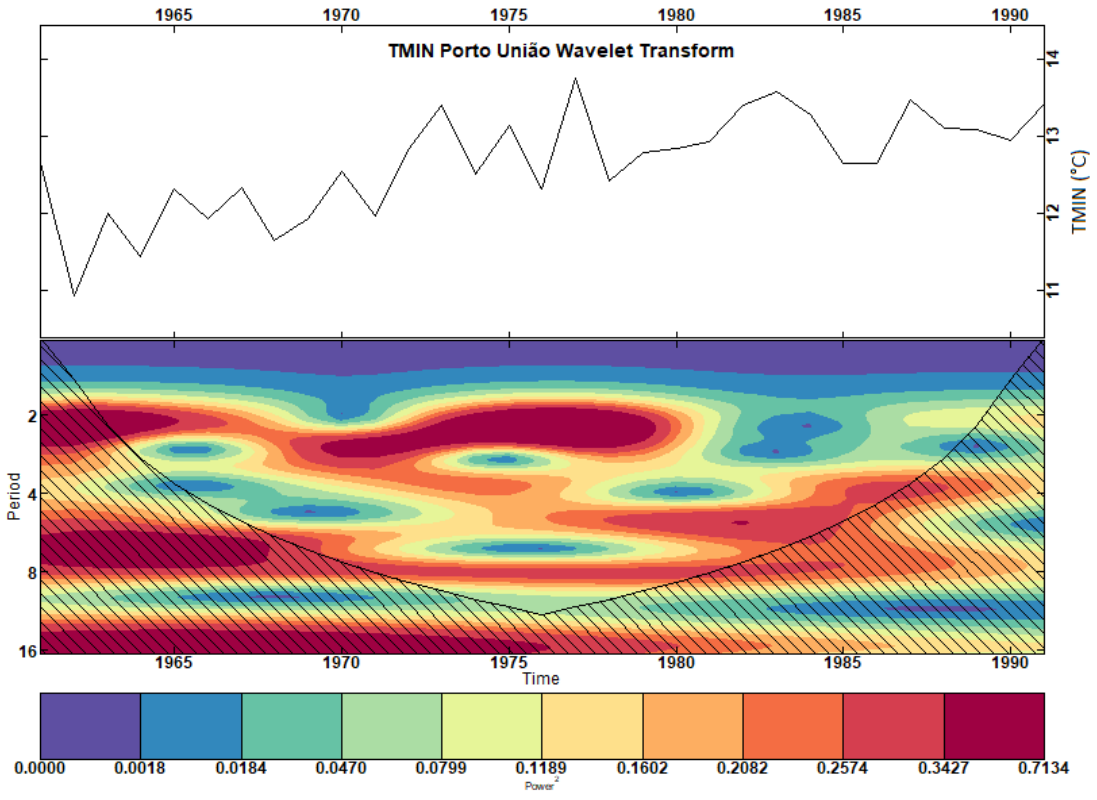

(d)

Source: The author.

Figure 58: Continuous Wavelet Transforms (CWTs) of Climate Variables at Joaçaba Station. (a) Precipitation, (b) Mean Temperature, (c) Minimum Temperature, and (d) Maximum Temperature. The black contours represent regions with a significance level greater than 0.95, indicating statistically significant patterns.

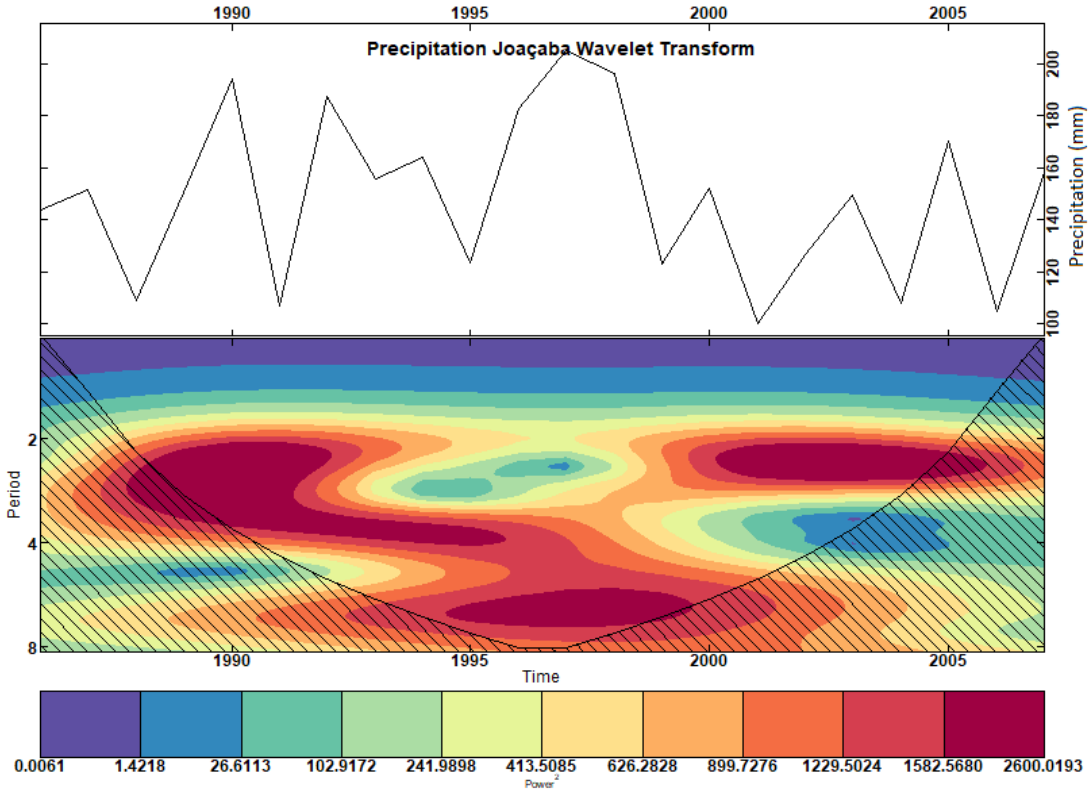

(a)

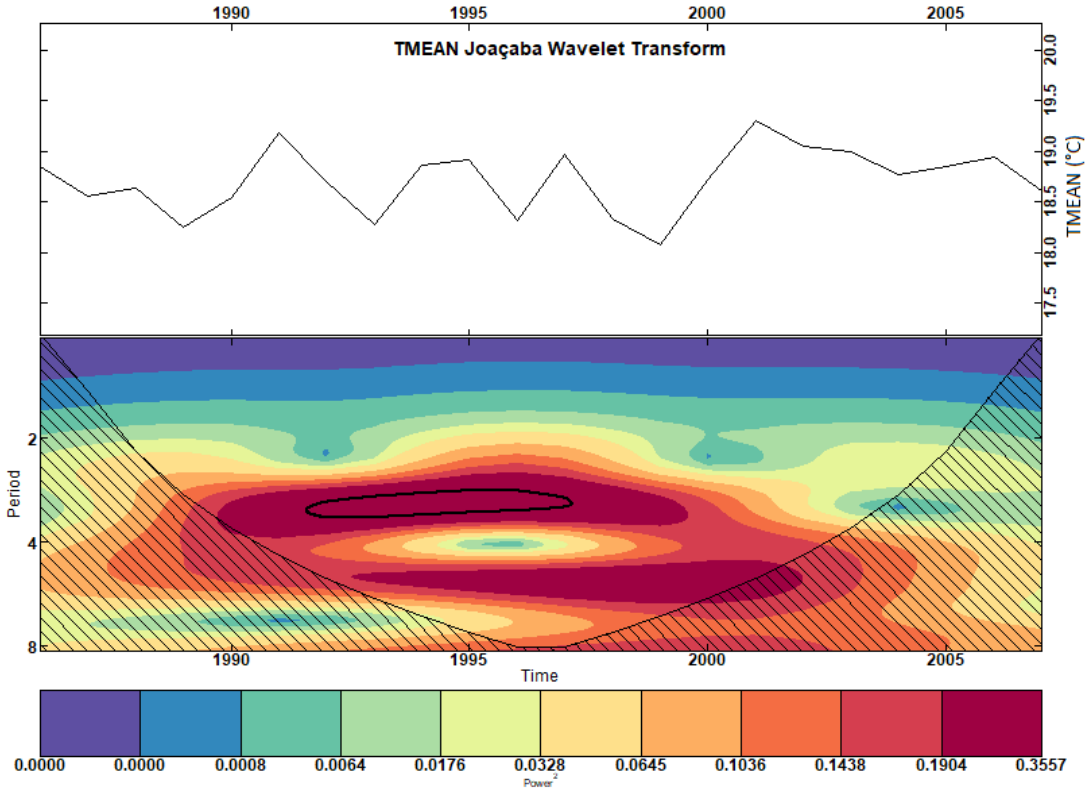

(b)

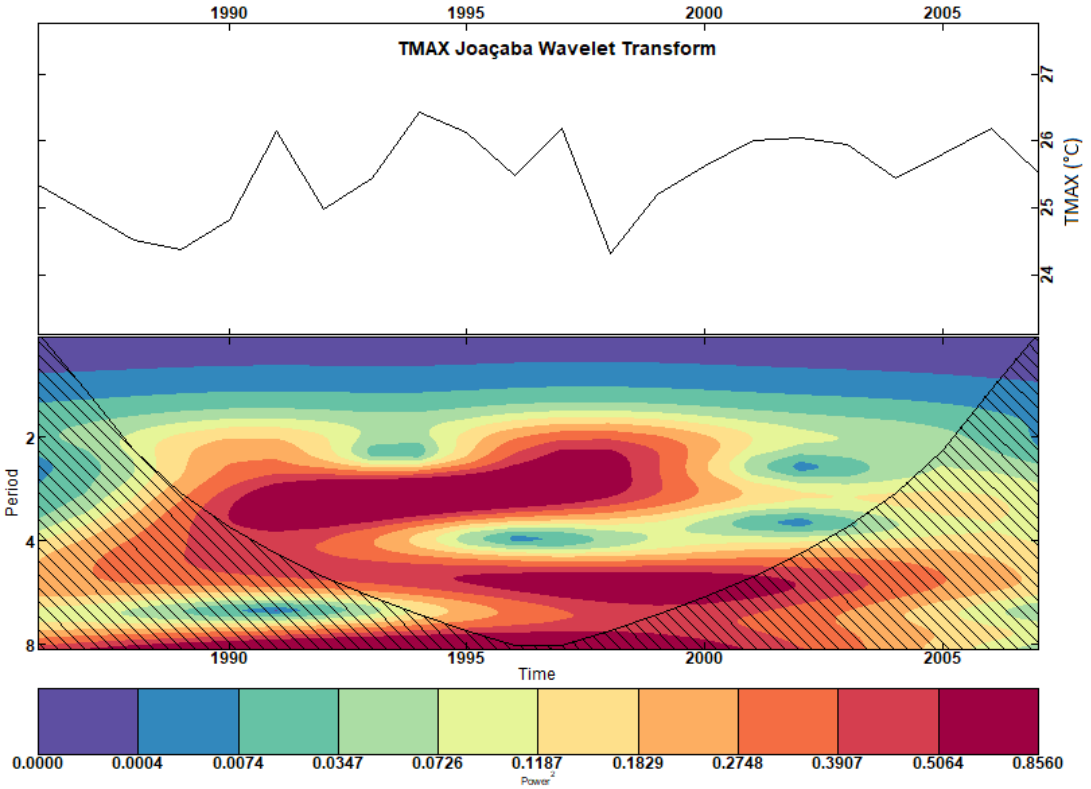

(c)

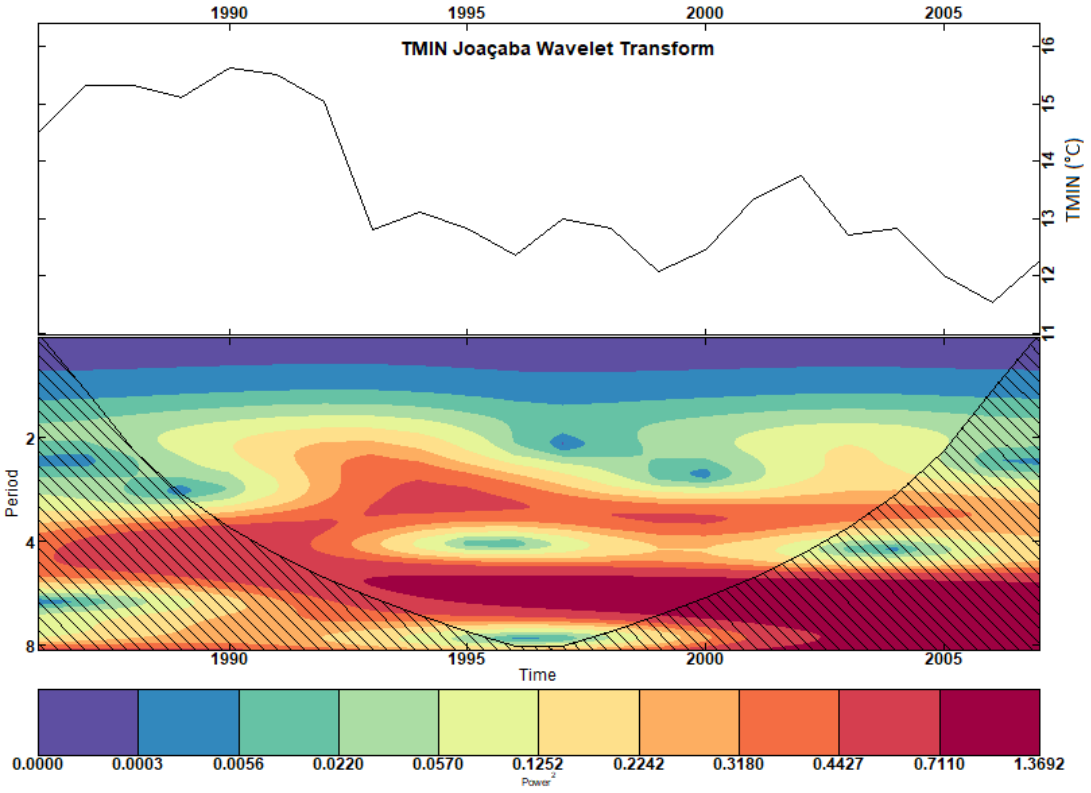

(d)

Source: The author.

APPENDIX C – CROSS WAVELET COHERENCE (WTC) FIGURES

In this appendix, we present the figures of the Cross Wavelet Coherence (WTC) analysis conducted to investigate the relationships between the Ring Width Index (RWI) and various ocean-atmosphere and solar parameters. The main goal of this investigation is to gain insights into the potential influences of these environmental and solar factors on the tree growth patterns captured by the RWI.

Figure 59: Cross Wavelet Coherence (WTC) Analysis between Açungui Ring Width Index (RWI) and Ocean-Atmosphere/Solar Parameters. Panels (a) to (h) display the WTC results between Açungui RWI and the Sunspot Number (SUNSPOT), Southern Oscillation Index (SOI), El Niño 3.4 Index (NIÑO 3.4), Atlantic Sea Surface Temperature (ATLSW), Precipitation (PREC), Maximum Temperature (TMAX), and Minimum Temperature (TMIN), Mean Temperature (TMEAN), respectively. The contours in black indicate regions of high coherence with a significance level > 0.95. The white arrows demonstrate the phase angle of the relationship between the RWI and each parameter. Rightward-pointing arrows signify an "in-phase" relationship. Contrary, leftward-pointing arrows indicate an "anti-phase" relationship.

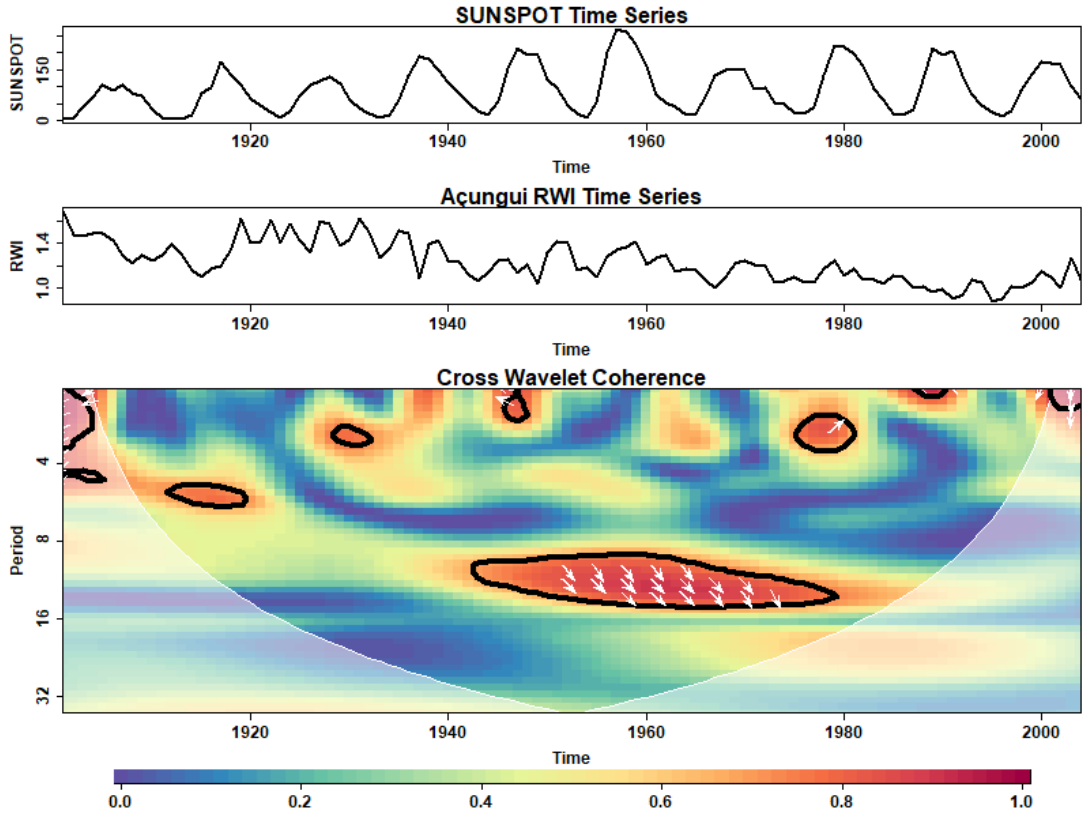

(a)

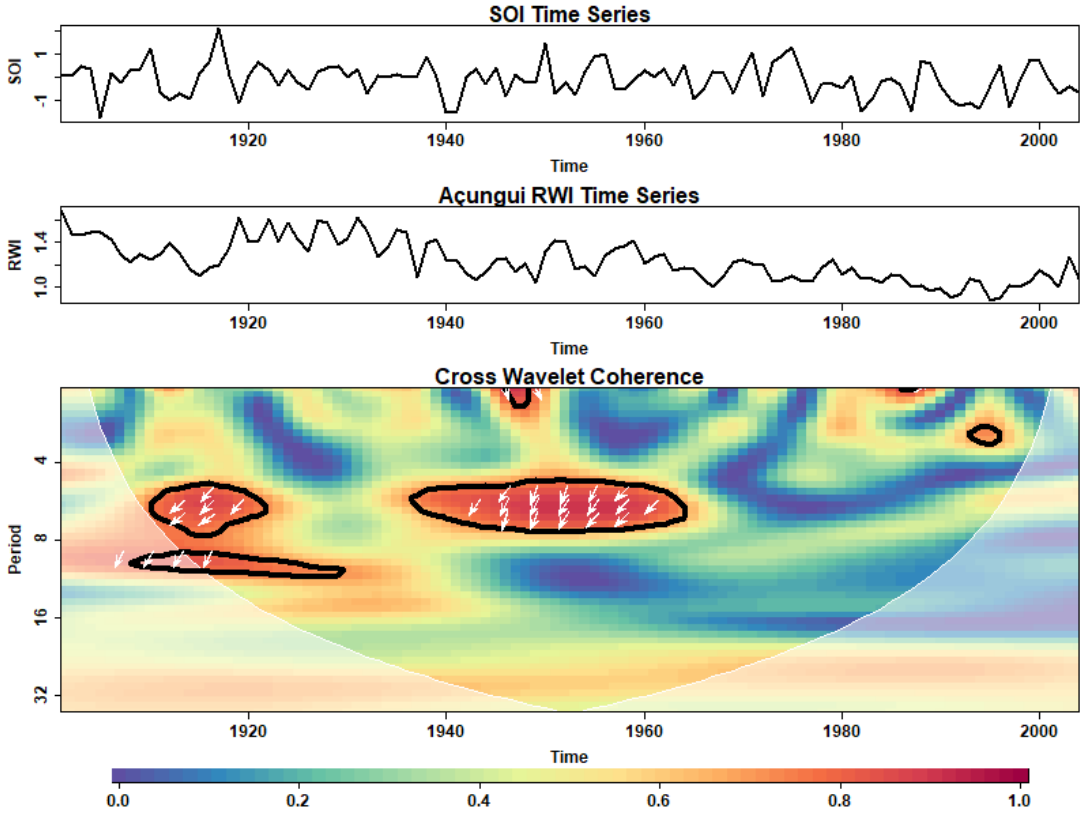
SOI Time Series
SOI
1
-1
1920
1940
1960
1980
2000
Time
Açungui RWI Time Series
RWI
1.4
1.0
1920
1940
1960
1980
2000
Time
Cross Wavelet Coherence
Period
4
8
16
32
1920
1940
1960
1980
2000
Time
0.0
0.2
0.4
0.6
0.8
1.0

(b)

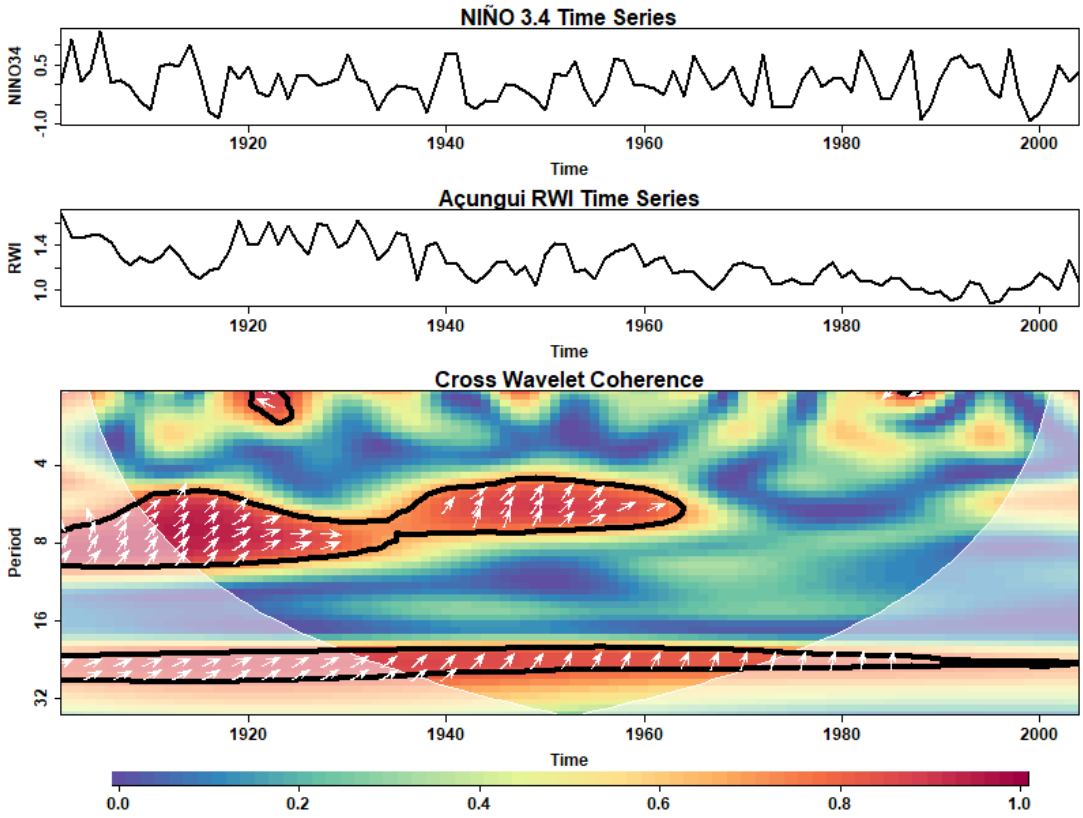
NIÑO 3.4 Time Series
NINO34
0.5
-1.0
1920
1940
1960
1980
2000
Time
Açungui RWI Time Series
RWI
1.4
1.0
1920
1940
1960
1980
2000
Time
Cross Wavelet Coherence
Period
4
8
16
32
1920
1940
1960
1980
2000
Time
0.0
0.2
0.4
0.6
0.8
1.0

(c)

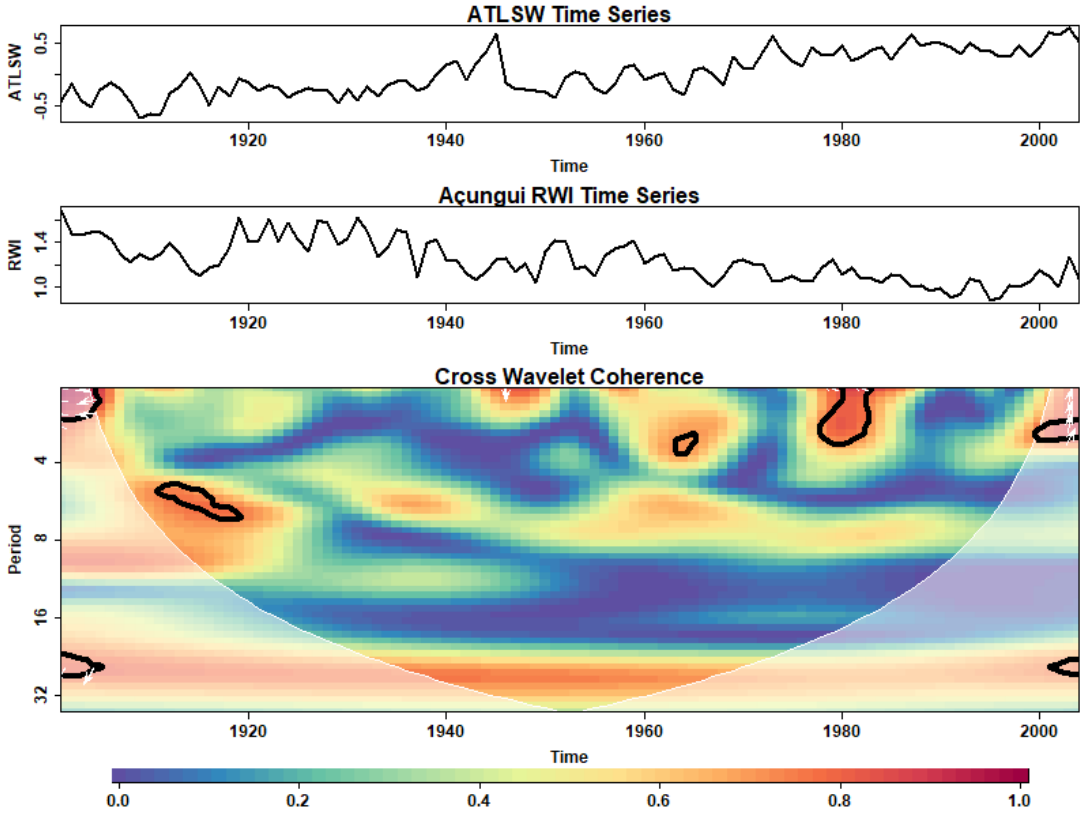
ATLSW Time Series
ATLSW
0.5
-0.5
1920
1940
1960
1980
2000
Time
Açungui RWI Time Series
RWI
1.4
1.0
1920
1940
1960
1980
2000
Time
Cross Wavelet Coherence
Period
4
8
16
32
1920
1940
1960
1980
2000
Time
0.0
0.2
0.4
0.6
0.8
1.0

(d)

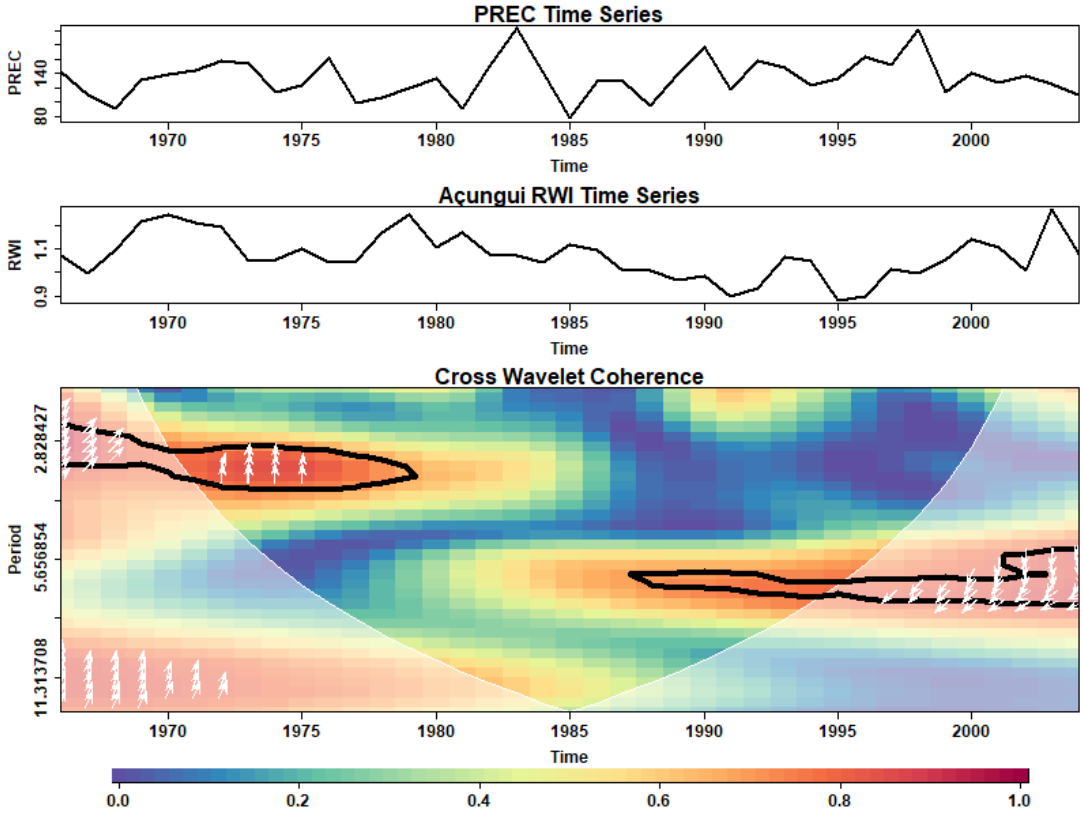
PREC Time Series
PREC
140
80
1970
1975
1980
1985
1990
1995
2000
Time
Açungui RWI Time Series
RWI
1.1
0.9
1970
1975
1980
1985
1990
1995
2000
Time
Cross Wavelet Coherence
Period
2.828427
5.656854
11.313708
1970
1975
1980
1985
1990
1995
2000
Time
0.0
0.2
0.4
0.6
0.8
1.0

(e)

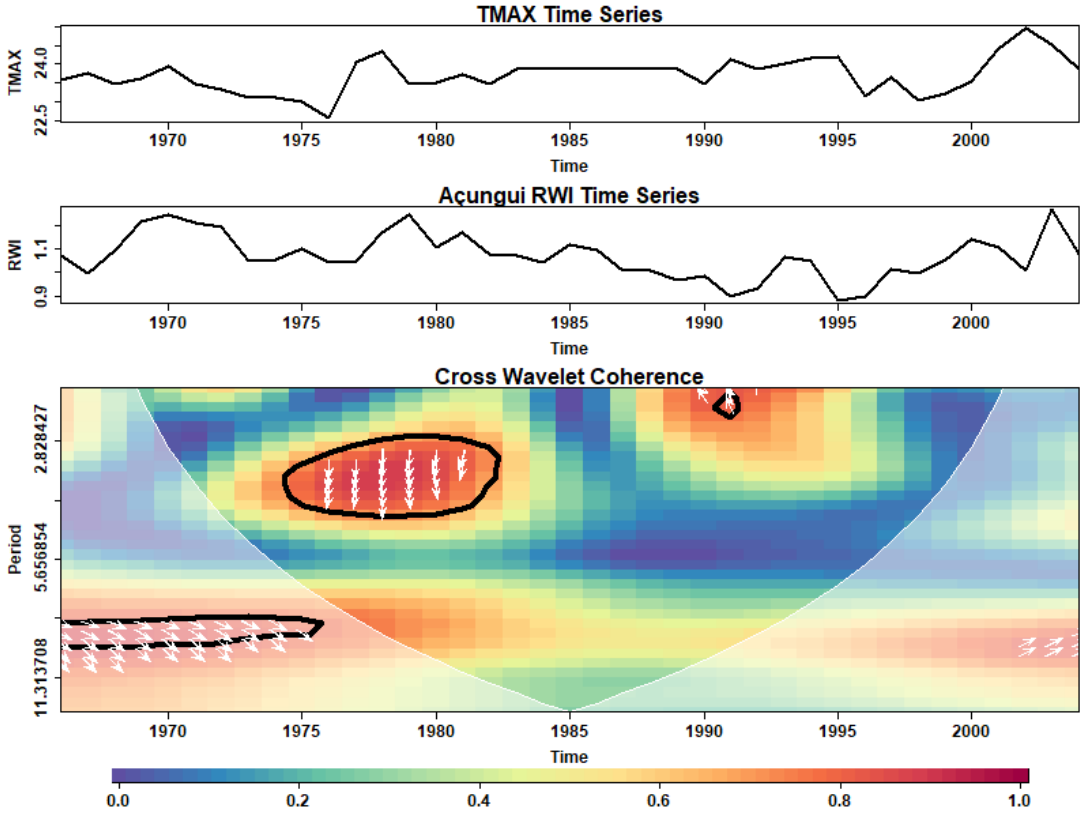
TMAX Time Series
TMAX
22.5
24.0
1970
1975
1980
1985
1990
1995
2000
Time
Açungui RWI Time Series
RWI
0.9
1.1
1970
1975
1980
1985
1990
1995
2000
Time
Cross Wavelet Coherence
Period
2.828427
5.656854
11.313708
1970
1975
1980
1985
1990
1995
2000
Time
0.0
0.2
0.4
0.6
0.8
1.0

(f)

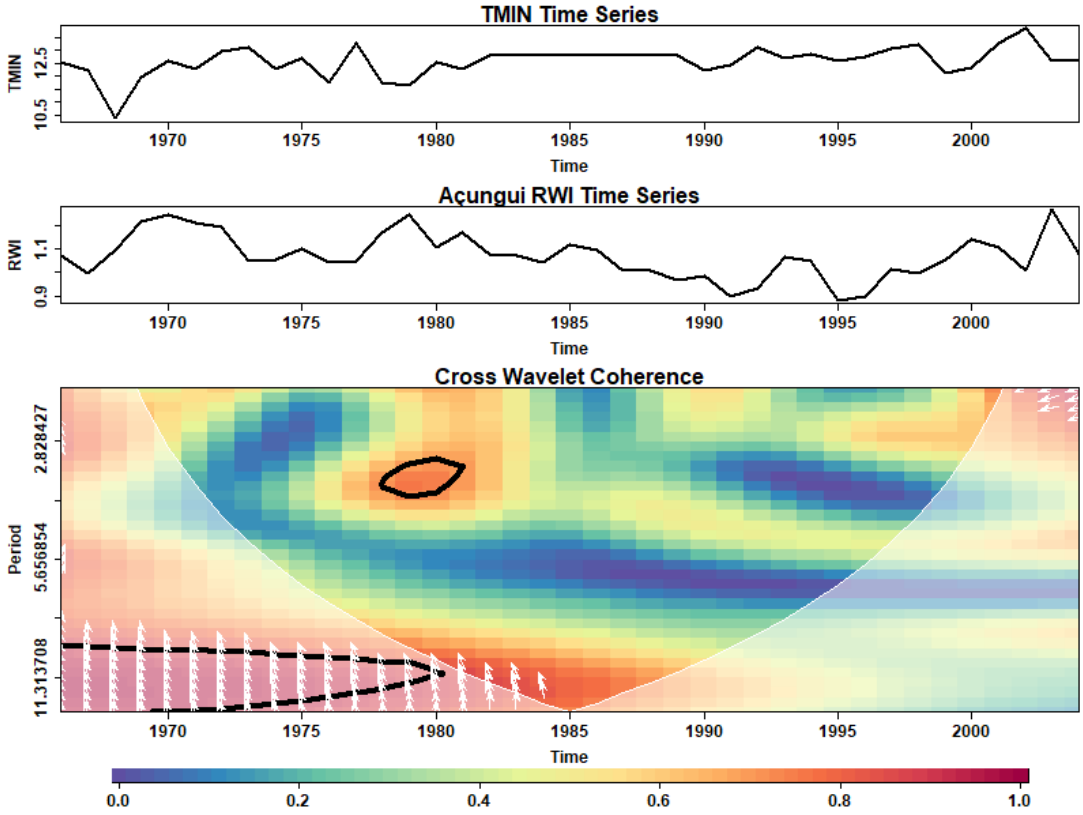
TMIN Time Series
TMIN
10.5
12.5
1970
1975
1980
1985
1990
1995
2000
Time
Açungui RWI Time Series
RWI
0.9
1.1
1970
1975
1980
1985
1990
1995
2000
Time
Cross Wavelet Coherence
Period
2.828427
5.656854
11.313708
1970
1975
1980
1985
1990
1995
2000
Time
0.0
0.2
0.4
0.6
0.8
1.0

(g)

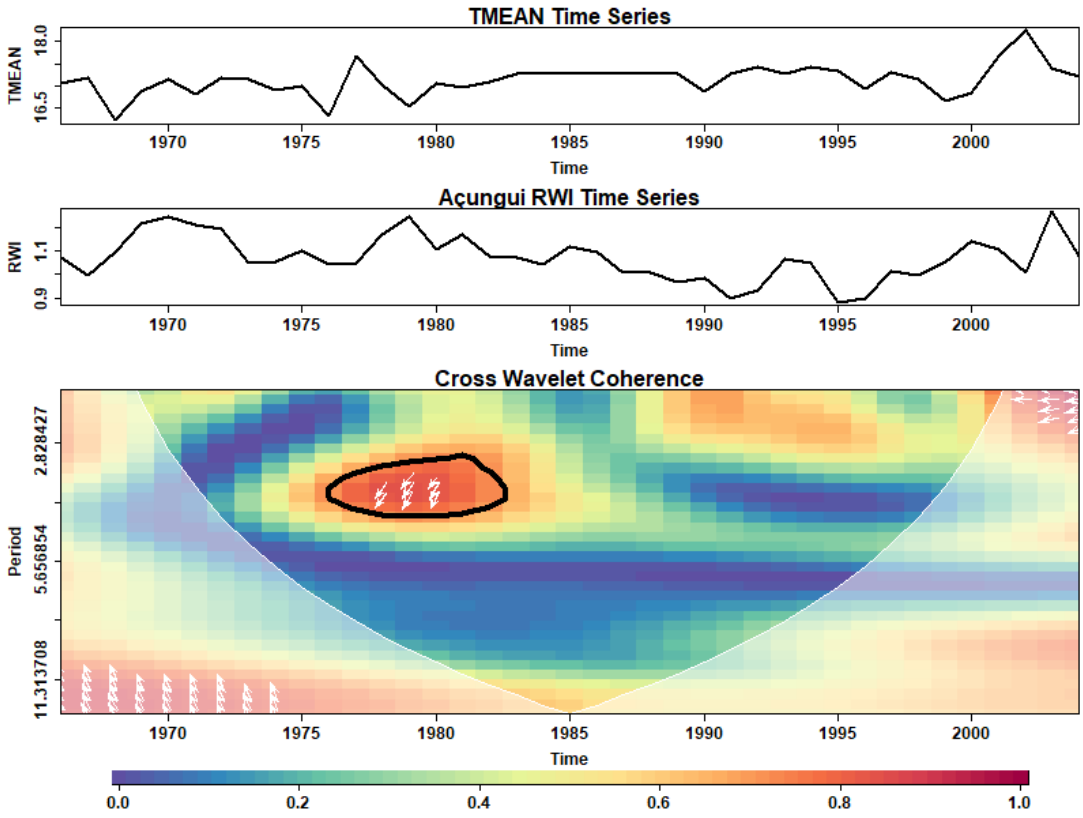

(h)
Source: The author.

Figure 60: Cross Wavelet Coherence (WTC) Analysis between Canela Ring Width Index (RWI) and Ocean-Atmosphere/Solar Parameters. Panels (a) to (h) display the WTC results between Canela RWI and the Southern Oscillation Index (SOI), El Niño 3.4 Index (NIÑO 3.4), Sunspot Activity (SUNSPOT), Atlantic Sea Surface Temperature (ATLSW), Precipitation (PREC), Mean Temperature (TMEAN), Maximum Temperature (TMAX), and Minimum Temperature (TMIN), respectively. The contours in black indicate regions of high coherence with a significance level > 0.95, unveiling potential associations and time-frequency relationships. The white arrows demonstrate the phase angle and direction of the relationship between the RWI and each parameter. Rightward-pointing arrows signify an "in-phase" relationship, indicating that both the RWI and the parameter share similar variations at specific time-frequency intervals. Contrary, leftward-pointing arrows indicate an "anti-phase" relationship, where the RWI and the parameter exhibit opposite variations at certain time-frequency regions.

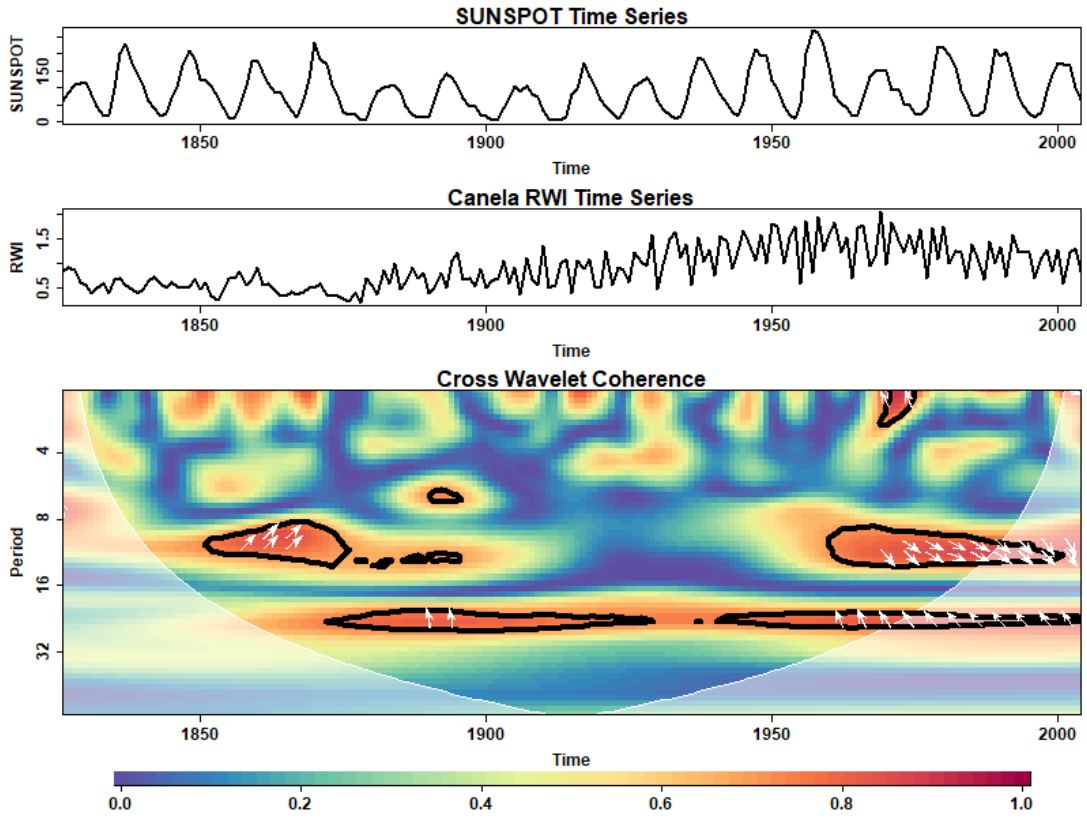

(a)

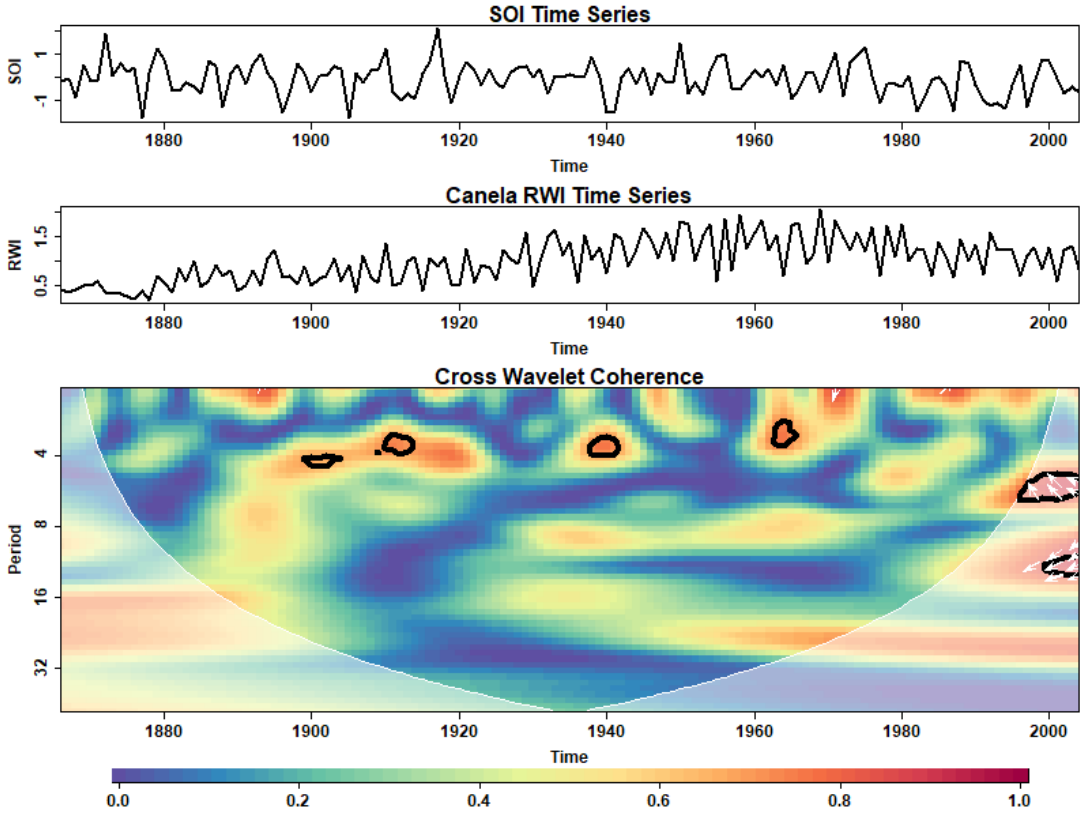
SOI Time Series
SOI
1
-1
1880
1900
1920
1940
1960
1980
2000
Time
Canela RWI Time Series
RWI
1.5
0.5
1880
1900
1920
1940
1960
1980
2000
Time
Cross Wavelet Coherence
Period
4
8
16
32
1880
1900
1920
1940
1960
1980
2000
Time
0.0
0.2
0.4
0.6
0.8
1.0

(b)

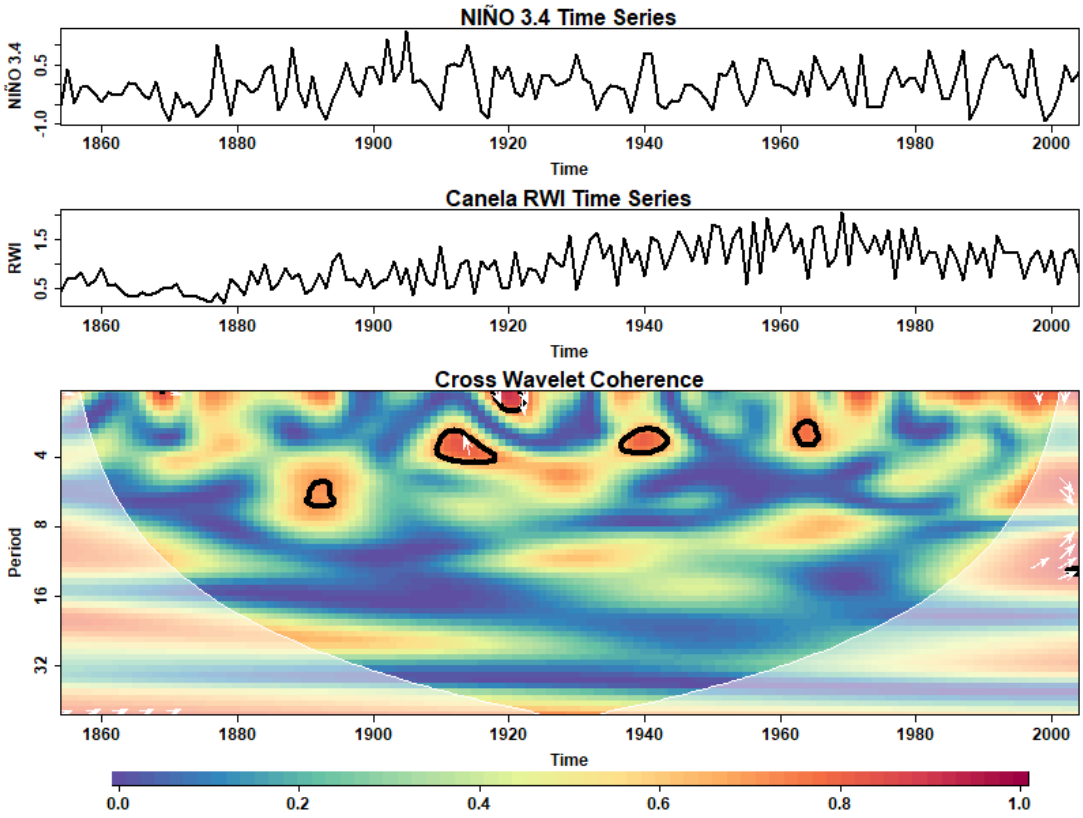
NIÑO 3.4 Time Series
NIÑO 3.4
0.5
-1.0
1860
1880
1900
1920
1940
1960
1980
2000
Time
Canela RWI Time Series
RWI
1.5
0.5
1860
1880
1900
1920
1940
1960
1980
2000
Time
Cross Wavelet Coherence
Period
4
8
16
32
1860
1880
1900
1920
1940
1960
1980
2000
Time
0.0
0.2
0.4
0.6
0.8
1.0

(c)

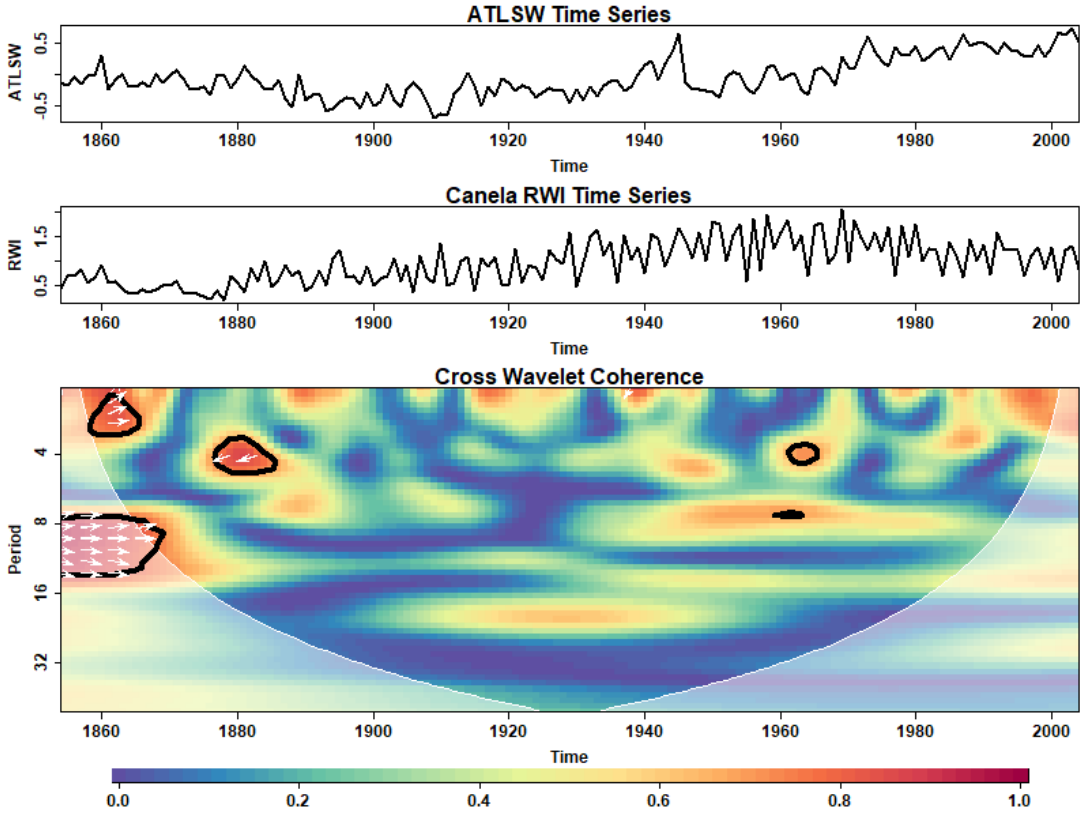
ATLSW Time Series
ATLSW
0.5
-0.5
1860
1880
1900
1920
1940
1960
1980
2000
Time
Canela RWI Time Series
RWI
1.5
0.5
1860
1880
1900
1920
1940
1960
1980
2000
Time
Cross Wavelet Coherence
Period
4
8
16
32
1860
1880
1900
1920
1940
1960
1980
2000
Time
0.0
0.2
0.4
0.6
0.8
1.0

(d)

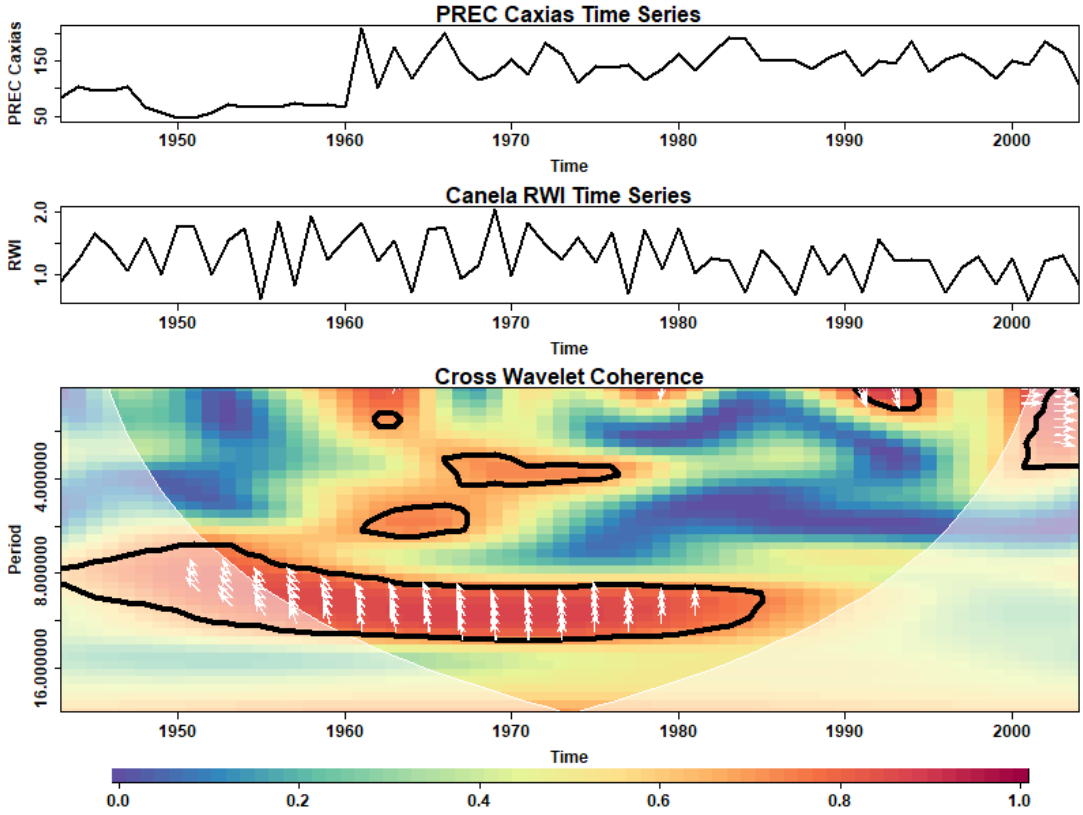
PREC Caxias Time Series
PREC Caxias
150
50
1950
1960
1970
1980
1990
2000
Time
Canela RWI Time Series
RWI
2.0
1.0
1950
1960
1970
1980
1990
2000
Time
Cross Wavelet Coherence
Period
4.000000
8.000000
16.000000
1950
1960
1970
1980
1990
2000
Time
0.0
0.2
0.4
0.6
0.8
1.0

(e)

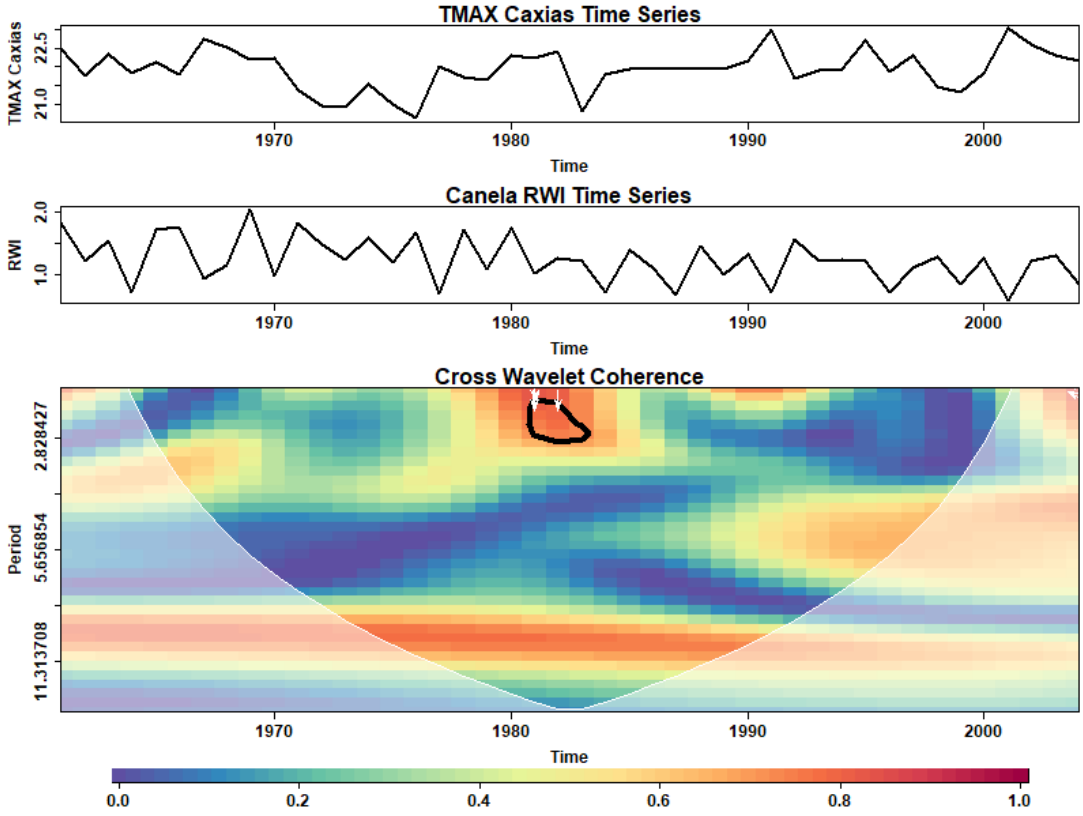
TMAX Caxias Time Series
TMAX Caxias
22.5
21.0
1970
1980
1990
2000
Time
Canela RWI Time Series
RWI
2.0
1.0
1970
1980
1990
2000
Time
Cross Wavelet Coherence
Period
2.828427
5.656854
11.313708
1970
1980
1990
2000
Time
0.0
0.2
0.4
0.6
0.8
1.0

(f)

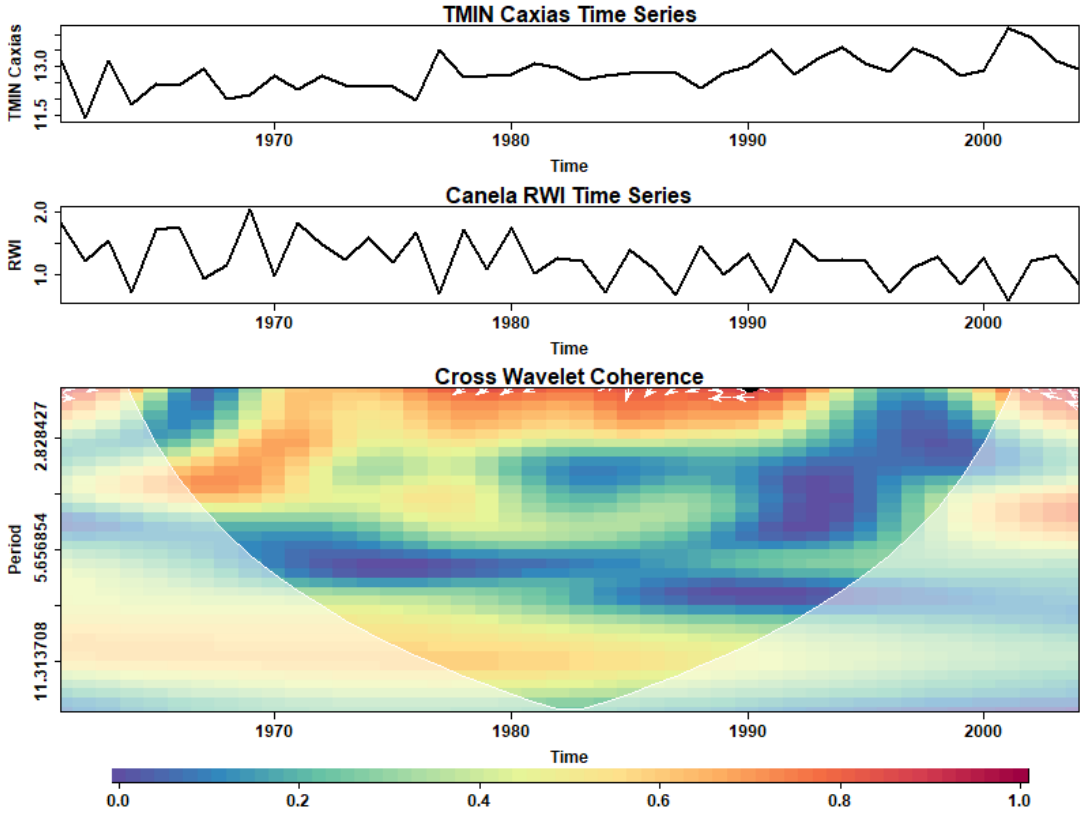
TMIN Caxias Time Series
TMIN Caxias
13.0
11.5
1970
1980
1990
2000
Time
Canela RWI Time Series
RWI
2.0
1.0
1970
1980
1990
2000
Time
Cross Wavelet Coherence
Period
2.828427
5.656854
11.313708
1970
1980
1990
2000
Time
0.0
0.2
0.4
0.6
0.8
1.0

(g)

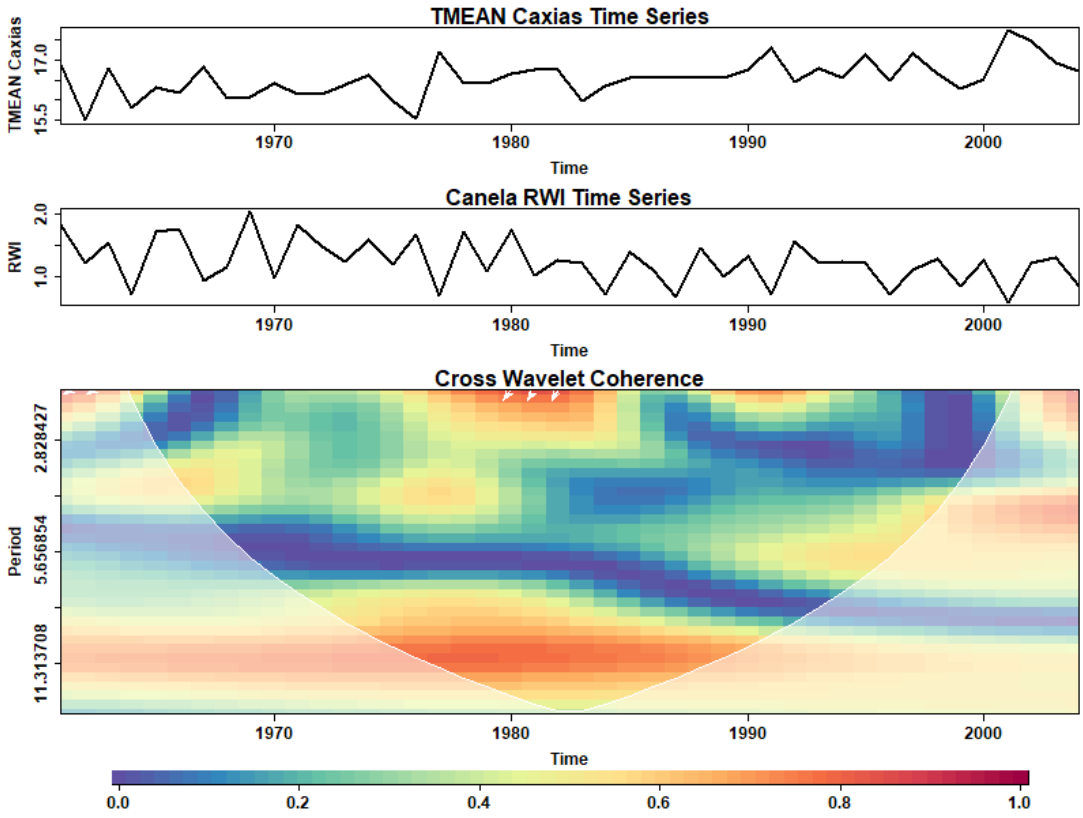

(h)
Source: The author.

Figure 61: Cross Wavelet Coherence (WTC) Analysis between Chapecó Ring Width Index (RWI) and Ocean-Atmosphere/Solar Parameters. Panels (a) to (h) display the WTC results between Chapecó RWI and the Southern Oscillation Index (SOI), El Niño 3.4 Index (NIÑO 3.4), Sunspot Activity (SUNSPOT), Atlantic Sea Surface Temperature (ATLSW), Precipitation (PREC), Mean Temperature (TMEAN), Maximum Temperature (TMAX), and Minimum Temperature (TMIN), respectively. The contours in black indicate regions of high coherence with a significance level > 0.95, unveiling potential associations and time-frequency relationships. The white arrows demonstrate the phase angle and direction of the relationship between the RWI and each parameter. Rightward-pointing arrows signify an "in-phase" relationship, indicating that both the RWI and the parameter share similar variations at specific time-frequency intervals. Contrary, leftward-pointing arrows indicate an "anti-phase" relationship, where the RWI and the parameter exhibit opposite variations at certain time-frequency regions.

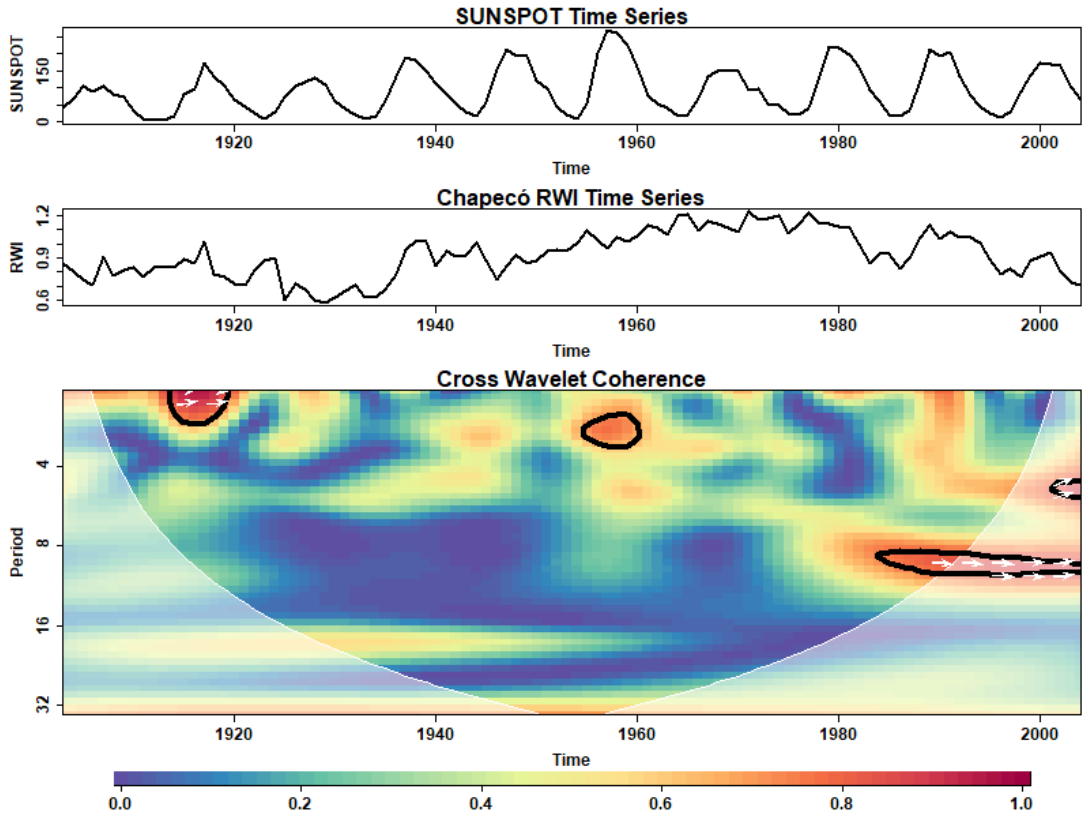

(a)

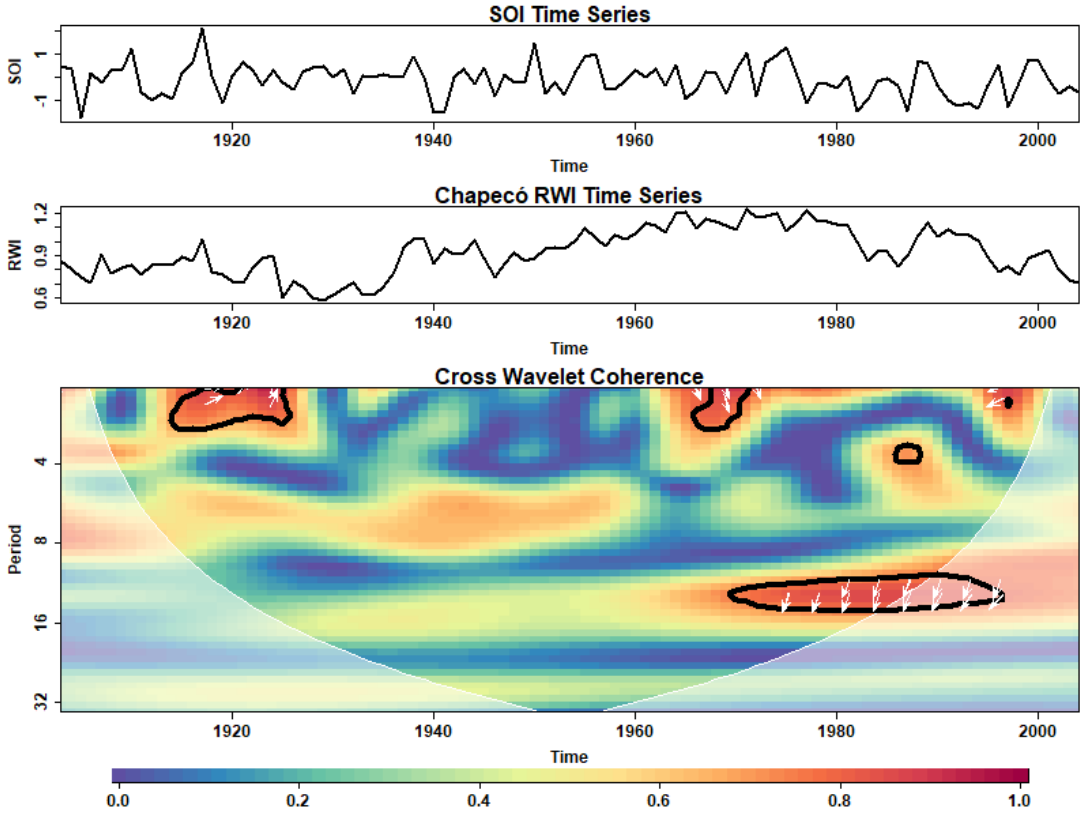
SOI Time Series
SOI
1
-1
1920
1940
1960
1980
2000
Time
Chapecó RWI Time Series
RWI
1.2
0.9
0.6
1920
1940
1960
1980
2000
Time
Cross Wavelet Coherence
Period
4
8
16
32
1920
1940
1960
1980
2000
Time
0.0
0.2
0.4
0.6
0.8
1.0

(b)

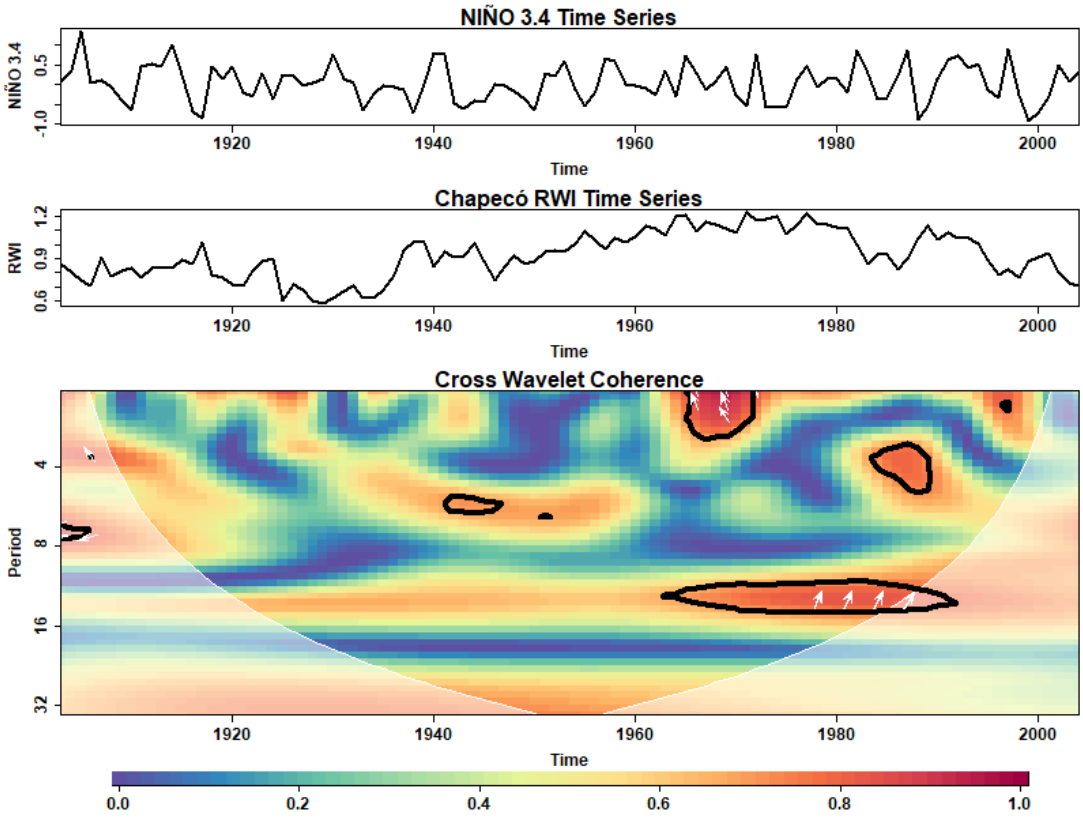
NIÑO 3.4 Time Series
NIÑO 3.4
0.5
-1.0
1920
1940
1960
1980
2000
Time
Chapecó RWI Time Series
RWI
1.2
0.9
0.6
1920
1940
1960
1980
2000
Time
Cross Wavelet Coherence
Period
4
8
16
32
1920
1940
1960
1980
2000
Time
0.0
0.2
0.4
0.6
0.8
1.0

(c)

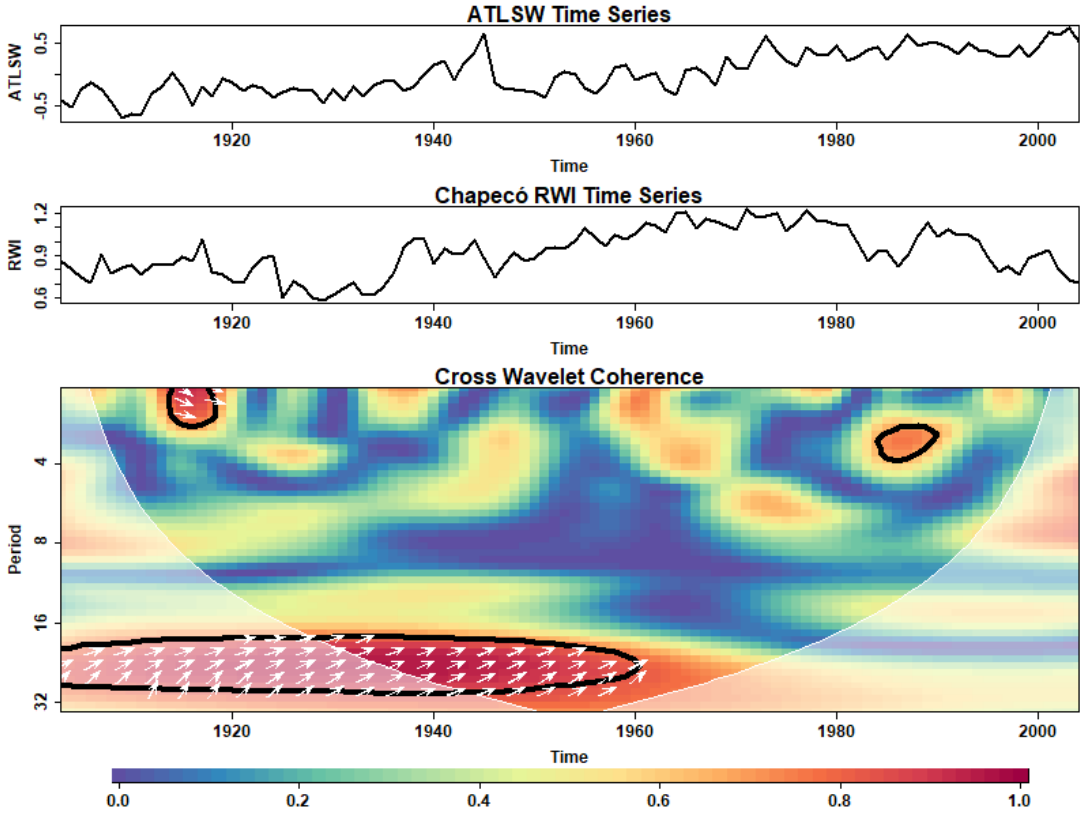
ATLSW Time Series
ATLSW
0.5
-0.5
1920
1940
1960
1980
2000
Time
Chapecó RWI Time Series
RWI
1.2
0.9
0.6
1920
1940
1960
1980
2000
Time
Cross Wavelet Coherence
Period
4
8
16
32
1920
1940
1960
1980
2000
Time
0.0
0.2
0.4
0.6
0.8
1.0

(d)

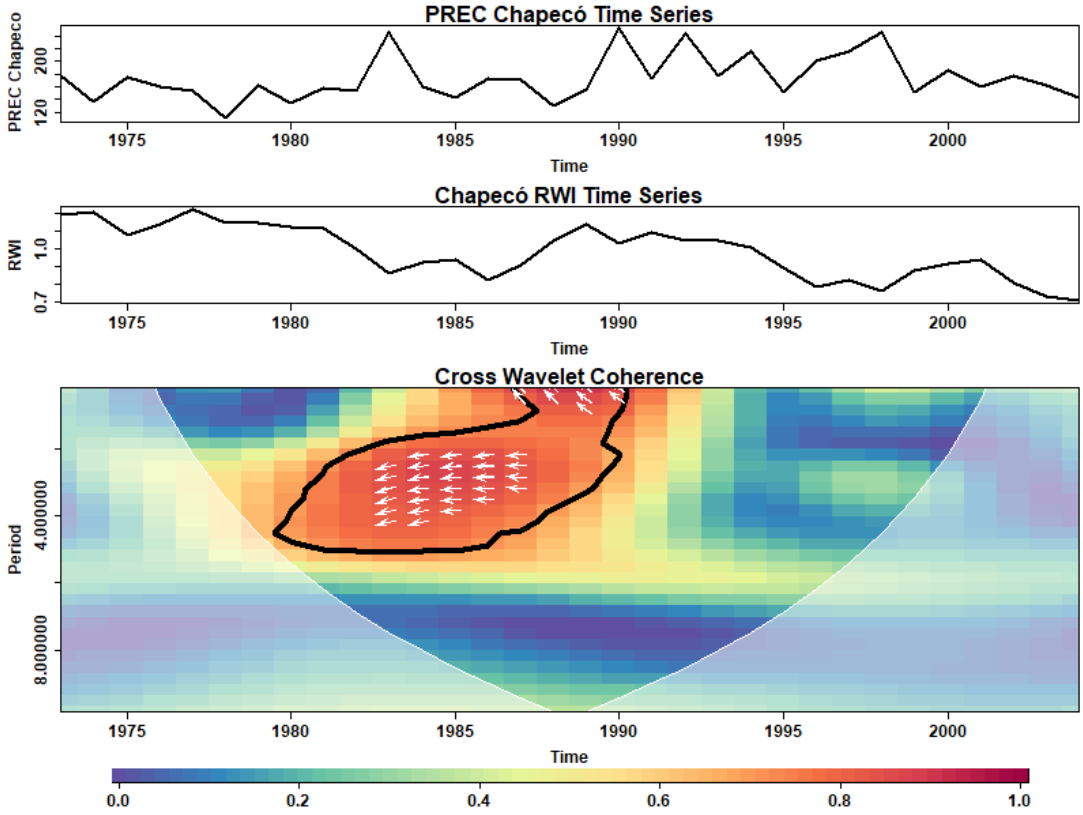
PREC Chapecó Time Series
PREC Chapeco
200
120
1975
1980
1985
1990
1995
2000
Time
Chapecó RWI Time Series
RWI
1.0
0.7
1975
1980
1985
1990
1995
2000
Time
Cross Wavelet Coherence
Period
4.000000
8.000000
1975
1980
1985
1990
1995
2000
Time
0.0
0.2
0.4
0.6
0.8
1.0

(e)

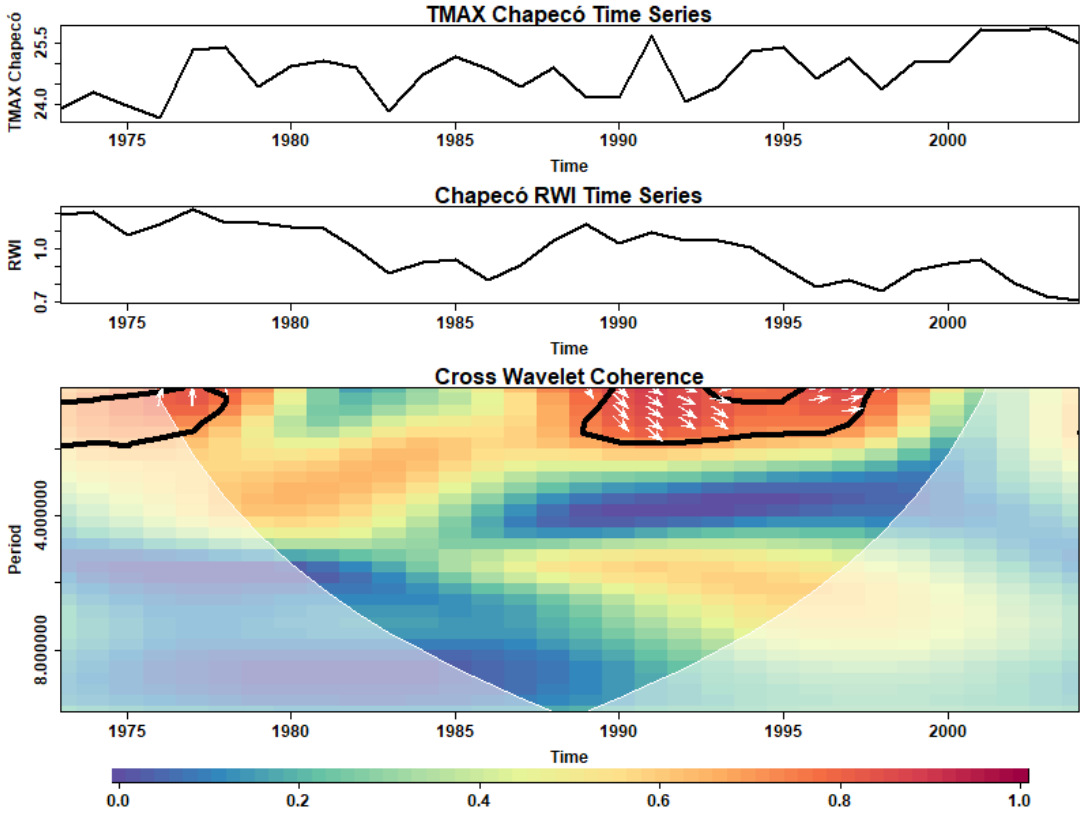
TMAX Chapecó Time Series
TMAX Chapecó
25.5
24.0
1975
1980
1985
1990
1995
2000
Time
Chapecó RWI Time Series
RWI
1.0
0.7
1975
1980
1985
1990
1995
2000
Time
Cross Wavelet Coherence
Period
4.000000
8.000000
1975
1980
1985
1990
1995
2000
Time
0.0
0.2
0.4
0.6
0.8
1.0

(f)

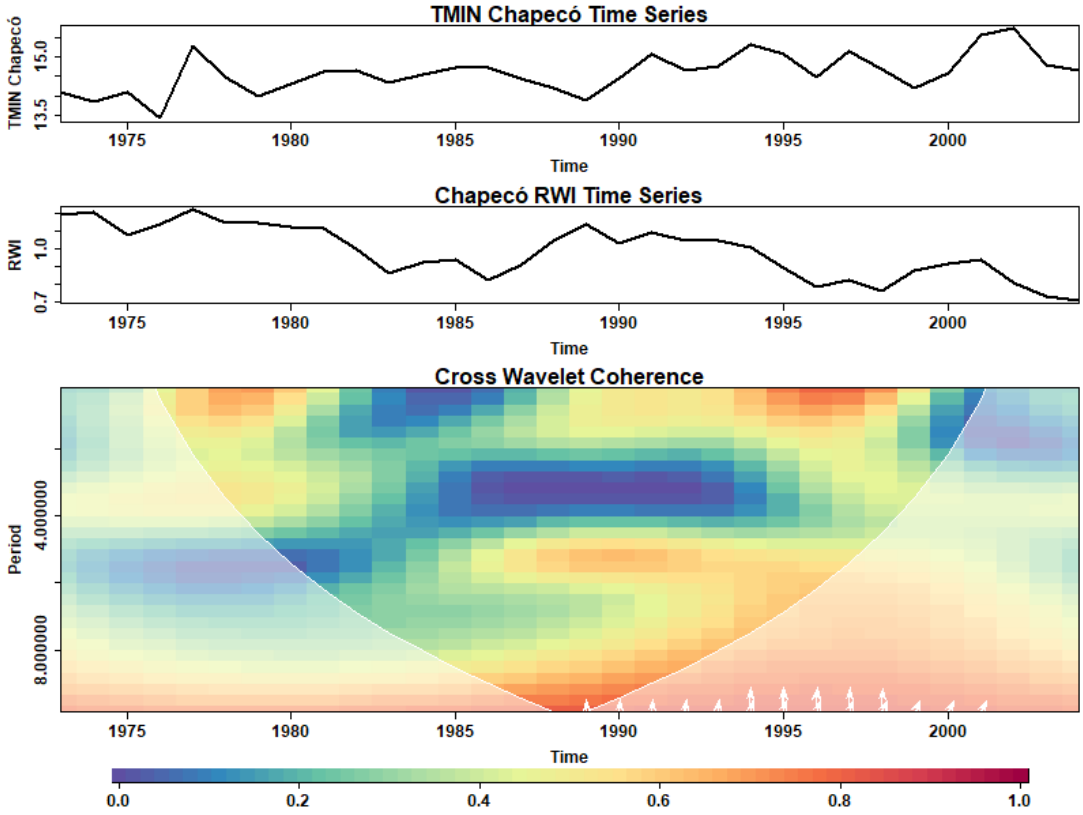
TMIN Chapecó Time Series
TMIN Chapecó
15.0
13.5
1975
1980
1985
1990
1995
2000
Time
Chapecó RWI Time Series
RWI
1.0
0.7
1975
1980
1985
1990
1995
2000
Time
Cross Wavelet Coherence
Period
4.000000
8.000000
1975
1980
1985
1990
1995
2000
Time
0.0
0.2
0.4
0.6
0.8
1.0

(g)

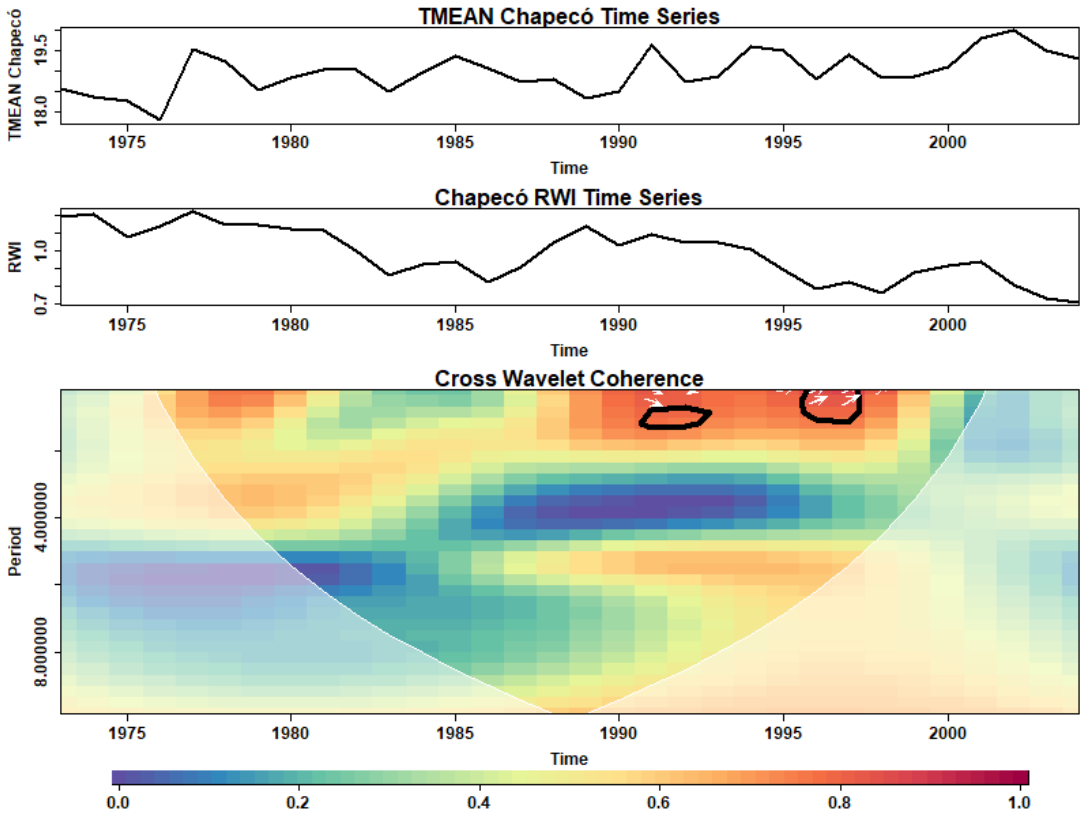

(h)
Source: The author.

Figure 62: Cross Wavelet Coherence (WTC) Analysis between Coxilha Ring Width Index (RWI) and Ocean-Atmosphere/Solar Parameters. Panels (a) to (h) display the WTC results between Coxilha RWI and the Southern Oscillation Index (SOI), El Niño 3.4 Index (NIÑO 3.4), Sunspot Activity (SUNSPOT), Atlantic Sea Surface Temperature (ATLSW), Precipitation (PREC), Mean Temperature (TMEAN), Maximum Temperature (TMAX), and Minimum Temperature (TMIN), respectively. The contours in black indicate regions of high coherence with a significance level > 0.95, unveiling potential associations and time-frequency relationships. The white arrows demonstrate the phase angle and direction of the relationship between the RWI and each parameter. Rightward-pointing arrows signify an "in-phase" relationship, indicating that both the RWI and the parameter share similar variations at specific time-frequency intervals. Contrary, leftward-pointing arrows indicate an "anti-phase" relationship, where the RWI and the parameter exhibit opposite variations at certain time-frequency regions.

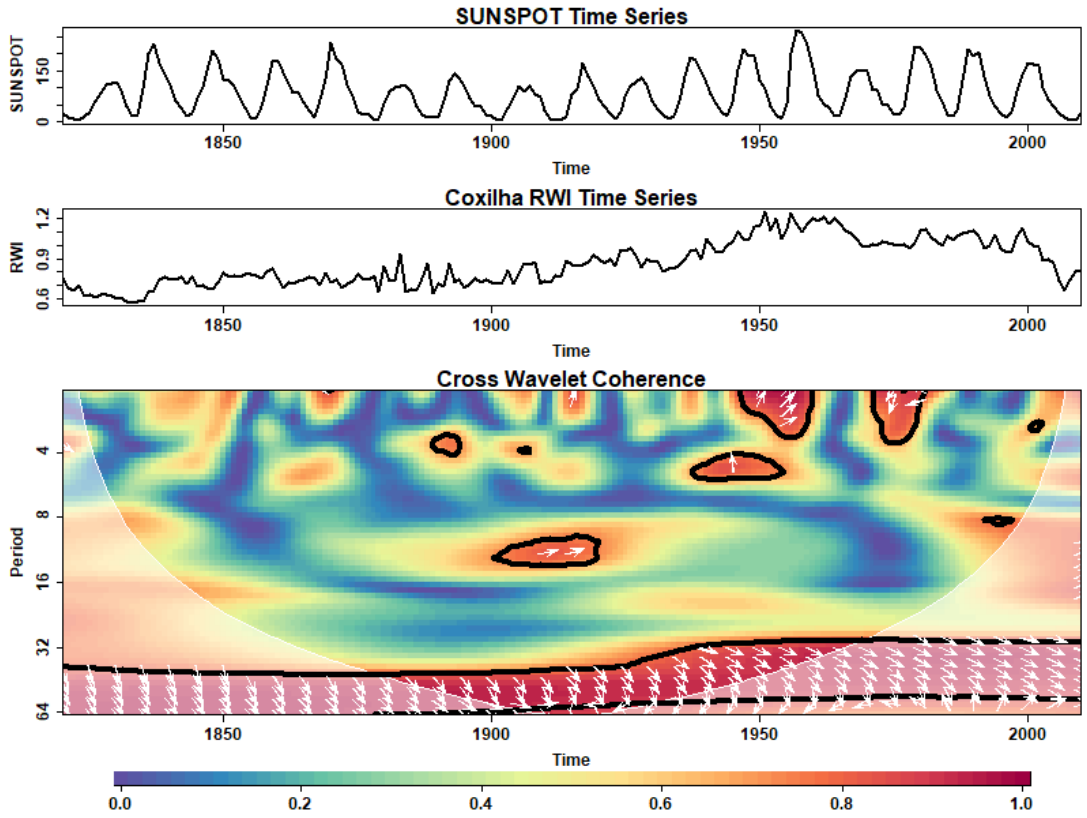

(a)

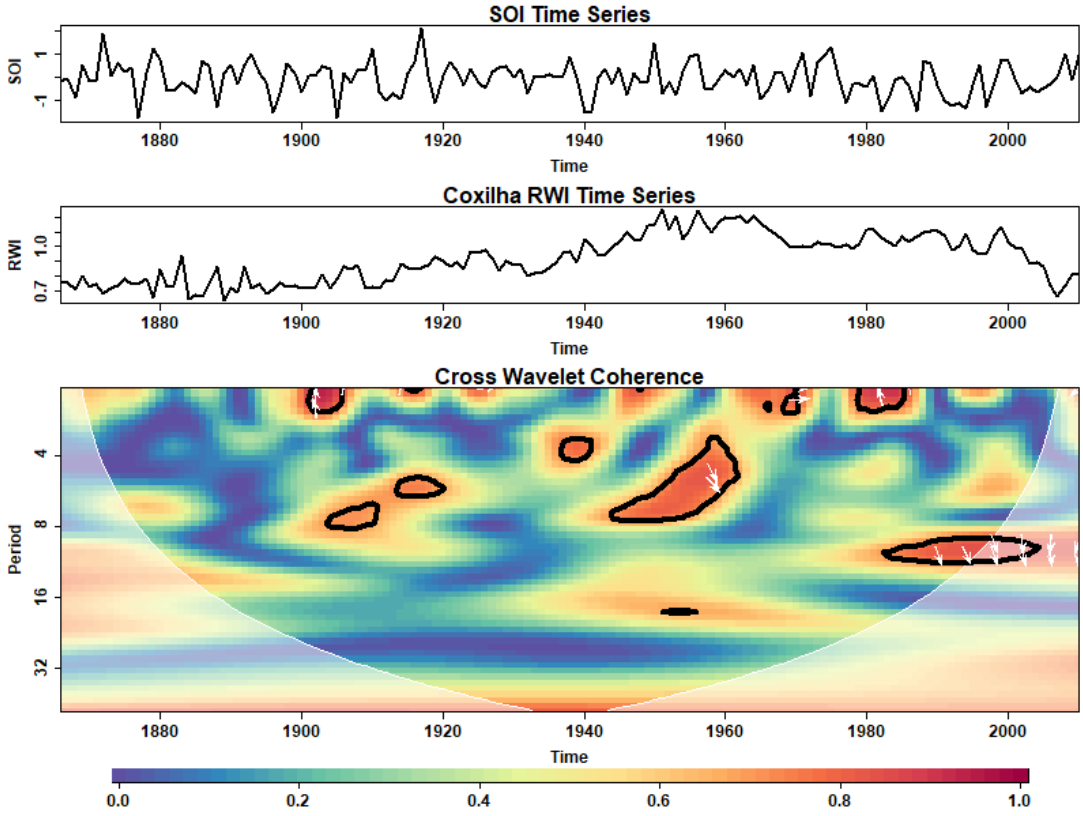
SOI Time Series
SOI
1
-1
1880
1900
1920
1940
1960
1980
2000
Time
Coxilha RWI Time Series
RWI
0.7
1.0
1880
1900
1920
1940
1960
1980
2000
Time
Cross Wavelet Coherence
Period
4
8
16
32
1880
1900
1920
1940
1960
1980
2000
Time
0.0
0.2
0.4
0.6
0.8
1.0

(b)

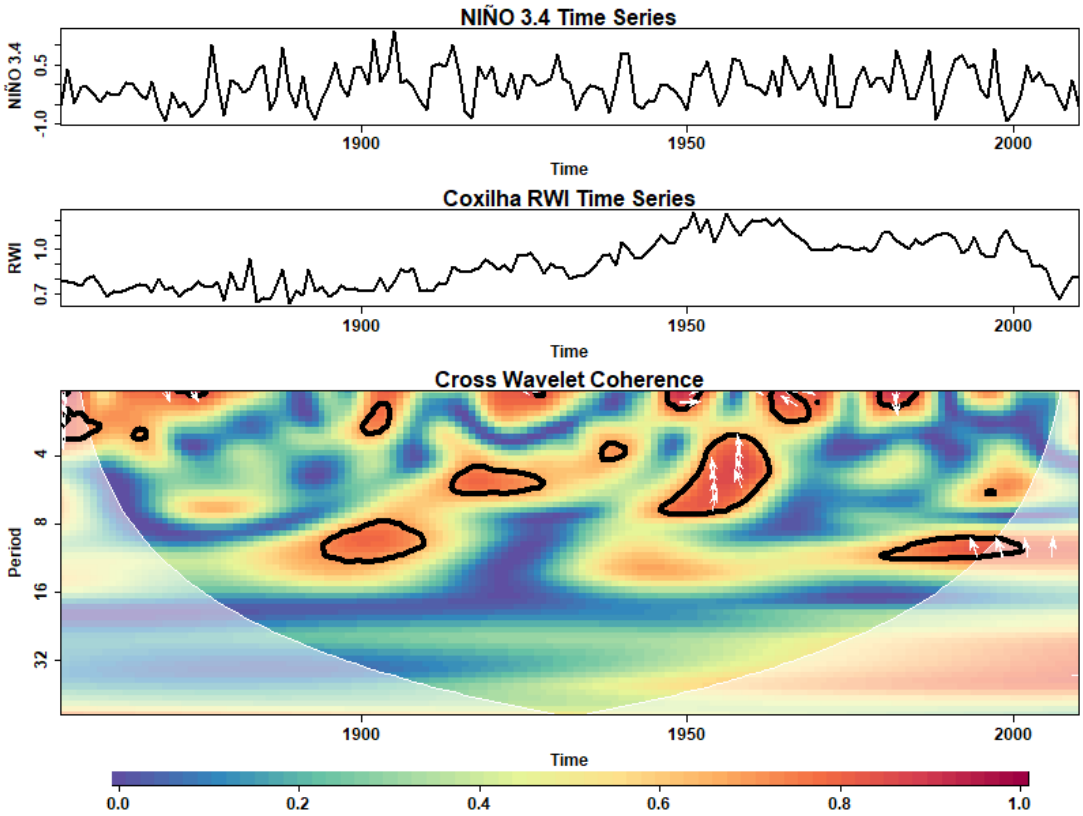
NIÑO 3.4 Time Series
NIÑO 3.4
0.5
-1.0
1900
1950
2000
Time
Coxilha RWI Time Series
RWI
0.7
1.0
1900
1950
2000
Time
Cross Wavelet Coherence
Period
4
8
16
32
1900
1950
2000
Time
0.0
0.2
0.4
0.6
0.8
1.0

(c)

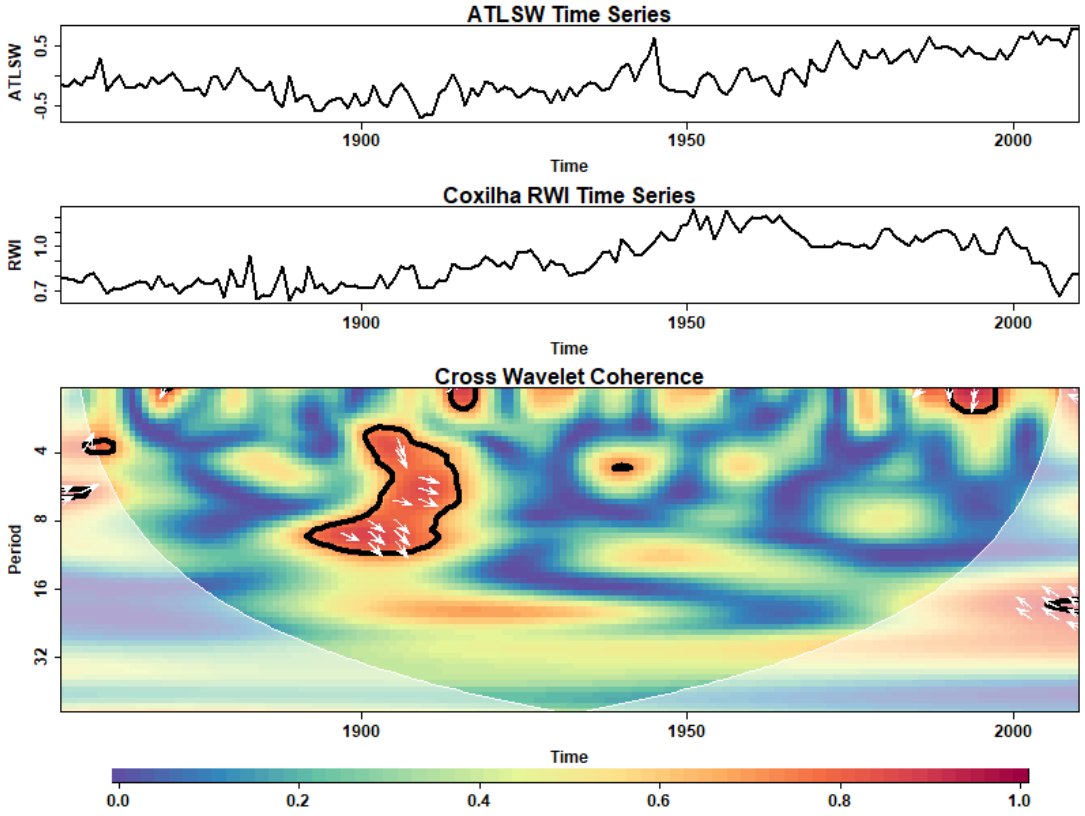
ATLSW Time Series
ATLSW
0.5
-0.5
1900
1950
2000
Time
Coxilha RWI Time Series
RWI
1.0
0.7
1900
1950
2000
Time
Cross Wavelet Coherence
Period
4
8
16
32
1900
1950
2000
Time
0.0
0.2
0.4
0.6
0.8
1.0

(d)

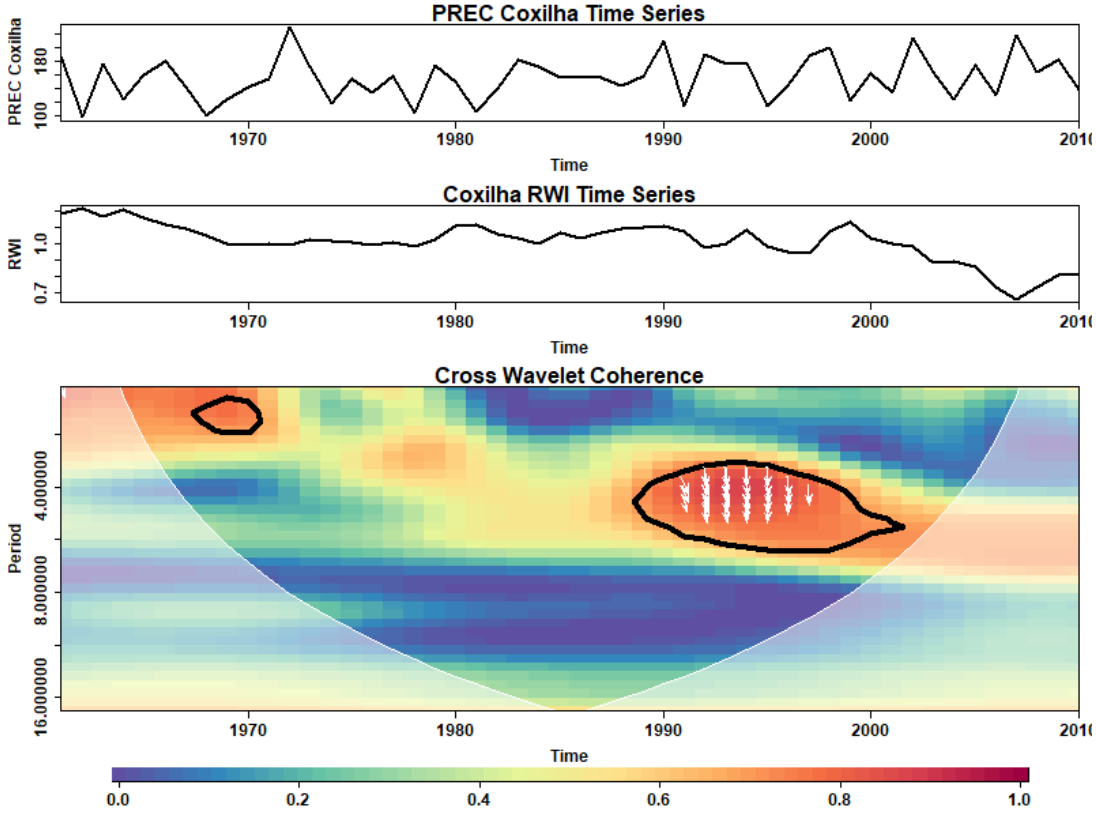
PREC Coxilha Time Series
PREC Coxilha
180
100
1970
1980
1990
2000
Time
Coxilha RWI Time Series
RWI
1.0
0.7
1970
1980
1990
2000
Time
Cross Wavelet Coherence
Period
4.000000
8.000000
16.000000
1970
1980
1990
2000
Time
0.0
0.2
0.4
0.6
0.8
1.0

(e)

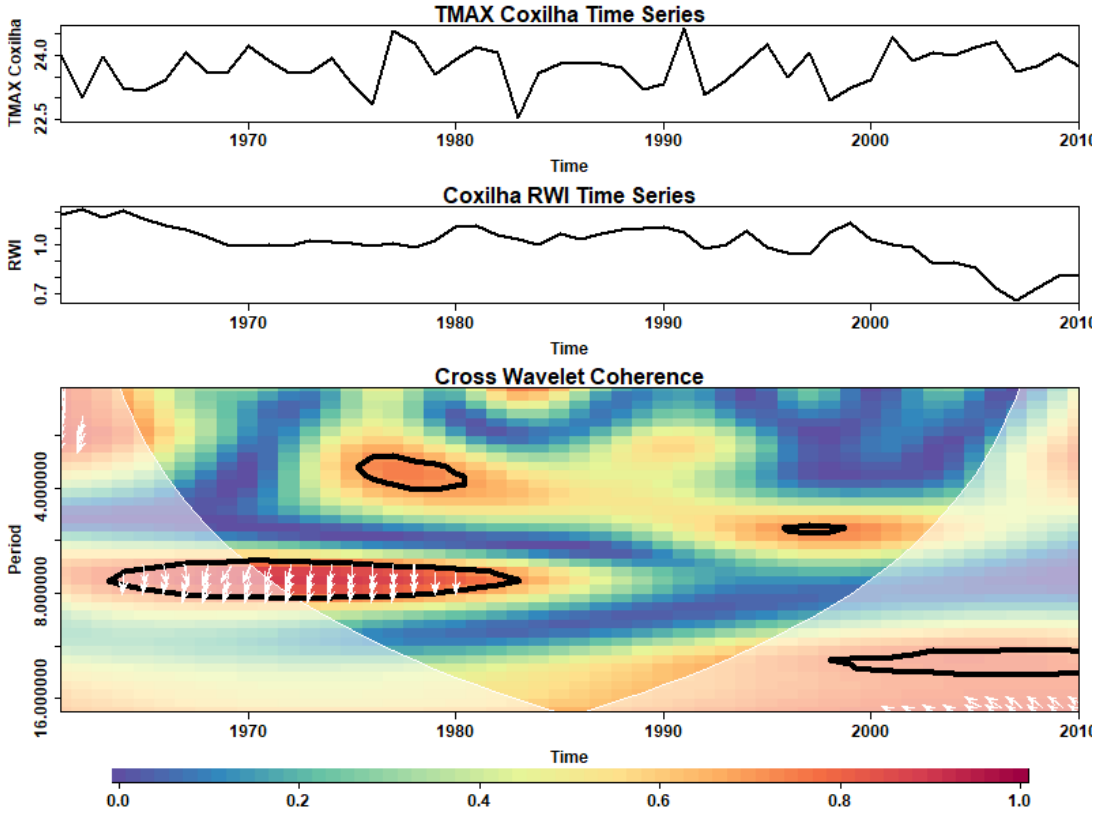
TMAX Coxilha Time Series
TMAX Coxilha
22.5
24.0
1970
1980
1990
2000
Time
Coxilha RWI Time Series
RWI
0.7
1.0
1970
1980
1990
2000
Time
Cross Wavelet Coherence
Period
16.000000
8.000000
4.000000
1970
1980
1990
2000
Time
0.0
0.2
0.4
0.6
0.8
1.0

(f)

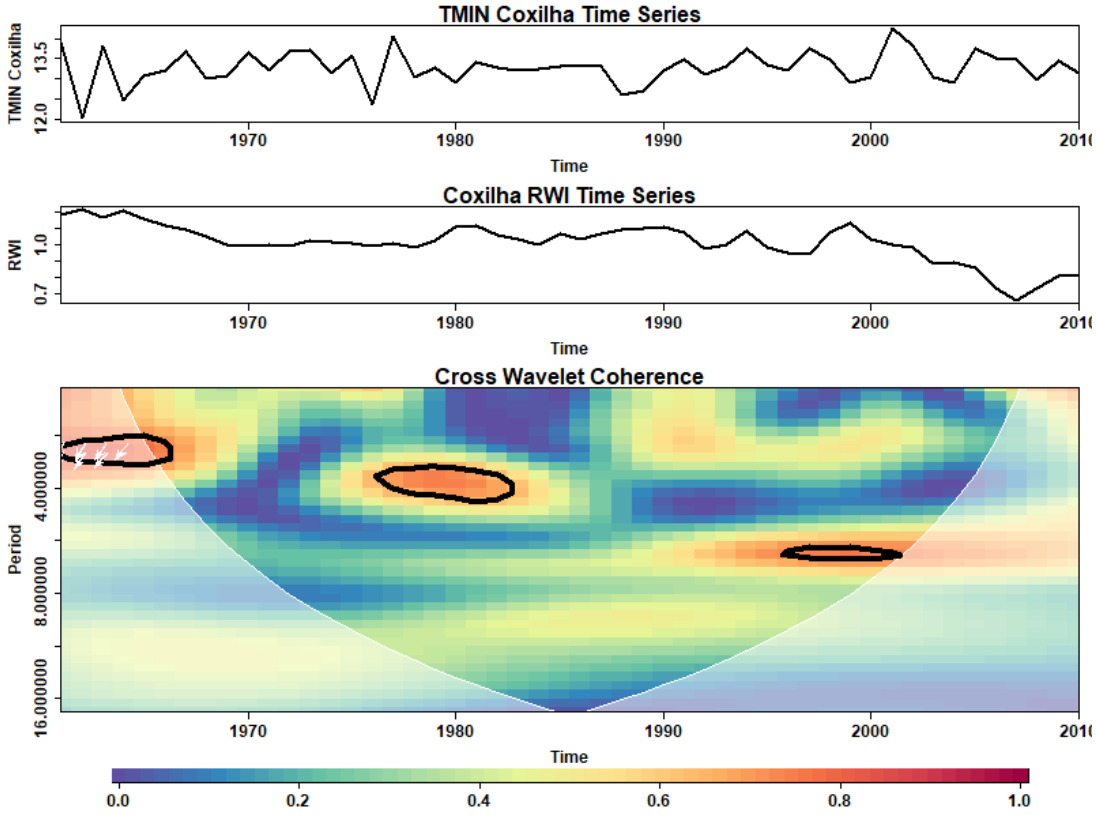
TMIN Coxilha Time Series
TMIN Coxilha
12.0
13.5
1970
1980
1990
2000
Time
Coxilha RWI Time Series
RWI
0.7
1.0
1970
1980
1990
2000
Time
Cross Wavelet Coherence
Period
16.000000
8.000000
4.000000
1970
1980
1990
2000
Time
0.0
0.2
0.4
0.6
0.8
1.0

(g)

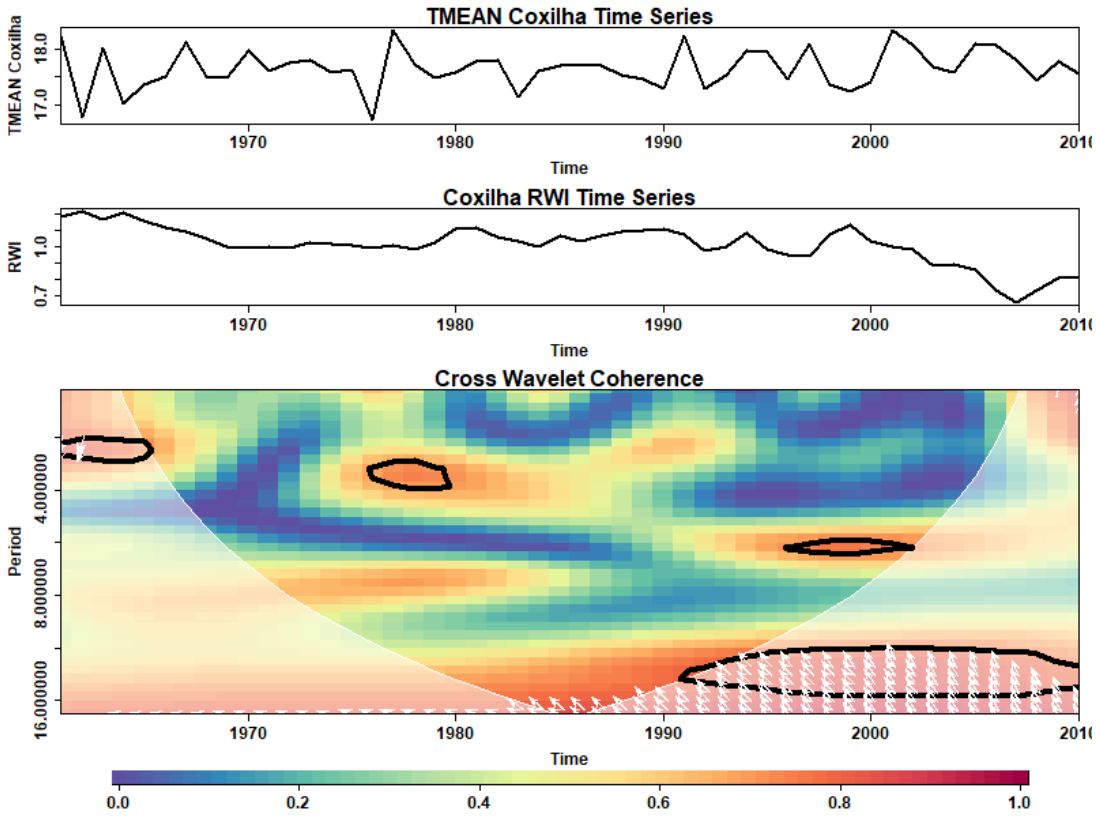

(h)
Source: The author.

Figure 63: Cross Wavelet Coherence (WTC) Analysis between Curitibanos Ring Width Index (RWI) and Ocean-Atmosphere/Solar Parameters. Panels (a) to (h) display the WTC results between Curitibanos RWI and the Southern Oscillation Index (SOI), El Niño 3.4 Index (NIÑO 3.4), Sunspot Activity (SUNSPOT), Atlantic Sea Surface Temperature (ATLSW), Precipitation (PREC), Mean Temperature (TMEAN), Maximum Temperature (TMAX), and Minimum Temperature (TMIN), respectively. The contours in black indicate regions of high coherence with a significance level > 0.95, unveiling potential associations and time-frequency relationships. The white arrows demonstrate the phase angle and direction of the relationship between the RWI and each parameter. Rightward-pointing arrows signify an "in-phase" relationship, indicating that both the RWI and the parameter share similar variations at specific time-frequency intervals. Contrary, leftward-pointing arrows indicate an "anti-phase" relationship, where the RWI and the parameter exhibit opposite variations at certain time-frequency regions.

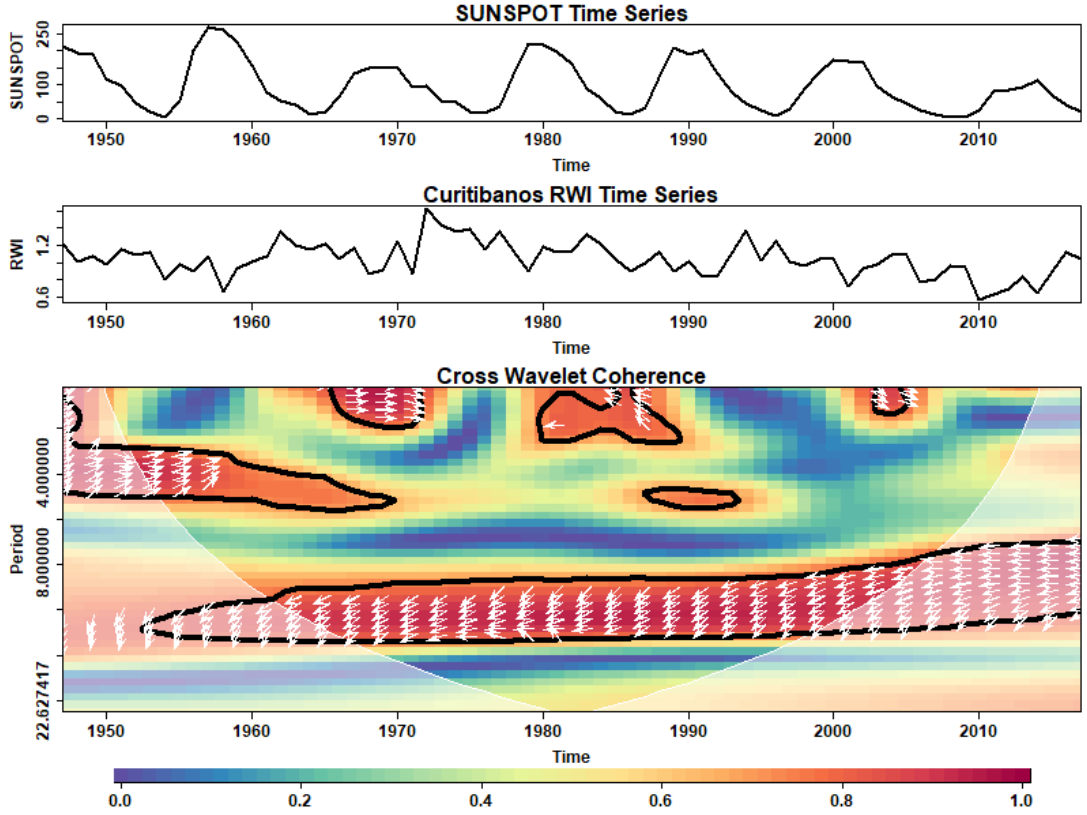

(a)

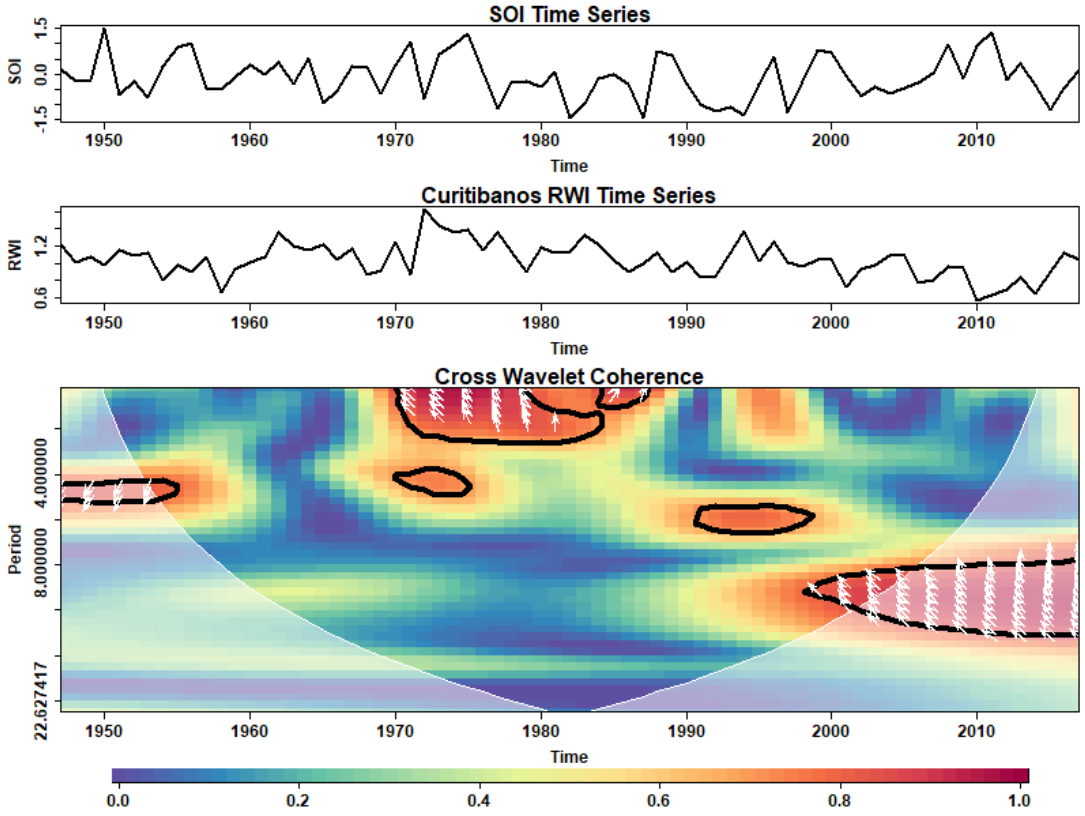
SOI Time Series
SOI
1.5
0.0
-1.5
1950
1960
1970
1980
1990
2000
2010
Time
Curitibanos RWI Time Series
RWI
1.2
0.6
1950
1960
1970
1980
1990
2000
2010
Time
Cross Wavelet Coherence
Period
4.000000
8.000000
22.627417
1950
1960
1970
1980
1990
2000
2010
Time
0.0
0.2
0.4
0.6
0.8
1.0

(b)

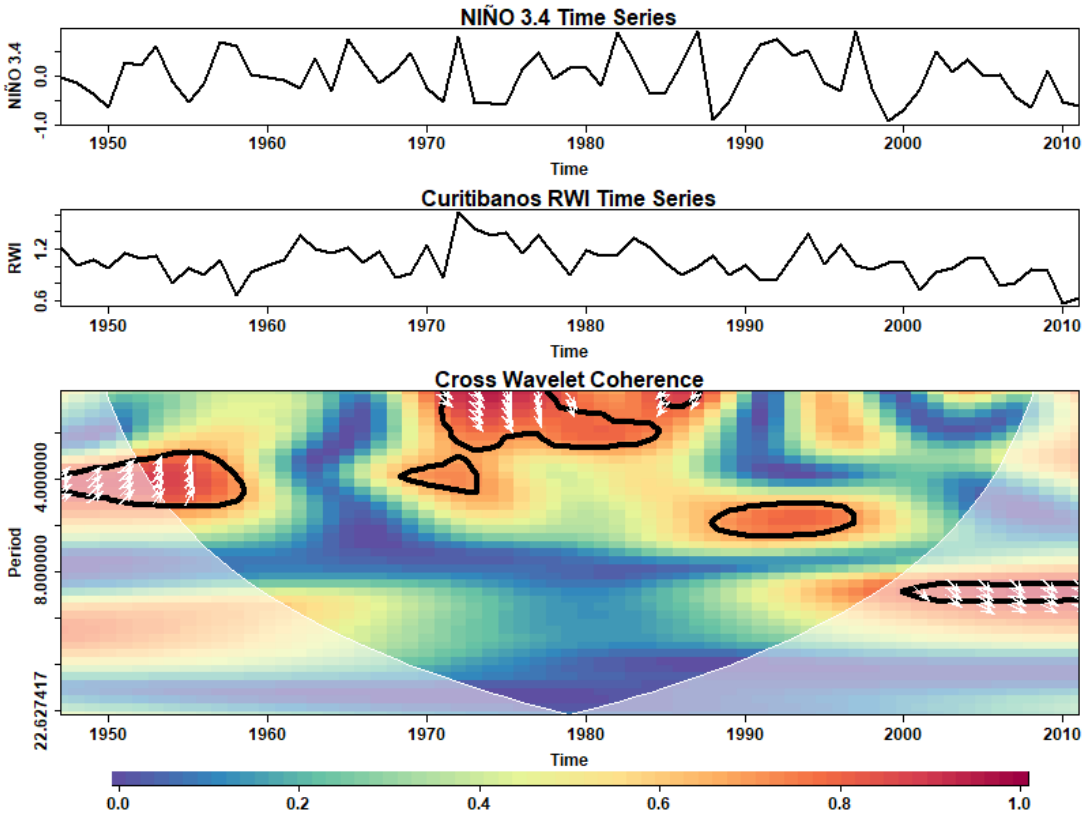
NIÑO 3.4 Time Series
NIÑO 3.4
0.0
-1.0
1950
1960
1970
1980
1990
2000
2010
Time
Curitibanos RWI Time Series
RWI
1.2
0.6
1950
1960
1970
1980
1990
2000
2010
Time
Cross Wavelet Coherence
Period
4.000000
8.000000
22.627417
1950
1960
1970
1980
1990
2000
2010
Time
0.0
0.2
0.4
0.6
0.8
1.0

(c)

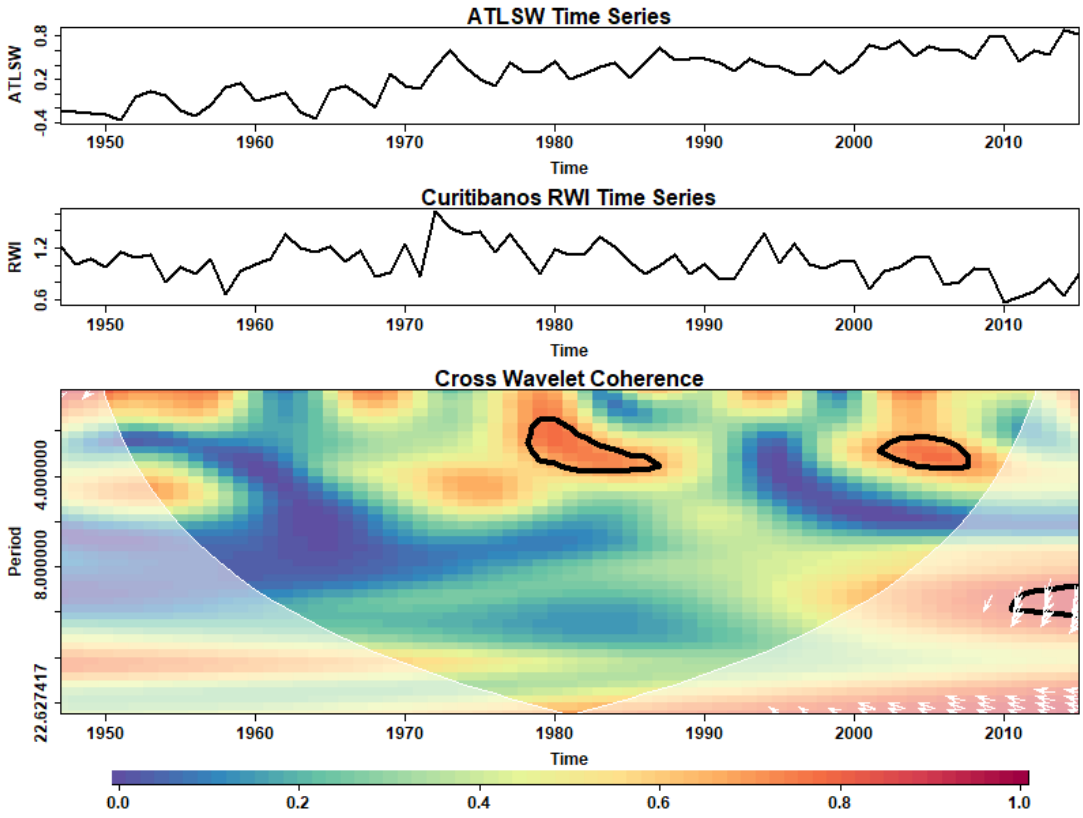

(d)
Source: The author.

Figure 64: Cross Wavelet Coherence (WTC) Analysis between General Carneiro (GCA) Ring Width Index (RWI) and Ocean-Atmosphere/Solar Parameters. Panels (a) to (h) display the WTC results between GCA RWI and the Southern Oscillation Index (SOI), El Niño 3.4 Index (NIÑO 3.4), Sunspot Activity (SUNSPOT), Atlantic Sea Surface Temperature (ATLSW), Precipitation (PREC), Mean Temperature (TMEAN), Maximum Temperature (TMAX), and Minimum Temperature (TMIN), respectively. The contours in black indicate regions of high coherence with a significance level > 0.95, unveiling potential associations and time-frequency relationships. The white arrows demonstrate the phase angle and direction of the relationship between the RWI and each parameter. Rightward-pointing arrows signify an "in-phase" relationship, indicating that both the RWI and the parameter share similar variations at specific time-frequency intervals. Contrary, leftward-pointing arrows indicate an "anti-phase" relationship, where the RWI and the parameter exhibit opposite variations at certain time-frequency regions.

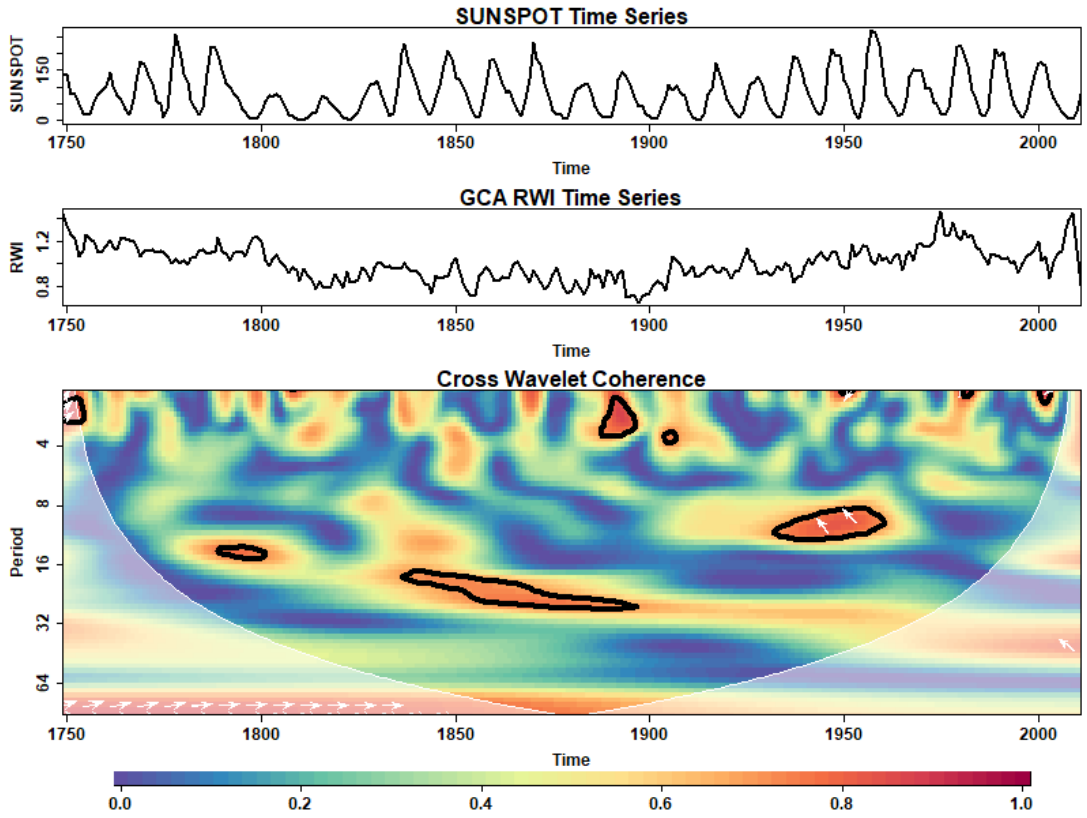

(a)

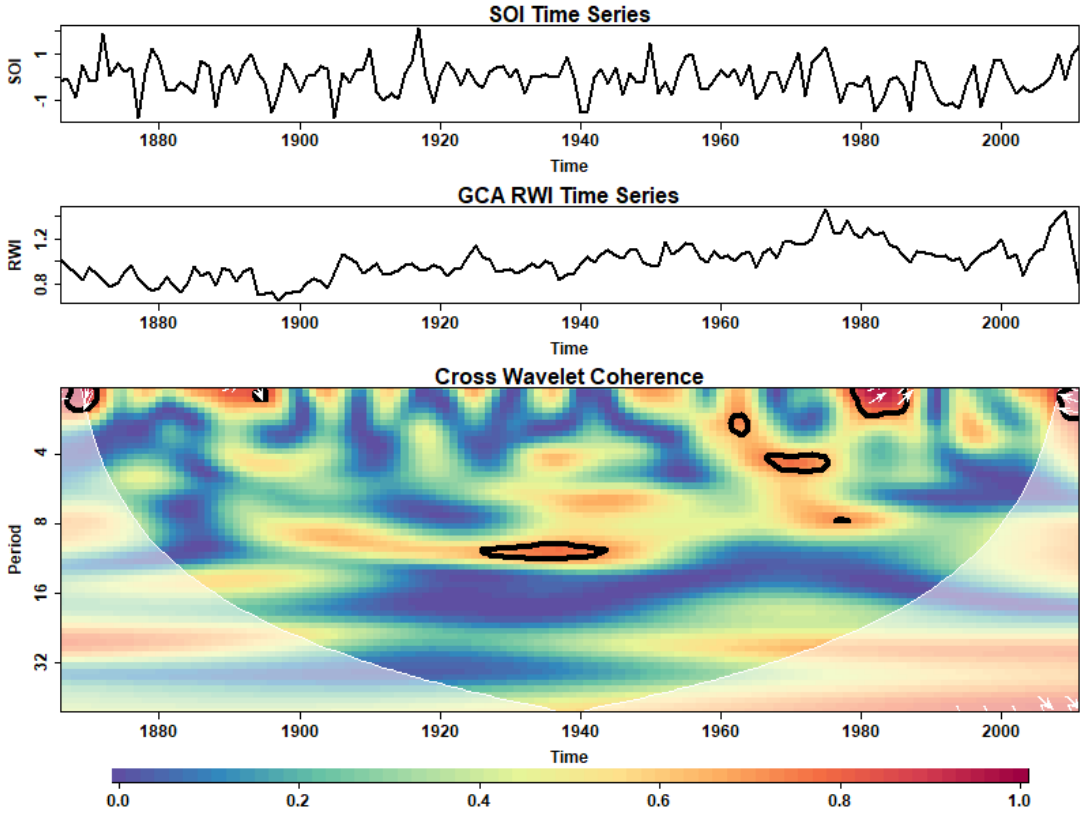
SOI Time Series
SOI
1
-1
1880
1900
1920
1940
1960
1980
2000
Time
GCA RWI Time Series
RWI
1.2
0.8
1880
1900
1920
1940
1960
1980
2000
Time
Cross Wavelet Coherence
Period
4
8
16
32
1880
1900
1920
1940
1960
1980
2000
Time
0.0
0.2
0.4
0.6
0.8
1.0

(b)

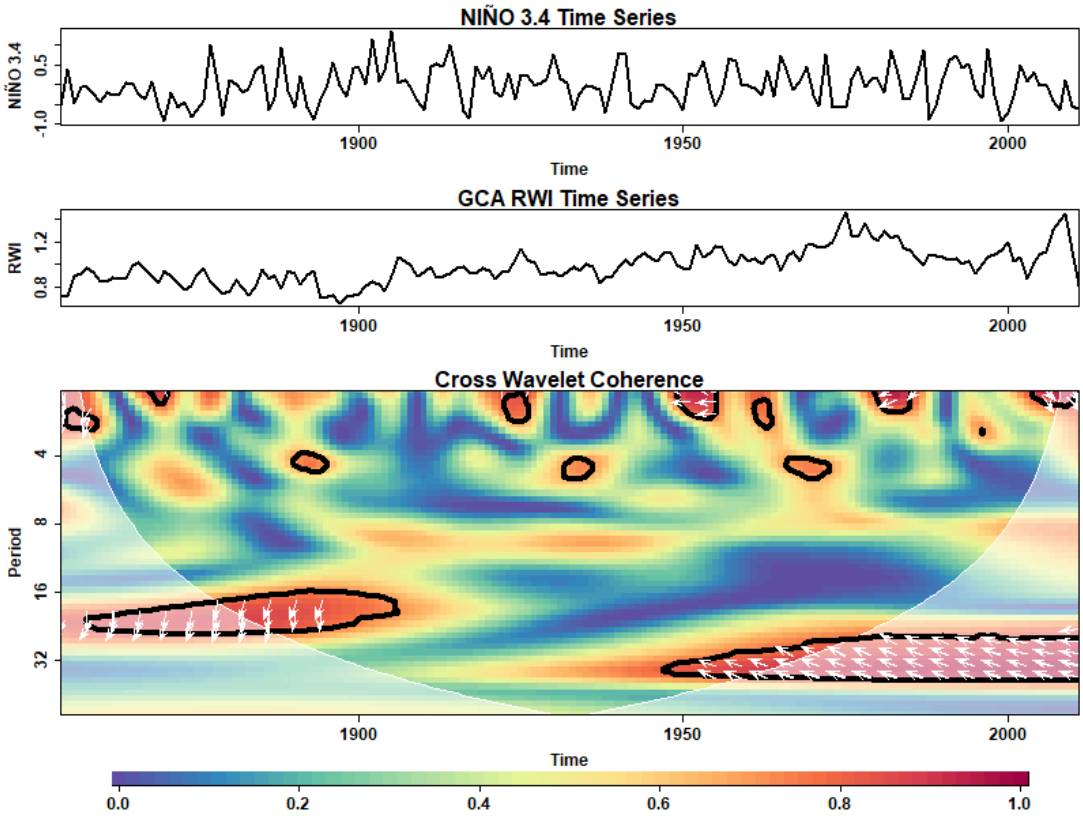
NIÑO 3.4 Time Series
NIÑO 3.4
0.5
-1.0
1900
1950
2000
Time
GCA RWI Time Series
RWI
1.2
0.8
1900
1950
2000
Time
Cross Wavelet Coherence
Period
4
8
16
32
1900
1950
2000
Time
0.0
0.2
0.4
0.6
0.8
1.0

(c)

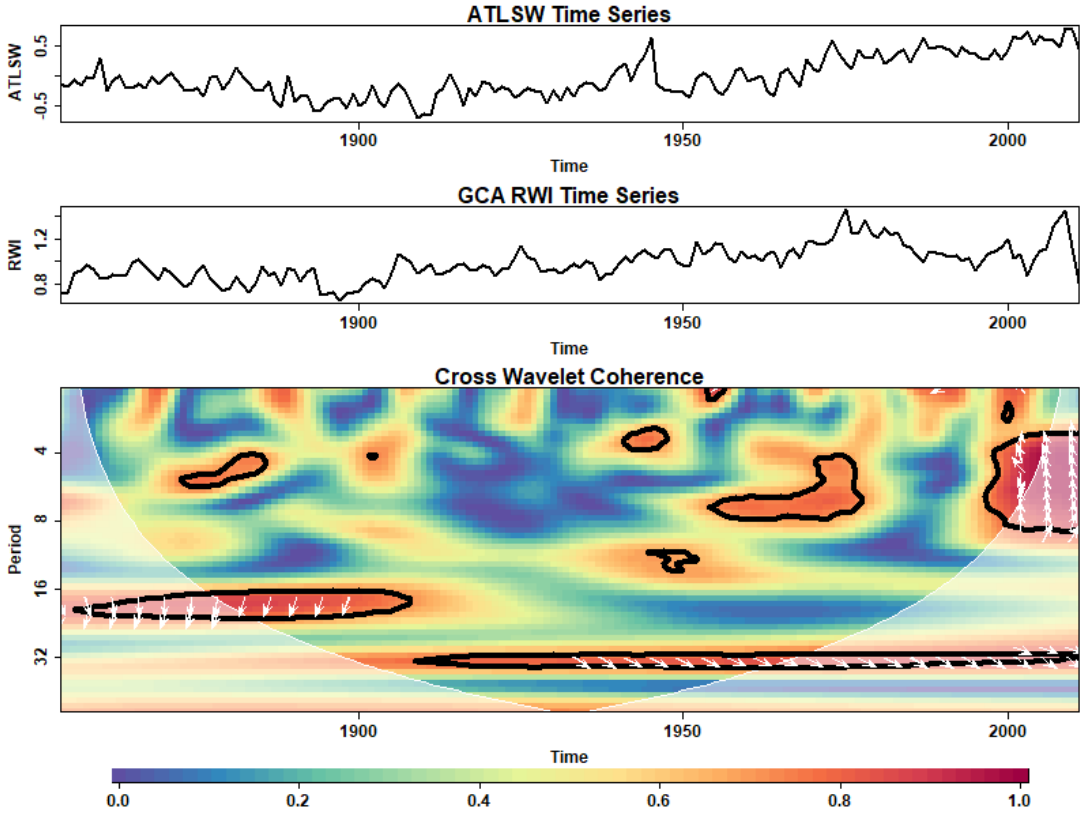
ATLSW Time Series
ATLSW
0.5
-0.5
1900
1950
2000
Time
GCA RWI Time Series
RWI
1.2
0.8
1900
1950
2000
Time
Cross Wavelet Coherence
Period
4
8
16
32
1900
1950
2000
Time
0.0
0.2
0.4
0.6
0.8
1.0

(d)

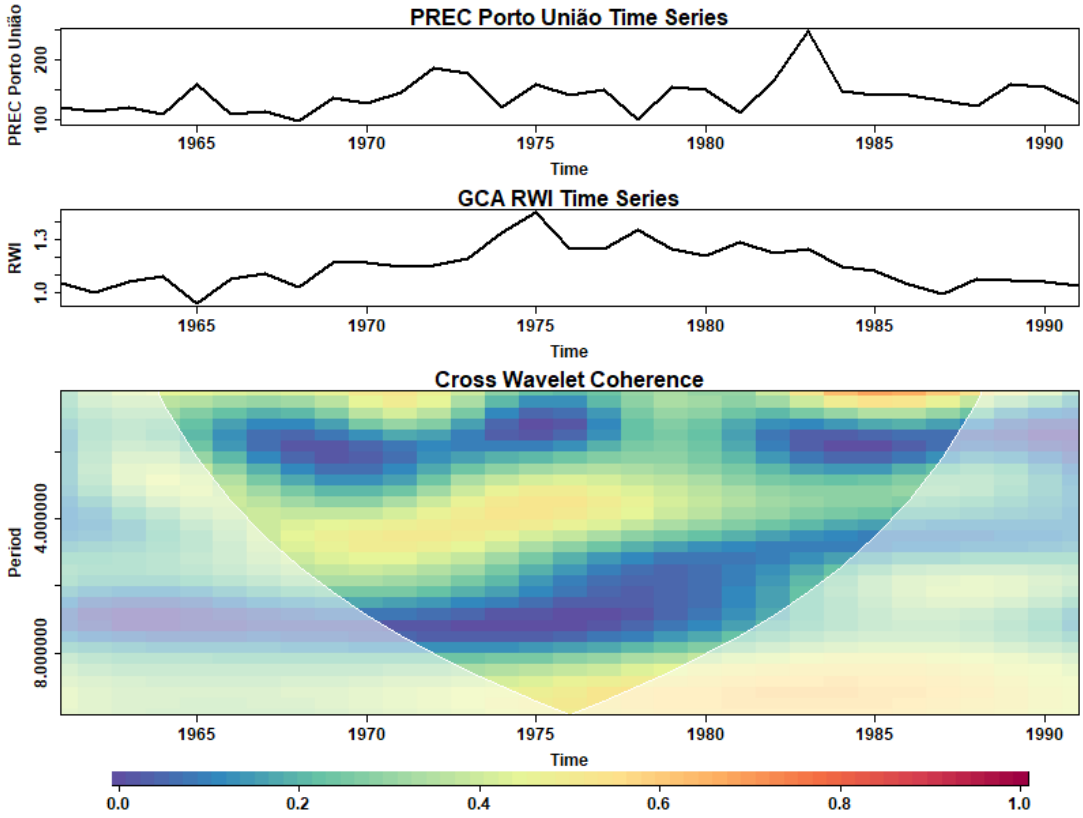
PREC Porto União Time Series
PREC Porto União
200
100
1965
1970
1975
1980
1985
1990
Time
GCA RWI Time Series
RWI
1.3
1.0
1965
1970
1975
1980
1985
1990
Time
Cross Wavelet Coherence
Period
4.000000
8.000000
1965
1970
1975
1980
1985
1990
Time
0.0
0.2
0.4
0.6
0.8
1.0

(e)

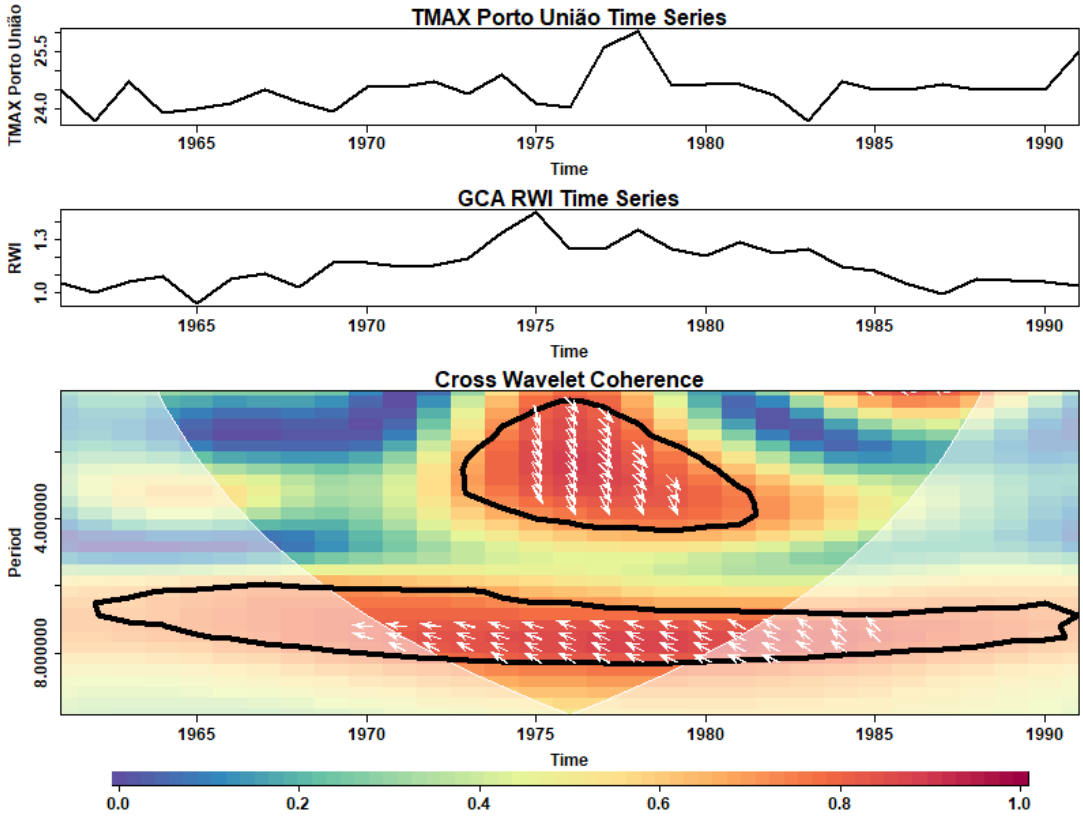
TMAX Porto União Time Series
TMAX Porto União
24.0
25.5
1965
1970
1975
1980
1985
1990
Time
GCA RWI Time Series
RWI
1.0
1.3
1965
1970
1975
1980
1985
1990
Time
Cross Wavelet Coherence
Period
4.000000
8.000000
1965
1970
1975
1980
1985
1990
Time
0.0
0.2
0.4
0.6
0.8
1.0

(f)

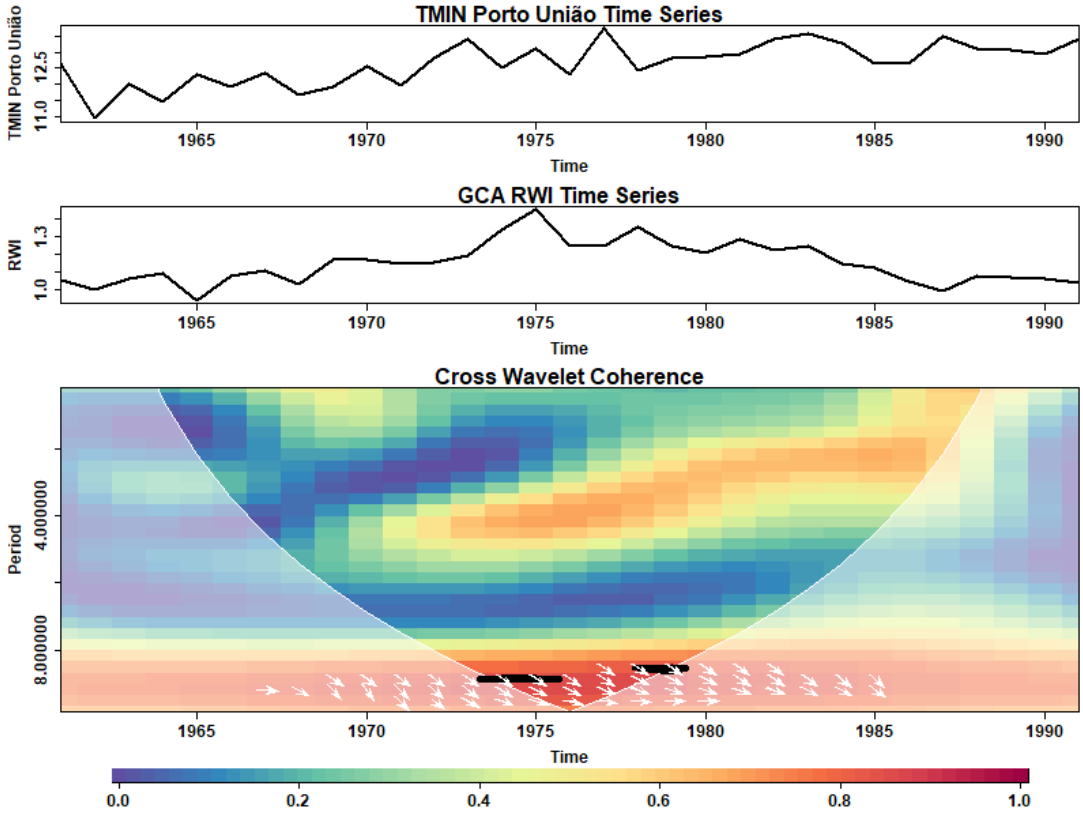
TMIN Porto União Time Series
TMIN Porto União
11.0
12.5
1965
1970
1975
1980
1985
1990
Time
GCA RWI Time Series
RWI
1.0
1.3
1965
1970
1975
1980
1985
1990
Time
Cross Wavelet Coherence
Period
4.000000
8.000000
1965
1970
1975
1980
1985
1990
Time
0.0
0.2
0.4
0.6
0.8
1.0

(g)

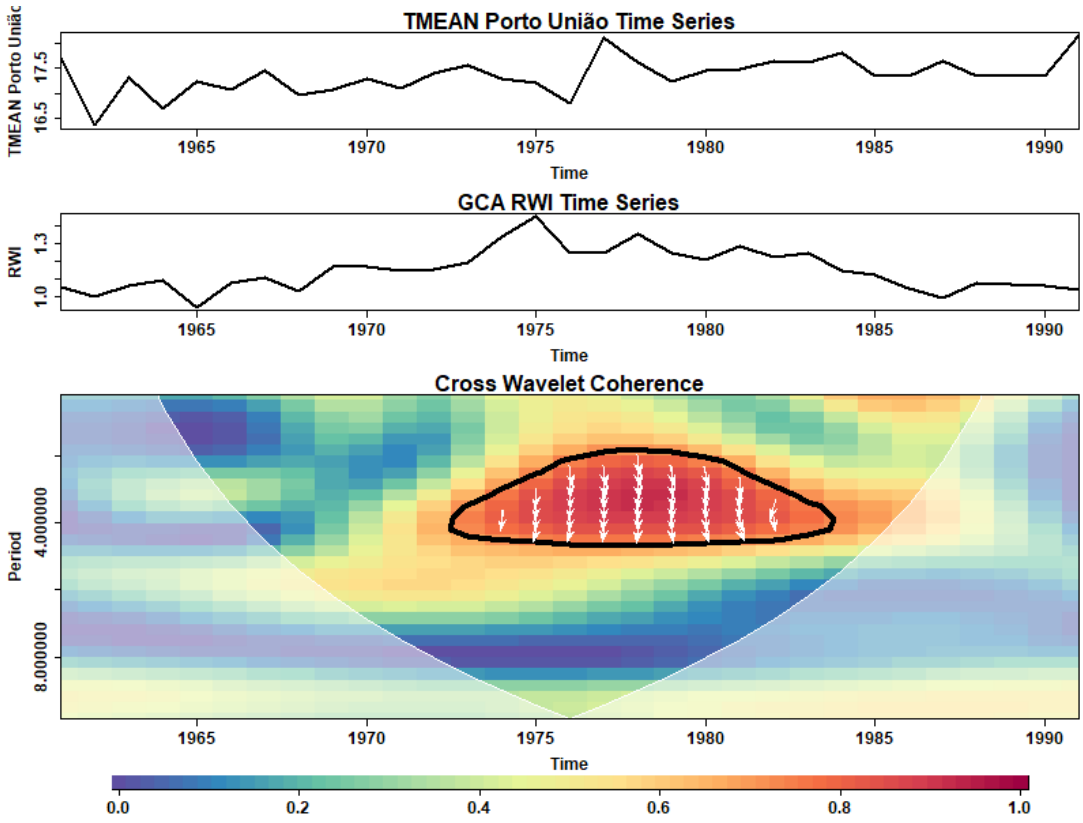

(h)
Source: The author.

Figure 65: Cross Wavelet Coherence (WTC) Analysis between Irani Ring Width Index (RWI) and Ocean-Atmosphere/Solar Parameters. Panels (a) to (h) display the WTC results between Irani RWI and the Southern Oscillation Index (SOI), El Niño 3.4 Index (NIÑO 3.4), Sunspot Activity (SUNSPOT), Atlantic Sea Surface Temperature (ATLSW), Precipitation (PREC), Mean Temperature (TMEAN), Maximum Temperature (TMAX), and Minimum Temperature (TMIN), respectively. The contours in black indicate regions of high coherence with a significance level > 0.95, unveiling potential associations and time-frequency relationships. The white arrows demonstrate the phase angle and direction of the relationship between the RWI and each parameter. Rightward-pointing arrows signify an "in-phase" relationship, indicating that both the RWI and the parameter share similar variations at specific time-frequency intervals. Contrary, leftward-pointing arrows indicate an "anti-phase" relationship, where the RWI and the parameter exhibit opposite variations at certain time-frequency regions.

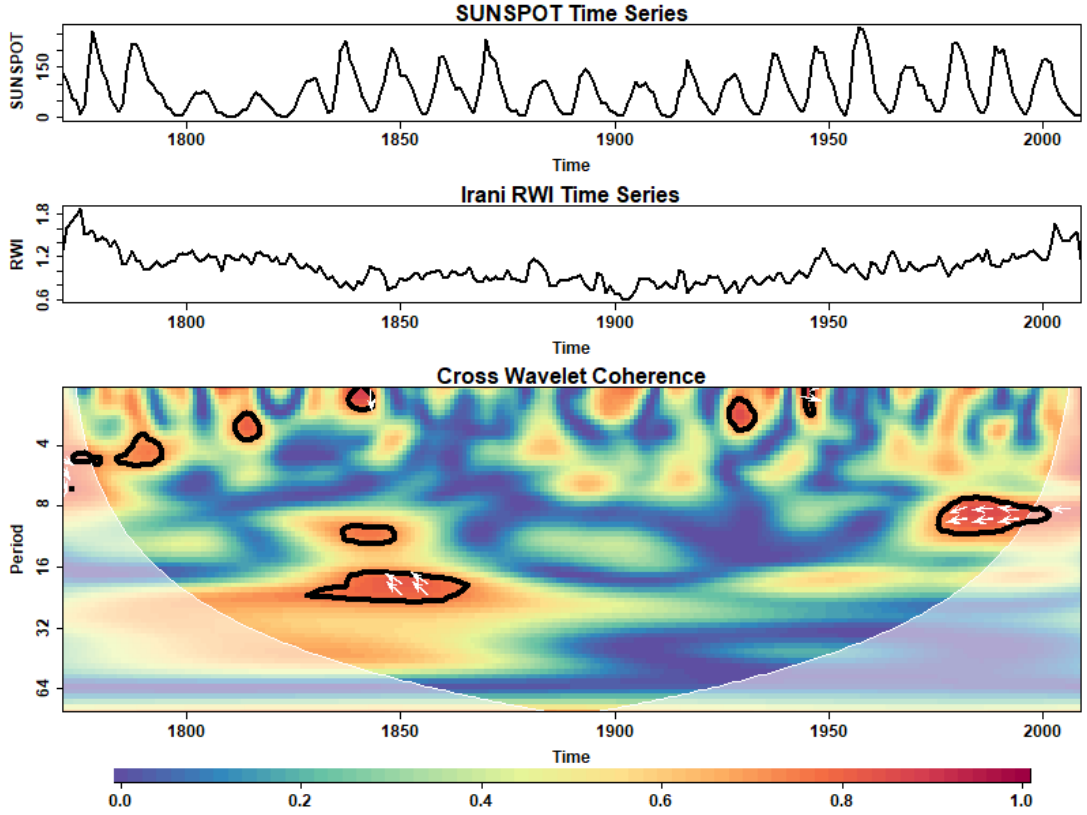

(a)

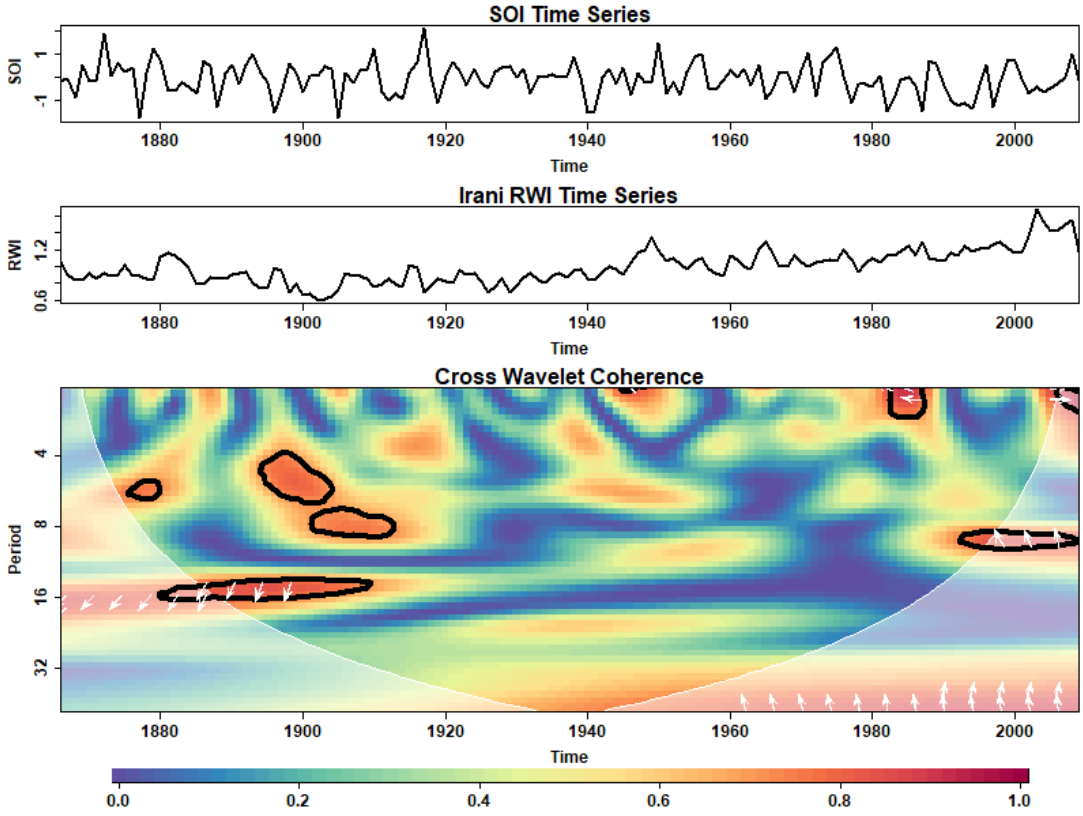
SOI Time Series
SOI
1
-1
1880
1900
1920
1940
1960
1980
2000
Time
Irani RWI Time Series
RWI
1.2
0.6
1880
1900
1920
1940
1960
1980
2000
Time
Cross Wavelet Coherence
Period
4
8
16
32
1880
1900
1920
1940
1960
1980
2000
Time
0.0
0.2
0.4
0.6
0.8
1.0

(b)

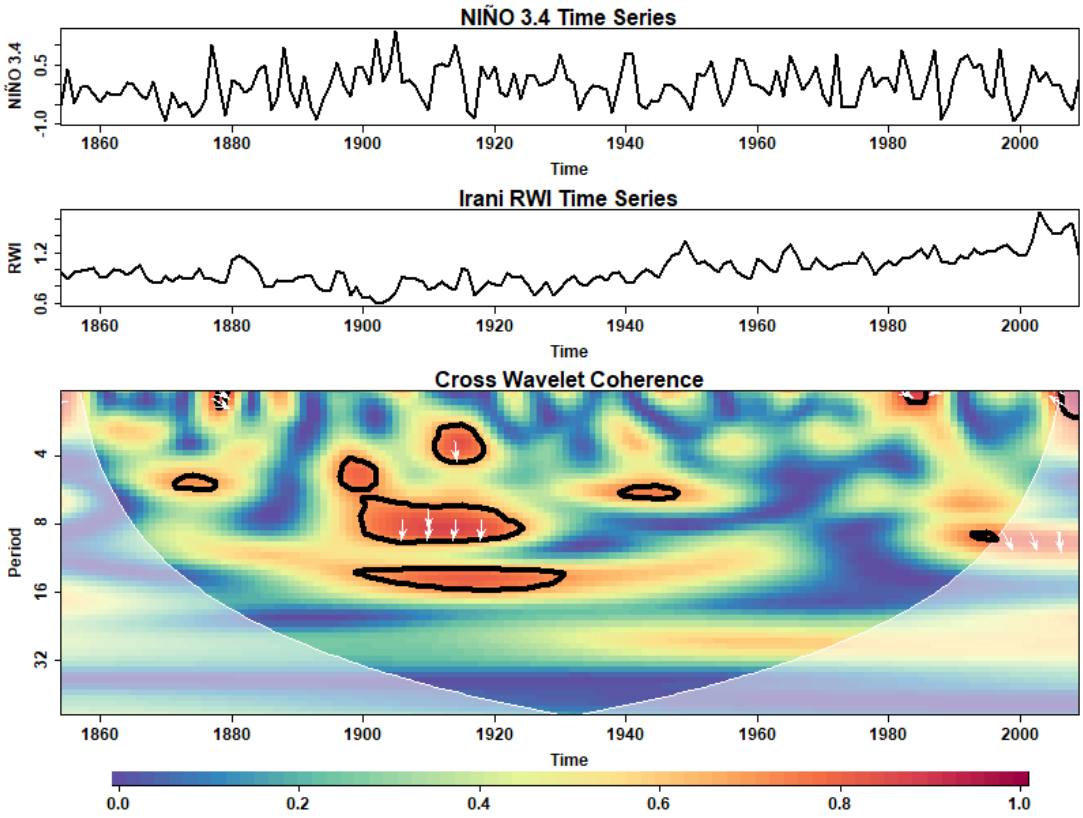
NIÑO 3.4 Time Series
NIÑO 3.4
0.5
-1.0
1860
1880
1900
1920
1940
1960
1980
2000
Time
Irani RWI Time Series
RWI
1.2
0.6
1860
1880
1900
1920
1940
1960
1980
2000
Time
Cross Wavelet Coherence
Period
4
8
16
32
1860
1880
1900
1920
1940
1960
1980
2000
Time
0.0
0.2
0.4
0.6
0.8
1.0

(c)

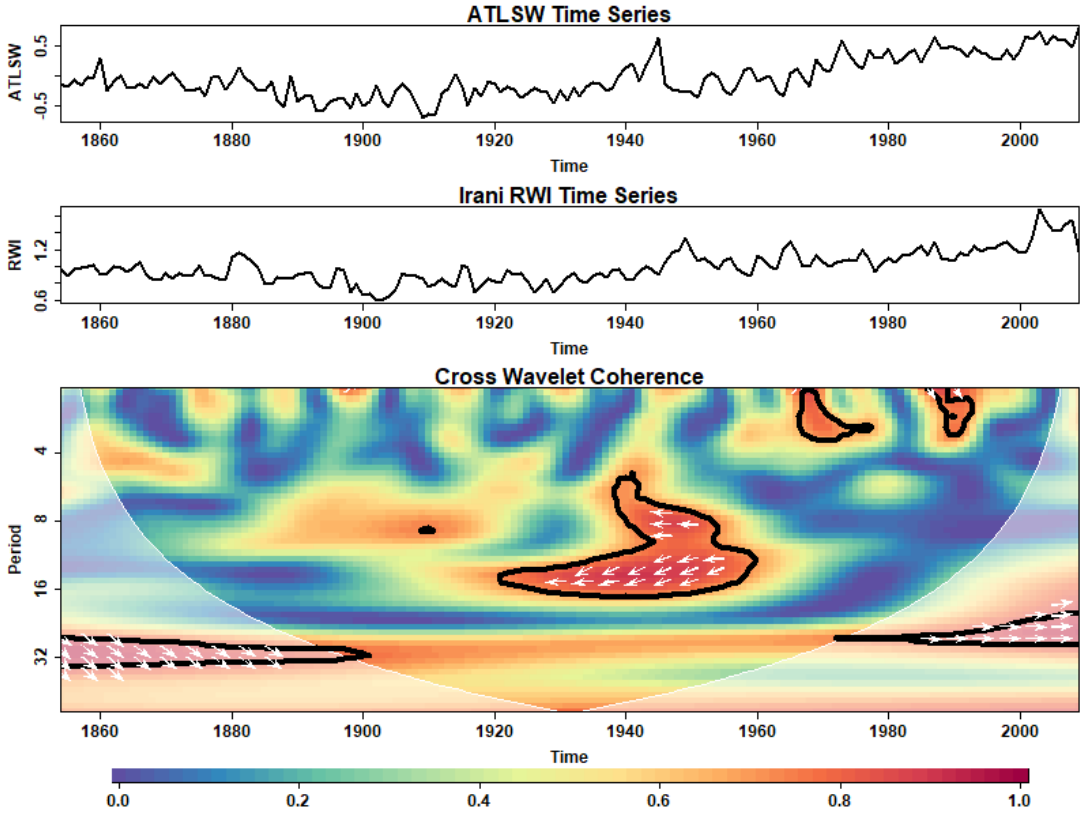
ATLSW Time Series
ATLSW
0.5
-0.5
1860
1880
1900
1920
1940
1960
1980
2000
Time
Irani RWI Time Series
RWI
1.2
0.6
1860
1880
1900
1920
1940
1960
1980
2000
Time
Cross Wavelet Coherence
Period
4
8
16
32
1860
1880
1900
1920
1940
1960
1980
2000
Time
0.0
0.2
0.4
0.6
0.8
1.0

(d)

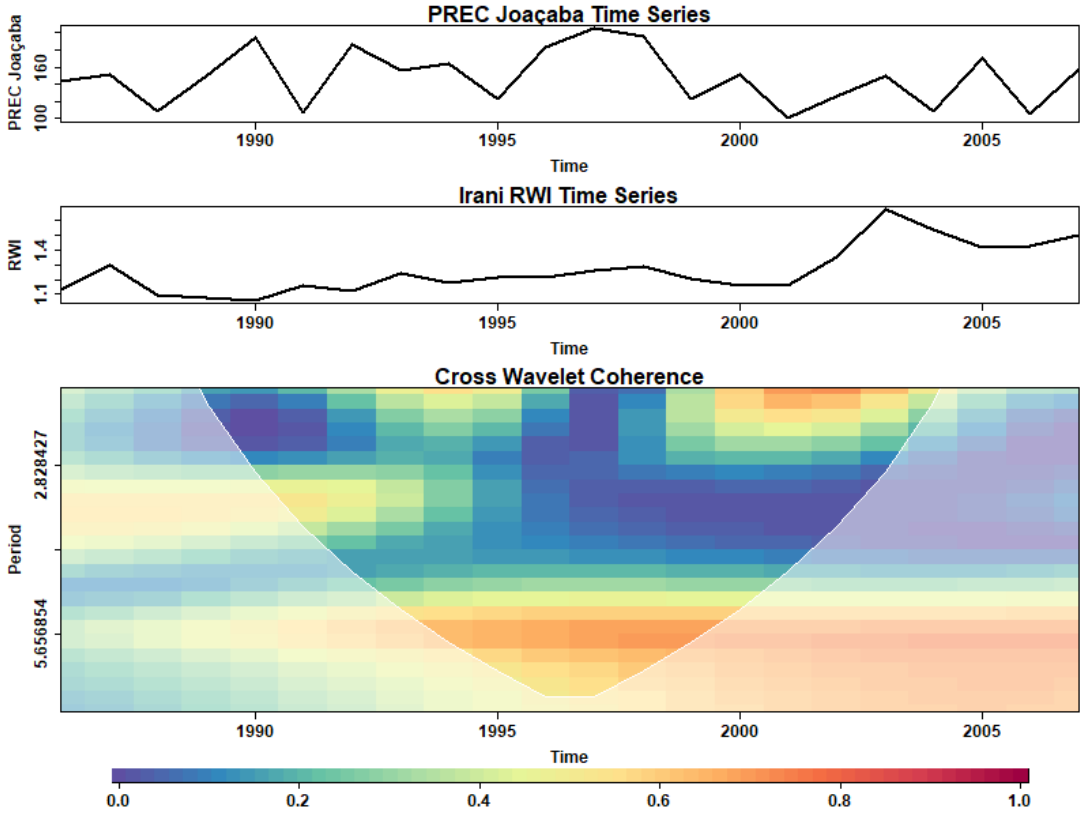
PREC Joaçaba Time Series
PREC Joaçaba
160
100
1990
1995
2000
2005
Time
Irani RWI Time Series
RWI
1.4
1.1
1990
1995
2000
2005
Time
Cross Wavelet Coherence
Period
2.828427
5.656854
1990
1995
2000
2005
Time
0.0
0.2
0.4
0.6
0.8
1.0

(e)

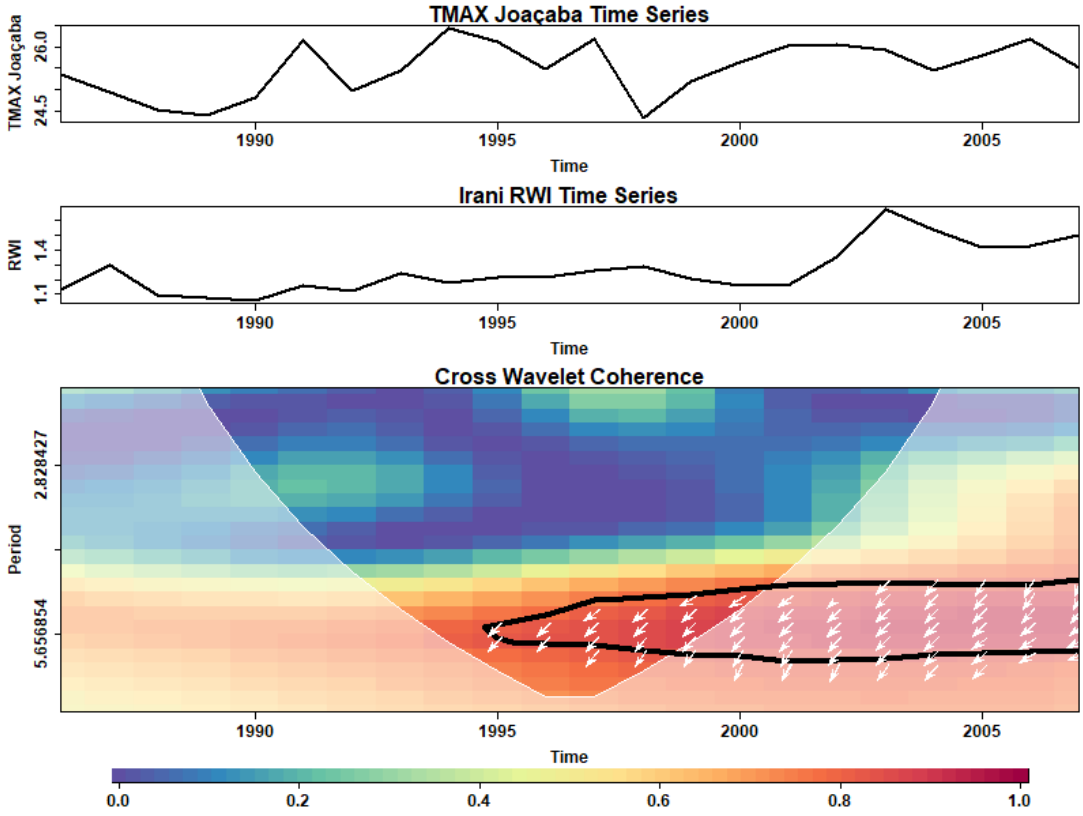
TMAX Joaçaba Time Series
TMAX Joaçaba
26.0
24.5
1990
1995
2000
2005
Time
Irani RWI Time Series
RWI
1.4
1.1
1990
1995
2000
2005
Time
Cross Wavelet Coherence
Period
2.828427
5.656854
1990
1995
2000
2005
Time
0.0
0.2
0.4
0.6
0.8
1.0

(f)

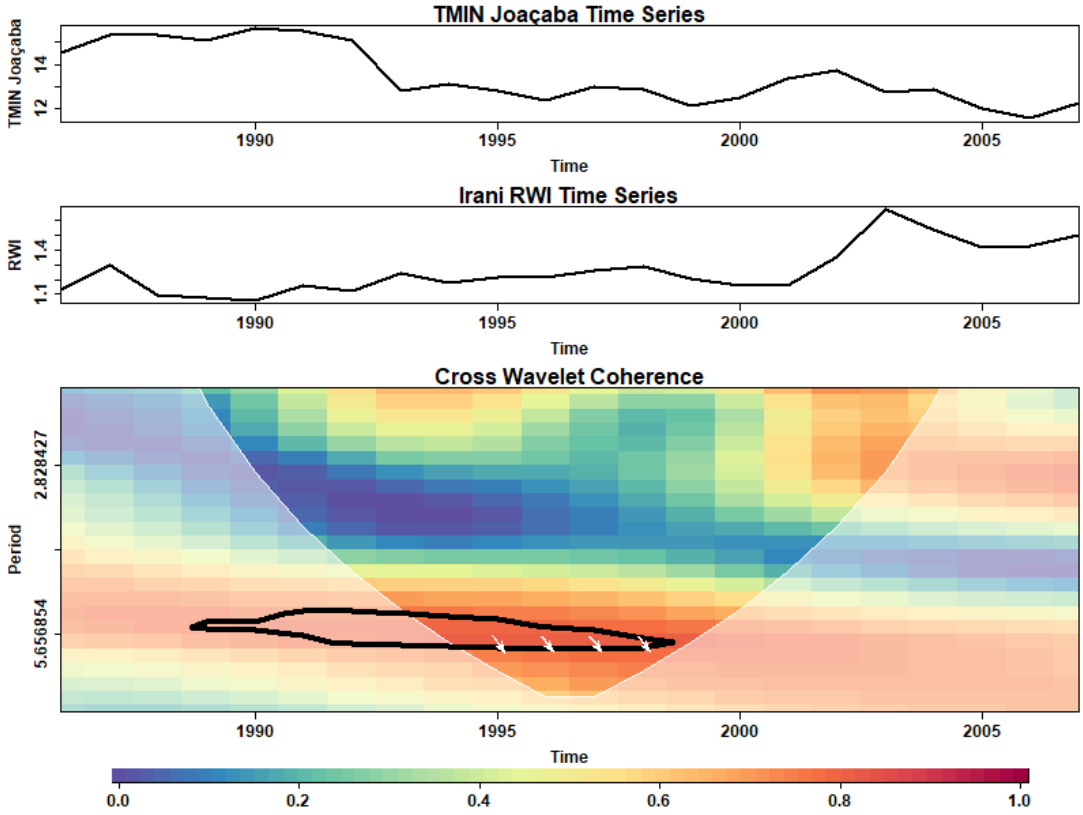
TMIN Joaçaba Time Series
TMIN Joaçaba
14
12
1990
1995
2000
2005
Time
Irani RWI Time Series
RWI
1.4
1.1
1990
1995
2000
2005
Time
Cross Wavelet Coherence
Period
2.828427
5.656854
1990
1995
2000
2005
Time
0.0
0.2
0.4
0.6
0.8
1.0

(g)

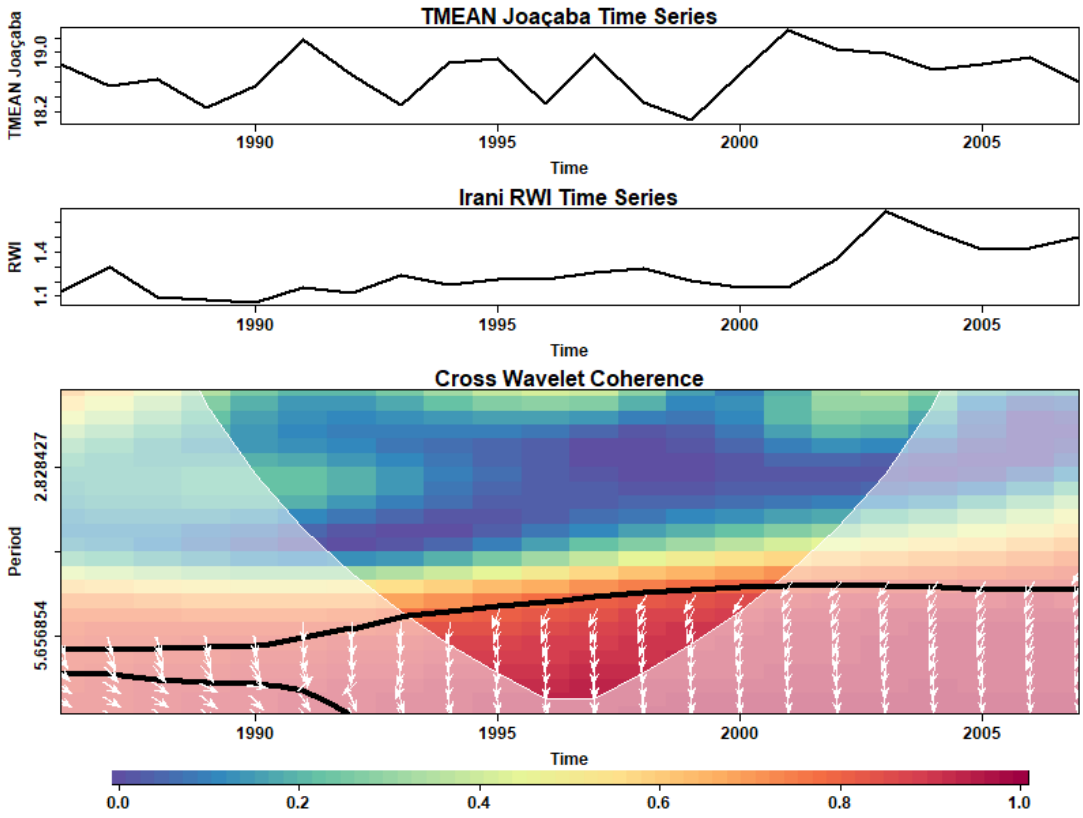

(h)
Source: The author.

Figure 66: Cross Wavelet Coherence (WTC) Analysis between Irineópolis Ring Width Index (RWI) and Ocean-Atmosphere/Solar Parameters. Panels (a) to (h) display the WTC results between Irineópolis RWI and the Southern Oscillation Index (SOI), El Niño 3.4 Index (NIÑO 3.4), Sunspot Activity (SUNSPOT), Atlantic Sea Surface Temperature (ATLSW), Precipitation (PREC), Mean Temperature (TMEAN), Maximum Temperature (TMAX), and Minimum Temperature (TMIN), respectively. The contours in black indicate regions of high coherence with a significance level > 0.95, unveiling potential associations and time-frequency relationships. The white arrows demonstrate the phase angle and direction of the relationship between the RWI and each parameter. Rightward-pointing arrows signify an "in-phase" relationship, indicating that both the RWI and the parameter share similar variations at specific time-frequency intervals. Contrary, leftward-pointing arrows indicate an "anti-phase" relationship, where the RWI and the parameter exhibit opposite variations at certain time-frequency regions.

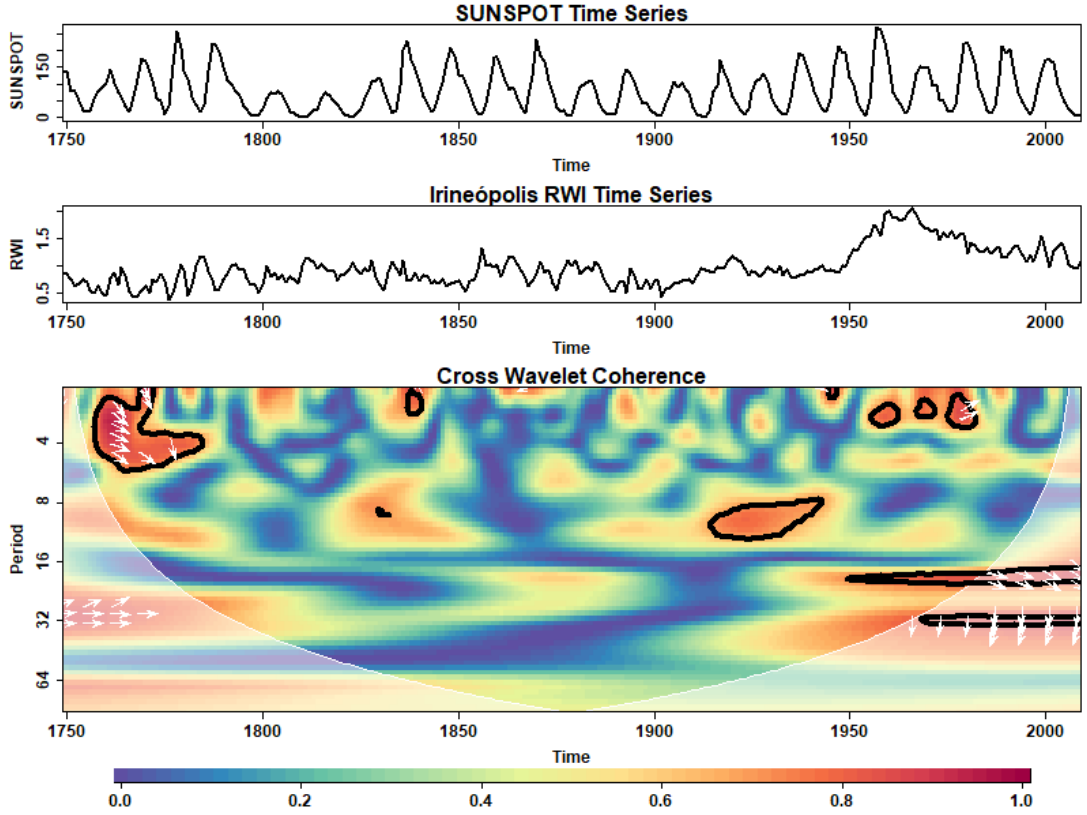

(a)

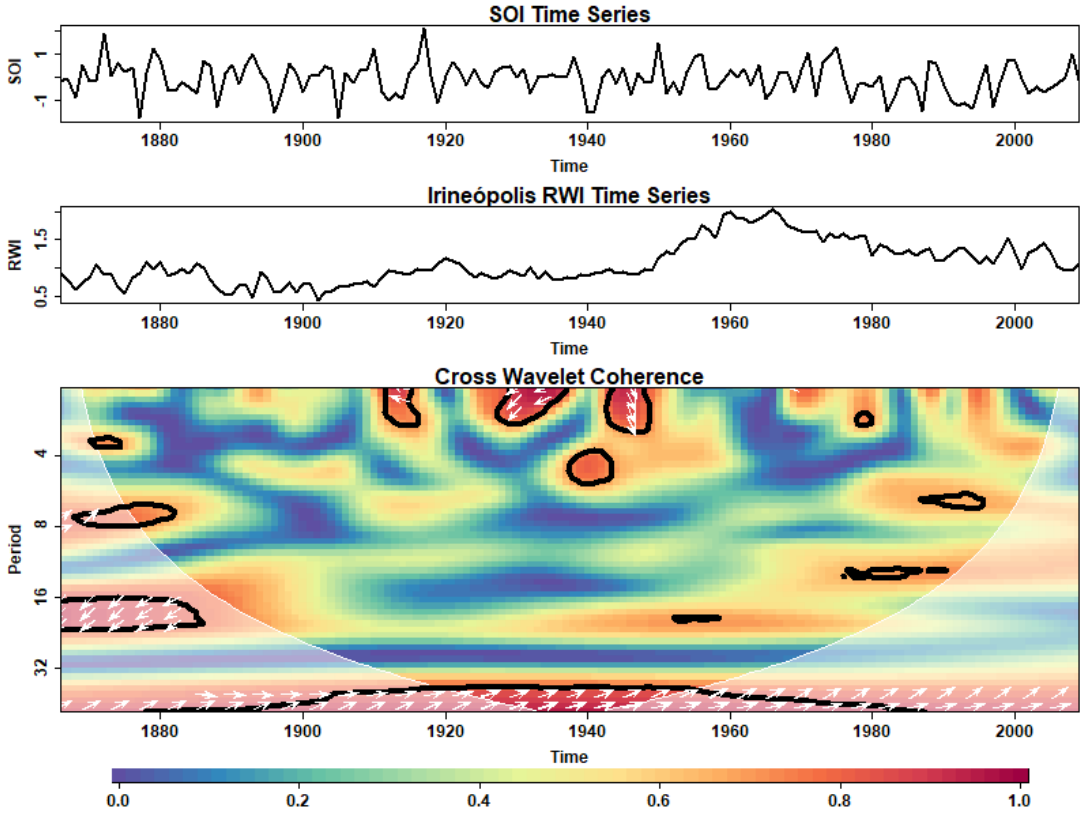
SOI Time Series
SOI
1
-1
1880
1900
1920
1940
1960
1980
2000
Time
Irineópolis RWI Time Series
RWI
1.5
0.5
1880
1900
1920
1940
1960
1980
2000
Time
Cross Wavelet Coherence
Period
4
8
16
32
1880
1900
1920
1940
1960
1980
2000
Time
0.0
0.2
0.4
0.6
0.8
1.0

(b)

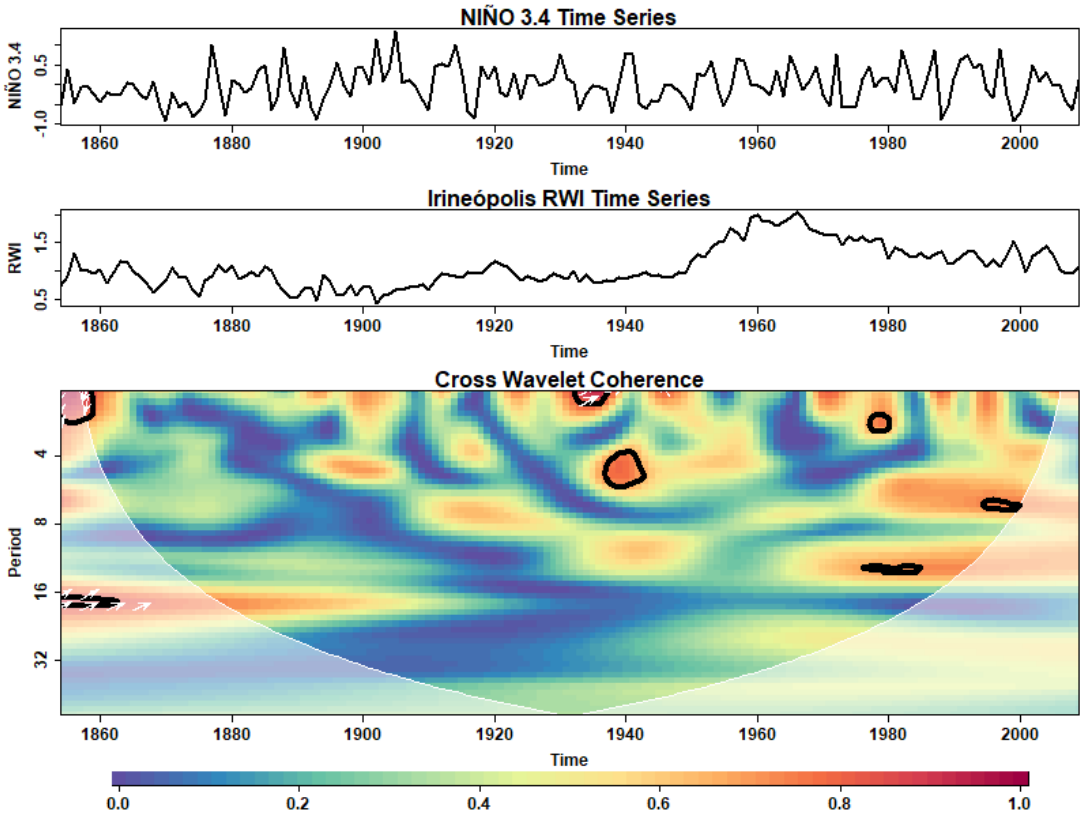
NIÑO 3.4 Time Series
NIÑO 3.4
0.5
-1.0
1860
1880
1900
1920
1940
1960
1980
2000
Time
Irineópolis RWI Time Series
RWI
1.5
0.5
1860
1880
1900
1920
1940
1960
1980
2000
Time
Cross Wavelet Coherence
Period
4
8
16
32
1860
1880
1900
1920
1940
1960
1980
2000
Time
0.0
0.2
0.4
0.6
0.8
1.0

(c)

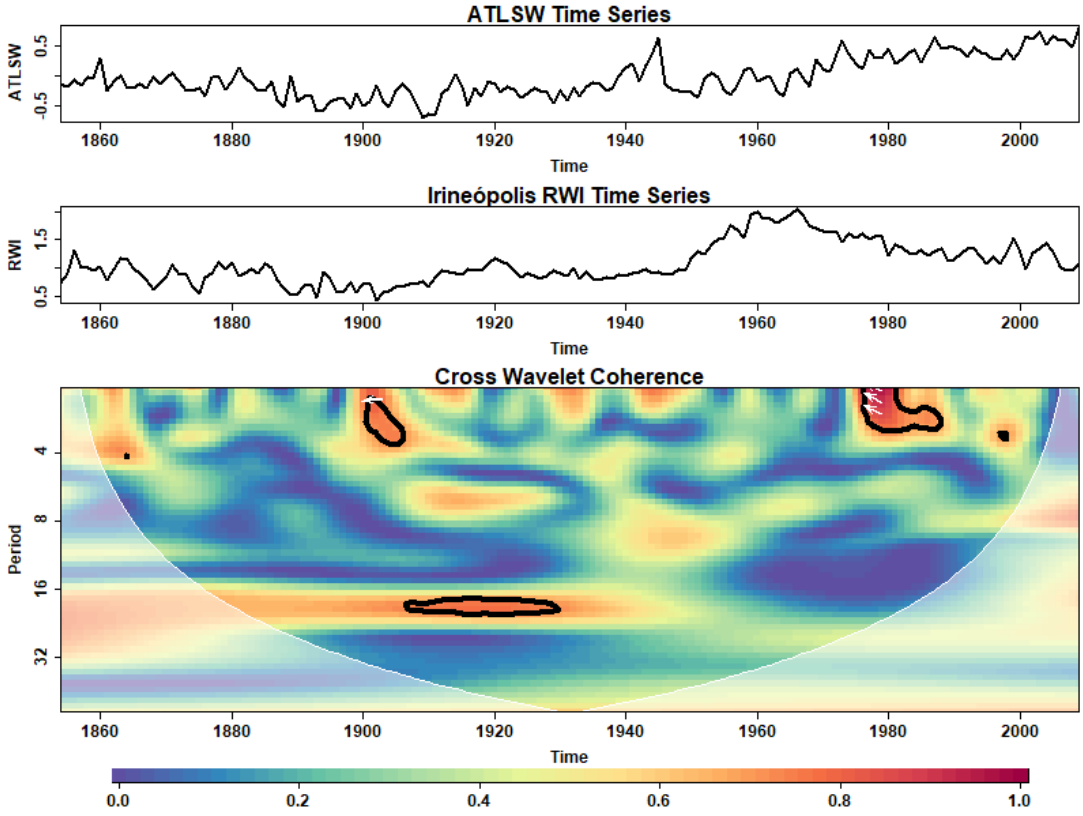
ATLSW Time Series
ATLSW
0.5
-0.5
1860
1880
1900
1920
1940
1960
1980
2000
Time
Irineópolis RWI Time Series
RWI
1.5
0.5
1860
1880
1900
1920
1940
1960
1980
2000
Time
Cross Wavelet Coherence
Period
4
8
16
32
1860
1880
1900
1920
1940
1960
1980
2000
Time
0.0
0.2
0.4
0.6
0.8
1.0

(d)

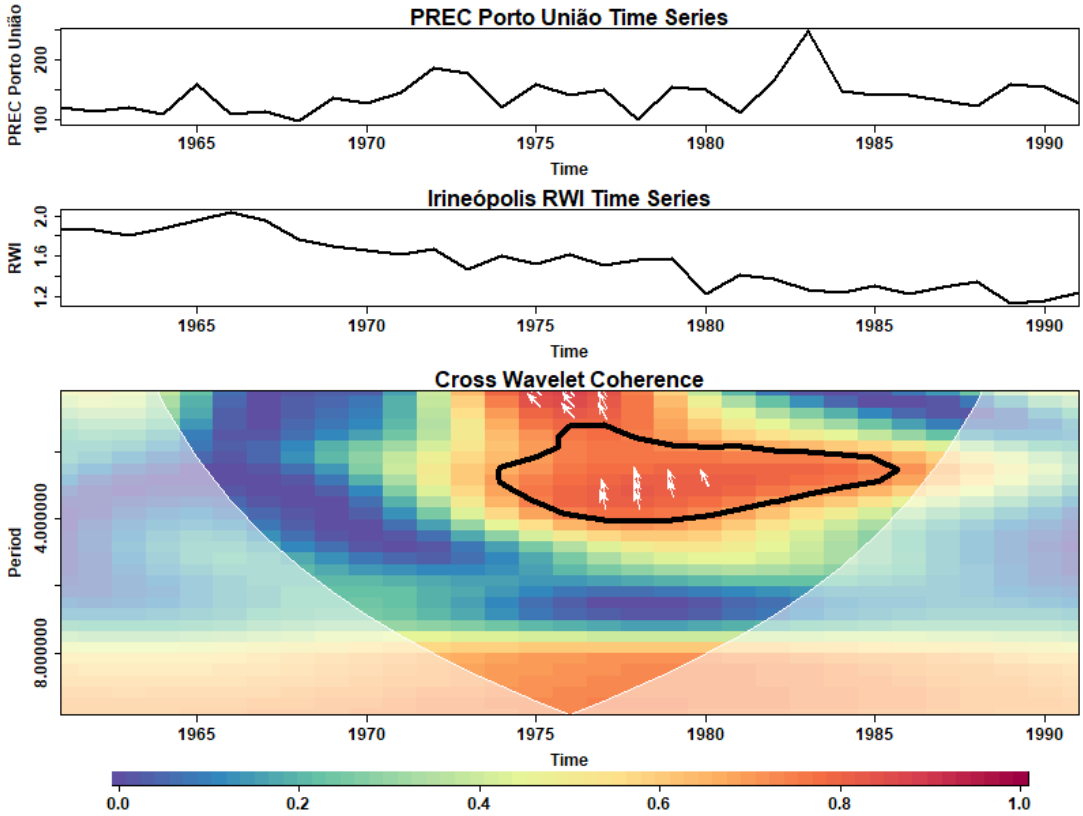
PREC Porto União Time Series
PREC Porto União
200
100
1965
1970
1975
1980
1985
1990
Time
Irineópolis RWI Time Series
RWI
2.0
1.6
1.2
1965
1970
1975
1980
1985
1990
Time
Cross Wavelet Coherence
Period
4.000000
8.000000
1965
1970
1975
1980
1985
1990
Time
0.0
0.2
0.4
0.6
0.8
1.0

(e)

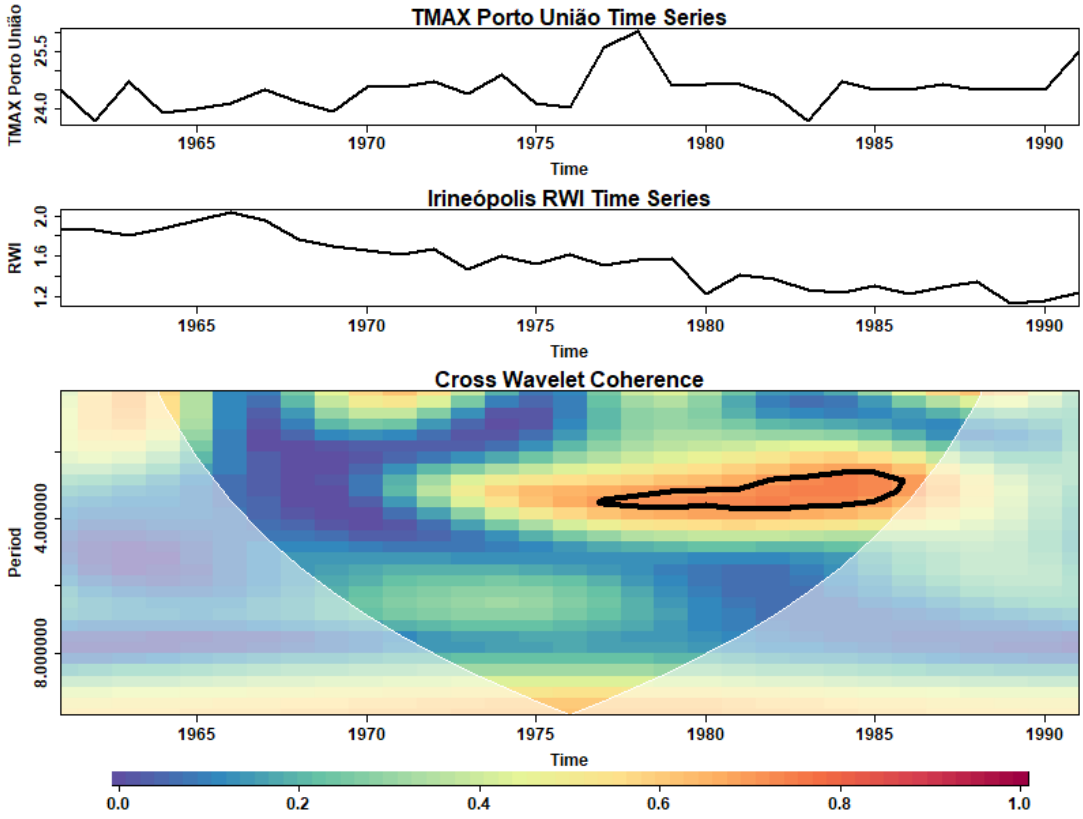
TMAX Porto União Time Series
TMAX Porto União
25.5
24.0
1965
1970
1975
1980
1985
1990
Time
Irineópolis RWI Time Series
RWI
2.0
1.6
1.2
1965
1970
1975
1980
1985
1990
Time
Cross Wavelet Coherence
Period
4.000000
8.000000
1965
1970
1975
1980
1985
1990
Time
0.0
0.2
0.4
0.6
0.8
1.0

(f)

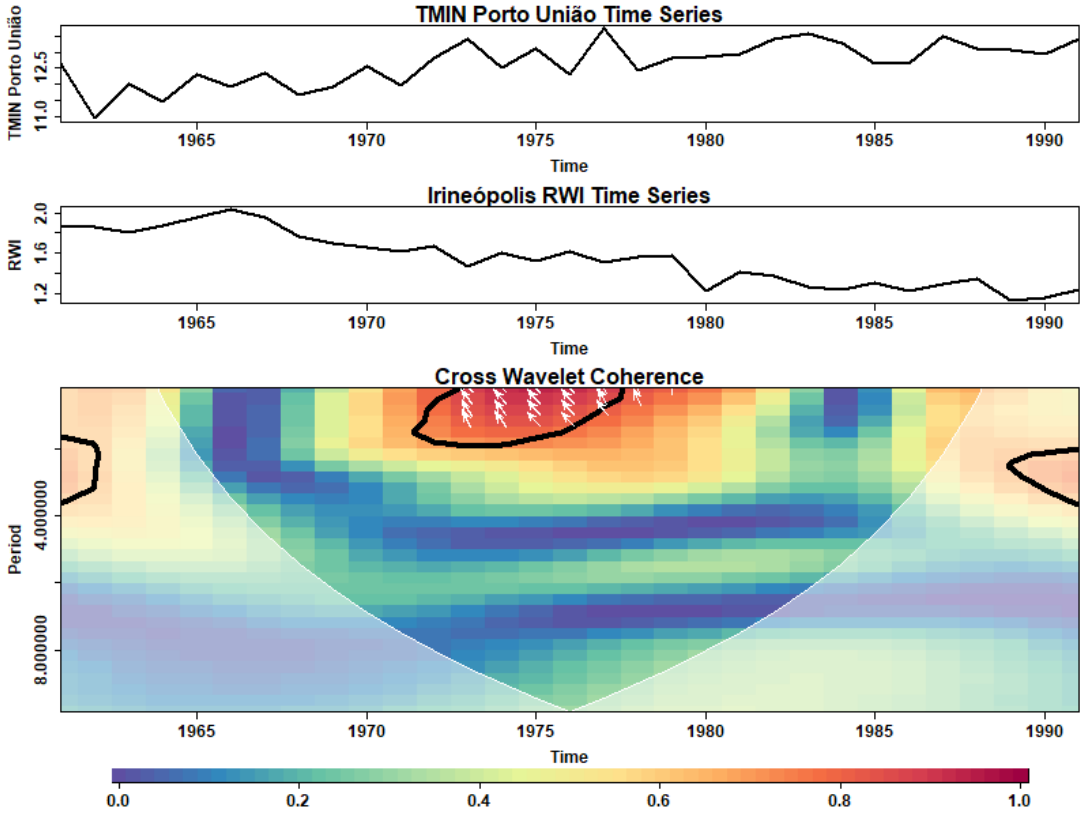
TMIN Porto União Time Series
TMIN Porto União
12.5
11.0
1965
1970
1975
1980
1985
1990
Time
Irineópolis RWI Time Series
RWI
2.0
1.6
1.2
1965
1970
1975
1980
1985
1990
Time
Cross Wavelet Coherence
Period
4.000000
8.000000
1965
1970
1975
1980
1985
1990
Time
0.0
0.2
0.4
0.6
0.8
1.0

(g)

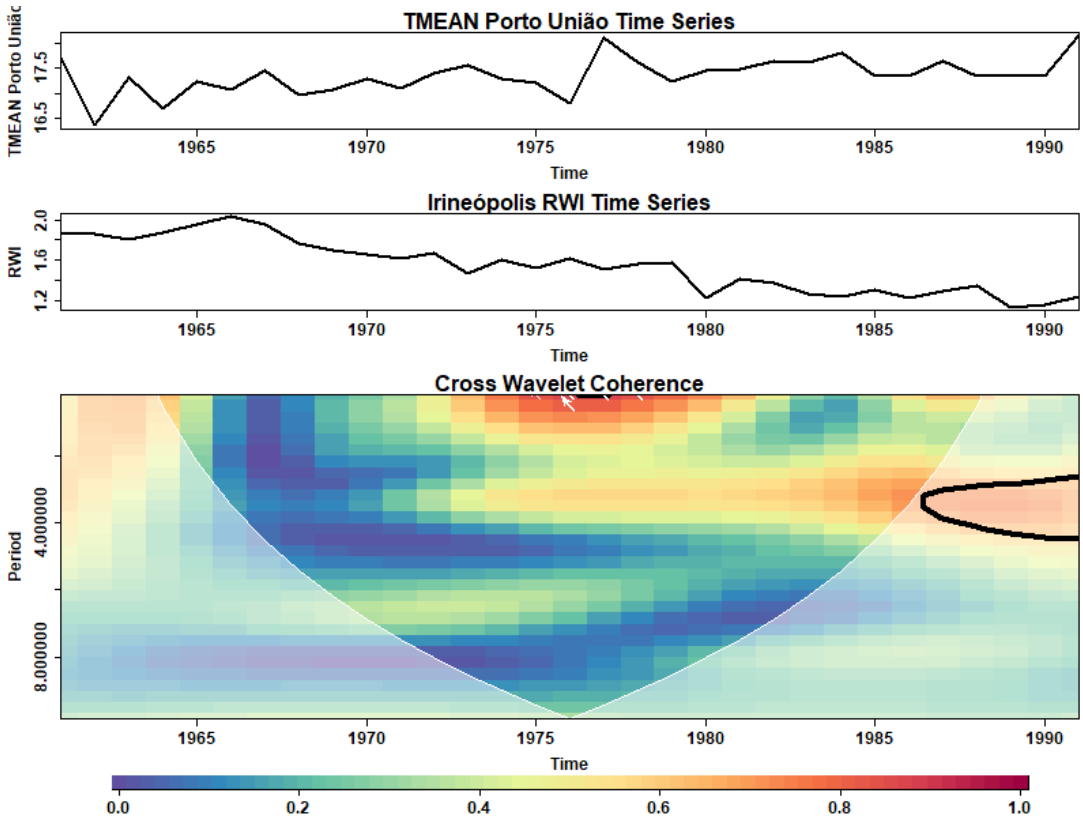

(h)
Source: The author.

Figure 67: Cross Wavelet Coherence (WTC) Analysis between Passo Fundo Ring Width Index (RWI) and Ocean-Atmosphere/Solar Parameters. Panels (a) to (h) display the WTC results between Passo Fundo RWI and the Southern Oscillation Index (SOI), El Niño 3.4 Index (NIÑO 3.4), Sunspot Activity (SUNSPOT), Atlantic Sea Surface Temperature (ATLSW), Precipitation (PREC), Mean Temperature (TMEAN), Maximum Temperature (TMAX), and Minimum Temperature (TMIN), respectively. The contours in black indicate regions of high coherence with a significance level > 0.95, unveiling potential associations and time-frequency relationships. The white arrows demonstrate the phase angle and direction of the relationship between the RWI and each parameter. Rightward-pointing arrows signify an "in-phase" relationship, indicating that both the RWI and the parameter share similar variations at specific time-frequency intervals. Contrary, leftward-pointing arrows indicate an "anti-phase" relationship, where the RWI and the parameter exhibit opposite variations at certain time-frequency regions.

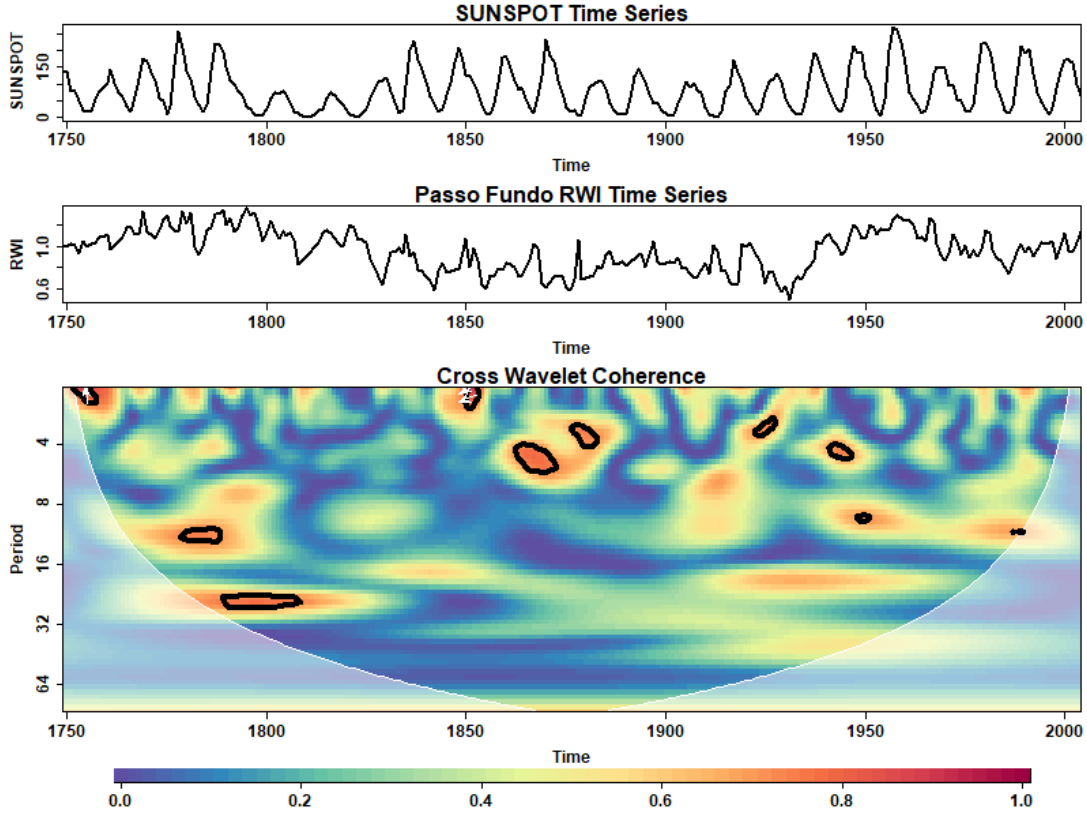

(a)

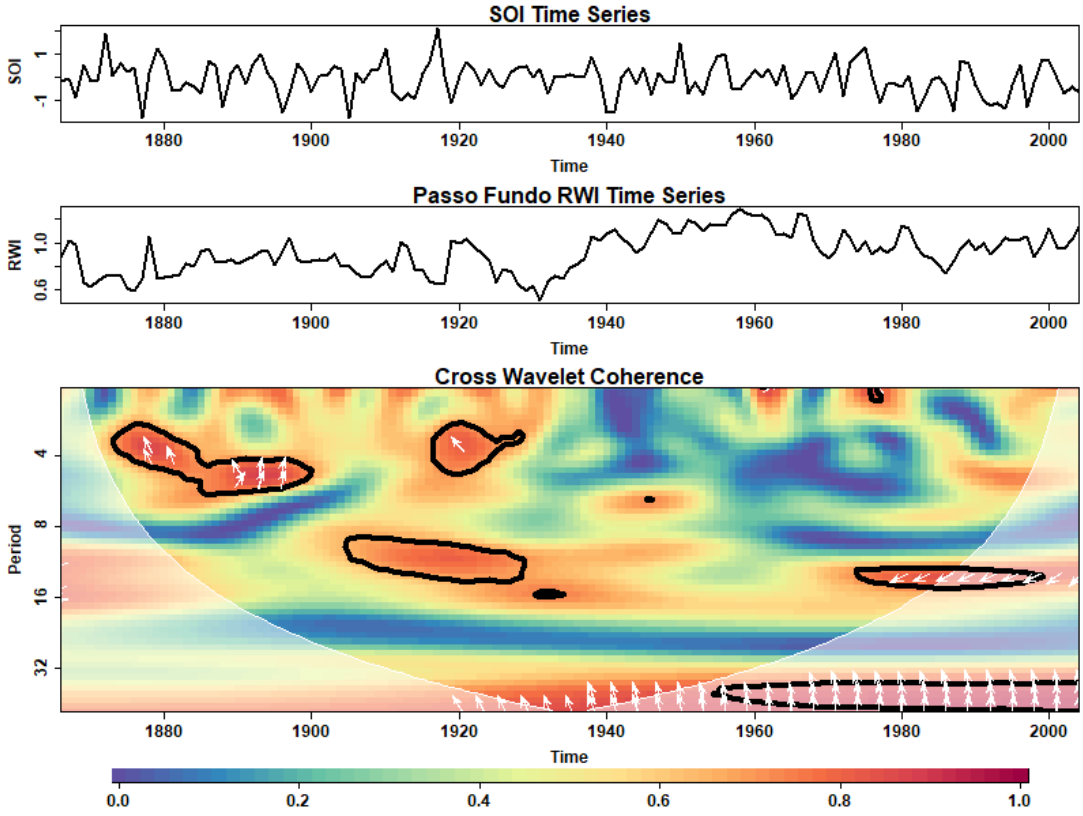
SOI Time Series
SOI
1
-1
1880
1900
1920
1940
1960
1980
2000
Time
Passo Fundo RWI Time Series
RWI
1.0
0.6
1880
1900
1920
1940
1960
1980
2000
Time
Cross Wavelet Coherence
Period
4
8
16
32
1880
1900
1920
1940
1960
1980
2000
Time
0.0
0.2
0.4
0.6
0.8
1.0

(b)

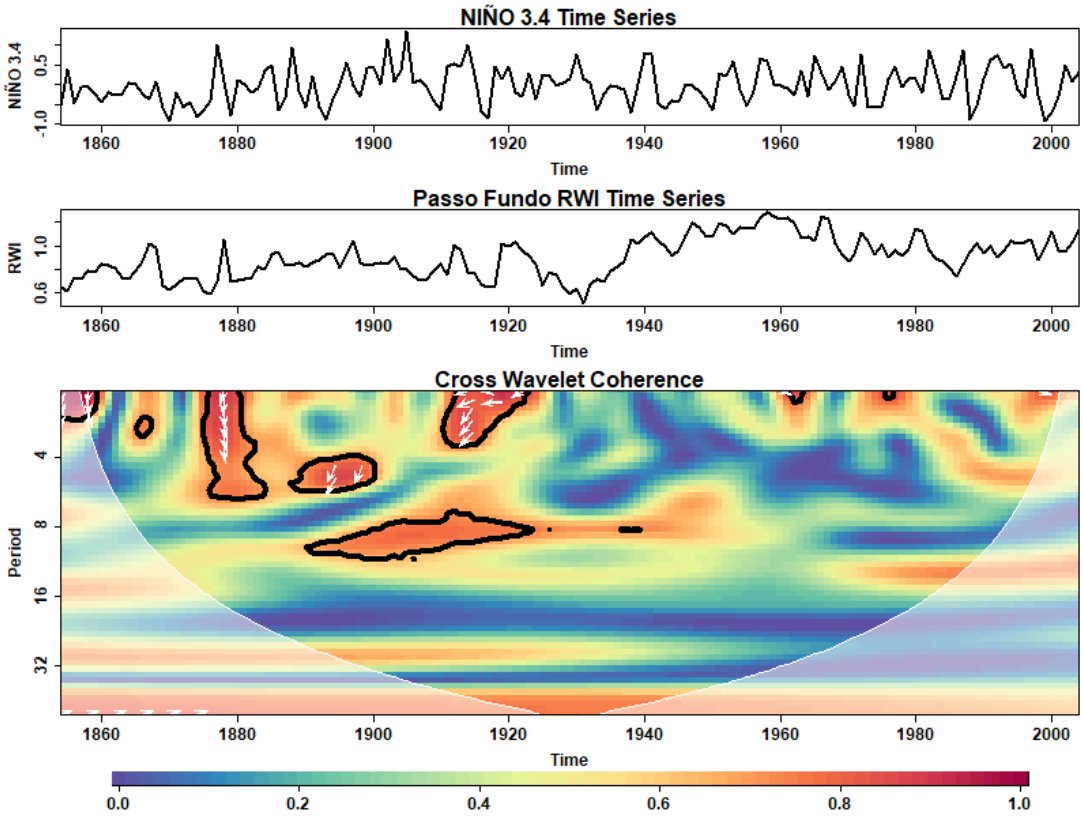
NIÑO 3.4 Time Series
NIÑO 3.4
0.5
-1.0
1860
1880
1900
1920
1940
1960
1980
2000
Time
Passo Fundo RWI Time Series
RWI
1.0
0.6
1860
1880
1900
1920
1940
1960
1980
2000
Time
Cross Wavelet Coherence
Period
4
8
16
32
1860
1880
1900
1920
1940
1960
1980
2000
Time
0.0
0.2
0.4
0.6
0.8
1.0

(c)

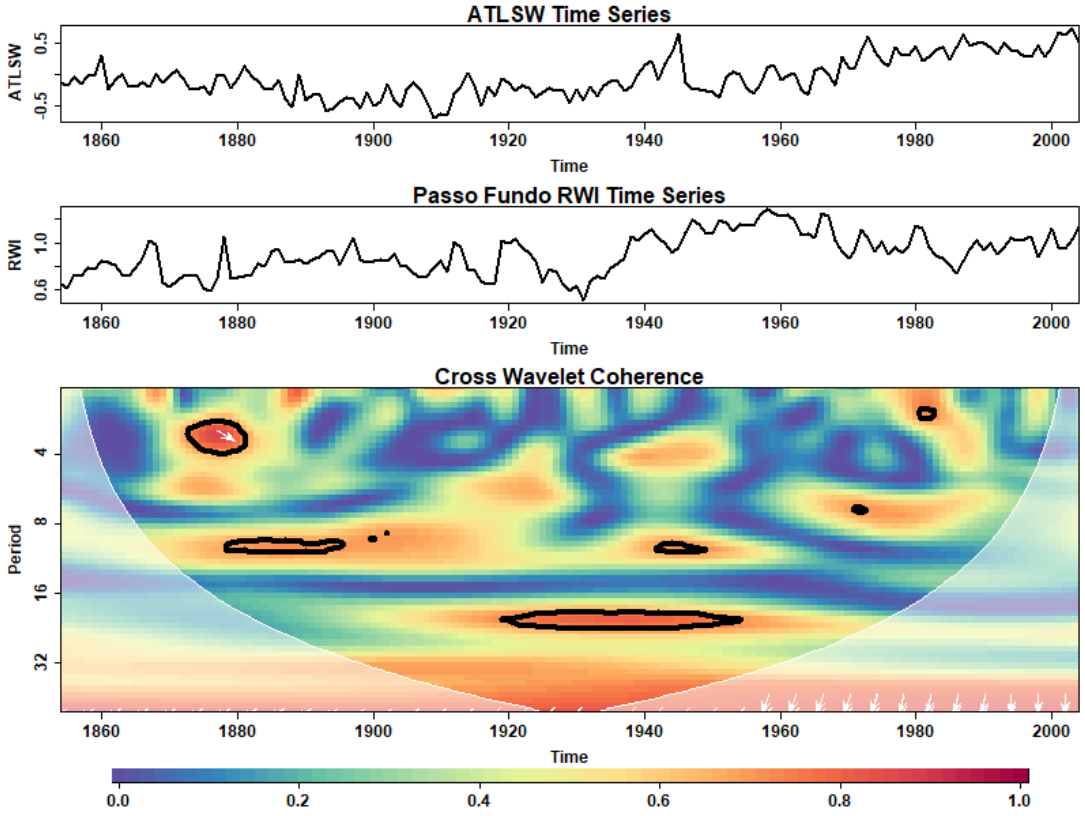
ATLSW Time Series
ATLSW
0.5
-0.5
1860
1880
1900
1920
1940
1960
1980
2000
Time
Passo Fundo RWI Time Series
RWI
1.0
0.6
1860
1880
1900
1920
1940
1960
1980
2000
Time
Cross Wavelet Coherence
Period
4
8
16
32
1860
1880
1900
1920
1940
1960
1980
2000
Time
0.0
0.2
0.4
0.6
0.8
1.0

(d)

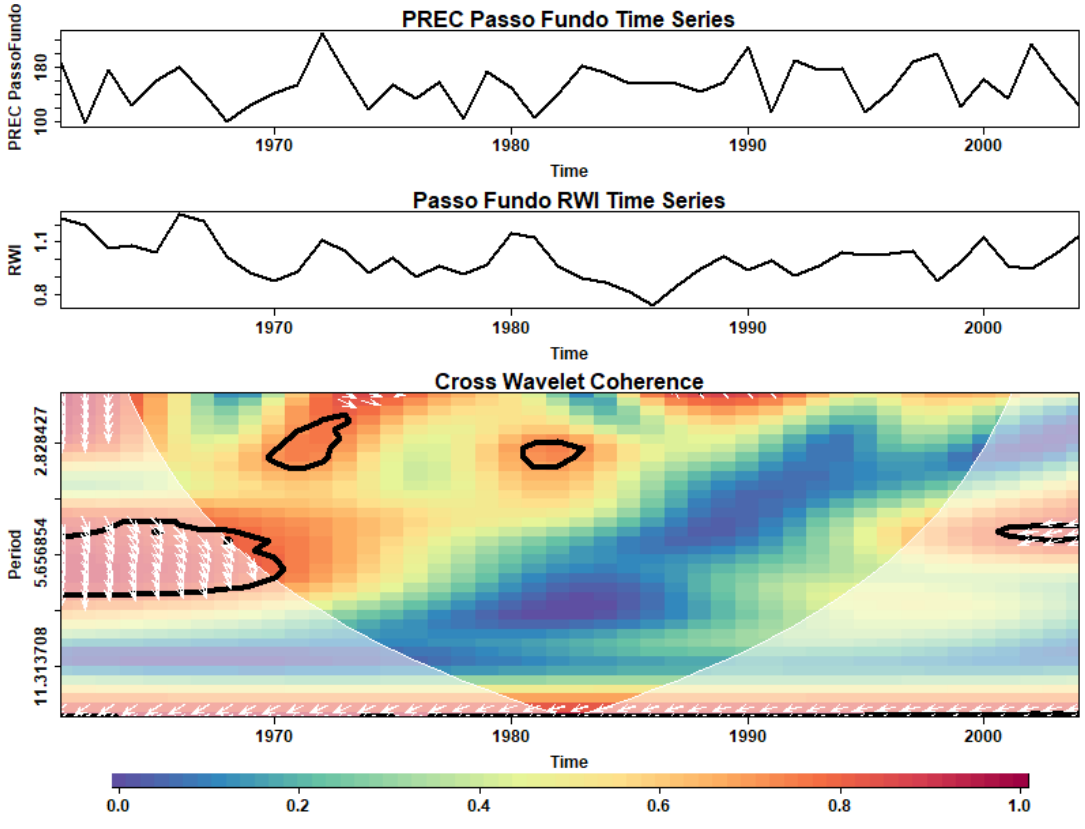
PREC Passo Fundo Time Series
PREC PassoFundo
180
100
1970
1980
1990
2000
Time
Passo Fundo RWI Time Series
RWI
1.1
0.8
1970
1980
1990
2000
Time
Cross Wavelet Coherence
Period
2.828427
5.656854
11.313708
1970
1980
1990
2000
Time
0.0
0.2
0.4
0.6
0.8
1.0

(e)

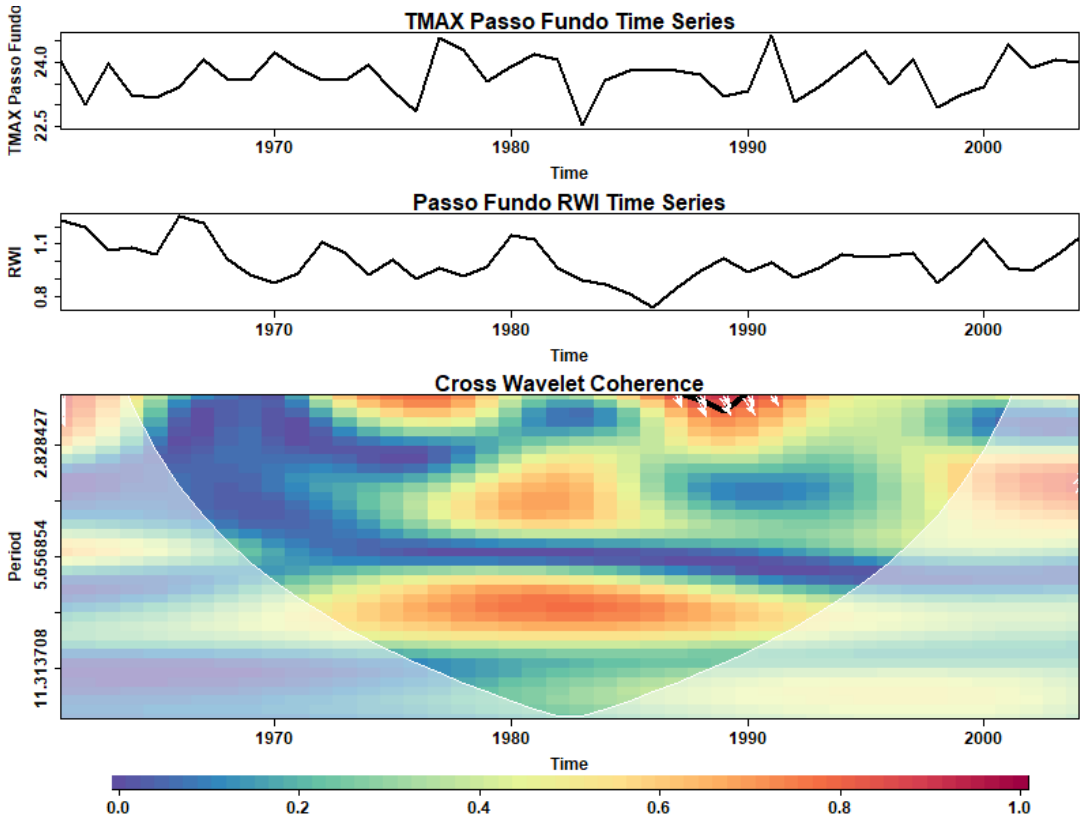
TMAX Passo Fundo Time Series
TMAX Passo Fundo
22.5
24.0
1970
1980
1990
2000
Time
Passo Fundo RWI Time Series
RWI
0.8
1.1
1970
1980
1990
2000
Time
Cross Wavelet Coherence
Period
2.828427
5.656854
11.313708
1970
1980
1990
2000
Time
0.0
0.2
0.4
0.6
0.8
1.0

(f)

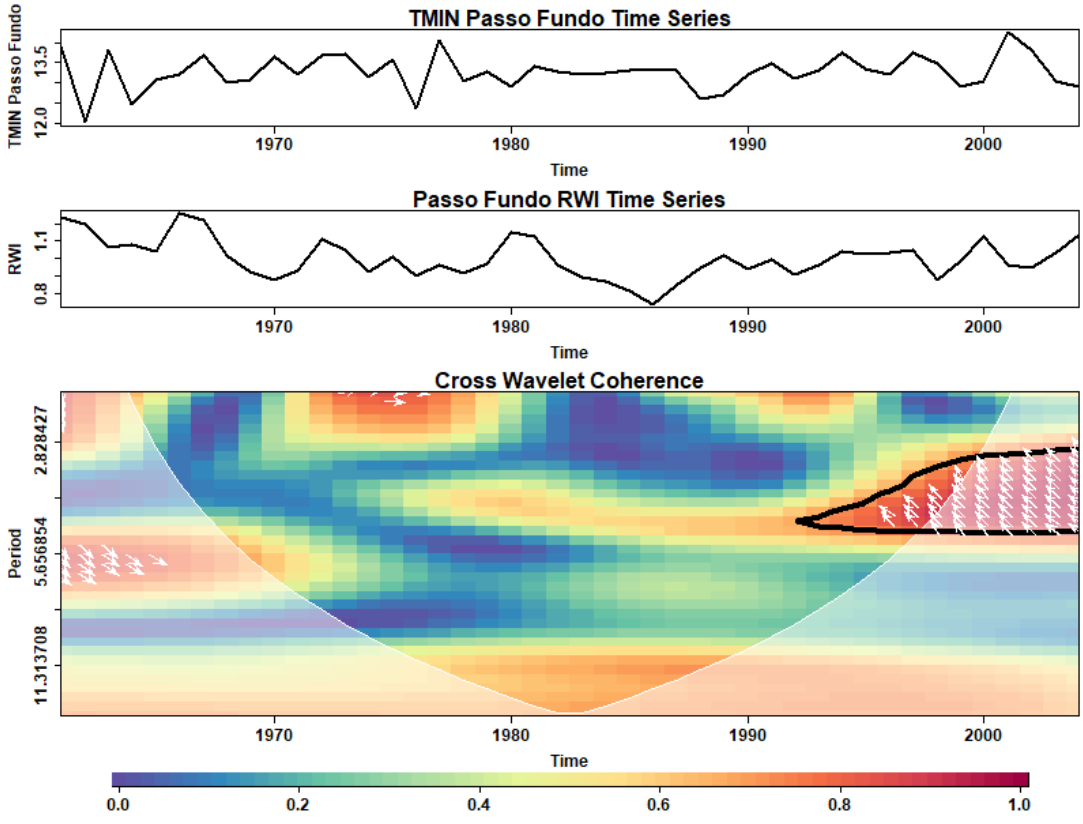
TMIN Passo Fundo Time Series
TMIN Passo Fundo
12.0
13.5
1970
1980
1990
2000
Time
Passo Fundo RWI Time Series
RWI
0.8
1.1
1970
1980
1990
2000
Time
Cross Wavelet Coherence
Period
2.828427
5.656854
11.313708
1970
1980
1990
2000
Time
0.0
0.2
0.4
0.6
0.8
1.0

(g)

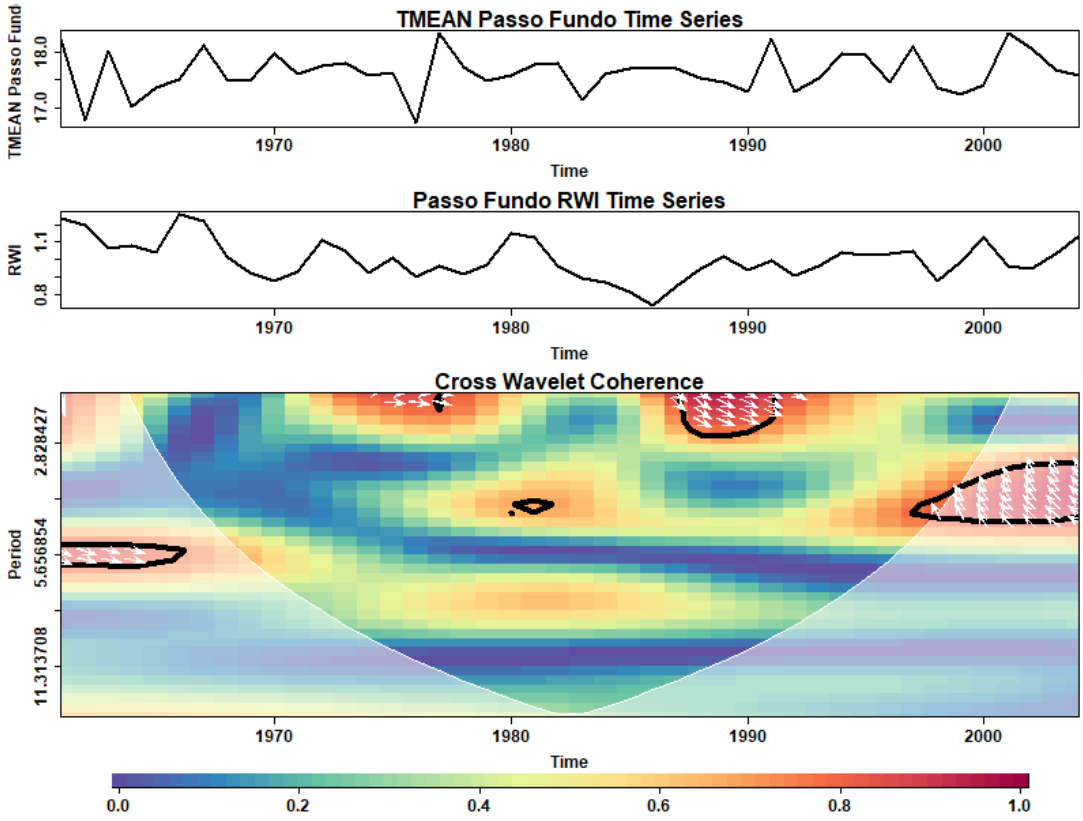

(h)
Source: The author.

Figure 68: Cross Wavelet Coherence (WTC) Analysis between São Francisco de Paula (SFP) Ring Width Index (RWI) and Ocean-Atmosphere/Solar Parameters. Panels (a) to (h) display the WTC results between (SFP) RWI and the Southern Oscillation Index (SOI), El Niño 3.4 Index (NIÑO 3.4), Sunspot Activity (SUNSPOT), Atlantic Sea Surface Temperature (ATLSW), Precipitation (PREC), Mean Temperature (TMEAN), Maximum Temperature (TMAX), and Minimum Temperature (TMIN), respectively. The contours in black indicate regions of high coherence with a significance level > 0.95, unveiling potential associations and time-frequency relationships. The white arrows demonstrate the phase angle and direction of the relationship between the RWI and each parameter. Rightward-pointing arrows signify an "in-phase" relationship, indicating that both the RWI and the parameter share similar variations at specific time-frequency intervals. Contrary, leftward-pointing arrows indicate an "anti-phase" relationship, where the RWI and the parameter exhibit opposite variations at certain time-frequency regions.

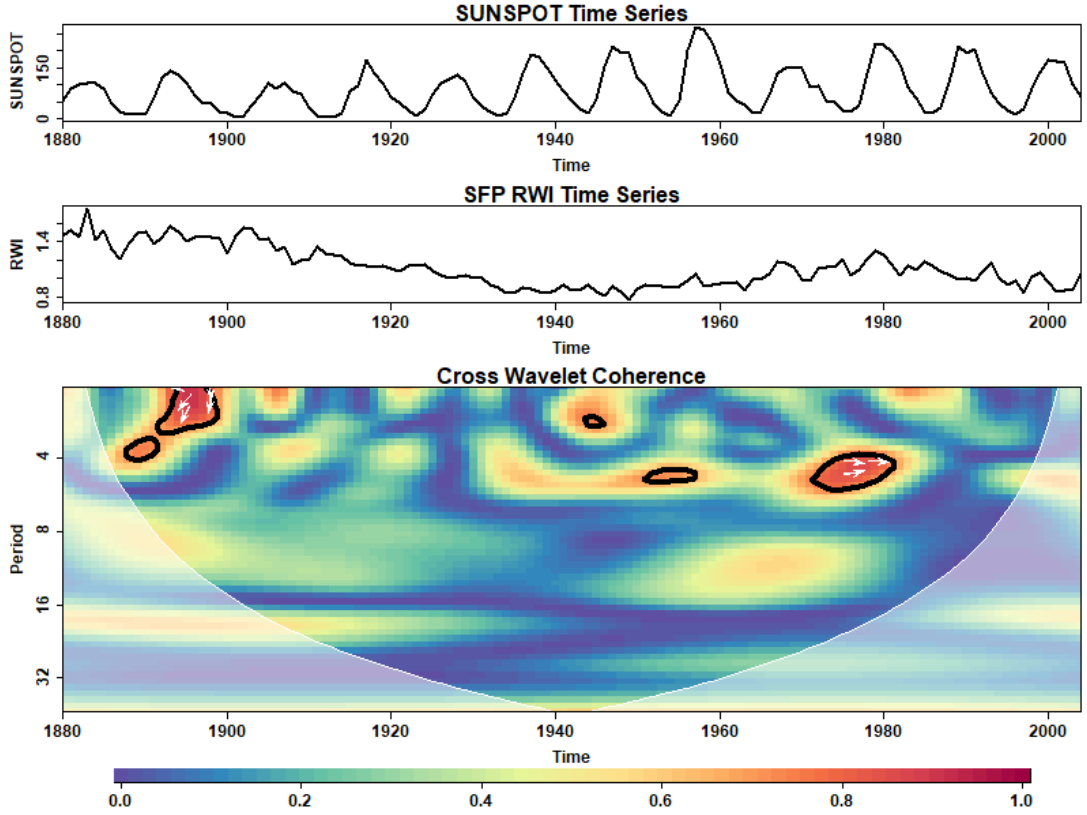

(a)

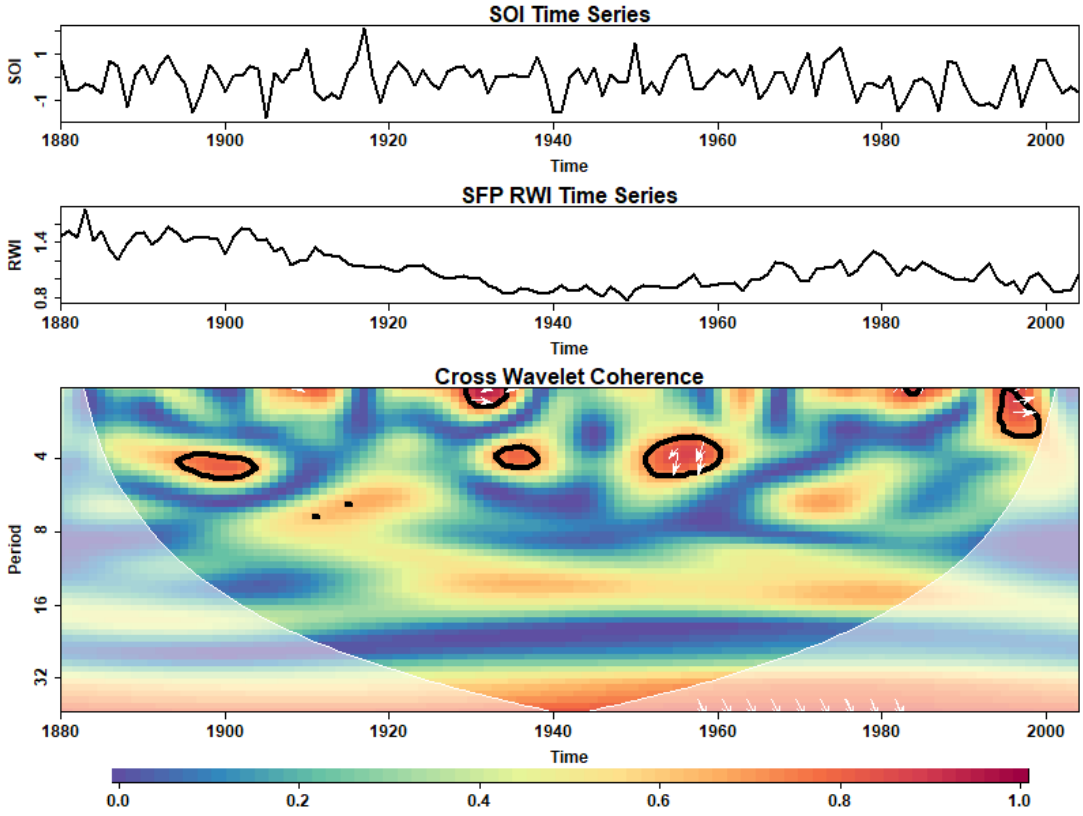
SOI Time Series
SOI
1
-1
1880
1900
1920
1940
1960
1980
2000
Time
SFP RWI Time Series
RWI
1.4
0.8
1880
1900
1920
1940
1960
1980
2000
Time
Cross Wavelet Coherence
Period
4
8
16
32
1880
1900
1920
1940
1960
1980
2000
Time
0.0
0.2
0.4
0.6
0.8
1.0

(b)

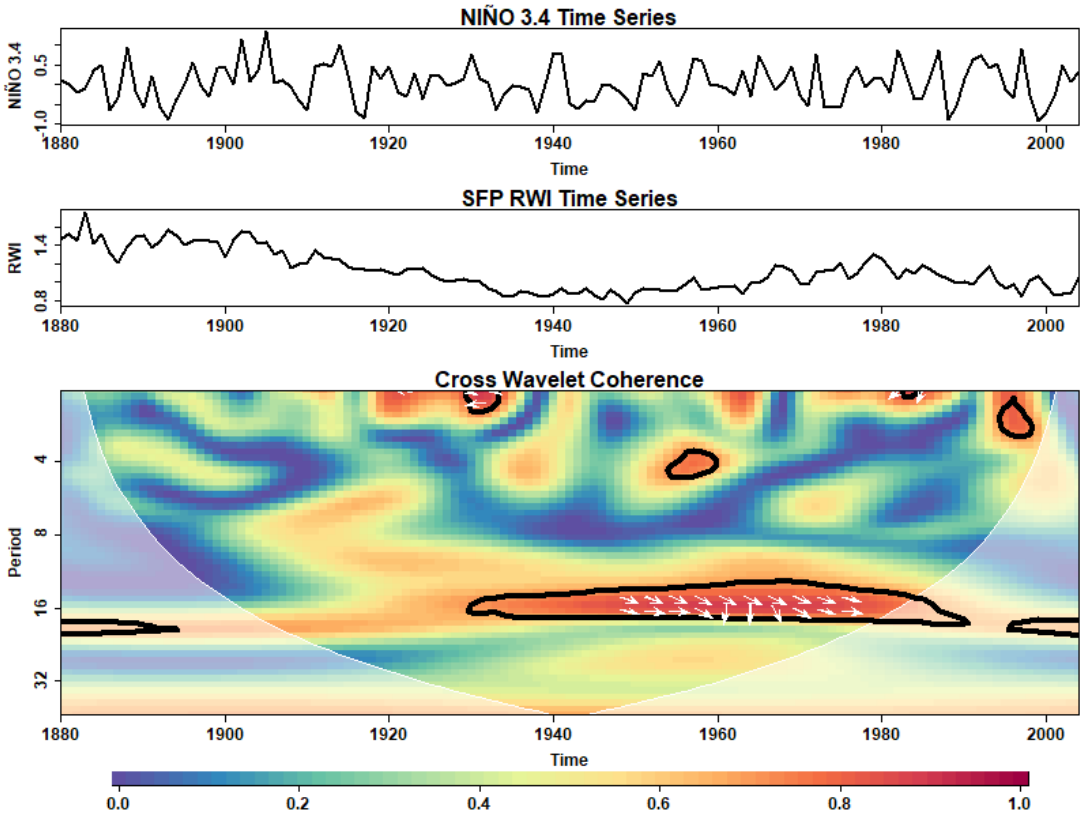
NIÑO 3.4 Time Series
NIÑO 3.4
0.5
-1.0
1880
1900
1920
1940
1960
1980
2000
Time
SFP RWI Time Series
RWI
1.4
0.8
1880
1900
1920
1940
1960
1980
2000
Time
Cross Wavelet Coherence
Period
4
8
16
32
1880
1900
1920
1940
1960
1980
2000
Time
0.0
0.2
0.4
0.6
0.8
1.0

(c)

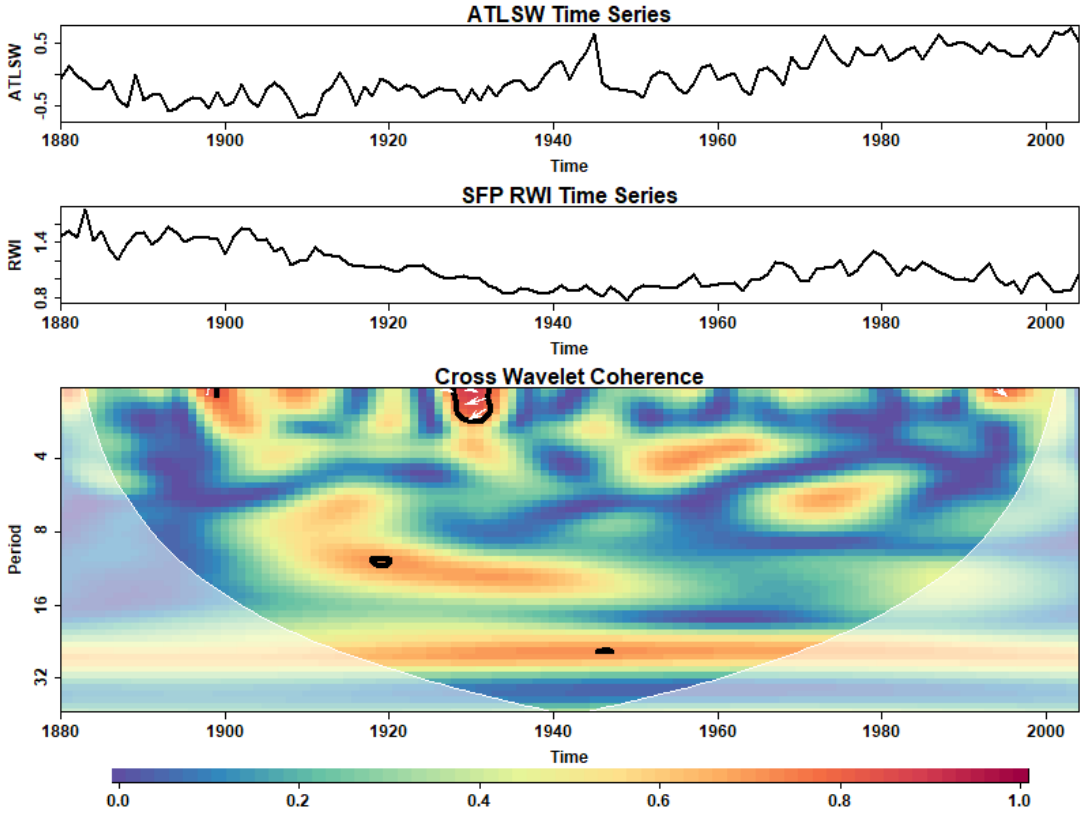
ATLSW Time Series
ATLSW
0.5
-0.5
1880
1900
1920
1940
1960
1980
2000
Time
SFP RWI Time Series
RWI
1.4
0.8
1880
1900
1920
1940
1960
1980
2000
Time
Cross Wavelet Coherence
Period
4
8
16
32
1880
1900
1920
1940
1960
1980
2000
Time
0.0
0.2
0.4
0.6
0.8
1.0

(d)

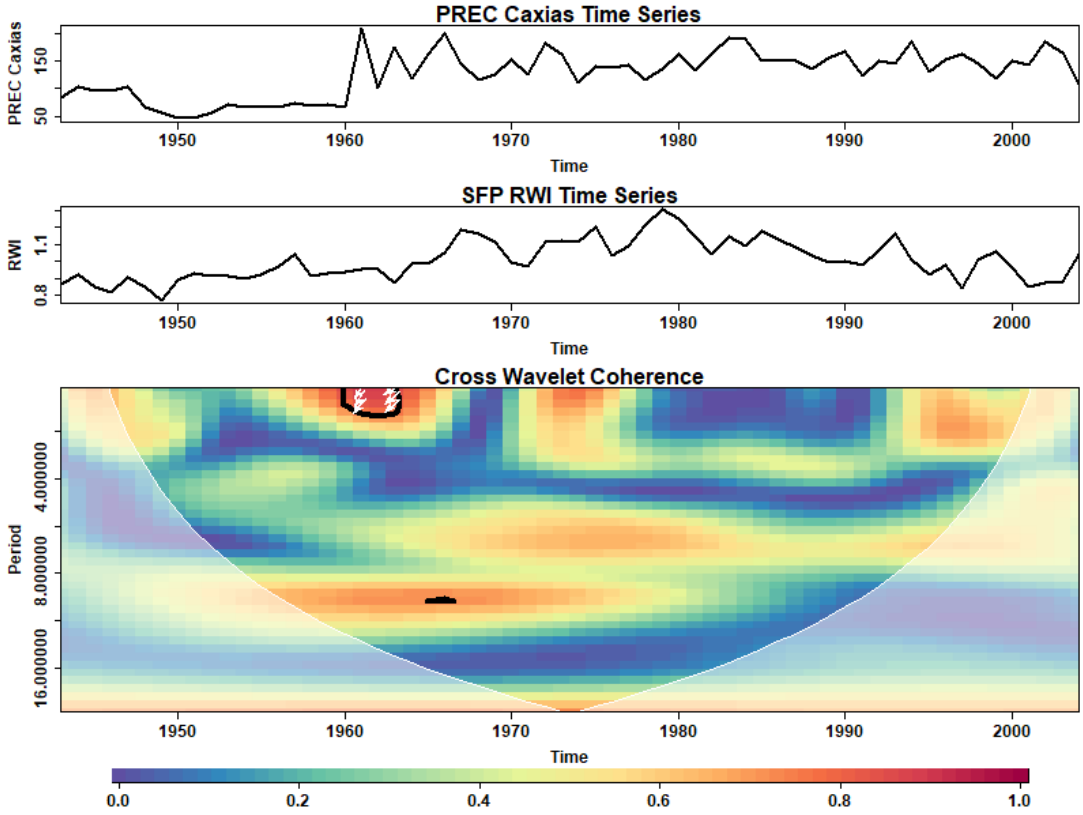
PREC Caxias Time Series
PREC Caxias
150
50
1950
1960
1970
1980
1990
2000
Time
SFP RWI Time Series
RWI
1.1
0.8
1950
1960
1970
1980
1990
2000
Time
Cross Wavelet Coherence
Period
4.000000
8.000000
16.000000
1950
1960
1970
1980
1990
2000
Time
0.0
0.2
0.4
0.6
0.8
1.0

(e)

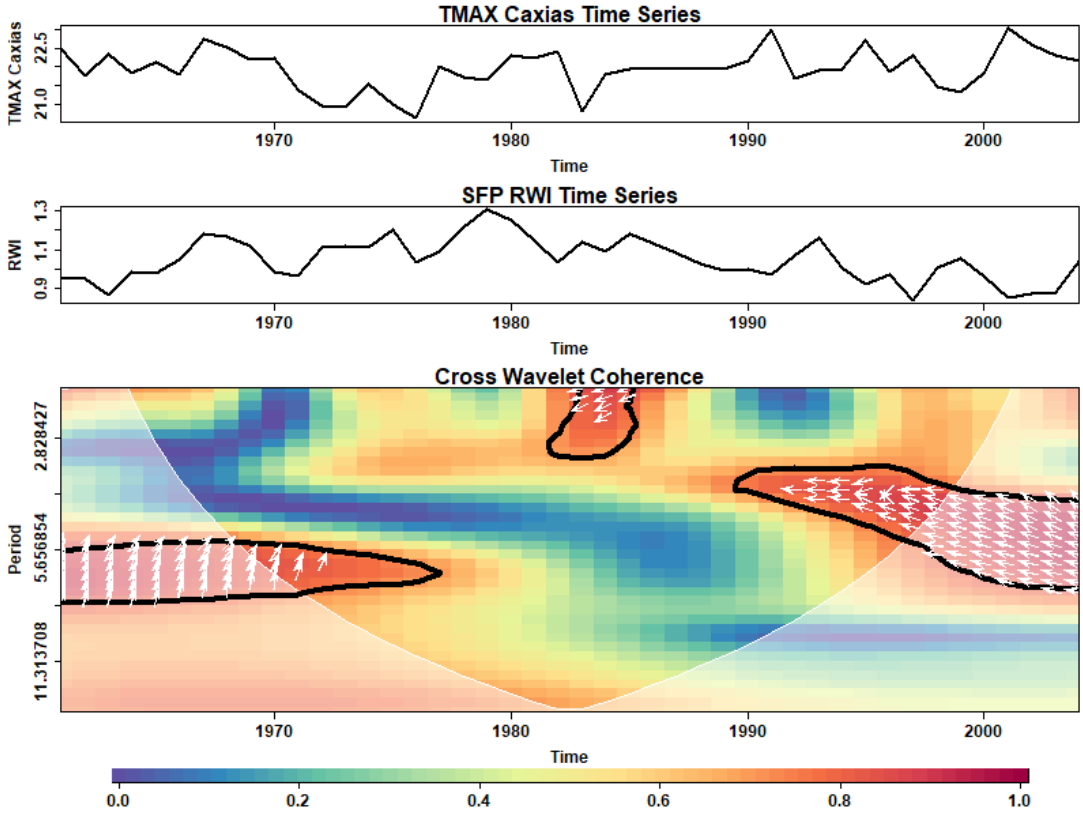
TMAX Caxias Time Series
TMAX Caxias
22.5
21.0
1970
1980
1990
2000
Time
SFP RWI Time Series
RWI
1.3
1.1
0.9
1970
1980
1990
2000
Time
Cross Wavelet Coherence
Period
2.828427
5.656854
11.313708
1970
1980
1990
2000
Time
0.0
0.2
0.4
0.6
0.8
1.0

(f)

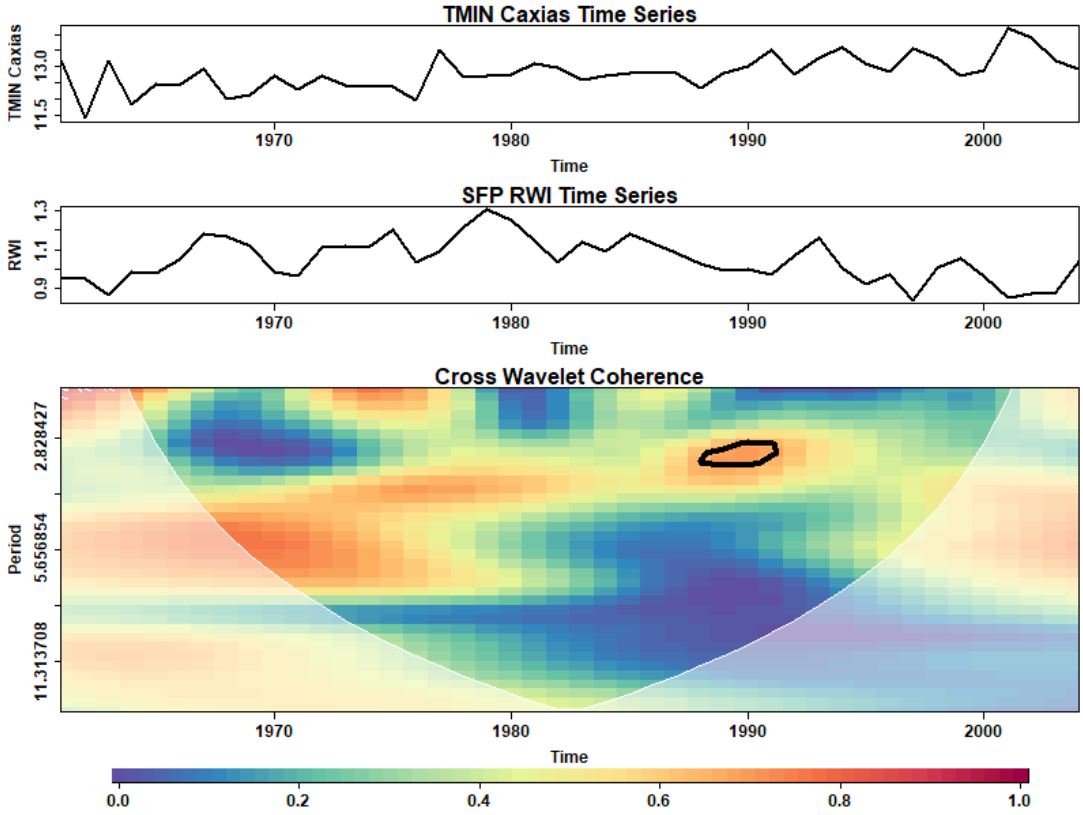
TMIN Caxias Time Series
TMIN Caxias
13.0
11.5
1970
1980
1990
2000
Time
SFP RWI Time Series
RWI
1.3
1.1
0.9
1970
1980
1990
2000
Time
Cross Wavelet Coherence
Period
2.828427
5.656854
11.313708
1970
1980
1990
2000
Time
0.0
0.2
0.4
0.6
0.8
1.0

(g)

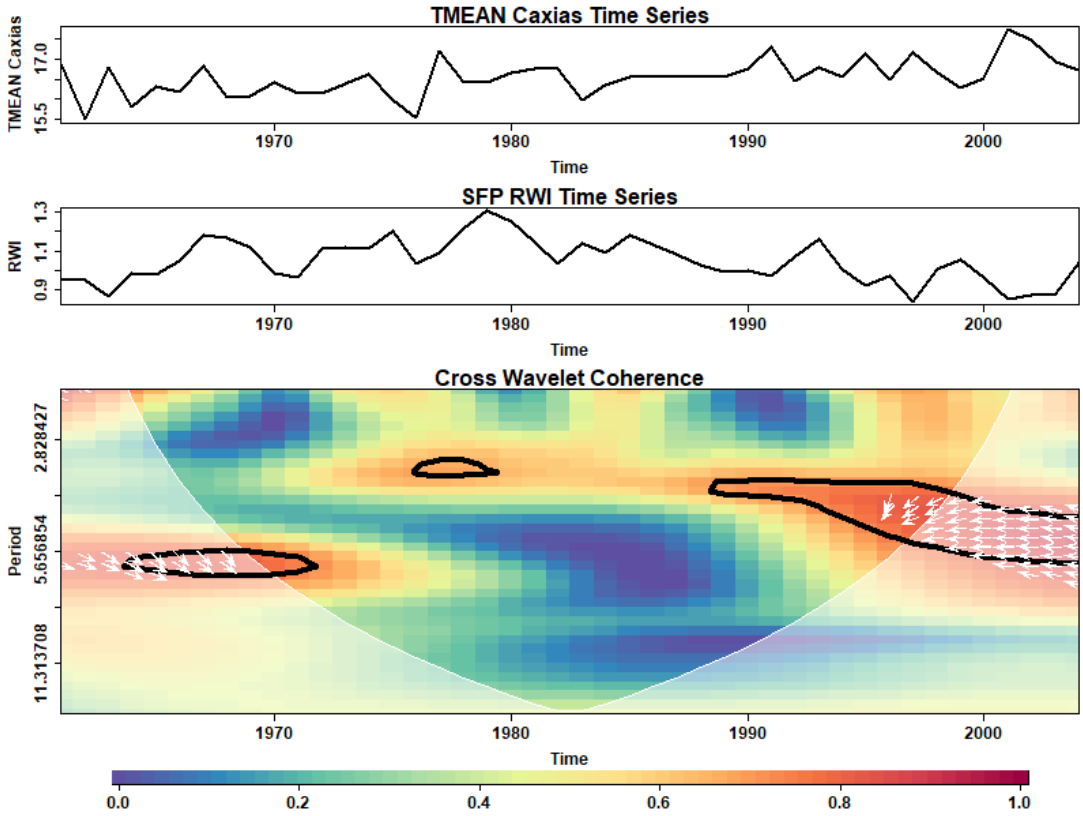

(h)
Source: The author.

APPENDIX D – PAPERS PUBLISHED DURING THE PH.D.

The following papers are directly related to this thesis. Other papers were published during the Ph.D. and can be found at Daniela Muraja Research Gate

Theoretical and Applied Climatology
https://doi.org/10.1007/s00704-023-04456-7

RESEARCH

Ocean–atmosphere interaction identified in tree-ring time series from southern Brazil using cross-wavelet analysis

Daniela Oliveira Silva Muraja[1] · Virginia Klausner[1] · Alan Prestes[1] · Iuri Rojahn da Silva[1]

Received: 19 April 2022 / Accepted: 5 April 2023

Abstract
Tropical dendrochronology has gained significant attention in recent years, particularly with the dendrochronological study of new species that produce annual growth rings and are responsive to environmental changes. Despite the progress, the extent to which ocean–atmosphere interactions influence regional climate and, consequently, tree growth, is not fully understood. Among the new species, *Ocotea porosa (Nees & Mart.) Barroso* (also known as *Imbuia*) has shown excellent potential for climate research. This study investigates the climatic and solar influences on a chronology of 41 *Imbuia* tree samples. Pearson's correlation was used alongside Wavelet transform to evaluate periodicities between the tree-ring chronology and climatic parameters such as the southern-oscillation index (SOI), annual precipitation, *El Niño* 3.4 (PACE), and the South Atlantic Index (ATLS). Our analysis revealed evidence of the influence of the *El Niño* Southern Oscillation (SOI) on rainfall variability in the region, the Hale and Gleissberg solar cycles causing precipitation variation, likely due to the influence of the Atlantic Ocean, and the Brückner-Egeson-Lockyer climatic cycle, which is correlated with sunspot activity. Furthermore, our wavelet analysis identified possible connections to the Eastern Pacific-type *El Niño* events during five specific periods: 1911–1912, 1918–1919, 1976–1977, 1982–1983, and 1986–1987. The results indicate that southern Brazil is affected by several climatic and geophysical parameters from both the Atlantic and Pacific oceans, which directly affect the growth of *Imbuia* trees as their tree-ring series display sensitivity to these parameters.

1 Introduction

The Brazilian territory is influenced by both the Atlantic and Pacific oceans, which interact with the lower atmosphere in different ways. These include 1) the winds above the sea surface, which are responsible for cooling the sea surface and balancing the heat flux, and are the main mechanisms that generate ocean circulation; 2) the evaporation from the ocean mixing across the marine atmospheric boundary layer, and subsequently transporting moisture to the troposphere; and 3) the atmospheric circulation driven by water vapor resulting from evaporation from the ocean, which releases latent heat associated with condensation of the vapor to form clouds and precipitation (Chelton and Xie 2010).

This interaction between the oceans and the lower atmosphere can result in climatic phenomena such as the *El Ninõ* Southern Oscillation (ENSO). The ENSO is associated with changes in the Sea Surface Temperature (SST) patterns and trade winds in the Equatorial Pacific region. It is defined as positive (*El Ninõ*) and negative (*La Ninã*) anomalies (Sampaio 2000), affecting South America (Garreaud et al 2009; Rigozo et al 2012), and specifically, Southern Brazil. In Southern Brazil, the *El Ninõ* events coincide with a higher frequency of heavy rains, and the *La Ninã* events correspond to severe droughts. Floods and severe droughts can cause problems with tree growth performance. Tree growth is highly dependent on the rainfall amounts in the most humid sector during the dry season, whereas in sites settled in areas of lower summer temperatures, the rainfall during the warm-rainy season is the main determining factor

Virginia Klausner, Alan Prestes and Iuri Rojahn da Silva contributed equally to this work.

Daniela Oliveira Silva Muraja
fys.dani@gmail.com

Virginia Klausner
viklausner@gmail.com

Alan Prestes
aprestes@gmail.com

Iuri Rojahn da Silva
iuri@univap.br

[1] Physics and Astronomy Department, University of Vale do Paraíba, Shishima Hifumi avenue, São José dos Campos 2911, São Paulo, Brazil

Published online: 18 June 2023

influencing tree-growth dynamics (Nordemann et al 2002; Venegas-González et al 2018).

The regional climate system is of paramount importance to the economy, particularly for services that depend directly on the climate, such as natural resource management and agriculture. Understanding environmental changes are also critical. Studies focused on agriculture illustrate the importance of analyzing climatic phenomena. For instance, Junior and Sentelhas (2019) found that soybean and corn crops in the Brazilian north region are negatively affected by the ENSO, while the same products in the Center-South region can be positively benefited. In 1982–1983, the intense rains caused floods in more than 400 municipalities in Paraná, Santa Catarina states, and Rio Grande do Sul state (Gasquez and Magalhães 1987). These climatic disasters are examples of ENSO consequences. During those years, the ENSO exhibited the widest range of extremes compared to any other similar period in the 20th century.

As discussed by Haigh (2007), the Sun exerts influence on various climate "modes of variability", for instance, the cycles of 11, 22, and 90 years found in climatic data are assumed to be associated with the solar variability (Currie 1974; Lassen and Friis-christensen 1995; Lean and Rind 1999; Hathaway 2010). To study climate variability and perform climate predictions, the understanding of oceanic and atmospheric circulation is fundamental, as they are interconnected. However, there is a lot of debate about whether the solar effect significantly contributes to global warming or not Scafetta (2009).

The solar activity presents several sub-intervals, including the Schwabe cycle, which corresponds to a period bandwidth of 8–13 years, the cycle of approximately 11 years related to the variability in sunspot numbers, and the Hale cycle of 17–26 years, which is related to the magnetic solar cycle of 22 years. The long-term variations in solar activity, which last 70–90 years, are called the Gleissberg cycle and can significantly affect terrestrial phenomena (Kivelson and Russell 1995; Hoyt and Schatten 1997; Ma 2009). The Gleissberg cycle can be directly linked to sunspot formation, and it is intrinsically related to features of the Schwabe cycle (Peristykh and Damon 2003). The 50- and 2- to 2.5-year cycles are possibly associated with the influences of the Gleissberg solar activity cycle and the interannual oscillations of land-atmospheric-ocean systems, respectively, as discussed by Zhang et al (2020). The cycles of approximately 18 years (Saros lunar cycle) and approximately 30 to 35 years (Brückner-Egeson-Lockyer climatic cycle) may be a combination of the Gleissberg and Hale cycles, as a result of the nonlinear effects of solar activity on the terrestrial environment (Solanki and Fligge 1998; Prestes et al 2018).

On the other hand, Scafetta (2010) investigated cycles with periods of 10–11, 12, 15, 20–22, 30, and 60 years using surface temperature records since 1850 and showed that these cycles could be easily linked to the orbits of Jupiter and Saturn. Additionally, the 9.1- and 18.6-year cycles were synchronized with the Moon's orbital cycles. While the idea that planetary motions might affect climate is intriguing, it remains controversial, and some scientists are skeptical of these claims. Nonetheless, the study of these long-term cycles can provide important insights into the natural variability of the climate system and may help to improve our understanding of the complex interactions between the Earth, the Sun, and the planets.

Dendrochronology is a widely used scientific technique that examines and dates events recorded in tree rings over the tree's lifetime (Speer 1971). The technique of cross-dating was introduced by Andrew E. Douglass, ensuring that each tree ring is assigned its exact year by using patterns of wide and narrow rings between cores from the same tree, making it the most critical principle for dendrochronology studies (Douglass 1919). In other words, tree ring data can be used to analyze the spatial and temporal patterns of climate variation and the solar cycle (Schweingruber 1988; Dergachev and Raspopov 2000; Raspopov et al 2004; Fye and Cleaveland 2001; Rigozo et al 2004a).

Several studies have shown evidence of the solar cycle's influence on tree rings, particularly related to the cycles of Schwabe (∼11 years), Hale (∼22 years), and Gleissberg (∼70 to ∼90 years) (Hathaway 2010; Rigozo et al 2004b; Prestes et al 2011, 2018). These studies indicate that variations in solar activity can influence tree growth, resulting in changes in tree-ring widths and patterns that reflect solar variability. However, it should be noted that other factors such as temperature, precipitation, and soil conditions can also influence tree growth, so the interpretation of tree-ring data requires careful consideration of all relevant environmental factors.

In this study, we will identify the climatic periodicities in the tree-ring series to understand the dynamics of the ocean–atmosphere interactions, and to evaluate how they affect or modify the regional climate system. The study of Rigozo et al (2012) found that tree-ring responses to the Southern Oscillation Index (SOI) in 4–8-year bandwidth, and higher and lower levels of rain due to the *El Ninõ* and *La Ninã*, respectively. In this sense, the Wavelet analysis is used here since it is a widely used tool for the study of non-stationary signals allowing us to identify the periodicities present in time series and investigate the mechanisms of climate influence (Velasco and Mendoza 2008; Ma 2009; Souza Echer et al 2012; Velasco Herrera 2016; Wang et al 2021).

2 Materials and methods

2.1 Study area and climate

The city of General Carneiro (latitude: 26°24'S - Longitude: 51°24'W - altitude: 983 m) is located in Paraná state, Southern Brazil (Fig. 1), and it was chosen as the collection site of the samples for this study.

The climatic characteristics of the Brazilian southern region are subtropical with well-distributed rains throughout the year. There is a slight decrease in the rainfall level during the winter, especially in August, and an increase during the summer. The Climograph of the region is shown in Fig. 2.

The southern region of Brazil is located outside the tropics, which results in it receiving less light than the Brazilian tropical regions. However, during the summer, the Earth's position allows for more insolation in this southern region, leading to high evaporation. Due to the southern region's proximity to the Atlantic Ocean, there is an increase in cloudiness, and as a consequence, there is an increase in the level of rainfall (Dittberner 2001).

The South Atlantic Anticyclone System (SAAS) has an indirect impact on the climate of General Carneiro city. The tropical marine mass originates from the SAAS, while the polar anticyclone originates the polar mass. The displacement of these masses, and their relationship with the warming of the Atlantic, is the primary cause for the abundant precipitation in spring and summer (Nimer 1989). Additionally, due to the polar fronts, General Carneiro city is subject to extreme weather events in any season. Therefore, the city experiences notable annual rainfall deviations in both summer and winter. However, the thermal variability does not vary with the same intensity (Leal 1999). From June to August, on average, there are 22 penetrations of frontal systems in the latitudinal range of 25° to 35° S (Oliveira 1986). The cold fronts induce the formation of instability lines, and in combination with other phenomena, it can accentuate the formation of convective precipitation.

Other important systems operating in this region are the Mesoscale Convective Complexes (MCC) and the South Atlantic Convergence Zones (SACZ). The MCC occurs mainly in spring and summer, and the SACZ generally occurs from September to October, and from March to April. These systems explain the famous "Summer rains" in Brazil (Nery 2005).

The climate circulation over Brazil is mainly driven by the South American Monsoon System (SAMS), which presents its maximum activity during the southern hemisphere summer. It is characterized as a rainy season. The SAMS is developed due to the large-scale thermal contrast between ocean and continent, and considering the effects of high topography, the Andes Mountains, the SAMS brings a large volume of moisture from the oceans to the continent (Zhou and Lau 1998). The SAMS also connects the Intertropical Convergence Zone (ITCZ) with the SACZ through a large-scale atmospheric circulation containing a low-level jet. The South American Low-Level Jet (SALLJ) starts in the northern region of South America following the Andes topography and transports heat and moisture from the Amazon Basin to the Rio da Prata Basin (Vera et al 2006). This transport, in its turn, is conditioned by the action of the low-pressure systems of the Chaco and Northern Argentina (Nogués-Paegle and Mo 1997). The portion of the low-level jets that goes towards the continent's Southeast region interacts with the winds formed by the high-pressure South Atlantic system. This event is considered the trigger to the SACZ formation (Saulo et al 2000).

Other important climatic features are the incursions of polar fronts arising from east of the Andes (Marengo and

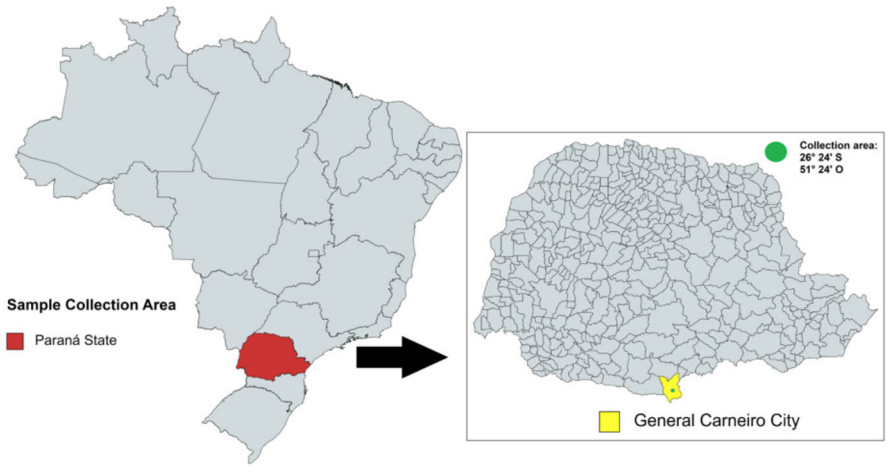

Fig. 1 The map of Brazil on which General Carneiro's city location is indicated. Source: MapChart (https://www.mapchart.net/)

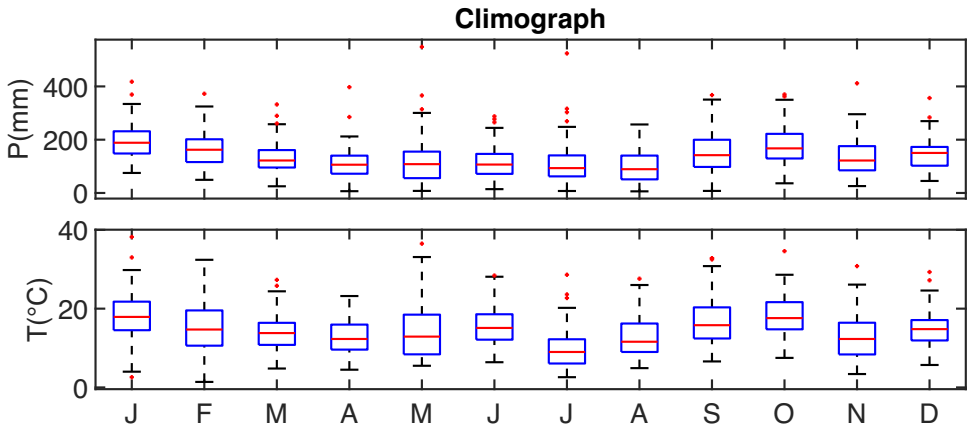

Fig. 2 Climograph of monthly climate data. Box shows the median and interquartile range (IQR). The whiskers indicate 1.5 IQR. Source: Data from Earth System Research Laboratory and graphic made by the authors

Rogers 2001), and the El Niño teleconnections that control rainfall and hydrology of major river systems (Aceituno 1988; Boulanger et al 2005).

2.2 Climatic Variables

For this analysis we choose the following representative parameters of ocean–atmosphere interaction:

- Southern-Oscillation Index (SOI) - The SOI is calculated by the difference in sea level air pressure (SLP) between Tahiti and Darwin (Australia), i.e., between the western and eastern tropical Pacific Ocean during El Niño and La Niña episodes;
- Annual precipitation - The precipitation data were obtained from reanalysis at Earth System Research Laboratory (http://www.esrl.noaa.gov), having a spatial resolution of 0.5° Latitude X 0.5° Longitude;
- El Niño 3.4 (PACE) - The SST index for the Pacific Ocean is used to verify the influence of the Equatorial Pacific (PACE) on precipitation and tree ring. The Niño 3.4 region (5° N - 5° S; 120X - 170X W) was selected because it represented the monthly index of the Equatorial Pacific; and
- South Atlantic Index (ATLS) - The SST index representing the Atlantic ocean is calculated as the area-averaged monthly SST anomalies between the latitudes 0° S and 20° S and longitudes 30° W and 10° E, available on the National Center for Environmental Prediction (NCEP) (http://www.cpc.ncep.noaa.gov/data/indices/).

The SST datasets for the Atlantic and Equatorial Pacific Oceans were obtained from the Climate Explorer site, available from the period 1854 to 2015. The atmospheric data selected for this work are the precipitation from 1900 to 2010, air temperature from 1948 to 2010, and SOI from 1880 to 2015.

2.3 Tree-ring data

The tree-ring data used in our analysis is the same dataset as used by Silva et al (2021). In their study, all data processing steps were described in detail, including the series detrending by Regional Curve Standardization (RCS) method. As discussed by Silva et al (2021), 64 tree-ring samples were collected in January 2013 from 21 different trees belonging to the native species *Ocotea porosa (Nees & Mart) Barroso*, commonly known as *Imbuia*. During the sample collection, it was ensured that the trees were not diseased or attacked by pests, to eliminate any influence on the tree-ring series. This species was selected based on its suitability for Tropical Dendrochronology, as it exhibits clear growth rings and annual periodicity (Nascimento 2022).

The preparation of the samples took place following these steps: (i) dry them in the shade; (ii) polished them on the transverse surface with 50–600 grit sandpaper to highlight the tree ring; (iii) demarcated the rings using a stereomicroscope (6 to 40 times magnification) with a fiber optic lighting system; (iv) measured the size of the rings using a VELMEX measuring table with an accuracy of 0.001 mm; and (v) arranged the tree-ring width values in spreadsheets corresponding to each sample. The dating was made from the tree bark to the pith. The last tree ring formed up to the date of the collection represents the year 2011.

To improve accuracy, the cross-validation technique was performed using a 50 years window to eliminate counting errors and identify false rings or partially missing rings (Helama et al 2004). From the initial 64 tree-ring samples, only 41 samples were chosen to compose our chronology from the year 1446 to 2011.

2.3.1 Chronology statistics

The chronology was estimated using Tukey's biweight robust mean. However, as the tree ring for the year 2012 had not completed its growth on the day of collection, the chronology

ends in 2011. This is because *Imbuia* tree ring formation occurs in summer/autumn, as reported by Filho et al (2003). We used trend variance in the chronology, as was done by Shiyatov and Mazepa (1987). Figure 3 shows that when the sample size is small (i.e., ≤ 5), corrections are needed to account for variations. On the other hand, in periods where there are more samples, no correction is necessary

Table 1 presents the chronology statistics. The mean series intercorrelation (Rbar) for the full period is around 0.15, which some dendrochronologists consider an acceptable value when working with a larger number of samples. In these studies of Cook et al (2004); Esper et al (2002); Anchukaitis et al (2017), the critical Rbar values used for sample selection ranged from 0.15 to 0.18. It's worth noting that the critical Rbar value used in any given study may depend on the specific research question, the quality of the samples, and the method of analysis used.

The mean sensitivity obtained is also high according to Locosselli (2012), exceeding 0.30, indicating that the time series are sensitive, which is defined as the difference between two successive rings divided by their mean Douglass (1919). However, it is worth noting that this value is still uncertain, and additional parameters are required, as discussed by Bunn et al (2013).

According to Cook and Kairiukstis (1990), an EPS value greater than 0.85 is obtained with a chronology of nearly 36 samples when the full-period intercorrelation value is approximately 0.1294, which agrees with our EPS results for the full period. An EPS value greater than the critical value indicates that the chronology is reliable, meaning that there is no single tree-ring series that dominates the chronology, and therefore it is homogeneous. We also obtained a signal-to-noise ratio of 6.086, although this value can be difficult to interpret, as it does not have an upper bound (Cook and Kairiukstis 1990).

2.4 Wavelet analysis

A wavelet transform is a useful tool for non-stationary signal analysis (Graps 1995). It allows identifying the periodicities of a time series and its location in time (Kumar and Foufoula-Georgiou 1997; Percival and Walden 2002). One of the limitations of the Fourier Transform lies in the fact that it does not allow the analysis of different parts of the signal separately (Haddad and Serdijn 2009). In addition, sine waves are well located in frequency, but not in time, as their supports are of infinite length. To overcome these problems, the wavelet transform was introduced.

As discussed by Torrence and Compo (1998), the continuous wavelet transform of a discrete sequence x_n is defined as the convolution of x_n with a scaled and translated version of the mother wavelet function ψ:

$$W_n(s) = \sum_{n'=0}^{N-1} x_{n'} \psi^* \left[\frac{(n' - n)\,\delta t}{s} \right] \tag{1}$$

where the $(*)$ indicates the complex conjugate. This transform uses windows of variable width (wavelet scale s), which can adjust to the characteristics of each signal segment. And by translating along the localized time index n, it is possible to construct a picture showing both the amplitude of any features versus the scale and how this amplitude varies with time. So, for example, if there is an increase in the resolution of the time domain, it implies a loss of location in frequency and vice versa. This fact is due to the Heisenberg Uncertainty principle. In 1927, the physicist Werner

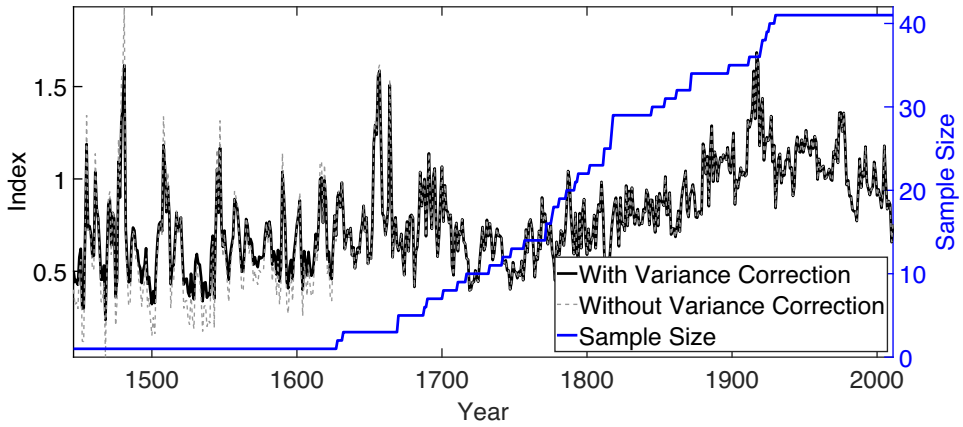

Fig. 3 The chronology of 41 *Imbuia* samples without the variance trend correction (light gray line) and with the variance trend correction (black line) based on the coefficient of variation. The change in the number of samples in the chronology is represented on the right y-axis (blue line)

Table 1 Chronology statistics used to interpret the chronology quality

Period	RBar	EPS
1687–1736	0.3475	0.727
1712–1761	0.2020	0.695
1737–1786	0.1799	0.707
1762–1811	0.1788	0.753
1787–1836	0.1865	0.821
1812–1861	0.1425	0.806
1837–1886	0.1382	0.823
1862–1911	0.1418	0.841
1887–1936	0.1287	0.834
1912–1961	0.1407	0.855
1937–1986	0.1505	0.879
1962–2011	0.1352	0.865
Full Period	0.1294	0.859
Nº of trees for EPS >0.85 = 10		
Mean Sensitivity = 0.3991		
Signal to Noise Ratio = 6.086		

A period of every 50 years was used to calculate the statistics, but the starting year starts in the middle of the previous period. RBar is the mean intercorrelation between the series. EPS is the Expressed Population Signal

Heisenberg determined that an object's position and speed cannot be measured accurately in time or even accurately described in theory. In signal processing, it is impossible to know simultaneously the frequency and the exact position at the time of this frequency of any signal. To determine the exact frequency of a signal, we must use an infinite support mother wavelet over time, or vice versa (Gabor 1946).

In this article, for the evaluation of the time-varying relationship between two-time series, we used the cross-wavelet transform (XWT) defined as

$$W_n^{XY}(s) = W_n^X(s) W_n^{Y*}(s), \tag{2}$$

where $W_n^X(s)$ and $W_n^Y(s)$ are the wavelet coefficients of the times series X and Y, respectively. Since we are using the Morlet as the mother wavelet, the cross-wavelet spectrum is complex, and the similarity of the two series can be given by the cross-wavelet power, i.e., $\mid W_n^{XY}(s) \mid$.

The CWT algorithm developed by Torrence and Compo (1998) was modified to suppress the effects of the border or edge. It is important to mention that the edge effects occur due to the limitation of the signal length, and will be treated here by the method of symmetrization. This method assumes that the signals can be recovered out of their original support through their symmetrical replication (signal mirroring), both to the left and to the right of their support. However, this method has the disadvantage of introducing discontinuities at the edges, but it works well in general. In addition, there is no loss of response due to wavelet truncation, and the cone of influence is not necessary as discussed in Prestes et al (2018).

At this point, one question arises: Is the data used in this work enough to show and explain the fluctuations related to the possible interrelation between climatic and solar forcing and the tree rings? As simply stated by the Nyquist criterion, only periodicities above at least twice the highest sampling period can be observed. On the other hand, the length of the signal limits the maximum observed period. For example, the precipitation series has a length of 110 years and a time resolution of 1 year, consequently, the cross-wavelet analysis can verify periodicities between 2 and 110-year bands as stated by the Nyquist criterion.

3 Results and discussion

To access the climate response of the trees, we performed the Pearson's (r) and Squared Pearson's Correlations (r^2), both computed for the full period of the chronology. The Significance Value (p) of the correlations was also computed, using the probability density functions obtained after 1000 Monte-Carlo iterations. Our correlation results (Table 2) indicate that they are not significantly correlated with the GCI concerning the full period of the chronology.

A moving correlation was performed (Fig. 4) using window sizes ranging from 2 to 33 years to examine the correlation coefficient point by point between the chronology and the climatic series. The white contours indicate the points with a significant correlation between the two series, i.e., p-value = 0.05.

The analysis of the moving correlation (Fig. 4) revealed that for PACE, there are consistently high and significant correlation coefficients between the chronology and the climatic series in the 2–15 year window for all years. Similarly, for SOI, the 2–15 year window also exhibited high correlation points for the entire series. Additionally, in the 10–33 year window, there were significant correlations between 1906–1936, 1960–1970, and 2000–2011. The ATLS also exhibited strong influences on tree-ring growth in the 2–15 year window throughout the full period, with an intense

Table 2 The results of Pearson correlation between the General Carneiro chronology and climatic parameters

Parameters	period	r	r^2	p
PACE	1854–2011	0.108	0.012	0.2931
SOI	1866–2011	0.051	0.003	0.4853
ATLS	1854–2011	−0.172	0.030	0.7116
Precipitation	1901–2010	−0.079	0.006	0.3997
SSN	1700–2011	0.103	0.011	0.1141

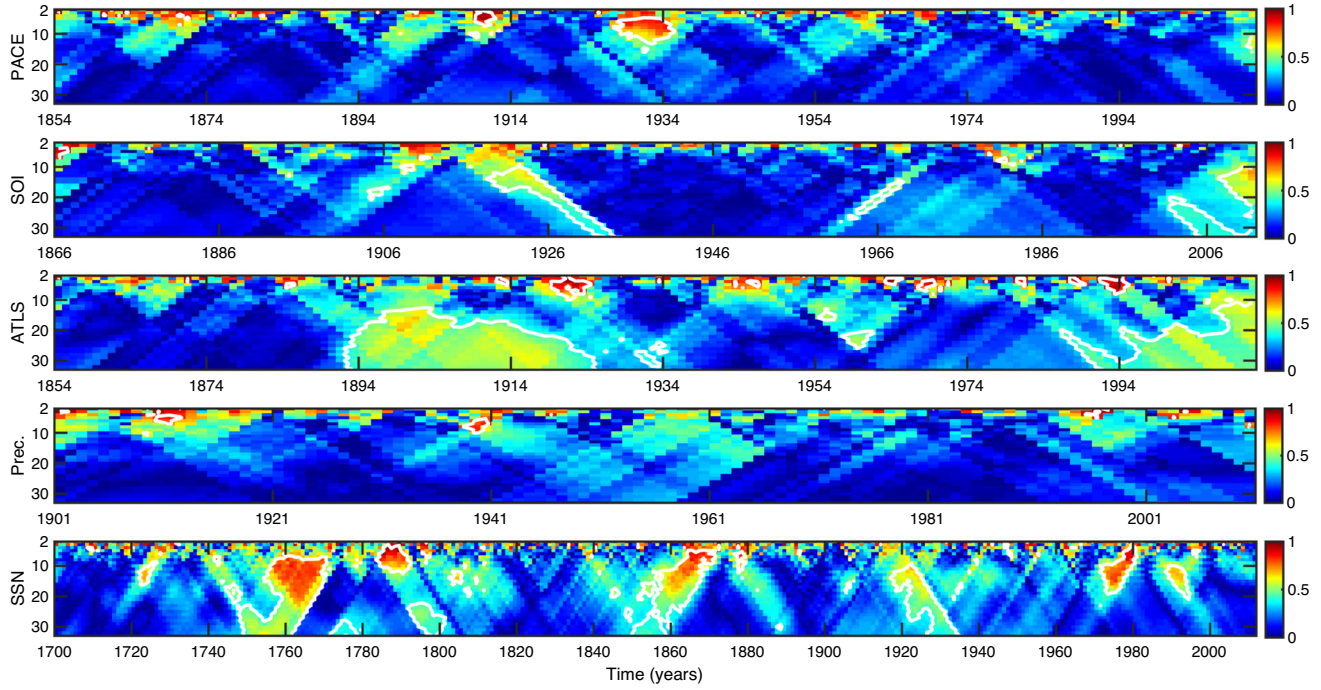

Fig. 4 Correlogram with 2–33-years moving windows, between the chronology and the climatic parameters. The white contours stand for a significant correlation at 0.05 level. The color bar represents the correlation coefficient in modulus

influence, in the 10–33 year window, between 1890–1925 and 1984–2011.

The moving correlation analysis revealed that precipitation had a consistent influence in the 2–15 year window throughout the full period, indicating a strong relationship between tree-ring growth and precipitation in the region. As for sunspot number, the analysis showed a consistent influence in the 2–15 year window throughout the series, but there were also intense influences during the years 1750–1770 and 1850–1870 for a 5–33 year window, and 1770–1780 and 1790–1802 for the 20–33 year window. These results suggest that solar variability may have had an impact on tree growth during those periods, possibly due to changes in the amount of energy received by the Earth's surface.

It should be noted that the high correlation coefficients in the moving correlation analysis do not necessarily indicate causation or prove a direct relationship between the climatic variables and tree-ring growth. Nonetheless, they provide useful information for further investigation and can help guide the development of more detailed models.

A time-dependent technique, known as the cross-wavelet transform, characterizes the interaction between the wavelet transform of two individual time series and enables the identification of significant interactions (at a significance level of 0.05) in a specific period-band over time. Figure 5(a) shows the cross-wavelet scalogram between our GCI and the *El Niño* 3.4 index, which monitors the tropical Pacific (PACE), during the period from 1854 to 2011. Figure 5(b) presents the cross-wavelet scalogram between GCI and the Southern Oscillation Index (SOI) for the period from 1866 to 2011. In both scalograms, the scale values are represented by periods in the range of 2 to 66 years.

In Fig. 5(a) and (b), significant periods with 95% confidence represent periodicities between 2 and 8-years, and ∼17 years. These periodicities between 2 and 8-years are located in the temporal space for PACE-GCI during the 1875–1890, 1906–1920, 1933–1952, 1985–2010 periods; and for SOI-GCI during the 1866–1890, 1904–1920, 1940–1950 periods. Whereas for ∼ 17 years, the temporal location is between 1970 - 1995 in both scalograms. As expected, the 95% confidence region is similar for both scalograms, especially in the range of 2 to 8-years, because ENSO is characterized by being an ocean–atmosphere interaction phenomenon in which the oceanic component is associated with variations in the sea surface temperature in the central and eastern waters of the Equatorial Pacific Ocean.

In the study of Magdoff (2005), the major ENSO events within our period of analysis were recorded in the years 1876–1878, 1972–1973, 1982–1983, and 1997–1998. Also, there were at least 30 *El Ninõ* events from 1900 to 2020. It is possible to notice that the cross-wavelet technique well-detected the major ENSO event influences in our chronology. Prestes (2009) and Silva (2013), studying dendrochronological series of *araucaria angustifolia* from southern Brazil, found equivalent results to those found here, both for the periodicities between 2 to 8-years and ∼ 17 years. It is inter-

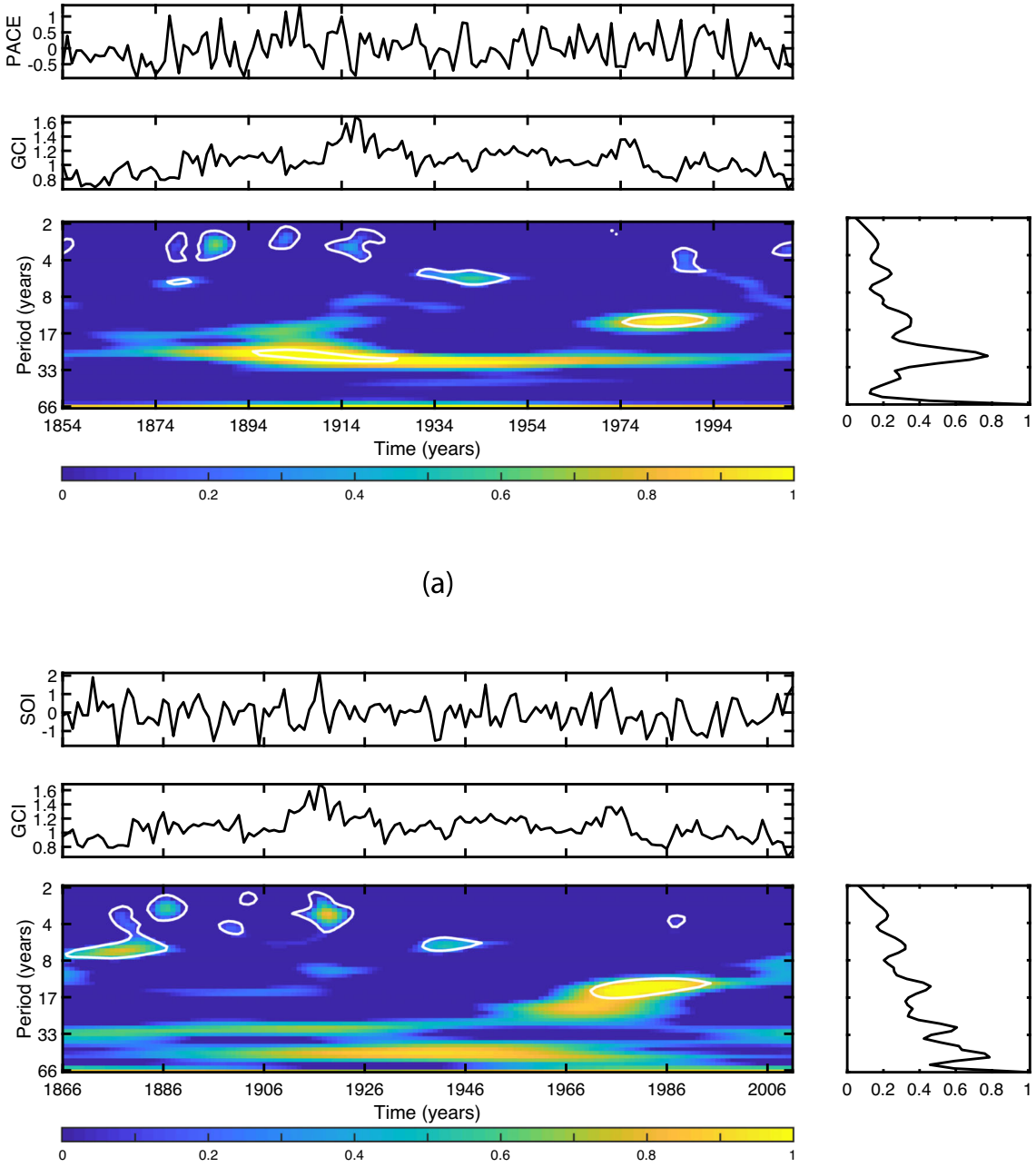

Fig. 5 The cross-wavelet spectrum using the Morlet wavelet between General Carneiro index (GCI) and (a) the *El Ninõ* 3.4 indexes to monitor the tropical Pacific (PACE); (b) Southern Oscillation Index (SOI). Top graphs: the climatic series used. Middle graphs: GCI chronology. Bottom graphs: the cross-wavelet power spectra (normalized), the squared cross-wavelet coefficient is normalized by its maximum, and therefore, areas of stronger wavelet power are shown in bright yellow ("1"), and areas of low wavelet power, in dark blue ("0"). The thick contour encloses regions of greater than 95% confidence for a red-noise process with a lag-1 coefficient of 0.72. Bottom right: the global wavelet spectrum (normalized)

esting to note that the periodicity of ∼ 17 years detected in the cross-wavelet analysis could be related to the Moon's orbital cycles, as suggested by Scafetta (2010). They found that long-term lunar cycles can induce a 9.1-year cycle in temperature records and possibly other cycles, including an 18.6-year cycle in some regions. However, it is worth noting that further research would be necessary to confirm this relationship and to understand the mechanisms behind it.

It is possible to notice cycles with periods of 20–22 (Fig. 5a), 30 and 60 years (Fig. 5b) which may be linked to the orbits of Jupiter and Saturn, as suggested by Scafetta (2010). The period of 20–22-years corresponds to the Hale solar cycle. The period of 30–40-years may also be related to the Brückner-Egeson-Lockyer climatic cycle that is correlated with sunspot activity. The results indicate a potential causal relationship between PACE-GCI and SOI-GCI in association

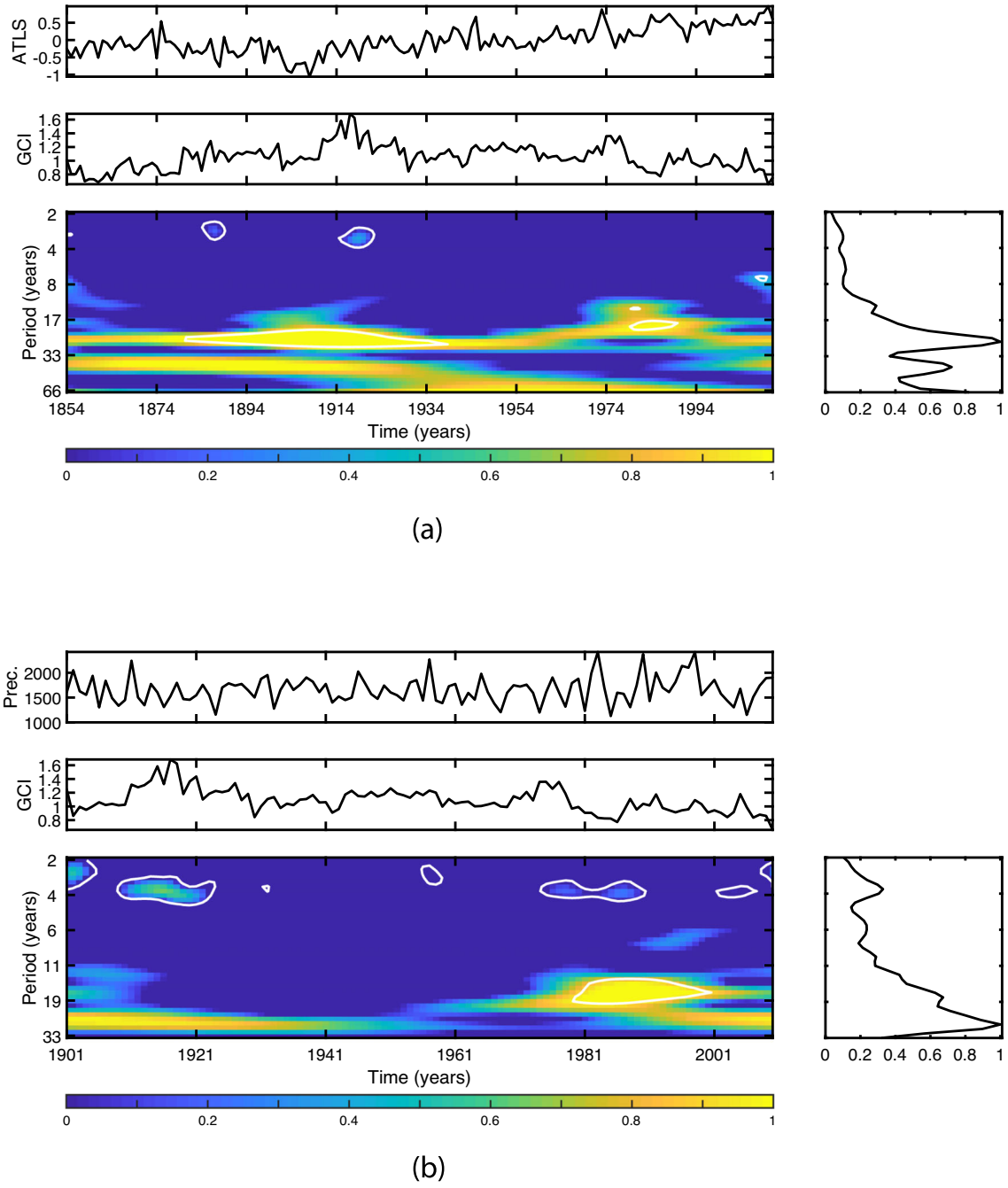

Fig. 6 The cross-wavelet spectrum using the Morlet wavelet between General Carneiro index (GCI) (a) Tropical Southern Atlantic index (ATLS); and (b) precipitation in the Brazilian southern region. Similar to Fig. 5

with the lunar and solar cycles, as well as, the orbital periods of Jupiter and Saturn.

In Fig. 6(a), the spectrum between GCI and ATLS presents sporadic regions with 2 to 5-years periodicities during 1880–1890 and 1914–1924, and with 17 years, during 1895–1925, and a period of ∼ 22 years appears between the years 1954 and 2011, similar to the wavelet spectra of PACE and SOI. White et al (1997) also found periodicities related to the solar forcing on a decadal scale (period of ∼ 11 years) and interdecadal (period of ∼ 22 years) in their analysis of Indian, Pacific, and Atlantic oceans. The highest correlations were found with a lag of 1–2-years between ocean temperatures and solar activity, which is approximately the time scale expected for the upper ocean layers (< 100 m) to reach equilibrium.

According to Rodrigues (2011), the Equatorial Atlantic (30° S a 30° N) can cause a temperature increase in the Brazilian southern region of up to 0.3 °C during summer and a decrease of 0.3 °C during winter. They also studied the influence of oceanic variability modes on the South American climate during the middle Holocene, and found that ENSO has a positive influence in southern Brazil with a tendency to increase precipitation up to 2.5 mm per day during the summer for the present climate. Prestes et al (2018) studied the response of *Araucaria angustifolia* growth in southern Brazil to solar and climatic variability, and their results showed significant periods of approximately 17 and 35 years, which may be related to the lunar and Brückner-Egeson-Lockyer climatic cycle, respectively. The period of ∼ 35 years may also be interconnected to the solar cycles of Hale and Gleissberg and their nonlinear effects on the atmospheric processes. However, tree growth is not linked only to solar radiation, but also to favorable weather conditions during its development. Here, we will verify the atmospheric influence on the *Imbuia* development by relating the tree ring to the annual precipitation in the region of General Carneiro city.

In Fig. 6(b), the spectrum between GCI and precipitation shows 3–5 years of periodicities during 1912–1922, and 1975–1986. There is also a consistently high cross-amplitude in the 22-year band over the entire analyzed interval. As reported by Viegas et al (2019), between the years 1905 and 1998, there were 10 observed *El Niño* events of the Eastern Pacific-type (or Canonical-type), 5 of which correspond to the years of periodicities found in our chronology (1911–1912, 1918–1919, 1976–1977, 1982–1983, and 1986–1987). Additionally, 14 Central Pacific-type (or Modoki-type) *El Niño* events were observed between 1902 and 2005, but only one event (1914–1915) occurred within the periodicities found in this study. This may indicate a positive response in tree growth to Eastern Pacific-type *El Niño* events, as they cause higher precipitation levels in southern Brazil due to their propagation further westward to the Eastern Equatorial Pacific from the coast of South America, as explained in Rasmusson and Carpenter (1982).

Souza Echer et al (2008) studied the annual precipitation series in Pelotas (southern Brazil) from 1894 to 1995 and its relationship with ENSO, using cross-wavelet analysis. They found significant cross-power for periodicities between 2 to 8 years in a temporal interval similar to those found here and argued its causal relationship with SOI. The precipitation in the South of Brazil is not well distributed or has a seasonal regime. Schossler et al (2018) observe an association between Southern Annular Mode, *El Ninõ*, and *La Ninã* with anomalous precipitation events. In general, the southern Brazilian region has rainfall above the climatological average during *El Ninõ* years from 1976 to 2010 (Teixeira Nery and Carfan 2014).

A significant period of ∼ 17–20 years is also observed between 1980 and 2001, which may correspond to the lunar cycle. As explained by Camuffo (2001), the Moon, with its tides, induces movement of the oceanic water and, consequently, the transport of heat, which influences the level of precipitation. It is also possible that the results attributed to the lunar cycle might be more appropriately attributed to the joint influence of Jupiter and Saturn or the Sun, or vice versa (Camuffo 2001).

In the analysis of the *araucaria* growth in southern Brazil to solar and climatic variability, Prestes et al (2018) found periodicities between 2 and 7 years related to the *El Ninõ* and *La Ninã* phenomena. They also found a period of ∼ 23 years related to changes in temperature, presenting a lag of 3 years with the series of the tree ring, and periods of ∼ 11, ∼ 80, and ∼ 200 years to solar activity. The period of ∼ 35 years, which is related to the Brückner-Egeson-Lockyer climatic cycle, was discussed by Prestes et al (2018) as being a combination of the Gleissberg and Hale cycles.

In Fig. 7, the spectrum for Sunspot Number displays two prominent periodicities: one around ∼100 years and another around 200 years. The ∼11 year period is intermittent, with variable energy over time. It exhibits significant inter-

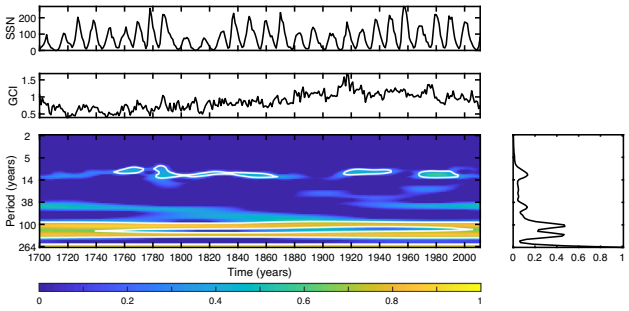

Fig. 7 The cross-wavelet spectrum using the Morlet wavelet between General Carneiro index (GCI) and SunSpot Numbers (SSN). Similar to Fig. 5

vals during the years 1745–1775, 1790–1870, 1910–1945, and 1970–1995. Lorensi (2016) found a similar spectrum between the SSN and the series of *Araucaria angustifolia* tree rings from General Carneiro, with the Gleissberg cycle displaying high wavelet-power energy. This cycle is also present in several other dendrochronological series from southern Brazil, including those studied by Rigozo et al (2008), Prestes et al (2011), Lorensi (2016), and Prestes et al (2018), and persists throughout the entire analyzed series.

4 Conclusion

The results can be summarized as follows:

1. The periodicities between 2 and 8 years found in the tree-ring chronology are likely due to the variability of the Pacific Ocean related to ENSO, which affects precipitation variability in General Carneiro city.
2. The 17-year period may be associated with the lunar cycle or the Hale and Gleissberg solar cycles, which are known to have non-linear effects on atmospheric processes.
3. The period of 22 years is mainly related to precipitation variation, possibly due to the influence of the Atlantic Ocean and/or its association with the Hale cycle.
4. The period of 30–40 years may also be related to the Brückner-Egeson-Lockyer climatic cycle, which is correlated with sunspot activity.
5. The rainfall regime in General Carneiro city has low annual variability, oscillating on average by ±10%. There was an increase in annual precipitation during the second half of the century, consistent with the rise in ocean temperatures, primarily related to the Atlantic Ocean.
6. The wavelet analysis identified periodicities in the years 1911–1912, 1918–1919, 1976–1977, 1982–1983, and 1986–1987, which may be indicative of Eastern Pacific-type or Canonical-type *El Niño* events. These periodicities were associated with increased precipitation, leading to higher tree growth.
7. Southern Brazil is under the influence of several climatic and geophysical parameters that result in ocean–atmosphere interactions of both the Atlantic and Pacific oceans. These parameters directly affect the development of *Imbuia* trees, as indicated by the sensitivity of the tree ring series. These results can serve as a first step for further studies, such as paleoclimate reconstructions.

Acknowledgements The authors would like to thank FAPESP (2009/02907-8), CAPES (88881.624415/2021-01), and CNPq (305249/2018-5, 308258/2021-5, and 407896/2021-0) for the financial support to perform fieldwork and scholarships.

Author Contributions All authors contributed to data analysis, methodology development, and writing and reviewing the manuscript

Funding The authors received no financial support for the research, authorship, and/or publication of this article

Availability of data and materials The datasets generated and analyzed during the current study are available under request

Declarations

Conflict of interest The authors declare that they have no conflict of interest

References

Aceituno P (1988) On the functioning of the southern oscillation in the south american sector. part i: Surface climate. Monthly Weather Review 116(3):505–524. https://doi.org/10.1175/1520-0493(1988)116<0505:OTFOTS>2.0.CO;2

Anchukaitis KJ, Wilson R, Briffa KR et al (2017) Last millennium northern hemisphere summer temperatures from tree rings: Part ii, spatially resolved reconstructions. Quaternary Science Reviews 163:1–22

Boulanger JP, Leloup J, Penalba O et al (2005) Observed precipitation in the Paraná-Plata hydrological basin: long-term trends, extreme conditions and ENSO teleconnections. Climate Dynamics 24(4):393–413. https://doi.org/10.1007/s00382-004-0514-x

Bunn AG, Jansma E, Korpela M et al (2013) Using simulations and data to evaluate mean sensitivity as a useful statistic in dendrochronology. Dendrochronologia 31(3):250–254. https://doi.org/10.1016/j.dendro.2013.01.004. https://www.sciencedirect.com/science/article/pii/S1125786513000295

Camuffo D (2001) Lunar Influences On Climate. Earth Moon and Planets 85:99–113. https://doi.org/10.1023/A:1017099427908

Chelton DB, Xie SP (2010) Coupled-ocean atmosphere at oceanic mesoscales. Oceanograph 23(4):52–69 (http://www.jstor.org/stable/24860862)

Cook E, Kairiukstis LA (1990) Methods of Dendrochronology: Applications in the Environmental Sciences. Springer

Cook ER, Woodhouse CA, Eakin CM et al (2004) Long-term aridity changes in the Western United States. Science 306(5698):1015–1018

Currie RG (1974) Solar cycle signal in surface air temperature. Journal of Geophysical Research (1896-1977) 79(36):5657–5660. https://doi.org/10.1029/JC079i036p05657

Dergachev V, Raspopov O (2000) The long-term solar cyclicity (210 and 90 years) and variation of the global terrestrial air temperatures since (1868) Solar and Space Weather Euroconference. The Solar Cycle and Terrestrial Climate 463:485

Dittberner MR (2001) Causas e efeitos das turbulências nas operações aéreas do aeroporto internacional hercílio luz, monografia (Monografia de Graduação). Departamento de Geografia - UFSC

Douglass AE (1919) Climatic Cycles and Tree-Growth. A Study of the Annual Rings of Trees in Relation to Climate and Solar Activity. the Carnegie Institution of Washington, Washington

Esper J, Cook ER, Schweingruber FH (2002) Low-frequency signals in long tree-ring chronologies for reconstructing past temperature variability. Science 295(5563):2250–2253

Filho AF, R. HS, Schaaf LB et al (2003) Avaliação do incremento em diâmetro com o uso de cintas dendrométricas em algumas espécies de uma floresta ombrófila mista localizada no sul do estado do paraná. Revista Ciências Exatas e Naturais 5(1)

Fye FK, Cleaveland MK (2001) Paleoclimatic analyses of tree-ring reconstructed summer drought in the united states, 1700–1978. Thee-Ring Research 57:31–34

Gabor D (1946) Theory of communication. part 1: The analysis of information. Journal of the Institution of Electrical Engineers- Part III: Radio and Communication Engineering 93(12):429–441

Garreaud RD, Vuille M, Compagnucci R et al (2009) Present-day south american climate. Palaeogeography, Palaeoclimatology, Palaeoecology 281(3):180–195. long-term multi-proxy climate reconstructions and dynamics in South America (LOTRED-SA): State of the art and perspectives. https://doi.org/10.1016/j.palaeo.2007.10.032

Gasquez M, Magalhães AR (1987) Climate anomalies and their impacts in brazil during the 1982-83 enso event. LUGANO Report: climate crises pp 30–36

Graps A (1995) An introduction to wavelets. IEEE Comput Sci Eng 2(2):50–61. https://doi.org/10.1109/99.388960

Haddad SAP, Serdijn WA (2009) Wavelet versus Fourier Analysis. Springer, Netherlands, Dordrecht. https://doi.org/10.1007/978-1-4020-9073-8_3

Haigh J (2007) The sun and the earth's climate. Living Rev Sol Phys 4(2). https://doi.org/10.12942/lrsp-2007-2

Hathaway D (2010) The solar cycle. Living Rev Sol Phys 7(1). https://doi.org/10.12942/lrsp-2010-1

Helama S, Lindholm M, Timonen M et al (2004) Detection of climate signal in dendrochronological data analysis: a comparison of tree-ring standardization methods. Theoretical and Applied Climatology 79

Hoyt DV, Schatten KH (1997) The Role of the Sun in Climate Change. Oxford University Press

Junior RSN, Sentelhas PC (2019) Soybean-maize off-season double crop system in brazil as affected by el niño southern oscillation phases. Agricultural Systems 173:254–267. https://doi.org/10.1016/j.agsy.2019.03.012 https://www.sciencedirect.com/science/article/pii/S0308521X18312691

Kivelson MG, Russell CT (1995) Introduction to Space Physics. Cambridge University Press

Kumar P, Foufoula-Georgiou E (1997) Wavelet analysis for geophysical applications. Reviews of Geophysics 35(4):385–412. https://doi.org/10.1029/97RG00427

Lassen K, Friis-christensen E (1995) Variability of the solar cycle length during the past five centuries and the apparent association with terrestrial climate. Journal of Atmospheric and Solar-Terrestrial Physics 57:835–845

Leal PC (1999) Sistema praial moçambique - barra da lagoa - ilha de santa catarina - brasil: Aspectos morfológicos, morfodinâmicos, sedimentológicos e ambientais. PhD thesis, Universidade Federal de Santa Catarina, Santa Catarina

Lean J, Rind D (1999) Evaluating sun-climate relationships since the little ice age. Journal of Atmospheric and Solar-Terrestrial Physics 61(1):25–36 https://doi.org/10.1016/S1364-6826(98)00113-8 https://www.sciencedirect.com/science/article/pii/S1364682698001138

Locosselli GM (2012) A multi-proxy dendroecological analysis of two tropical species (hymenaea spp., leguminosae) growing in a vegetation mosaic. Trees 27

Lorensi C (2016) Resposta dos anéis de crescimento de araucaria angustifolia (bertol.) o. kuntze da região sul do brasil aos forçantes geofísicos e climáticos. PhD thesis, Universidade do Vale do Paraíba - UNIVAP, Instituto de Pesquisa e Desenvolvimento Programa de Pós-Graduação em Física e Astronomia

Ma L (2009) Gleissberg cycle of solar activity over the last 7000years. New Astronomy 14(1):1–3 https://doi.org/10.1016/j.newast.2008.04.001 https://www.sciencedirect.com/science/article/pii/S1384107608000511

Magdoff F (2005) Book review: Late victorian holocausts: El niño famines and the making of the third world. by mike davis 2001. verso, London and New York. isbn 1-85984-739-0, cloth. Renewable Agriculture and Food Systems 20(3):190–192. https://doi.org/10.1079/RAF2005109

Marengo J, Rogers J (2001) Polar air outbreaks in the americas: Assessments and impacts during modern and past climates. Interhemispheric Climate Linkages, pp 31–51

Nascimento T (2022) Imbuias multisseculares: Dendrocronologia e propriedades físico-anatômicas da madeira de ocotea porosa, completion of the Undergraduate Course in Forestry Engineering at the Center for Rural Sciences. Universidade de Santa Catarina - Departamento de Agricultura, Biodiversidade e Florestas

Nery JT (2005) Dinâmica climática da região sul do brasil. Revista Brasileira de Climatologia 1(1)

Nimer E (1989) Climatologia do Brasil. IBGE, Rio de Janeiro

Nogués-Paegle J, Mo KC (1997) Alternating wet and dry conditions over south america during summer. Monthly Weather Review 125(2):279–291

Nordemann DJR, Rigozo NR, Echer E et al (2002) Solar activity and el ninõ effects on southern brazil araucaria ring widths (1955-1997). INTERNATIONAL CONFERENCE ON DENDROCHRONOLOGY (Poster)

Oliveira AS (1986) Interações entre sistemas na américa do sul e convecção na amazônia. PhD thesis, Instituto Nacional de Pesquisas Espaciais

Percival D, Walden AT (2002) Introduction to Wavelets. University of Washington

Peristykh AN, Damon PE (2003) Persistence of the gleissberg 88-year solar cycle over the last ∼ 12,000 years: Evidence from cosmogenic isotopes. Journal of Geophysical Research 108:1003

Prestes A (2009) Relação sol-terra estudada através de anéis de crescimento de coníferas do holoceno recente e triássico. 2009. PhD thesis, Instituto Nacional de Pesquisas Espaciais, São José dos Campos

Prestes A, Rigozo NR, Nordemann DJR et al (2011) Sun-earth relationship inferred by tree growth rings in conifers from severiano de almeida, southern brazil. Journal of Atmospheric and Solar-Terrestrial Physics 73:1587–1593

Prestes A, Klausner V, Rojahn I et al (2018) Araucaria growth response to solar and climate variability in south brazil. Annales Geophysicae 36:717–729. https://doi.org/10.5194/angeo-36-717-2018

Rasmusson E, Carpenter T (1982) Variation in tropical sea surface temperature and surface wind fields associated with southern oscillation/el niño. Monthly Weather Review 110(5):354–384

Raspopov O, Dergachev V, Kolström T (2004) Periodicity of climate conditions and solar variability derived from dendrochronological and other palaeoclimatic data in high latitudes. Palaeogeography, Palaeoclimatology, Palaeoecology 209(1):127–139. high Latitude Eurasian Palaeoenvironments. https://doi.org/10.1016/j.palaeo.2004.02.022. https://www.sciencedirect.com/science/article/pii/S0031018204001154

Rigozo N, Evangelista H, Nordemann D et al (2008) The medieval and modern maximum solar activity imprints in tree ring data from chile and stable isotope records from antarctica and peru. Journal of Atmospheric and Solar-Terrestrial Physics 70:1012–1024. https://doi.org/10.1016/j.jastp.2008.01.002

Rigozo N, Lisi C, Filho M et al (2012) Solar-terrestrial signal record in tree ring width time series from brazil. Pure and Applied Geophysics 169. https://doi.org/10.1007/s00024-012-0480-x

Rigozo NR, Nordemann DJR, Echer E et al (2004) Search for solar periodicities in tree-ring widths from concórdia (s.c., brazil). Pure and Applied Geophysics 161:221–233. https://doi.org/10.1007/s00024-003-2427-8

Rigozo NR, Nordemann DJR, Echer E et al (2004b) Search for solar periodicities in tree-ring widths from concórdia (s.c., brazil). Pure and Applied Geophysics 161(1):221–233

Rodrigues JM (2011) Influência dos modos de variabilidade oceânica no clima da américa do sul durante o holoceno médio. Master thesis, Universidade Federal de Viçosa., Viçosa - MG

Sampaio G (2000) El Niño e Você - o fenômeno Climático. Editora Transtec, São José dos Campos

Saulo AC, Nicolini M, Chou SC (2000) Model characterization of the south american low-level flow during the 1997–1998 spring-summer season. Climate Dynamics 16:867–881. https://doi.org/10.1007/s003820000085

Scafetta N (2009) Empirical analysis of the solar contribution to global mean air surface temperature change. Journal of Atmospheric and Solar-Terrestrial Physics 71(17):1916–1923. https://doi.org/10.1016/j.jastp.2009.07.007

Scafetta N (2010) Empirical evidence for a celestial origin of the climate oscillations and its implications. Journal of Atmospheric and Solar-Terrestrial Physics 72(13):951–970 https://doi.org/10.1016/j.jastp.2010.04.015 https://www.sciencedirect.com/science/article/pii/S1364682610001495

Schossler V, Simões JC, Aquino FE et al (2018) Precipitation anomalies in the brazilian southern coast related to the sam and enso climate variability modes. Brazilian Journal of Water Resources 23. https://doi.org/10.1590/2318-0331.231820170081. Accessed 10 Aug 2021

Schweingruber FH (1988) Tree Rings: Basics and Applications of Dendrochronology. D. Reidel Publishing Company

Shiyatov SG, Mazepa VS (1987) Some New Approaches in the Consideration of More Reliable Dendroclimatological Series and in the Analysis of Cycle Components. Methods of Dendrochronology, Kairiukstis, L. et al. (eds.), International Institute for Applied Systems Analysis, Laxenburg, Austria and Polish Academy of Sciences-System Research Institute, Warsaw, Poland

Silva AC (2013) Análise dendroclimática da região de três barras e canoinhas-sc. Phd thesis, Universidade do Vale do Paraíba

Silva DO, Klausner V, Prestes A et al (2021) Principal components analysis: An alternative way for removing natural growth trends. Pure and Applied Geophysics. https://doi.org/10.1007/s00024-021-02776-1

Solanki SK, Fligge M (1998) Solar irradiance since 1874 revisited. Geophysical Research Letters 25(3):341–344. https://doi.org/10.1029/98GL50038

Souza Echer M, Echer E, Rigozo N et al (2012) On the relationship between global, hemispheric and latitudinal averaged air surface temperature (giss time series) and solar activity. Journal of Atmospheric and Solar-Terrestrial Physics 74:87–93 https://doi.org/10.1016/j.jastp.2011.10.002. https://www.sciencedirect.com/science/article/pii/S1364682611002756

Souza Echer MP, Echer E, Nordemann DJ et al (2008) Wavelet analysis of a centennial (1895–1994) southern brazil rainfall series (pelotas, 31°46'19"s 52°20' 33"w). Climatic Change 87:489–497

Speer JH (1971) Fundamentals of Tree-Ring Research. Library of Congress Cataloging-in-Publication Data

Teixeira Nery J, Carfan AC (2014) Re-analysis of pluvial precipitation in southern brazil. Atmósfera 27(2):103–115. https://doi.org/10.1016/S0187-6236(14)71104-X

Torrence C, Compo GP (1998) A Practical Guide to Wavelet Analysis. Bulletin of the American Meteorological Society 79(1):61–78

Velasco V, Mendoza B (2008) Assessing the relationship between solar activity and some large scale climatic phenomena. Advances in Space Research 42(5):866–878 https://doi.org/10.1016/j.asr.2007.05.050 https://www.sciencedirect.com/science/article/pii/S0273117707005418

Velasco Herrera G (2016) Mexican forest fires and their decadal variations. Advances in Space Research 58(10):2104–2115. space and Geophysical Research related to Latin America - Part 2. https://doi.org/10.1016/j.asr.2016.08.030. https://www.sciencedirect.com/science/article/pii/S0273117716304835

Venegas-González A, Roig FA, Lisi CS et al (2018) Drought and climate change incidence on hotspot cedrela forests from the mata atlântica biome in southeastern brazil. Global Ecology and Conservation 15(e00):408. https://doi.org/10.1016/j.gecco.2018.e00408, https://www.sciencedirect.com/science/article/pii/S2351989418300945

Vera C, Silvestri G, Liebmann B et al (2006) Climate change scenarios for seasonal precipitation in south america from ipcc-ar4 models. Geophysical Research Letters 33(13). https://doi.org/10.1029/2006GL025759

Viegas J, Andreoli RV, Kayano MT et al (2019) Caracterização dos diferentes tipos de *El Niño* e seus impactos na américa do sul a partir de dados observados e modelados. Revista Brasileira de Meteorologia 34(34). https://doi.org/10.1590/0102-7786334015

Wang H, Zhang Y, Shao X (2021) A tree-ring-based drought reconstruction from 1466 to 2013 ce for the aksu area, western china. Climatic Change 165

White W, Lean J, Cayan D et al (1997) Response of global upper ocean temperature to changing solar irradiance. Journal of Geophysical Research 102:3255–3266. https://doi.org/10.1029/96JC03549

Zhang T, Shang H, Fan Y et al (2020) A 475-year tree-ring-width record of streamflow for the qingshui river originating in the southern slope of the central tianshan mountains, china. Geografiska Annaler: Series A, Physical Geography 102(3):247–266. https://doi.org/10.1080/04353676.2020.1769887

Zhou J, Lau KM (1998) Does a monsoon climate exist over South America? Journal of Climate 11(5):1020–1040. https://doi.org/10.1175/1520-0442(1998)011<1020:DAMCEO>2.0.CO;2

atmosphere

MDPI

Article

Climate Influence in Dendrochronological Series of *Araucaria angustifolia* from Campos do Jordão, Brazil

Daniela Oliveira da Silva *, Alan Prestes, Virginia Klausner and Táyla Gabrielle Gonçalves de Souza

Laboratório de Registros Naturais, Programa de Pós-Graduação em Física e Astronomia Brazil, Instituto de Pesquisa e Desenvolvimento, Universidade do Vale do Paraíba, São José dos Campos 12244-390, Brazil; prestes@univap.br (A.P.); virginia@univap.br (V.K.); taylagabrielle@gmail.com (T.G.G.d.S.)

* Correspondence: fys.dani@gmail.com

Abstract: A dendrochronological series of *Araucaria angustifolia* was analyzed for a better understanding of the climatic factors that operate in Campos do Jordão city, São Paulo state, Brazil. The dendroclimatic analysis was carried out using 45 samples from 16 *Araucaria angustifolia* trees to reconstruct the precipitation and the temperature over the 1803–2012 yearly interval. To this end, Pearson's correlation was calculated between mean chronology and the climatic time series using a monthly temporal resolution to calibrate our models. We obtained correlations as high as $r = 0.22$ $(\alpha = 0.1)$ for precipitation (February), and $r = 0.21$ $(\alpha = 0.1)$ for temperature (March), both corresponding to the end of the summer season. Our results show evidence of temporal instabilities because the correlations for the halves of 1963–2012 were very different, as well as for the full period. To overcome this problem, the dendrochronological series and the climatic data were investigated using the wavelet techniques searching for time-dependent cause–effect relationships. From these analyses, we find a strong influence of the region's precipitation and temperature on the growth of tree ring widths.

Keywords: dendrochronology; *Araucaria angustifolia*; tree rings

Citation: da Silva, D.O.; Prestes, A.; Klausner, V.; de Souza, T.G.G. Climate Influence in Dendrochronological Series of *Araucaria angustifolia* from Campos do Jordão, Brazil. *Atmosphere* **2021**, *12*, 957. https://doi.org/10.3390/atmos12080957

Academic Editor: Jeong-Wook Seo

Received: 30 May 2021
Accepted: 22 July 2021
Published: 25 July 2021

1. Introduction

Trees are used as a natural record of climate variability in the regions in which they grow. The study of the climate–time relationship using the variation in the width of the tree ring growth is known as dendroclimatology. By analysing the tree ring widths, it is possible to access how the trees responded to the regional climatic conditions. There are many studies that prove this growth variation response [1,2], and it can vary from species to species. Dendroclimatology determines the age of the trees by measuring the growth of tree rings formed year by year and establishes its relationship with climatic events [3]. This technique extracts the memory of climatic variations of the environment recorded by their tree ring widths [4].

In regions where there is a contrast between the climate seasons, that is, mid and high latitudes, the rings are generally well marked. Some tree species, such as pines, araucarias, and cypress trees, have well-demarcated rings even in regions of low contrast between the seasons [4]. Trees growing in mountain regions are excellent sources of paleoenvironmental records because their physical and biological systems are highly sensitive to climatic variations. Tree rings from high elevation sites provide climate-sensitive records that can reach over a thousand years or more with annual to seasonal resolution [5]. Among the species most used in dendrochronology, the use of *Araucaria angustifolia* stands out due to the high longevity of the species, as well as its sensitivity to the climate [6–8].

Araucaria angustifolia is a subtropical and tropical conifer from South America [9–11]. This native tree of the Atlantic Forest is easily found in the southern and southeastern Brazilian states and areas of Argentina and Paraguay. It belongs to Mixed Ombrophilous Forests, also known as "Araucaria Forests", due to the high occurrence of this species. It is common to find individuals of *Araucaria angustifolia* in high altitudes, for instance,

in mountainous areas in the States of Rio de Janeiro and Minas Gerais [12–14]. This species still suffers from human exploration, causing environmental impact in the short and long term, due to the alarming reduction of the original total forest area [15–19].

According to [20], about 60% of the Brazilian Atlantic Forest is located in southeastern Brazil. The state of São Paulo has the highest level of fragmentation and deforestation in this biome compared to other states in the southeastern. The Campos do Jordão city, in the state of São Paulo, has well-defined climates as a striking feature. Its Köppen climate classification is Cfb (temperate, no dry season, cool summer). In the study of [21], on the structure and aspects of the natural regeneration of the Mixed Rainforest, it was found that management actions are necessary for the in situ conservation of local conifers.

Many studies of *Araucaria angustifolia* were performed in southern Brazil, while the development of dendroclimatic studies with this species in southeastern Brazil is quite recent, and may contribute to the understanding of its growth dynamics concerning the regional climate. To this end, our paper aims to obtain information on climate variability in Campos do Jordão city, São Paulo, located in southeastern Brazil. We use a time-varying correlation between the dendrochronological series of *Araucaria angustifolia* and the regional climatic data (temperature and precipitation) using wavelet techniques.

2. Materials and Methods

2.1. Study Area and Species

Araucaria angustifolia trees stand out in dendrochronological studies due to their excellent temporal resolution. When these trees present wide rings, it is possible to infer which years had environmental conditions favorable to their development. On the other hand, narrower rings correspond to years unfavorable to their growth [22,23]. Figure 1 shows a specimen of *Araucaria angustifolia* in the collection area, *Pedra do Baú*.

Figure 1. Samples of *Araucaria angustifolia* located at *Pedra do Baú*, 2013.

The Campos do Jordão city was selected for this study due to (i) its geographical position and altitude; (ii) being an endemic region for the *Araucaria angustifolia* trees; and (iii) the tree's longevity. Campos do Jordão city is an Environmental Protection Area (Ordinary Law No. 4105, dated 26 June 1984), which is located at the east of the São Paulo Capital, in Serra da Mantiqueira (Figure 2), at an altitude of 1597 m (more information in http://www.camposdojordao.sp.gov.br/portal/index.php/cidade/informacoes/localizacao (accessed on 8 May 2012). Prefeitura de Campos do Jordão).

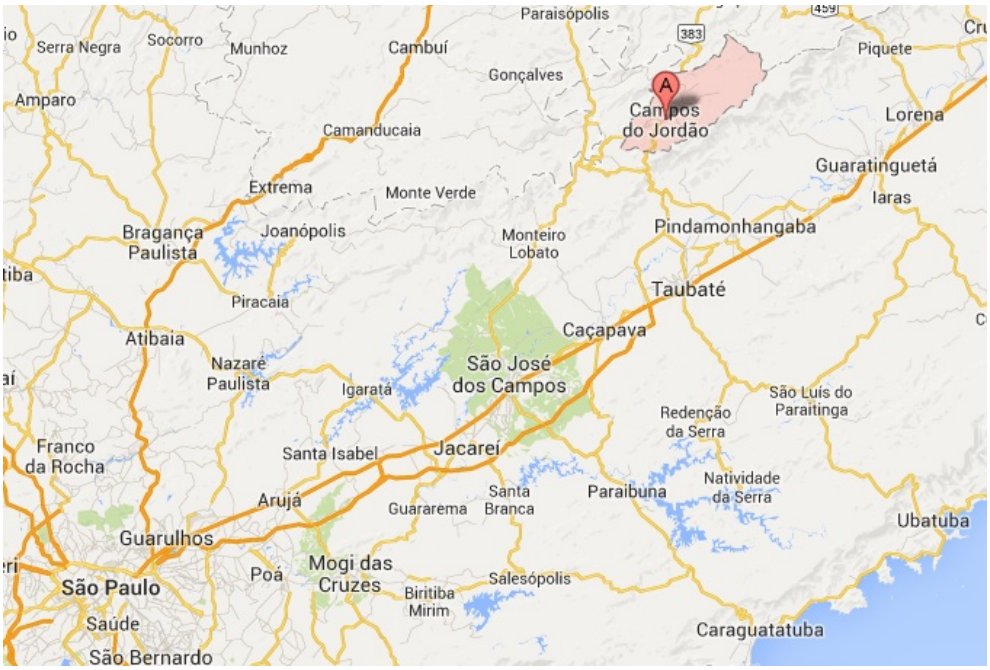

Figure 2. Location of Campos do Jordão city (Red Point). Source: maps.google.com.br, accessed on 10 February 2021.

According to the Köppen classification, the climate of Campos do Jordão city is Cfb, which corresponds to a subtropical climate of altitude, mesothermal and humid, without drought, with a maximum temperature below 22 °C [24].

2.2. Samples Collection and Preparation

Samples of native *Araucaria angustifolia* woods were collected, under license from the Brazilian Institute of the Environment and Renewable Natural Resources (IBAMA) in the Campos do Jordão city in the state of São Paulo.

Through the macroscopic analysis of the wood, it is possible to observe the anatomy of the tree rings of *Araucaria angustifolia*. Two parts are well-distinguished in the growth layer: (i) earlywood (spring) and (ii) latewood (autumn or summer). The earlywood corresponds to the tree's growth at the beginning of the vegetative period, usually in the spring or when conditions are favorable to the natural growth. In other words, when the plants are awakened from the dormancy period and resume their physiological activities with all vigor. As autumn approaches, environmental conditions (e.g., climate, water availability, etc.) become increasingly restrictive to plant growth, causing the vascular exchange and the cells to gradually decrease their physiological activity. As a result, the cell walls become thicker and their cavities smaller. In general, this fact gives the latewood a darker appearance [25].

In our first campaign, we collected four samples from eight individual trees. This campaign occurred in October 2012, within the area of the *Universidade do Vale do Paraíba*, located in the central perimeter of Campos do Jordão (−22°44 and −45°36 and altitude 1520 m a.s.l.). The same number of trees and samples per tree were collected in our second campaign carried out in March 2013 at *Pedra do Baú* in São Bento do Sapucaí city, a municipality covered by Campos do Jordão (−22°40 and −45°39, and altitude 1835 m a.s.l.).

The samples were taken by the non-destructive method with the aid of an increment borer (Pressler probe), which removes wooden cores from live trees. An incision of 1.30 m diameter at breast height was made to remove each sample. To succeed in our analyses, the samples were glued on support and polished with a sequence of sandpapers of different granulations (from 50 to 400 grains). From the 16 *Araucaria angustifolia* trees (64 samples), only 45 samples were considered viable. The other unused samples were broken, incomplete, too dark, or with resin stains.

2.3. The Chronologies

The tree ring analyses were performed at the Natural Registry Laboratory (*Laboratório de Registros Naturais* (LRN)), located at the *Instituto de Pesquisa e Desenvolvimento* (IP&D) of the *Universidade do Vale do Paraíba* (UNIVAP). The samples considered viable for the study were examined under a stereomicroscope (SMZ 168, with increases of 6.3 to 40 times), and a fiber optic lighting system. Using this procedure, we demarcated the annual natural tree ring width and excluded the false rings using COFECHA for cross-dating. The tree rings were counted to determine the tree ages. Afterwards, they were correlated with their respective calendar year. The measurement of the tree ring width was performed on a Velmex Table.

The natural growth rate varies according to the biological characteristics of each species; in order to maximize climate signals, a detrending in each series must be performed. The detrending model depends on the study goal [26]. As this study aims to determine the climatological variabilities, the following steps were: (1) to obtain the tree ring widths for each (Figure 3); (2) to detrend the tree ring series using the 67% nspline (two-third spline) with 50% of frequency cutoff as the individual growth trend; (3) to subtract the trend from each tree series sample; (4) to calculate the mean chronology vising to minimize anomalies and/or damage or any other sporadic phenomenon that may occur in any tree (Figure 3); and (5) to improve the quality of the mean chronology, we used the statistical program COFECHA to find possible errors between samples and to check the synchronization between the tree ring series and the master series [27,28]. The traditional approach to standardizing tree ring indices is to divide tree ring series by the detrended 67% nspline [29]. However, the tree ring indices are computed as residuals due to the non-heteroscedastic nature of our tree ring series, as suggested by [28].

To measure the common variability in the chronology we calculate the value of the expressed population signal (EPS) using

$$EPS(t) = \frac{t\ x\ R_{bt}}{t\ x\ R_{bt} + (1 - R_{bt})}. \quad (1)$$

The average number of tree series used is given by t and the mean between-tree correlation is given by R_{bt}. According to [30], when the EPS < 0.85, it means that the chronology is starting to be dominated by the individual signal of each tree series. However, the tree series can still be used for dendrochronology as long as it is not extremely low [31]. In Table 1, one can see that the EPS value for this study is 0.86. Therefore, the series has a coherent stand-level signal although it only contains 16 tree series.

Furthermore, we performed the variance correction due to the different sample numbers used in each time interval [32]. It is important to use as much of the tree ring series as possible. A subset of size between one and ten reflects an increase in variance [33]. Given this circumstance, the variance correction should be applied to produce a corrected tree ring chronology. The uncorrected and corrected chronologies are shown in Figure 4. In our case, there was a contraction in the variance of the corrected chronology below 15 samples.

2.4. Climatic Data and Analysis

In this study, monthly and annual temperature and precipitation series of the Campos do Jordão station—SP (OMM: 83714)—were used. These series are available at the INMET site (*Instituto Nacional de Meteorologia*). In this paper, we use the MATLAB functions developed by [34], `Seascorr`, to summarize the seasonal climate signal in our tree ring mean chronology. Figure 5 shows the climograph of the region. It can be observed that both precipitation and temperature follow the same pattern of monthly distribution. However, it can be noted that the precipitation does not vary much during the year (∼200 mm) and, also, the temperature (∼10 °C). The intercorrelation between the climatic variables (precipitation and temperature) was also evaluated, and has low correlation along the computed periods, with the majority below 50% (Figure 6).

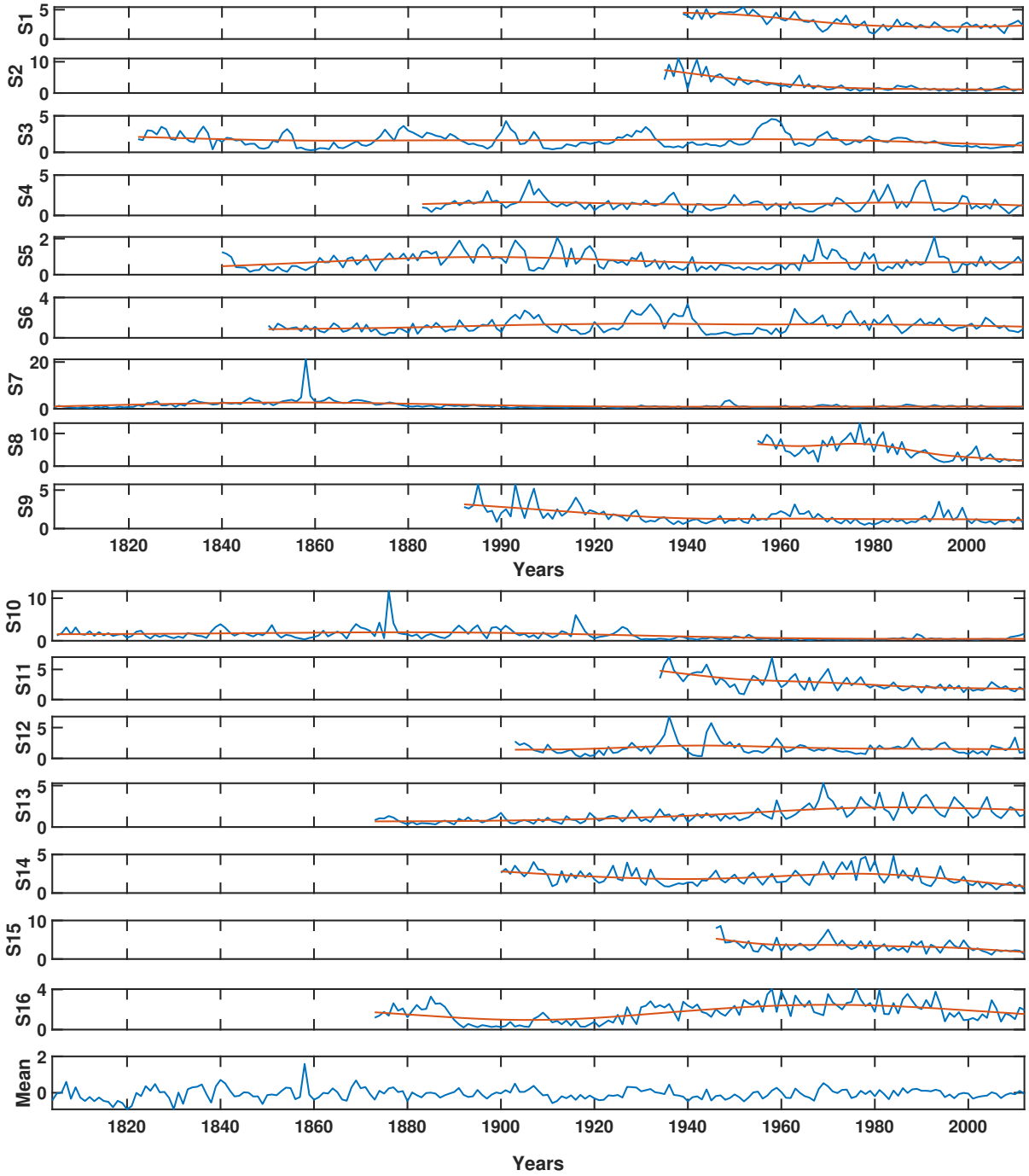

Figure 3. Tree ring series of each tree from Campos do Jordão (Si in mm, where $i = 1, 2, \ldots, 16$). Mean chronology (Mean in mm, the last panel). The 67% nsplines (two-third splines) with 50% of frequency cutoff were applied to remove the age trend (red lines).

Table 1. Tree ring series parameters.

Number of Tree Series (t)	Period	Mean between-Tree Correlation (Rbt)	Expressed Population Signal (EPS)
16	1803–2012	0.28	0.86

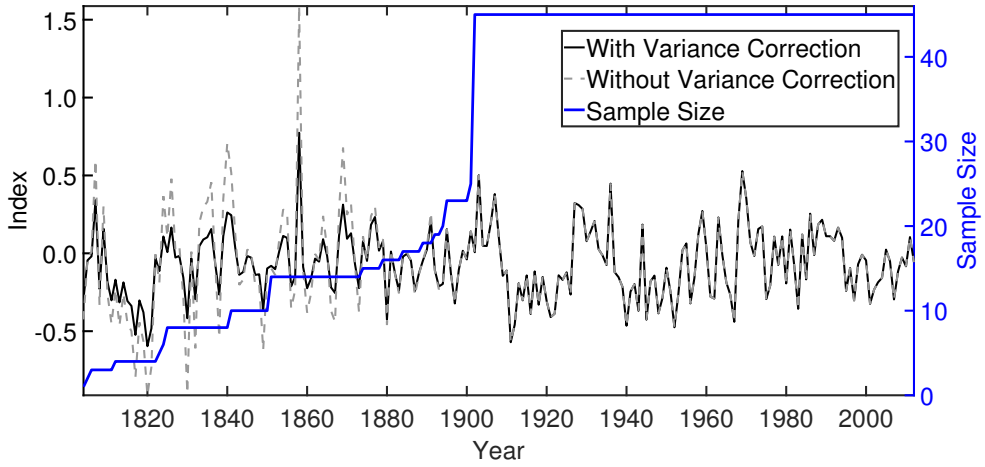

Figure 4. The corrected mean chronology (black line), the change in sample size (blue line), and the mean chronology without variance correction (light gray dashed line).

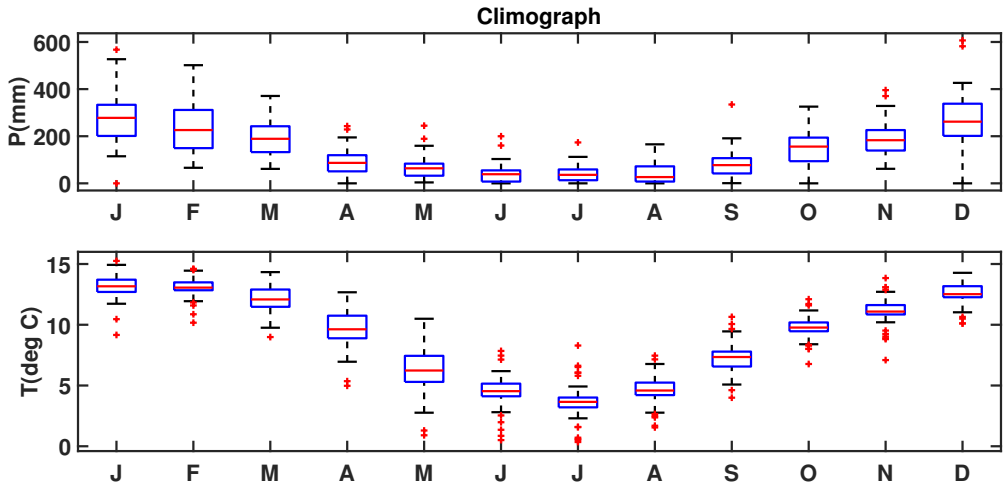

Figure 5. Climograph of Campos do Jordão city. (**Top**): Precipitation. (**Bottom**): Temperature.

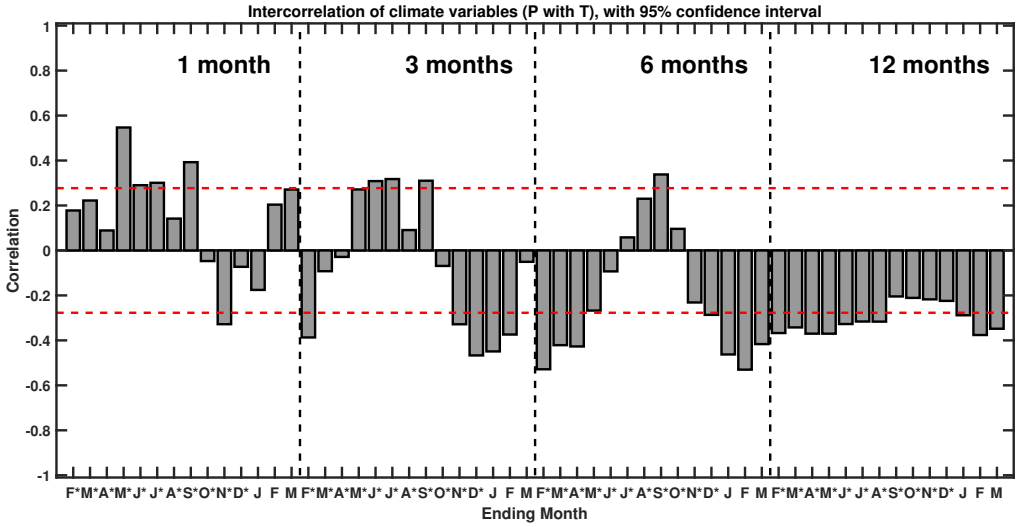

Figure 6. Intercorrelation of the climatic variable (precipitation and temperature) for 1, 3, 6, and 12 month-period moving correlation.

In the second step, we tested the temporal instability in the relationship between the mean chronology and our primary climate variables using the Pearson correlation. The correlation of mean chronology with our primary climate variables was also calculated in two sub-periods: in the early period between 1961–1978, and the late period, 1979–2012.

In the third step, the relationship between the mean chronology and our primary climate variables was also analyzed by the wavelet spectral techniques, which performs the search for periodicities and the extraction of non-periodic signals [35]. Morlet's cross-wavelet spectrum shows what is common between two-time series. In the scalograms, the Y-axis represents the scale (periods) of the spectrum in years, the X-axis is time, also in years, and the color scale indicates the energy power for each periodicity at a given time. The scalogram also shows the cone of influence (delimited by a white curve), in which the outer region of this curve is where the border effects exist [36]. Here, we use the wavelet cross-correlation to analyze the data dependent on the scales, in which each one represents the behavior of a different frequency band. We used an updated version of the CWT algorithm with the Morlet as the analyzing wavelet [36]. We used the symmetrization method, to deal with the border effects [8]. Therefore, there is no need for a cone of influence in our scalograms.

2.5. Results and Discussions

We calculated the Pearson's correlations and partial correlations between the mean chronology and precipitation/temperature series (Figure 7). The partial correlation was used to remove the influence of one climatic variable from another using the `Seascorr` written with MATLAB Release 2010b by [34]. Therefore, it is possible to assess the importance of only one climatic variable in the mean chronology. In the case of the southern hemisphere, the growing season ends in March. Consequently, the correlations and partial correlations were computed for individual months from February of the previous year to March of the current year, 3-month seasons ending in February of the previous year to March of the current year, and so on. The monthly temperature is significantly negatively correlated ($\alpha = 0.05$) with the mean chronology in three-month lengths ending in December (partial correlation—without the precipitation influence). The analysis of Figure 7 shows that the highest correlations for precipitation are in February, February#, April#, and July# for the 1, 3, 6, and 12-month lengths, respectively, where # means "previous year". In the same sense, the highest correlations for temperature are in March, May#, March#, and September#, respectively. The non-exceedance probabilities are listed in Table 2 for each computed "season". We note that the correlations for the observed precipitation and temperature are higher than those for any of the corresponding 1000 simulations in February and March, respectively. The confidence intervals for the correlations are derived by Monte Carlo simulation, and the Empirical non-exceedance probabilities for the simulation-based correlations were computed using the Weibull formula, as discussed by [34].

In Table 3, we present the correlation and α for full, early and late periods, for the precipitation and temperature as our primary variable. The α indicates that the parameters used in this analysis are not significantly correlated concerning the full period. The month with the highest correlation for the full period is February. In the present study, considering the seasons of the southern hemisphere, the precipitation during February (ending of the summer season) was considered the best control factor for the growth of *Araucaria angustifolia* located in Campos do Jordão city. We also tested the temporal instability using the correlation values obtained in the splitting periods. The splitting time correlation analysis reveals temporal instability between tree ring width and summer precipitation presenting correlations of 0.34 for the early period and -0.07 for the late period. This low correlation between the tree ring series and monthly total precipitation in the late period suggests caution in climatic reconstructions and also in our interpretation of the relationship between the tree natural growth and precipitation. To overcome this problem, we used a time-dependent correlation; in other words, the wavelet cross-correlation. From the

spectral analysis (Figure 8), it is possible to verify that there is a significant correlation ($\alpha = 0.05$) around the 2–3 year band during 1974–1986, around the 3–7 year band during ∼ 1961–1977, and around the 7–11 year band during 1967–1980.

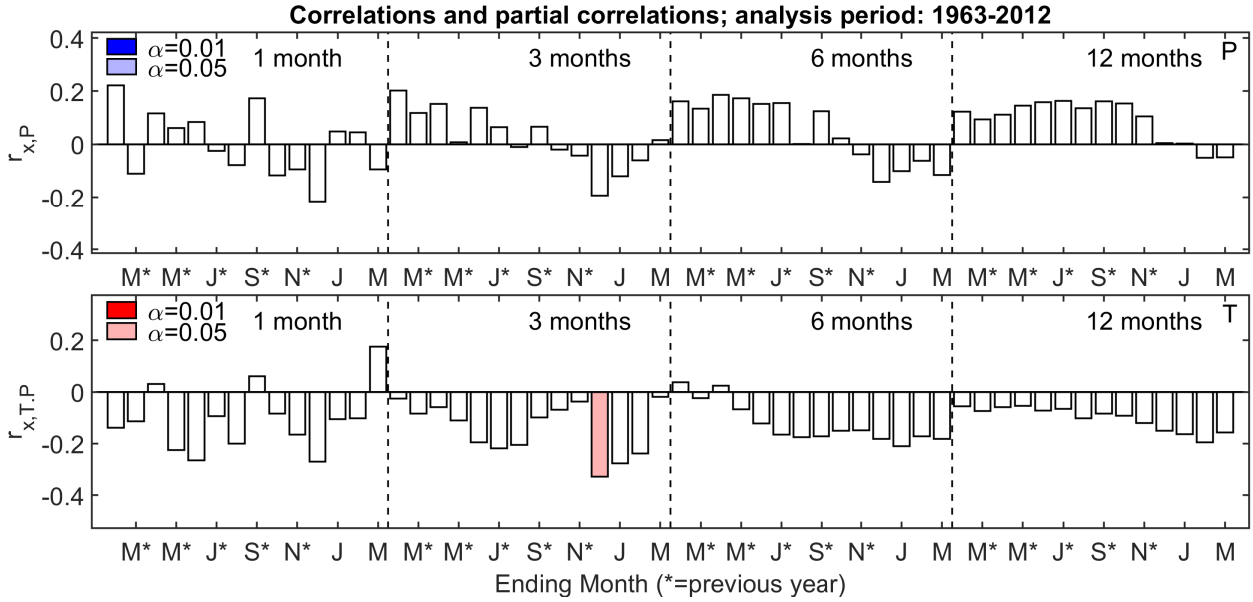

(**a**)

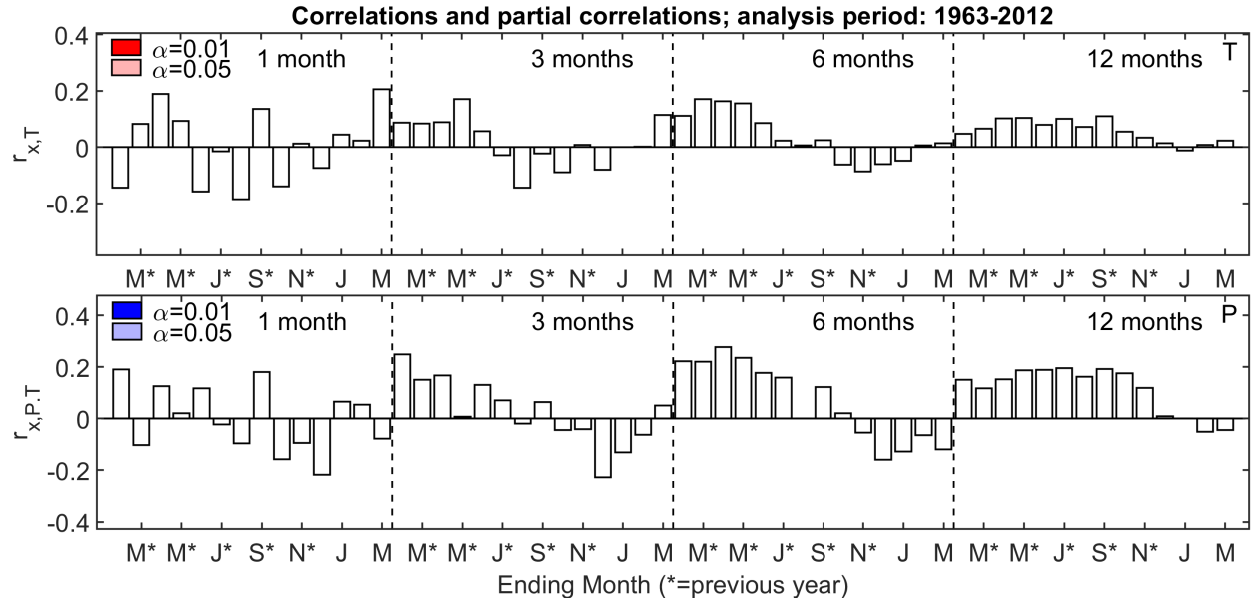

(**b**)

Figure 7. Correlations (**top panel**) and partial correlations (**bottom panel**) of mean chronology with the precipitation (P) and temperature (T). In each top panel are the simple correlations with the primary climate variable, and in each bottom panel, the partial correlations of mean chronology with the secondary climate variable. Significance at $\alpha = 0.05$ and $\alpha = 0.01$ color-coded. Notation $r_{x,P}$ ($r_{x,t}$) means correlation of x (mean chronology) with P (T); $r_{x,T.P}$ ($r_{x,P.T}$) means partial correlation of x with T (P), controlling for influence of P (T). (**a**) **Top**—Precipitation simple correlation. **Bottom**—Temperature partial correlation. (**b**) **Top**—Temperature simple correlation. **Bottom**—Precipitation partial correlation.

Table 2. Highest-correlated seasons of mean chronology with precipitation and temperature. The period analyzed is 1963–2012 with 1000 simulations. # means "previous year".

Precipitation				
m	**Ending Month**	**r**	**α**	**Nonexceedance Probability**
1	February	0.22	0.1	0.9462
3	February #	0.20	0.2	0.8866
6	April #	0.19	0.3	0.8477
12	July #	0.16	0.4	0.8092
Temperature				
1	March	0.21	0.1	0.9348
3	May #	0.17	0.3	0.8725
6	March #	0.17	0.3	0.8602
12	September #	0.11	0.5	0.7464

Table 3. Temporal stability of Pearson correlation of mean chronology with precipitation and temperature from early to late sub-periods. Full = 1961–2012, early = 1963–1987, late = 1988–2012.

Precipitation								
Season		**Correlation**			**Sample Size**		**Test Results**	
Months	**Length**	**Full**	**Early**	**Late**	**N1**	**N2**	**Δ Z**	**α**
February	1	0.22	0.34	−0.07	24	24	0.4286	0.162
December–February	3	0.20	0.25	−0.04	21	21	0.2975	0.377
November–April	6	0.19	0.24	−0.04	18	18	0.2762	0.445
August–July	12	0.16	0.18	−0.03	17	17	0.2189	0.557
Temperature								
March	1	0.21	0.36	0.02	24	24	0.3602	0.243
March–May	3	0.17	0.38	0.03	22	22	0.3647	0.258
October–March	6	0.17	0.38	−0.01	22	22	0.4190	0.193
October–September	12	0.11	0.41	−0.10	19	19	0.5399	0.122

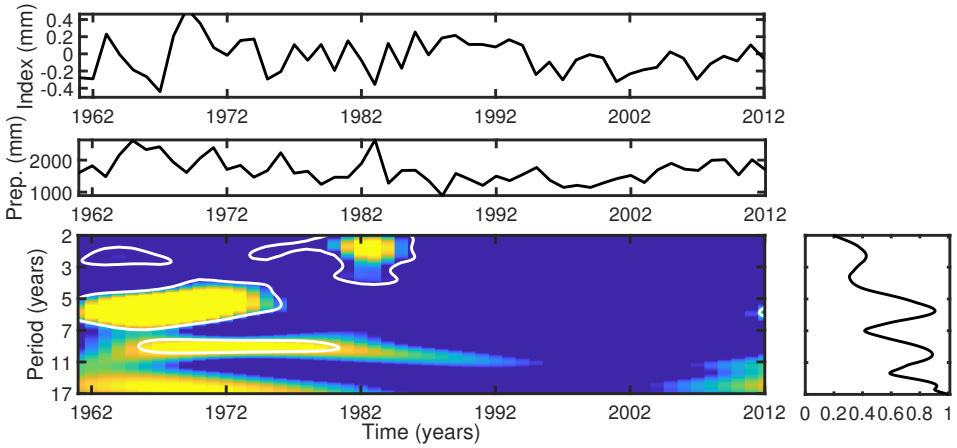

Figure 8. Cross-wavelets between the average growth rings' dendrochronological series and February precipitation time-series with the global spectrum (bottom right panel) and the confidence level of 95% (white contours).

For the full period, the highest correlation using temperature as a primary climate variable is **0.21** for March (Table 3). In the same sense, the results for the halves of 1963–2012 are **0.36** and **0.02**, respectively. This low correlation between the tree ring series and monthly temperature in the late period once more suggests caution in climatic reconstructions.

The α indicates that the parameters used in this analysis are not significantly correlated with the full period. Figure 9a shows the influence of the mean temperature, especially around the 3–7 year band during ~ 1964–1983, and an 8–17 year band during 1962–1969. In Figure 9b, we can verify three bands of maximum temperature influence, a 2–3 year band during ~1961–1967, a 4–7 year band during 1961–1968, and a 2–5 year band during 1968–1987. Finally, in Figure 9c, we can verify only one band of minimum temperature influence, a 4–9 year band during ~1961–1981.

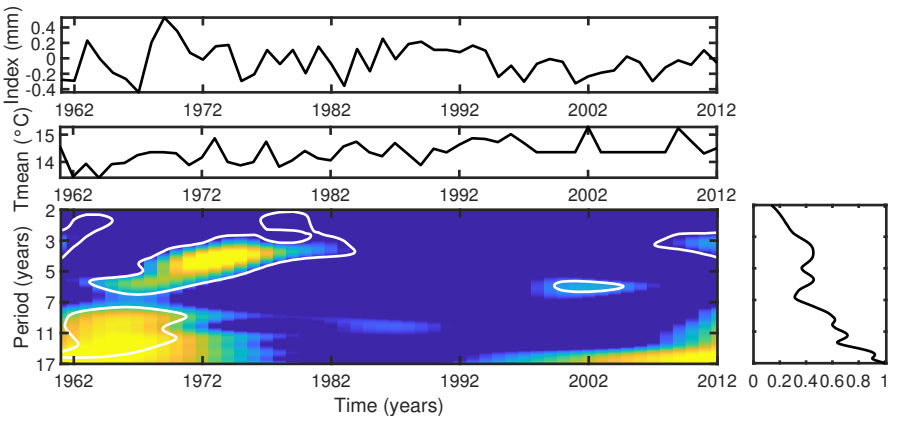

(**a**)

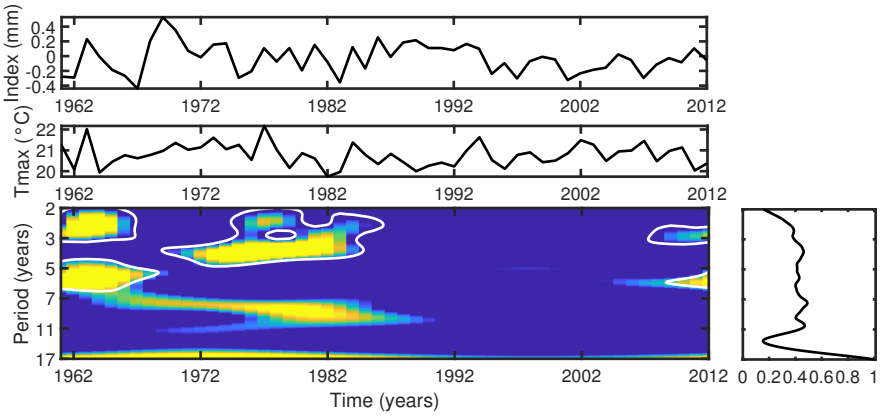

(**b**)

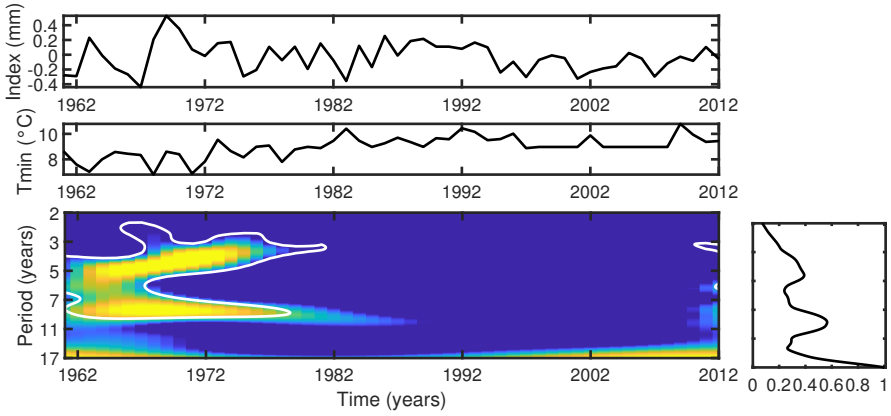

(**c**)

Figure 9. Cross-wavelets between the average growth rings dendrochronological series and mean March temperature (**a**), with maximum March temperature (**b**) and with minimum March temperature (**c**) time-series, respectively, with the global spectrum (**bottom right panel**) and the confidence level of 95% (white contours).

As a result of the analyses mentioned above, we constructed the data scatter plot (Figure 10) between the mean chronology and our primary climate variables for period-groups with higher correlations. The precipitation was more significant and well-correlated with the mean chronology, indicating that the species is sensitive to meteorological fluctuations. According to [37], the trees show a reaction to the environmental variables that affect their innumerable physiological processes, such as breathing, sap flow, transpiration, rate of cell divisions, and so forth, reflecting on the exchange activity, and, consequently, on the anatomy of the wood. However, some authors compared the meteorological variations with the periodicity of the growth of forest species and concluded that the lack of seasonality of temperature or precipitation in some regions makes it difficult to determine the periodic activity of the vascular change [38].

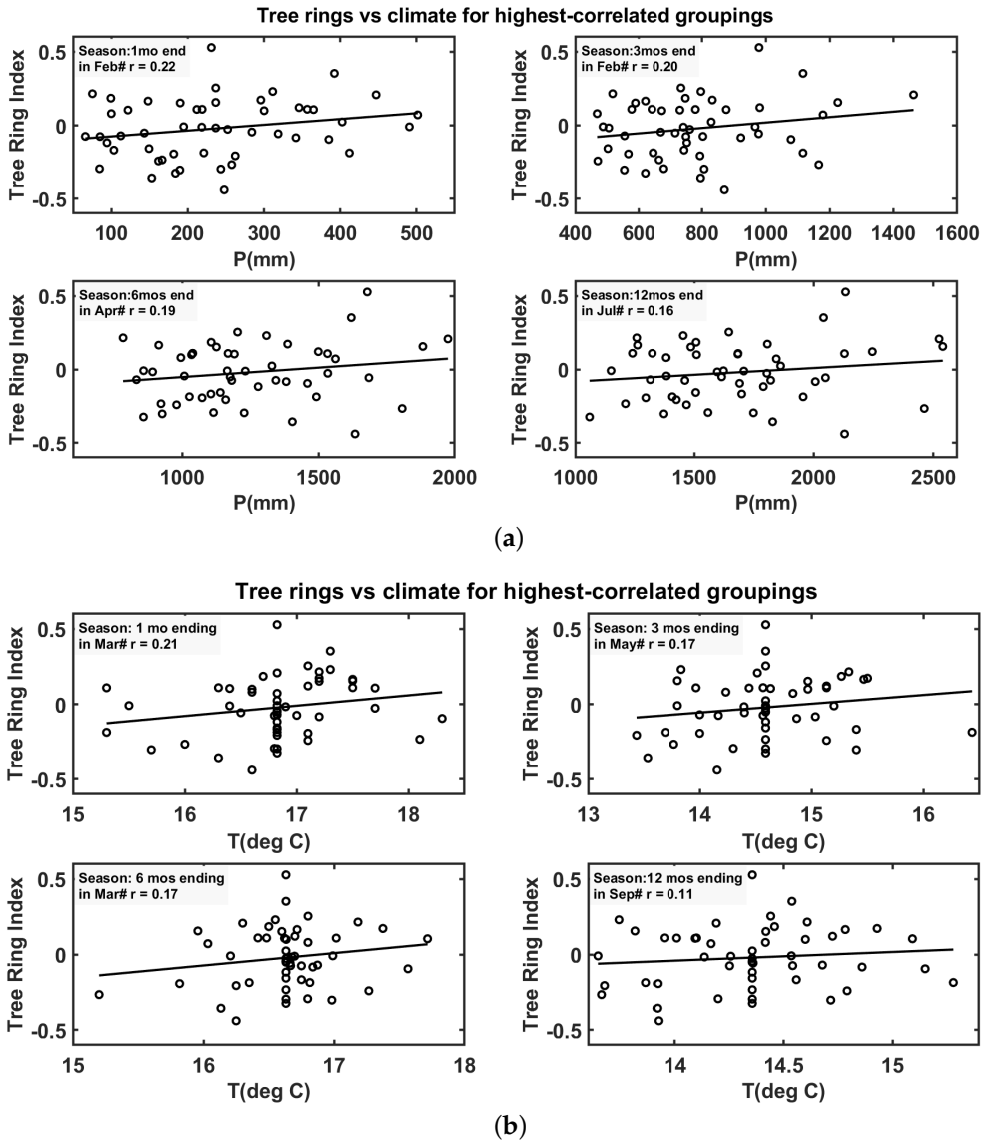

Figure 10. Data distribution between mean chronology and the precipitation (**a**) and the temperature (**b**).

A study described by [39] related the growth of *Araucaria angustifolia* with climatological data and observed that January was responsible for an increase of about 22% in the annual diametric increment of the trees. At the end of January, 57.42% of the accumulated annual increment of the trees occurred. Another study on the seasonal growth of *Araucaria*

angustifolia concluded that in regions with regular rainfall during the year, together with other environmental factors, such as temperature, may cause the growth to decrease [40].

As discussed by [41], water stress affects other physiological processes besides photosynthesis. Growth is likely to be slowed down by inhibiting many sensitive processes such as cell elongation and protein synthesis. The authors of [42] comment on the influence of water on the physiology of plants. According to them, the availability of water in the leaf is closely related to physiological activities such as leaf turgor, growth, stomatal conductance, transpiration, photosynthesis and respiration.

Variations in temperature, precipitation and solar radiation, among other meteorological elements, are more significant in areas of temperate climate than in tropical, when discussing the growth rate of the trees [43]. The relationship between meteorological variables and the exchange activity of *Araucaria angustifolia* trees has been observed by several authors [4,6,8,44,45], through growth rings that present a seasonal rhythm. However, the exchange activity of *Araucaria angustifolia* presents a difference between the sample sites regarding the periods of initial and latewood formation. It is known that the temperature affects the vapor pressure in the leaf so that the water activity can be influenced by the temperature. Temperatures below zero can lead to the formation of air bubbles and freezing, making it difficult to transport water, which decreases or ceases biological activities [41]. In our studied region, the temperature did not show periodic or seasonal influence on the growth of *Araucaria angustifolia*, as we can see in Figure 9. It suggests a good adaptation of this tree population to the variations of maximum and minimum temperatures. Other studies consider temperature as a limiting factor [39,40].

Our results corroborate that the tree ring growth of *Araucaria angustifolia* is seasonal. The exchange rate activity, determined by the patterns of earlywood and latewood formation, suggests seasonal variability regulated by the annual variation in precipitation. We can consider that the high availability of water is a limiting factor to the growth and development of the *Araucaria angustifolia* trees, since the excess of water available in the soil causes a decrease in the photosynthetic rate, reflected in the decrease of the tree's growth. The behavior of the *Araucaria angustifolia* in relation to water depends on the precipitation availability in the region.

3. Conclusions

The mean chronology of tree ring width in the region of Campos do Jordão-SP covered the time interval from 1803 to 2012. Our chronology was compared to the precipitation and temperature datasets employing Pearson correlation and cross-wavelet analysis. Our results corroborate that the tree ring growth of *Araucaria angustifolia* is seasonal. The rate of exchange activity determined the patterns of earlywood and latewood formation. This fact suggests that exchange rate seasonality may be regulated by the months at the end of the summer season, February (precipitation) and March (temperature).

Our results show evidence of temporal instabilities for both splitting time correlation analysis using precipitation and temperature, especially in the last halves of 1963–2012. To address this issue, the dendrochronological series and the climatic data were investigated using the wavelet cross-correlation searching for 95% significant time-dependent cause–effect relationships. From these analyses, we find a strong influence of the region's precipitation and temperature on the growth of tree rings.

A difficulty in the development of this work was the lack of longer and more complete climatic series in the region, and this will be our next task for better results.

Author Contributions: D.O.d.S. made a major contribution to preparing the introduction, dataset and methodology , and conclusions. A.P. developed the idea for this manuscript. V.K. collaborated in the revision of the text and description of the results. T.G.G.d.S. was responsible for the acquisition of the dataset and its preconditioning. All authors have read and agreed to the published version of the manuscript

Funding: This research received no external funding.

Institutional Review Board Statement: Not applicable.

Informed Consent Statement: Not applicable.

Data Availability Statement: To obtain the data for this study, please contact the authors via email.

Acknowledgments: The authors would like to thank FAPESP (Fundação de Amparo à Pesquisa do Estado de São Paulo.) for its assistance in the Prestes A. FAPESP project—(2009/02907-8), and CNPq (305249/2018-5).

Conflicts of Interest: The authors declare no conflict of interest.

Abbreviations

The following abbreviations are used in this manuscript:

IP&D	Instituto de Pesquisa e Desenvolvimento
UNIVAP	Universidade do Vale do Paraíba

References

1. Das Neves Brandes, A.F.; Albuquerque, R.P.; Lisi, C.S.; de Lemos, D.N.; Nicola, L.R.M.; Melo, A.L.F.; Barros, C.F. The growth responses of Araucaria angustifolia to climate are adjusted both spatially and temporally at its northern distribution limit. *For. Ecol. Manag.* **2021**, *487*, 119024. [CrossRef]
2. Venegas-González, A.; Roig, F.A.; Lisi, C.S.; Albiero-Junior, A.; Alvares, C.A.; Tomazello-Filho, M. Drought and climate change incidence on hotspot Cedrela forests from the Mata Atlântica biome in southeastern Brazil. *Glob. Ecol. Conserv.* **2018**, *15*, e00408. [CrossRef]
3. Schweingruber, F.H. *Tree Rings: Basics and Applications of Dendrochronology*; D. Reidel Publishing Company: Dordrecht, Hollan, 1988.
4. Nordemann, D.J.R.; Rigozo, N.R. Árvores Contam uma História do Sol. *Sci. Am.* **2003**, *2*, 30–37.
5. Luckman, B.H. Using Multiple High-Resolution Proxy Climate Records to Reconstruct Natural Climate Variability: An example from the Canadian Rockies. In *Mountain Environments in Changing Climates*; Routledge: London, UK, 1994; pp. 42–59.
6. Rigozo, N.; Lisi, C.; Filho, M.; Prestes, A.; Nordemann, D.; Pereira de Souza Echer, M.; Echer, E.; Evangelista, H.; Rigozo, V. Solar-Terrestrial Signal Record in Tree Ring Width Time Series from Brazil. *Pure Appl. Geophys.* **2012**, *169*. [CrossRef]
7. Lorensi, C.; Prestes, A. Dendroclimatological Reconstruction of Spring-Summer Precipitation for Fazenda Rio Grande, PR, with samples of Araucaria angustifolia (Bertol.) Kuntze. *Rev. Árvore* **2016**, *40*, 347–354. [CrossRef]
8. Prestes, A.; Klausner, V.; Rojahn da Silva, I.; Ojeda-González, A.; Lorensi, C. Araucaria growth response to solar and climate variability in South Brazil. *Ann. Geophys.* **2018**, *36*, 717–729. [CrossRef]
9. Fontana, C.; Reis-Avila, G.; Nabais, C.; Botosso, P.C.; Oliveira, J.M. Dendrochronology and climate in the Brazilian Atlantic Forest: Which species, where and how. *Neotrop. Biol. Conserv.* **2018**, *13*, 321–333. [CrossRef]
10. Lisi, C.S.; Pessenda, L.C.R.; Tomazello Fo., M.; Rozanski, K. 14C Bomb efects on tree rings of tropical and subtropical species of Brazil. *Tree-Ring Res.* **2001**, *57*, 191–196.
11. Roig, F.A. *Dendrocronologia en América Latina*; EDIUNC: Mendoza, Argentina, 2000.
12. Carvalho, P. Pinheiro-do-Paraná. Technical Report 60, Circular Técnica Embrapa. 2002. Available online: http://www.infoteca.cnptia.embrapa.br/infoteca/handle/doc/304455 (accessed on 20 March 2021).
13. Wrege, M.; Sousa, V.; Fritzsons, E.; Soares, M.; Aguiar, V.A. Predicting current and future geographical distribution of araucaria in Brazil for fundamental niche modeling. *Environ. Ecol. Res.* **2017**, *4*, 269–279. [CrossRef]
14. Wrege, M.S.; Fritzsons, E.; Soares, M.T.S.; Bognola, I.A.; de Sousa, V.A.; de Sousa, L.P.; Gomes, J.B.V.; de Aguiar, A.V.; Gomes, G.C.; Matos, M.; et al. Distribuição natural e habitat da araucária frente às mudanças climáticas globais. *Pesqui. Florest. Bras.* **2017**, *37*, 331. [CrossRef]
15. Guerra, M.; Silveira, V.; Reis, M.; Schneider, L. Exploração, manejo e conservação da araucária (Araucaria angustifolia). In *Sustentável Mata Atlântica—A Exploração de Seus Recursos Florestais*; Simões, L.L., Lino, C.F., Eds.; Editora Senac: São Paulo, Brazil, 2002; pp. 85–102.
16. Ribeiro, M.C.; Metzger, J.P.; Martensen, A.C.; Ponzoni, F.J.; Hirota, M.M. The Brazilian Atlantic Forest: How much is left, and how is the remaining forest distributed? Implications for conservation. *Biol. Conserv.* **2009**, *142*, 1141–1153. [CrossRef]
17. Carvalho, M.M.X.; Nodari, E.S. As fases da exploração madeireira na floresta com Araucária e os progressivos avanços da indústria madeireira sobre as florestas primárias (1870–1970). In *Anais do Simpósio Internacional de História Ambiental e Migrações*; UFSC: Florianópolis, Brazil, 2010.
18. Thomas, P. Araucaria Angustifolia. The IUCN Red List of Threatened Species 2013. Technical Report, Online Document. 2013. Available online: https://doi.org/10.2305/IUCN.UK.2013-1.RLTS.T32975A2829141.en (accessed on 13 May 2021).
19. Brazil. Portaria N° 443, de 17 de Dezembro de 2014. Technical Report, Diário Oficial da União. 2014; pp. 110–121. Available online: http://cncflora.jbrj.gov.br/portal/static/pdf/portaria_mma_443_2014.pdf (accessed on 21 April 2021).

20. Rodrigues, R.; Brancalion, P.; Isernhagen, I. Pacto Pela Restauração da Mata Atlântica: Referencial dos Conceitos e Ações de Restauração Florestal. Technical Report, Escola Superior de Agricultura Luiz de Queiroz & Instituto BioAtlântica. 2009. Available online: https://www.ipe.org.br/ultimas-noticias/1911-ipe-esta-no-conselho-de-coordenacao-do-pacto-pela-restauracao-da-mata-atlantica?gclid=Cj0KCQjw9O6HBhCrARIsADx5qCSaSwOsx3voien-9Nz2wcP6esrNTnHLCfejR5tdMjWz5aqor-jSK8kaAvdiEALw_wcB (accessed on 20 March 2021).
21. Souza, R.O.M.; Souza, V.C.; Polisel, R.T.; Ivanauskas, N.M. Estrutura e aspectos da regeneração natural de Floresta Ombrófila Mista no Parque Estadual de Campos do Jordão, SP, Brasil. *Hoehnea* **2012**, *39*, 387–407. [CrossRef]
22. Lisi, C.S. Atividade de Î4C do Fallout e Razão Isotópica Î3C/Î2 em Anéis de Crescimento de Clima Tropical e Subtropical do Brasil. Ph.D. Thesis, CENA Science PG, Universidade de São Paulo, São Paulo, Brazil, 18 January 2001.
23. Raven, P.; Evert, R.; Eichhorn, S. *Biologia Vegetal*, 6th ed.; Guanabara Koogan: Rio de Janeiro, Brazil, 1999.
24. Do Estado de São Paulo, G. Plano de Manejo do Parque Estadual de Campos do Jordão. Technical Bulletin, Governo do Estado de São Paulo. 1975. Available online: https://www.infraestruturameioambiente.sp.gov.br/fundacaoflorestal/planos-de-manejo/planos-de-manejo-planos-concluidos/planos-de-manejo-pe-de-campos-do-jordao/ (accessed on 20 March 2021).
25. Botosso, P. *Identificação Macroscópica de Madeiras: Guia práTico e Noções Básicas para o seu Reconhecimento*; Embrapa Florestas Colombo: Paraná, Brazil, 2011.
26. Silva, D.; Klausner, V.; Prestes, A.; Gimenes, H.M.; Aakala, T.; Silva, I.R. Principal Components Analysis: An Alternative Way for Removing Natural Growth Trends. *Pure Appl. Geophys.* **2021**. [CrossRef]
27. Holmes, R.L. Computer assisted quality control in tree-ring dating and measurement. *Tree Ring Bull.* **1983**, *43*, 69–78.
28. Helama, S.; Lindholm, M.; Timonen, M.; Eronen, M. Detection of climate signal in dendrochronological data analysis: A comparison of tree-ring standardization methods. *Theor. Appl. Climatol.* **2004**, *79*, 239–254. [CrossRef]
29. Fowler, A.M. Variance Stabilization Revisited: A Case For Analysis Based On Data Pooling. *Tree-Ring Res.* **2009**, *65*, 129–145. [CrossRef]
30. Speer, J.H. *Fundalmentals of Tree-Ring Research*; Library of Congress Cataloging-in-Publication Data; Library of Congress: Washington, DC, USA, 1971.
31. Ferrio, J.P.; Díez-Herrero, A.; Tarrés, D.; Ballesteros-Cánovas, J.A.; Aguilera, M.; Bodoque, J.M. Using stable isotopes of oxygen from tree-rings to study the origin of past flood events: First results from the iberian peninsula. *Quaternaire* **2015**, *26*, 67–80. [CrossRef]
32. Shiyatov, S.G.; Mazepa, V.S. *Some New Approaches in the Consideration of More Reliable Dendroclimatological Series and in the Analysis of Cycle Components*; Methods of Dendrochronology; Kairiukstis, L., Cook, E.R , Eds.; International Institute for Applied Systems Analysis, Laxenburg, Austria and Polish Academy of Sciences-System Research Institute: Warsaw, Poland, 1987.
33. Cook, E.; Briffa, K.; Shiyatov, S.; Mazepa, V.; Jones, P.D. Data Analysis. In *Methods of Dendrochronology: Applications in the Environmental Sciences*; Cook, E.R., Kairiukstis, L.A., Eds.; Springer: Dordrecht, The Netherlands, 1990; pp. 97–162. [CrossRef]
34. Meko, D.M.; Touchan, R.; Anchukaitis, K.J. Seascorr: A MATLAB program for identifying the seasonal climate signal in an annual tree-ring time series. *Comput. Geosci.* **2011**, *37*, 1234–1241. [CrossRef]
35. Rigozo, N.R.; Echer, E.; Vieira, L.E.A.; Nordemann, D.R. Reconstruction of Wolf sunspot numbers on the basis of spectral characteristics and estimates of associated radio flux and solar Wind parameters for the last millennium. *Sol. Phys.* **2001**, *203*, 179–191. [CrossRef]
36. Torrence, C.; Compo, G.P. A Practical Guide to Wavelet Analysis. *Bull. Am. Meteorol. Soc.* **1998**, *79*, 61–78. [CrossRef]
37. Tomazello Filho, M.; Botosso, P.C.; Lisi, C.S. Análise e aplicação dos anéis de crescimento das árvores como indicadores ambientais: Dendrocronologia e dendroclimatologia. In *Indicadores Ambientais: Conceitos e Aplicações*; EDUC, COMPED, INEP: Piracicapa, São Paulo, Brazil, 2002; pp. 117–143.
38. Cardoso, N.S. Caracterização da Estrutura Anatômica da Madeira, Fenologia e Relações com a Atividade Cambial de Arvores de Teça (Tectona Grandis)— Verbanaceae. Master's Thesis, Escola Superior de Agricultura "Luiz de Queiroz", Universidade de São Paulo, Piracicaba, Brazil, 1991.
39. Zanon, M.L.B. Crescimento da Araucaria Angustifolia (Bertol.) Kuntze Diferenciado por Dioicia. Ph.D. Thesis, Universidade Federal de Santa Maria, Santa Maria, Brazil, 2007.
40. Santarosa, E.; Oliveira, J.M.; Roig, F.A.; Pillar, V.P. Crescimento Sazonal em Araucaria angustifolia: Evidências Anatômicas. *Rev. Bras. BiociêNcias* **2007**, *5*, 618–620.
41. Lambers, H.; Chapin, F.; Pons, T. *Plant Physiological Ecology*; Springer: New York, NY, USA, 1998.
42. Kramer, P.J.; Boyer, J. *Water Relations of Plants and Soils*; Academic Pres: San Diego, CA, USA, 1995; p. 495.
43. Jacob, G.C. Overview of tree-rings analysis in tropical regions. *IAWA Bull. New Ser.* **1989**, *10*, 99–108. [CrossRef]
44. Rigozo, N.; Evangelista, H.; Nordemann, D.; Echer, E.; Pereira de Souza Echer, M.; Prestes, A. The Medieval and Modern Maximum solar activity imprints in tree ring data from Chile and stable isotope records from Antarctica and Peru. *J. Atmos. Sol. Terr. Phys.* **2008**, *70*, 1012–1024. [CrossRef]
45. Scipioni, M.C.; Fontana, C.; Oliveira, J.M.; Santini Junior, L.; Roig, F.A.; Tomazello-Filho, M. Effects of cold conditions on the growth rates of a subtropical conifer. *Dendrochronologia* **2021**, *68*, 125858. [CrossRef]